Modelling the Mechanical Response of Japanese Lacquer (*Urushi*) to Varying Environmental Conditions

by

Xinyi Liu

A doctoral thesis submitted in partial fulfilment of the requirements for the award of Doctor of Philosophy of Loughborough University

Wolfson School of Mechanical and Manufacturing Engineering

Dedicated to my parents and fiancee

Abstract

Urushi is a complex natural polymer that has been used to protect and decorate objects for many hundreds of years. *Urushi* is an important material as decorated objects can obtain great value and historical worth. A star item of *urushi* lacquerwares, the Mazarin Chest, property of Victoria & Albert (V&A) Museum in London, is famous as one of the finest pieces of Japanese lacquerware in the world, dating back to as early as the late 1630s. These *urushi* lacquerwares are often exposed to environments that are detrimental to both their aesthetic appeal and structural performance, and restoration and conservation procedures are needed to preserve these objects over long periods of time. However, the precise behaviour of *urushi* lacquers is not sufficiently understood to allow accurate prediction of the material response to environmental effects or of the effectiveness of any proposed conservation procedure. Thus a need exists for a comprehensive understanding of this material and a finite element (FE) model to predict the mechanical response to varying environmental conditions.

The aim of this research was to model the hygro-mechanical effects during the environmental ageing process of *urushi* films by means of FE modelling, which will help to make decisions about the environmental conditions required for storage and exhibition. This was achieved by a combination of experimental and computational methods. A synthetic thermosetting (crosslinked) lacquer, polyurethane (PU), was initially studied to develop the methodology of the experimental and numerical studies and to provide a comparison to the natural lacquer.

Experimental work was carried out to characterise the material behaviour of both materials, such as hygroscopic expansion, moisture diffusion kinetics and mechanical behaviour under various environmental conditions. Moisture diffusion in the two lacquer films was well described by Fick's law. However, different sorption isotherm models, Flory-Huggins model for PU and Guggenheim-Anderson-de-Boer (GAB) model for *urushi*, were required to model the equilibrium sorption of these two materials. The mechanical properties of the lacquer films were found to have a complex dependence on environmental conditions. The tensile properties of both lacquer films were shown to change significantly after UV ageing. With increasing time of ultraviolet (UV) irradiation, Young's Modulus and tensile strength increased dramatically, but the maximum strain decreased. With water absorption, both Young's modulus and tensile strength decreased, and maximum strain increased. The two lacquer films were found to behave with a non-linear viscoelasticity, which was highly

dependent on environmental conditions. A modified Burger's model was found to provide a good fit to experimental creep data for the PU lacquer well at different stress levels, suggesting this is a satisfactory method for characterising PU rheological behaviour. A novel modified generalized Kelvin fluid (MGKF) model was found to be a powerful non-linear viscoelastic model capable of representing the rheological behaviour of the *urushi* below the yield stress. However, in order to include the post yield behaviour a visco-elastic-plastic model is required.

A hygro-mechanical model of the *urushi* behaviour based on the MGKF viscoelastic model was developed and tested. Through careful determination of the mechanical behaviour the constitutive properties of a thin layer of lacquer were determined and used as an input to a FE based model of the deformation and stresses that develop in response to changes in the environmental conditions. The model was validated using experimental results that showed the depth averaged stress in a thin layer deposited on a glass substrate, which allowed insight into the time dependent and spatially varying stresses within the layer. It was shown that the regions of highest stress were found in areas of highest moisture ingress, emphasising the need for control of the environment in which *urushi* covered artefacts are stored.

In order to perform a predictive study on the bending behaviour of *urushi* films with cracks, as can be seen in aged lacquers, a model with a grooved *urushi* film on an aluminium substrate was created and subjected to bending loads. The time-dependency of the *urushi* material properties seems to hardly affect the bending behaviour of the model, however, the profile of the displacement field around the groove was found to be considerably affected by the geometry of the groove. To evaluate the effectiveness of a traditional Japanese consolidation method for lacquerware objects, known as *urushi-gatame,* a strain-based progressive damage failure model was used to model the continuum failure in the bi-material strip under an increasing bending load. The behaviour of damage initiation and evolution was modelled for an unfilled groove, a filled groove with fresh filler and filled groove with UV aged filler. From the finite element analysis (FEA) results, the introduction of the filler, as a simple mimic of the consolidation method, does enable the strip to sustain a higher bending load. However, this effectiveness is weakened as the material is aged, with it behaving similar to a groove without any filler.

Table of Content

List of Figures

List of Tables

Symbols

a_w	Water activity
C	Concentration of diffusing substance
C_{sat}	Concentration at saturatino
d	Parameter of Ducker-Prager model
d_c	Crack depth
D	Diffusion coefficient
E	Elastic modulus
E_0	Instantaneous modulus
E_T	Tensile elastic modulus
$E(t)$	Relaxation modulus
F	Rate of transfer per unit area
F_Y	Yield function
f	Flux
g	Flow potential
G_i	Deviatoric modulus
G_c	Critical strain energy release rate
H	Height of pile-up
H_a	Hardening parameters
I_1	First invariant of the stress tensor
J_2	Second deviatoric invariant of the stress tensor
$J(t)$	Creep compliance
K_i	Volumetric modulus
K_c	Critical stress intensity factor

L	Length
l_d	Delamination length
m_1	Mass of the specimen after drying
m_2	Mass of the specimen at specified time intervals
M_m	Monolayer moisture content
$M(t)$	Mass of the total amount of penetrant absorbed at time t
$M(\infty)$	Weight gain at equilibrium
$p_t\|_0$	Initial average tensile strength
q	Von Mises equivalent stress
s_{ij}	Components of the stress deviator tensor
t	Time
V	Volume fractions
u	Molar volume
α	Friction angle
β	Coefficient of hygroscopic expansion
β'	Parameter of Ducker-Prager model
σ	Stress
σ_B	Tensile strength at break
σ^{dev}	Stress deviator tensor
σ_{eq}	von Mises equivalent stress
σ_f	In-film stress
σ_x	Normal stress components in the x directions
σ_y	Normal stress components in the y directions
σ_{xy}	Shear stress in x-y plane

σ_{xx}	Longitudinal stress
$\dot{\sigma}$	Stress rate
$\bar{s}$	Yield stress
τ	Retardation time
τ_Y	Yield stress under pure shear load
δ	Curvature
ε	Strain
ε_1	Initial elastic strain
ε_2	Transient creep region
ε_3	Secondary creep region
ε_{33}	Out-of plane strain
ε_B	Strain at break
ε_c	Creep strain
ε_d	Strain of dashpot component
ε_h,	Hygroscopic strain
e^{pl}	Equivalent plastic strain
ε_s	Strain of spring component
$\dot{\varepsilon}$	Strain rate
$\dot{\varepsilon}_{eq}^{cr}$	Uniaxial equivalent creep strain rate
$\dot{\varepsilon}_{ij}$	Multi-direction creep strain rate tensor
$\dot{\varepsilon}_d$	Strain rate of dashpot component
$\dot{\varepsilon}_{eq}^{c}$	Equivalent creep strain rate scalar
$\dot{\varepsilon}_s$	Strain rate of spring component

θ	Temperature
φ	Density of diffusing material
c_d	Polymer-penetrant interaction index
ρ	Density
η	Dashpot constant

Acronyms

2D	Two Dimensional
3D	Three Dimensional
CDM	Continuum Damage Mechanics (CDM)
CHE	Coefficient of Hygroscopic Expansion
DP	Degree of Polymerization
EMC	Equilibrium Moisture Concentration
FE	Finite Element
FEA	Finite Element Analysis
FEM	Finite Element Method
FT-IR/ATR	Transform Infrared–Attenuated Total Reflectance
HALS	Hindered Amine Light Stabiliser
GAB	Guggenheim-Anderson-de-Boer
MBM	Modified Burger's Model
MC	Moisture Content
MGKM	Modified Generalized Kelvin Model
PL	Purified *Urushi*
PU	Polyurethane
PID	Proportional with Integral and Derivative
RH	Relative Humidity
SEM	Scanning Electron Microscopy
TBC	Thermal Barrier Coating
TPU	Thermoplastic Polyurethane
UV	Ultraviolet

UVA   Ultraviolet A

UVB   Ultraviolet B

V&A   Victoria & Albert

Acknowledgement

I am deeply indebted to my supervisors Prof R. D. Wildman and Prof I. A. Ashcroft at Loughborough University. Their patient guidance, stimulating suggestions and enthusiastic encouragement helped me through the whole process of this research till the writing of this thesis.

Special thanks are due to Shayne Rivers at the Victoria & Albert (V&A) Museum for her advice on conservation of *urushi* lacquerwares.

Thanks are also due to the staff of the Wolfson School of Mechanical and Manufacturing Engineering for their support and help. I appreciate the guidance provided by Mr. Max Farrand and Mr. Andy Sandaver during the experimentation and characterisation phases of the research.

I would also like to extend my gratitude to my fellow researchers; Dr. Aamir Mubashar, Dr. Juan Pablo Casas Rodriguez, Dr. Vikram Shenoy, Dr. Kazim Altaf, Mr George Tsigkourakos, Mr Tho Nguyen and Miss Maryam Haghihi-Abayneh for their help and friendship throughout the research.

Publications

Liu, X., Elmahdy, A.E., Ashcroft, I.A. and Wildman, R.D., 2011, *"A Methodology for Modelling the Mechanical Response of Urushi Lacquer under Varying Environmental Conditions"*. In East Asian Lacquer: Material Culture, Science and Conservation, Shayne Rivers, Rupert Faulkner and Boris Pretzel, Archetype Publications, London ISBN: 9781904982609.

Liu, X., Elmahdy, A.E., Wildman, R.D., Ashcroft, I.A. and Ruiz, P.D., 2011 *"Experimental Investigation and Material Modelling of Fresh and UV Aged Japanese Lacquer (Urushi)"*. Progress in Organic Coatings, **70**(4), 160-169.

Liu, X. Wildman, R.D., Ashcroft, I.A. and Ruiz, P.D., *"Experimental Investigation and Numerical Modelling on UV and Humidity Related Mechanical Properties of Polyurethane Lacquer Films"*. being submitted to Plastics, Rubber and Composites.

Liu, X. Wildman, R.D., Ashcroft, I.A. and Ruiz, P.D., *"Modelling the Mechanical Response of Urushi Lacquer under Varying Environmental Conditions"*, being submitted to Proceedings of Royal Scoiety. A: Mathematical, Physical and Engineering Science.

Chapter 1 Introduction

1.1 Overview of Mazarin Chest

The Mazarin Chest, property of Victoria & Albert Museum (V&A) in London, is famous as one of the finest pieces of Japanese lacquerware in the world. The chest, shown in Figure 1-1, was manufactured in Kyoto in the late 1630s or early 1640s and has been regarded as a precious Japanese national treasure and item of cultural heritage [1].

Figure 1-1: The Mazarin Chest, in V&A Museum in London [2].

The chest measures 59 cm high, 101.5 cm wide and 63.9 cm deep, with the name Mazarin derived from having once been owned by the Mazarin-La Meilleraye family, whose coat of arms is carried on the chest's French steel key. It is made of black-lacquered wood in a European style for export purposes at the time. It is lavishly decorated on both internal and external surfaces, with vivid scenes from Japanese traditional tales, including portraits, palaces, bridges and other decorative patterns [3]. This wooden masterpiece is a solid representation of a wide range of Japanese traditional decoration techniques and the outstanding skill of the craftsmen who made the chest. Each detail on this work is of great technical and artistic importance for both Japan and the West [4].

The Mazarin Chest is constructed from straight grain wood and cross grain pinewood. Once the wooden structure of the Mazarin Chest was built, numerous foundation layers, consisting

of oriental lacquer mixed with other materials such as wheat flour paste and water mixed with clay, were applied to the surface of the wooden structure. Finally, the chest was coated with multiple layers of coloured lacquer and decorated using a range of traditional Japanese techniques [5]. In the years since its manufacture, the Mazarin Chest has suffered from different kinds of damage during its storage and display in fluctuating environmental conditions, particularly the relative humidity (RH), which is high in Japan compared to relative humidity in Europe. It has also been exposed to potentially harmful lighting conditions for long periods, and has suffered from previously applied Western coatings that were used in an attempt to restore the original appearance and lustre of the lacquer [5].

As a result of this exposure to fluctuating environmental conditions, micro-cracks have appeared in the lacquer, leading to significant discoloration and fading of the originally glossy surface. In addition, there is damage to the wooden structure, in the form of cracks, due to the expansion and contraction of the wood. The lacquer film around these cracks has lifted and there has been a loss of lacquer coating with extensive loosening and wrinkling of adhered decorative elements, including silver and gold foils. There has also been extensive lifting of the mother-of-pearl decoration.

As a consequence of the damage suffered by the Mazarin Chest, it was not stable enough for display or transport and is also at risk of further deterioration. Even if it simply remained in storage without conservation, access to the chest within the V&A would be severely limited. In addition any requests for the loan of this object could not be supported, preventing the chest from playing a wider role in the international field of art history. Every loss to the original decoration represented a loss of meaning and cultural value of the object and as a result, conservation was urgently needed. Therefore, the V&A, with the support of the Toshiba Foundation and other charitable bodies, initiated a project to consider the most appropriate methodologies for conserving this object for future generations.

At the point of initiation of this project, the traditionally favoured method for the conservation of natural lacquer objects was to apply another layer of lacquer (usually diluted) to the damaged surface. This has the effect of filling any holes or micro-cracks. This contrasts with the Western approach of preserving the object in its current state. Conservators do not know for sure, however, which method is the most effective in minimising the negative long term impact of environmental ageing effect [5].

1.2 Mazarin Chest conservation project

The Mazarin Chest conservation project is a combination of art, historical and scientific research. The stated aims of the Mazarin Chest conservation project are to develop a comprehensive interdisciplinary methodology for the conservation of Japanese lacquer objects held in Japan and Western collections and develop a theoretical framework for the collaborative conservation treatment of the V&A Mazarin Chest and similar lacquer objects in Japan and in the West.

The Mazarin Chest conservation project consists of a network of partnerships of universities and specialist institutions with the V&A, which include Loughborough University, the Polish Academy of Sciences, Imperial College London and the Dresden Academy of Fine Arts.

The Institute of Catalysis and Surface Chemistry, within the Polish Academy of Sciences, is investigating moisture absorption by wood and lacquer, the dimensional response (swelling isotherm) of wood and lacquer due to fluctuations in relative humidity, the rate at which moisture moves through each of these materials, and the effects of the moisture distribution in the wood and lacquer on cracks, as they respond to fluctuations in relative humidity [6].

The Chemistry Department at Imperial College is studying the effect of Western varnishes on the Chest's lacquer. Western varnishes have been applied in an attempt to restore the original colour and gloss of the aged lacquer. Unfortunately, they do not replicate the original appearance of the *urushi* lacquer. Further, Western varnishes can damage the original lacquer as they age and degrade in turn. The more aged the lacquer surface and the more degraded and oxidised the Western coating, the more difficult it is to remove the varnish without damaging the original lacquer. The problem of removing degraded Western varnishes from oriental lacquer affects a substantial proportion of such objects held in public collections in the West. Analysing the interpretation and presentation of Japanese lacquer in Western collections, identifying the aesthetic criteria applied to Japanese lacquer in Japan and the West, and understanding the cultural belief systems that define conservation ethics in Japan and the West will provide a framework for proposing an experimental conservation methodology [6].

Dresden Academy of Fine Arts in Germany is investigating problems encountered by conservators in their working practice when consolidating degraded oriental lacquers. The main research strands are [6] identification and characterisation of the typical

problems/different types of deterioration/modes of failure of the lacquer layer structure, and review of the materials used for consolidation in conservation (i.e. collagen glues, Polyvinyl acetates (PVA) glues, acrylics, traditional Japanese consolidation materials).

The Wolfson School of Mechanical and Manufacturing Engineering at Loughborough University is focused on developing an understanding of the basic mechanics of *urushi* layers. The aim of this focus is to understand and be able to predict the effect of ageing on the ability of *urushi* layers to support stresses that are generated through interaction with typical environments.

1.3   Aims and objectives of the Project

As an important aspect of the scientific research of the Mazarin Chest conservation project, this PhD project aims to model the hygro-mechanical effects during the environmental ageing process of *urushi* films by means of finite element (FE) modelling. This will help to make decisions about the environmental conditions required for storage and exhibition, and is of great significance as a part of the scientific research in the Mazarin Chest Project. To meet this aim, the project had objectives to:

l   Experimentally characterise the hygro-mechanical properties of *urushi* with environmental effects,

l   Find or develop appropriate material models that can be used to describe the material behaviour under various environmental conditions,

l   Propose and validate an FE model that is able to predict the mechanical response of *urushi* lacquer to varying environmental conditions.

This work will result in two major advances in this area. First, a material model that can describe the non-linear and time-dependent stress-strain behaviour of coating materials under changing environmental conditions will be developed for first time. Secondly, a methodology on modelling mechanical response to varying environmental conditions will be developed for coating material. The research outcomes will support the V&A conservators in making informed decisions about conservation treatment options and help understand the material behaviour observed during conservation work.

1.4   Research methodology and thesis structure

The methodology of the research has been designed to achieve the specified aim and objectives. The experimental programme in this project, investigating the effects of the moisture on the urushi film which has been aged under different periods of ultraviolet (UV) exposure, is shown schematically in Figure 1-2. Computer simulation, using finite element analysis (FEA), was applied in this research and the commercial FE package ABAQUS (v6.9 and 6.10, Dassault Systems, Providence, RI, USA) was used in all the modelling work. The basic modelling methodology is illustrated in Figure 1-3. A FE model was created and material properties defined as a function of environmental conditions. A load was then applied by means of a varying external humidity. This was implemented in the FE model by varying the boundary conditions of the diffusion model as a function of time.
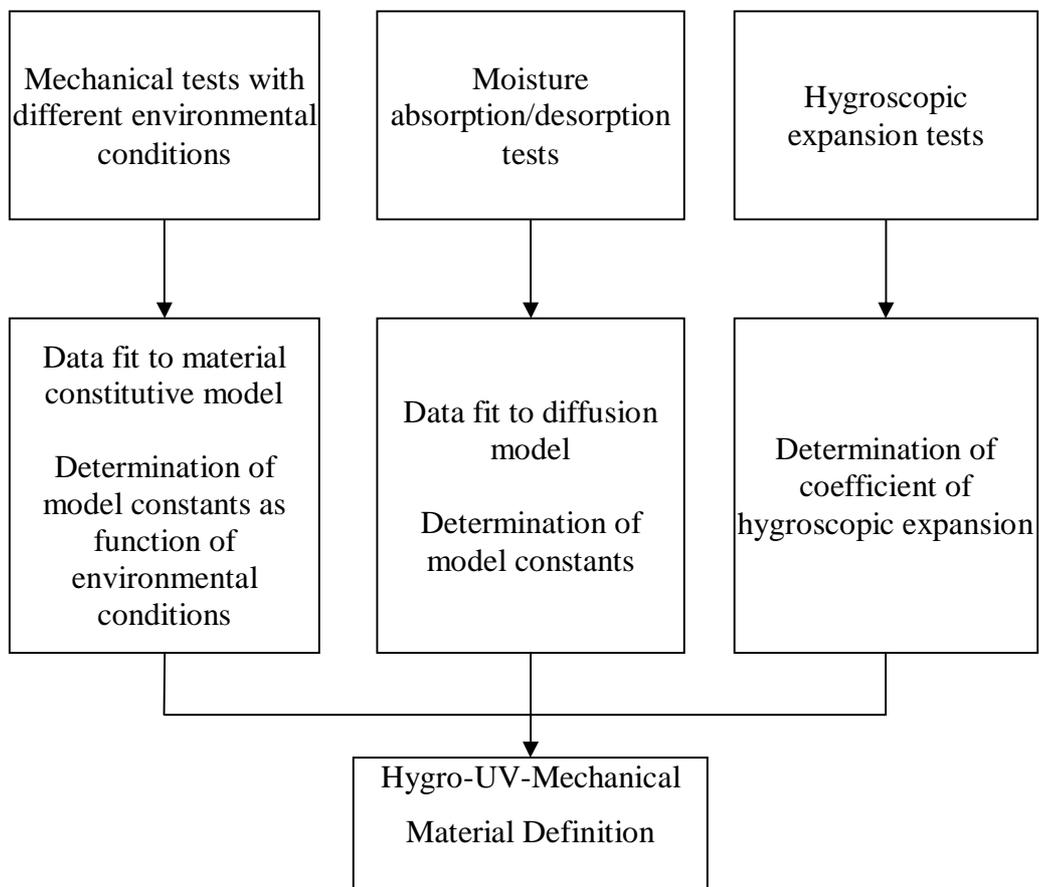
Figure 1-2: Overall framework of experimentation.

```
┌──────────────────┐  ┌──────────────┐  ┌─────────────────────┐  ┌──────────────────┐
│ Material Properties│  │   Loading    │  │ Boundary conditions │  │ Geometry and mesh│
└──────────────────┘  └──────────────┘  └─────────────────────┘  └──────────────────┘
```

┌ ─ ┐

```
   ┌──────────────────┐   ┌──────────────────┐
   │ Material properties│   │   Fluctuating    │
   │   as function of   │   │  environmental   │
   │   environmental    │   │    conditions    │
   │     conditions     │   │                  │
   └──────────────────┘   └──────────────────┘
```

└ ─ ┘

```
┌────────────────────────────────────────────────────┐
│ Finite element analysis                            │
│                                                    │
│   • Coupled stress-diffusion analysis              │
│   • Failure analysis                               │
│                                                    │
└────────────────────────────────────────────────────┘
```
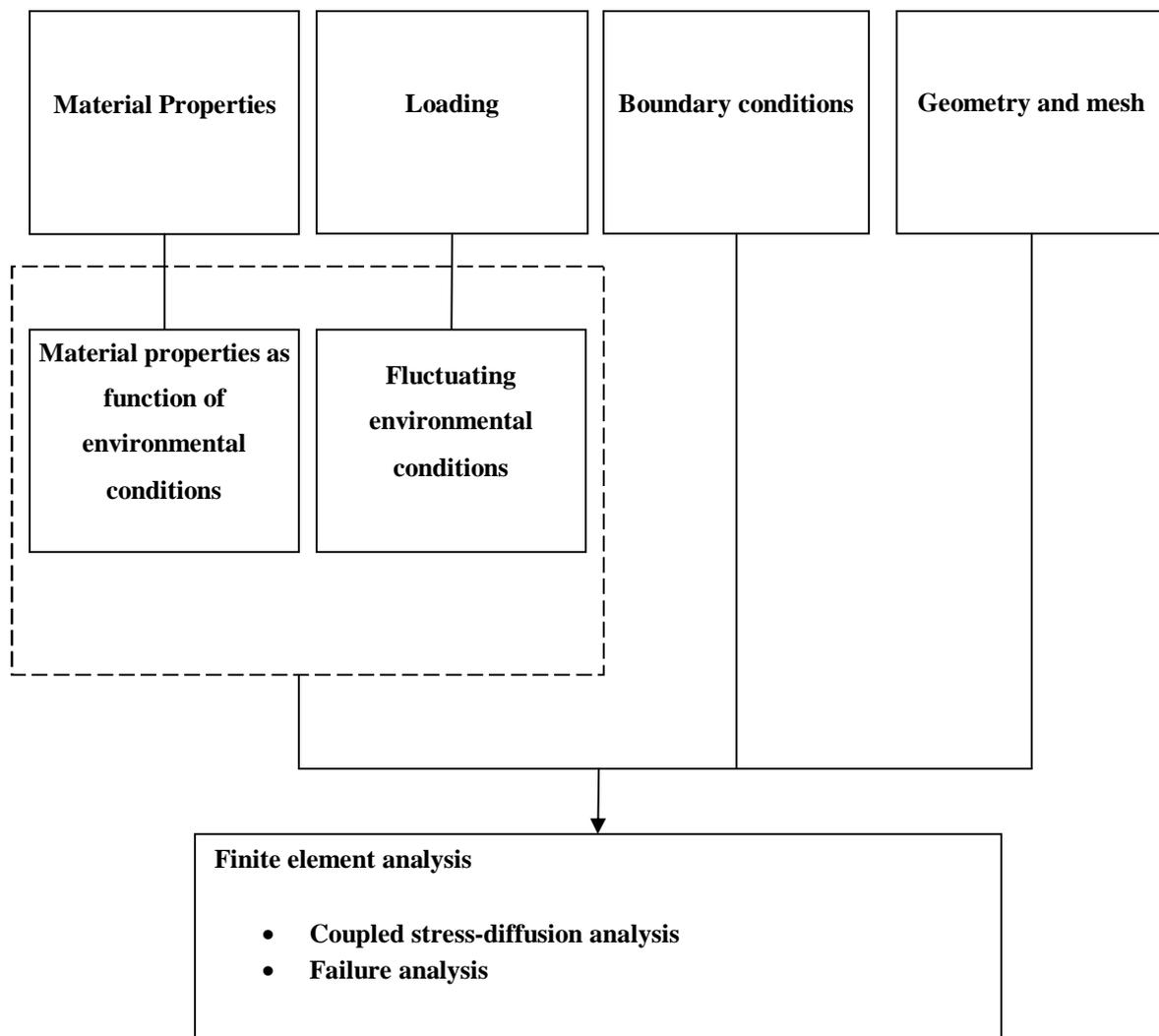
Figure 1-3: The modelling methodology.

A brief description of the contents of the remaining chapters of the thesis is given below.

Chapter 2 gives an introduction to the nature of *urushi* material as a natural polymer. It describes the published literature on *urushi,* with special emphasis on the effect of the environmental conditions (temperature, humidity and exposure to UV radiation) on the properties of *urushi*. A survey of the current literature on various potential material models for *urushi* is also presented in this Chapter.

Chapter 3 presents the experimental method used to prepare samples and characterise material properties. Experimental control techniques are also detailed in this chapter.

Chapter 4 describes the numerical techniques involved in the project and provides details of the FE modelling methods used. The method used to determine model constants is discussed.

The geometry, boundary condition, meshing methodology, choice of elements and details of material model benchmarking analysis, hygro-mechanical coupled analysis, and 3-point bending analysis are presented.

Chapter 5 presents an investigation of the mechanical and hygroscopic behaviour of a commercial PU lacquer film. From experimental result of water absorption and desorption tests, the diffusion coefficient and coefficient of hygroscopic expansion were determined. The complex dependence of material properties on environmental conditions is discussed according to the results of tensile tests at constant displacement rates and creep tests under different loads and UV/humidity ageing conditions. On the basis of the viscoelastic behaviour observed from the mechanical tests, a material model is proposed to describe the rheology of PU lacquer films under various environmental conditions.

Chapter 6 provides an assessment on the efficiencies of various rheological models in terms of their usefulness and feasibility in the FEA of *urushi* coatings. A modified generalised Kelvin model is found to be the best model to describe viscoelastic behaviour of *urushi* film. The environmental effect on the rheology is quantitively analysed based on the parameters studied in this model. The dependence of rheological properties on UV ageing of *urushi* film properties is also studied.

Chapter 7 presents a hygro-mechanical FE model for predicting the humidity-dependent mechanical behaviour of *urushi* films. It also provides a validation of the FE methodology by predicting stress evolution of *urushi* film on a glass substrate experiencing humidity fluctuation. The material model is tested by comparing the predicted stress evolution to experimental data.

In Chapter 8, the mechanical response of a grooved *urushi*/aluminium bi-material strip to a 3-point bending load is modelled using the FE method, as a reference study of *urushi* films with a notch subjected to a bending load in service. On the basis of this model, the failure behaviour of a bi-material strip when subjected to bending loads was modelled by introducing a strain-based damage model, with the aim of assessing traditional Japanese consolidation methods for lacquerware objects.

Chapter 9 is the concluding part of this thesis. Key achievements of the research and suggestions for future work are presented in this chapter. The publications that have resulted from this research are listed after the Acknowledgements.

Chapter 2 Literature Review

The purpose of this literature review is to provide background information on the issues to be considered in this project and to emphasise the relevance of the project. This chapter provides a review of the mechanical and hygroscopic properties of polymeric coating materials, including synthetic and natural (*urushi*) lacquers, and the effect that environmental factors have on the performance of coating materials. This is followed by a description of the various material models, including time dependent constitutive models and failure models, which can be applied in modelling the mechanical response of *urushi* subjected to environmental ageing. Whilst the review attempts to provide an overview of these areas of research, the emphasis is on the materials and methods used in this project.

2.1 Lacquers

2.1.1 Introduction

The term *coating* is used to describe a material, usually a liquid, that is applied for protective or decorative purposes to an underlying substrate, such as wood, metals and ceramics, the resulting dry material and the process of the application depending on the context [7]. Coatings may be differentiated as being either organic or inorganic. Organic coatings can be classified as either architectural coatings (house, wall and ceiling coatings) or industrial coatings (appliance, furniture, automobile, coil coatings) [8].

Coating materials for wood finishes can be made from natural or synthetic resins. Natural resins and oils have been used for decorative and protective purposes for centuries. They are derived from natural sources such as plants, animals and fossilised remains [9]. The main material used in the coating and decoration of the Mazarin Chest is a natural lacquer known as *urushi*, which is characterised by its smooth and glossy surface, its durability and solvent resistance. *Urushi* is a completely natural material, gathered and refined from the sap of the *urushi* (lacquer) tree grown in China, Japan, Korea and eastern Himalayas region, scientifically named as *Rhus vernicifera* and a member of the *Anacardiaceae* family [10]. *Urushi* does not cure in the same way as other natural resins, which are usually dissolved in a solvent. The resulting mixture is applied as a coating and the resin hardens into a solid film as the solvent evaporates. On the other hand, *urushi* cures as a result of a complex internal chemical crosslinking and, uniquely, does so only in the presence of high relative humidity.

The resulting material is polymerised (like a plastic), it is very hard, glossy and durable, resistant to water, acids, scratches, heat and exhibits excellent resistance to weathering indoors. These properties of *urushi* led to it being used as a protective, decorative and adhesive material in Japan and other oriental countries since ancient times [10]. Examples include surfaces in shrines and temples, wooden bowls (lacquerware) and chests. Many of these objects are exhibited in museums in Japan, USA and Europe [11-14]. The deep black colour and the beautiful lustre of *urushi* are also regarded as a symbol of the national beauty of Japan. In the Shosoin temple in Japan, a great number of wares coated with *urushi* have been preserved for more than one thousand years without losing their original elegant beauty [15].

The first entirely synthetic coating resin, phenol-formaldehyde, were launched on the market in 1907, followed in rapid succession by vinyl resins, urea resins and, from the 1930s onwards, alkyd resins, acrylic resins, polyurethane (PU) resins and melamine resins [16]. Polyurethanes (PUs) are well known resins used for both commercial and technical applications and are conventional coating materials for wood finishing [17]. Obataya *et al* [18] compared the mechanical properties of *urushi* film and conventional synthetic coatings and found that the *urushi* film is similar to the polyurethane lacquer in terms of its viscoelastic properties, suggesting the possibility of polyurethane as a replacement for *urushi* in some cases.

2.1.2   *Urushi*

2.1.2.1   Chemistry of *Urushi*

The variety of sap *Rhus vernicifera* [19-20] is a very common natural product. Commercially available sap is a blend collected at different times. The constituent materials are water (20-30%), *urushiol* (60-65%) and an acetone-insoluble powder, a mixture of water-insoluble glycoprotein (3-5%), water soluble plant gum (6.5-10%) and enzymes (<1%). The plant gum contains mono-, oligo- and polysaccharides (5-7%), and the enzymes are laccase, lactase (a copper-glycoprotein enzyme having 4 atoms of copper in a molecule), stellacyanin, and peroxides. In sap, a water-in-oil type emulsion, a major part of the gum and the enzymes may be dissolved in the water phase, and the glycoproteins are in the oil (*urushiol*) phase [21-23].

The main component of the sap of the *urushi* tree is *urushiol*, whose chemical structure is shown in Figure 2-1 [11-12, 24-26].
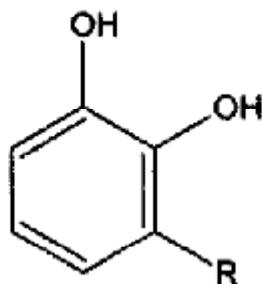
R	: $(CH_2)_{14}$-CH_3	4 wt %
	: $(CH_2)_7$-CH=CH-$(CH_2)_5$-CH_3	21 wt %
	: $(CH_2)_7$-CH=CH-CH_2-CH= CH-$(CH_2)_2$	4 wt %
	: $(CH_2)_7$-CH=CH-CH_2-CH= CH-CH=CH-CH_3	70 wt %
	other constituent compounds with a C_{17}- side chain	1 wt %

Figure 2-1: Typical chemical structure and composition of *urushiol* [10].

2.1.2.2 Preparation, application and curing mechanism

Preparation of the *urushi* has an important effect on the performance of *urushi* films. Raw *urushi* sap is a non-stable water-in-oil type emulsion. As a result of the naturally high moisture content, the water soluble polysaccharides in the sap can aggregate to form large irregular islands during drying [27]. First of all, the sap collected from lacquer trees is stirred in a specially designed open vessel at room temperature for about 1.5 hours. Then the temperature is increased to about 45°C and kept at this temperature for 2-4 hours to reduce the water content to 2%-4%. This is called the *kurome* process or *Sugugome* process, with the detail a closely guarded commercial secret which differs from manufacturer to manufacturer [28]. After the *kurome* process, the resulting raw lacquer, which is ready for application, consists of *urushiol* oligo-*urushiol* and dimers (about 5-10%). The raw lacquer is a phenolic material and its polymerisation is achieved by means of the catalysis of an enzyme to form a very strong crosslinked network structure [21, 28]. The temperature cycle must be carefully controlled to keep the enzyme activated enough. Ultimately, the curing of the lacquer is a process of enzymatic oxidation.

The process of stirring and heating the sap, or *kurome*, results in the evaporation of water, polymerisation of *urushiol* and the reaction of glycoproteins with the *urushiol*. The ingredients of the lacquer are homogenised and polysaccharides are dispersed into the oil

phase after the *Kurome* process. Spherical grains of polymerised *urushiol* are surrounded by a thin wall of polysaccharides, which looks like a very fine core-wall structure. This structure is the reason for the outstanding durability of *urushi* film because the polysaccharide wall isolates the *urushi*-coated surface from oxygen [27, 29-31]. The inner structure of sap and *Kurome* treated *urushi* is shown in Figure 2-2
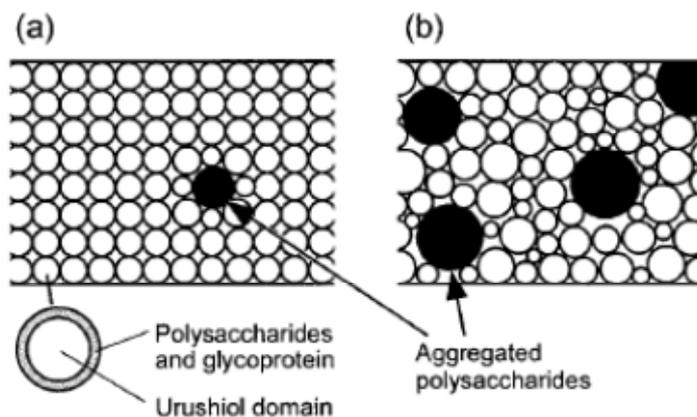
Figure 2-2: Schematic illustration of the structure of *Kurome*-treated lacquer film (a) and that of sap film (b) [27].

Urushi is applied by painting layer by layer, and some high quality products may need as many as 30-40 layers. Also, painting and curing must be done under high relative humidity of 65-80%. Although there is no acknowledged conclusion on the detailed nature of the curing processes, it is normally thought to be long as it is known that the curing is not complete even after one month [21].

There are 3 common *urushi* products, which are commercially available; clear, virgin and black lacquers, or C, V and B *urushi* lacquer. Clear lacquers and black lacquers have a lower moisture content (MC) of about 3% and a higher degree of polymerisation (DP) due to different *Kurome* treatments. Although clear lacquer results in a dark brownish film, it is called clear lacquer according to its Japanese name, *suki sugurome urushi*, which means clear kuromo-treated lacquer. Virgin lacquer is a neat filtered sap which has a high MC of more than 20% and low DP [27].

2.1.3 Polyurethane lacquer

Otto Bayer and coworkers at I.G. Ferbenindustri, Germany in 1937 were the first to discover PUs [32]. PU is a type of reaction polymer compound, which also include epoxies, unsaturated polyesters, and phenolics [33-35]. A urethane linkage is produced by reacting an

isocyanate group, -N=C=O, with a hydroxyl (alcohol) group, -OH, as shown in Figure 2-3. PU is produced by the polyaddition reaction of a polyisocyanate with a polyalcohol (polyol) in the presence of a catalyst and other additives. The formation of PU polymers requires an isocyanate with two or more functional groups. One of the most important isocyanates is 1, 6-hexamethylene diisocyanate (HDI), which is extensively used for weather and abrasion resistant coatings and lacquers [33-37].

$$R^1\text{-}N\text{=}C\text{=}O \ + \ R^2\text{-}O\text{-}H \ \longrightarrow \ R^1\text{-}\overset{\overset{\displaystyle H}{|}}{N}\text{-}\overset{\overset{\displaystyle O}{||}}{C}\text{-}O\text{-}R^2$$
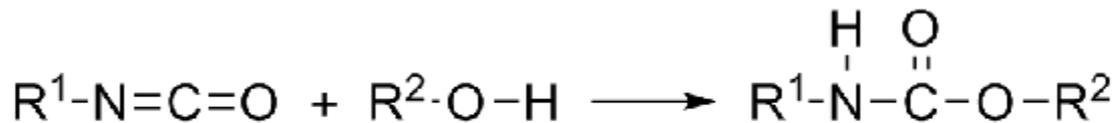
Figure 2-3: Generalised reaction to produce a urethane linkage [33].

PU lacquers have a clear, durable, water-resistant finish, which seals the pores of the wood and provides a very durable finish. PU can be purchased in a high-gloss form or satin form. PU dries quickly and is applied like a varnish [38].

2.2 **The effect of environmental conditions on the properties of *lacquers***

2.2.1 **Introduction**

The use of organic coatings in a variety of conditions such as weather exposure and aggressive elements (sunlight, UV exposure, water (humidity), polluting agents and temperature) can significantly affect their durability. In the case of wood coating for lacquerwares, the Mazarin Chest for example, the main aspects of intent are humidity and UV exposure. There has been a small amount of research performed in the last few decades to study the effect of humidity and UV exposure on coating behaviour and this will be reported here.

2.2.2 **Humidity**

2.2.2.1 *Urushi*

Lacquerware is susceptible to damage from exposure to very dry conditions or fluctuating humidity. Relative humidity (RH) fluctuation causes the wooden substrate to shrink and expand thus causing the *urushi* to crack to relieve the stress and to lose adherence to the substrate. For this reason, cracks most often appear along seams and joints, and usually in the

direction of the grain of the underlying wood substrate as there is almost no shrinkage in the direction of the wood's grain (lengthwise). If the shrinkage becomes permanent then the *urushi* surface will no longer lie flat [39-40]. In low RH condition, water, an essential part of *urushi* structure is lost and as a result *urushi* becomes more brittle, less strong and susceptible to attack by water and oxygen. If *urushi* is exposed to cycles of low and high humidity it will eventually start to flake off its wooden core. It is important not to let the humidity drop too low or fluctuate wildly to keep lacquerware in prime condition [41]. In museums, a constant humidity of 50% to 60% is usually recommended during storage, treatment and display. In Japan the most valuable pieces of lacquerware are stored in silk bags or wooden boxes and brought out only for special occasions. The box serves a number of functions: it keeps the item from exposure to light, protects it from structural damage and buffers any changes in humidity [41].

Bratasz *et al* [42] studied moisture absorption and transport, the resulting dimensional response and the related stress fields in materials constituting lacquer furniture. Wood of the *hinoki*-Japanese cypress (*Chamaecyparis obtusa*) was used in this study, which is similar to that used in Mazarin Chest. Ground layers and lacquer surface coatings were investigated. Figure 2-4 shows the equilibrium moisture content (EMC), moisture content at equilibrium state, for the *hinoki* wood and specimens of new lacquer, exposed and unexposed historic *urushi* lacquer. The lacquer can be seen to absorb considerable amounts of moisture especially at high humidity regions. The EMC increases for historic, naturally-aged material due to the formation of an increased amount of polar oxygen-containing adsorption sites. Obataya *et al* [27] studied the water sorption of C and V *urushi* lacquer films aged over a thousand days (shown in Figure 2-5). The EMC of the V *urushi* film was higher than that of the C *urushi* film over the RH range (10%-90%) tested. Obataya *et al* [27] found that the hygroscopicity of polysaccharides is higher than that of the polymerised *urushiol*. Furthermore, the hygroscopicity of polysaccharides in the V *urushi* film must be higher than that in the C *urushi* film because the former is held more loosely among the *urushiol* domains. Thus, the higher moisture content of the V *urushi* film is attributable to the hygroscopicity of polysaccharide aggregated during drying.
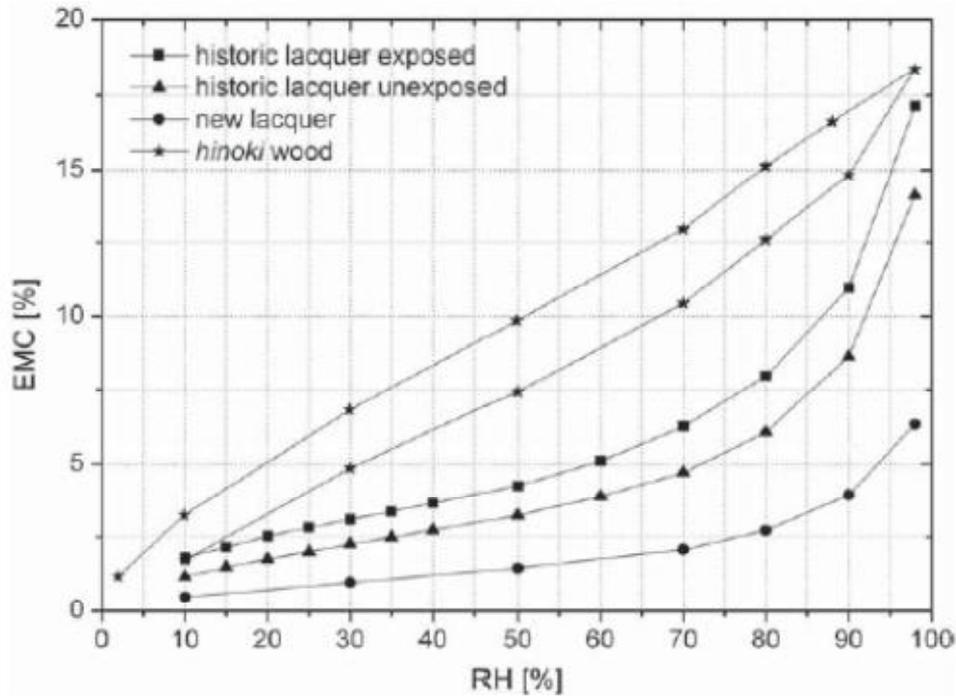
Figure 2-4: Equilibrium moisture content (EMC) for hinoki wood as well as new and aged lacquer at 24 °C [42].
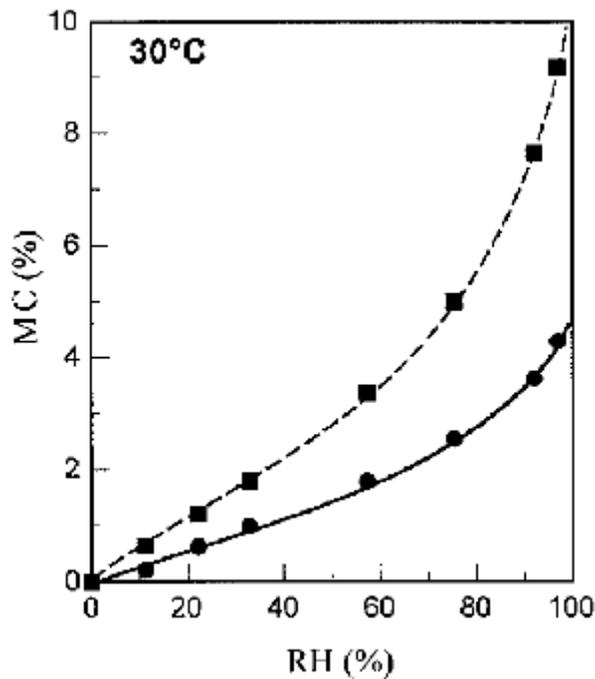
Figure 2-5: Moisture content (MC) at equilibrium of the clear (●), and virgin (■) *urushi* films aged over 1000 days [27].

Ogawa *et al* [10] investigated the effect of water on the mechanical properties of *urushi* film of constant thickness at 25 °C. Curing was achieved through three steps: 60% RH for 4 hours,

70% RH for 18 hours, and 80% RH for 24 hours. Tensile stress-strain tests were conducted under various degrees of humidity (15%-100%) as shown in Figure 2-6. The relationships between tensile properties and humidity are summarised in Figure 2-7. In general, *urushi* films become more flexible after water absorption, leading to an increase in the strain at break and a decrease in the elastic modulus, demonstrating that the water serves as a plasticiser.
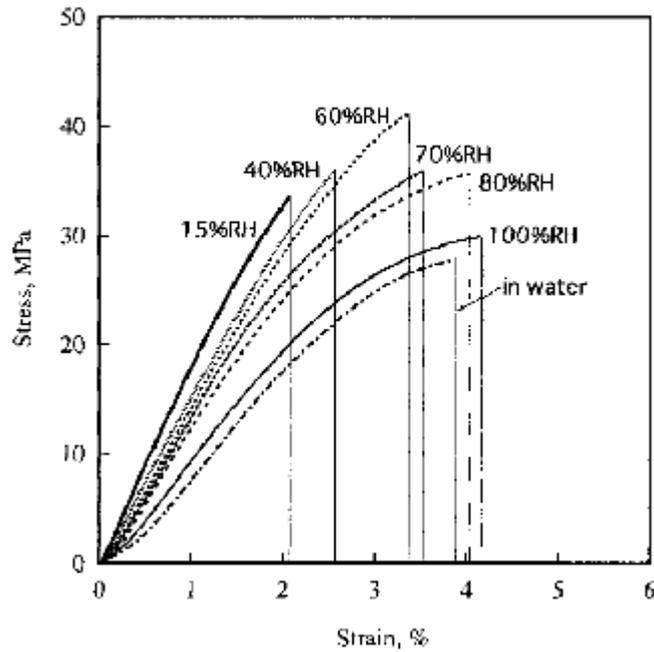
Figure 2-6: Effect of humidity on the tensile stress-strain curves for *urushi* film [10].
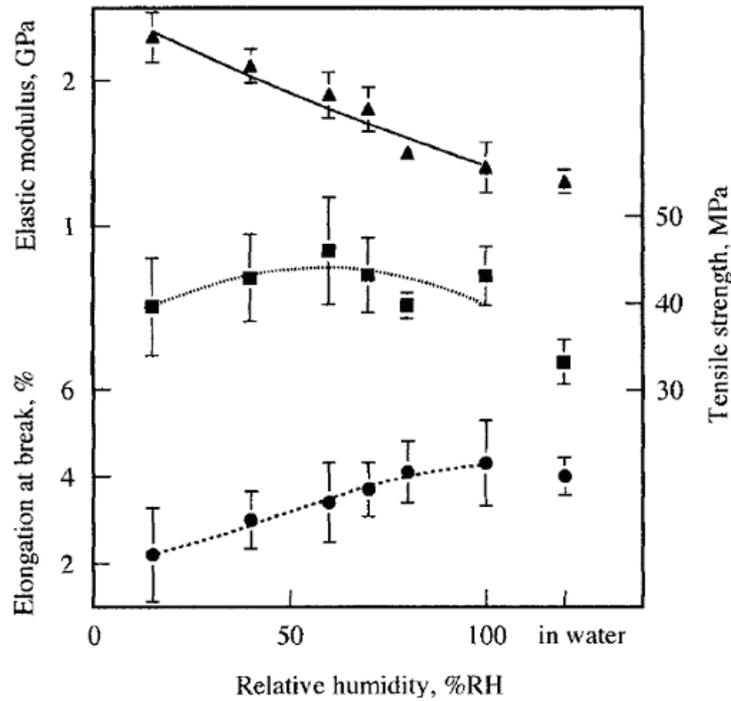
Figure 2-7: Relation between stress-strain properties and RH: (▲) elastic modulus, (■) tensile strength, and (●) strain at break [10].

The fundamental difference between polymers and other materials resides in the inherent rheological or viscoelastic properties [43], which have been reported many times in the literature [10, 18, 27, 44-45]. Ogawa *et al* [10] also investigated changes in the relaxation modulus, $E(t)$, of *urushi* over 100 hours. The stress relaxation tests were conducted using a dynamic viscoelastometer at a set temperature and humidity. The testing result shows the relaxation modulus of the film decreases with increasing RH.

It can be seen that *urushi* film has a tendency to become brittle under dry conditions and more ductile under wet conditions. On the other hand, the film can become sticky and soft under very high humidity or immersed in water [10]. When lacquerwares are used under these conditions, stress builds up between *urushi* and the substrate, which is usually wood, because of different hygroscopic expansion of *urushi* and substrates. This stress decreases the bonding strength between *urushi* and the substrate, which can be defined as the load required to break an adhesive assembly, with failure occurring in or near the plane of the bond.

As a result of these stresses, *urushi* will eventually peel off from the substrate. It was concluded by Ogawa *et al* that water is one of the most important influences on the durability of lacquerware [46].

2.2.2.2 Polyurethane

As one of the most useful and flexible commercial classes of polymers, PU has found extensive use in numerous commercial applications, such as in plastic products, as a coating material, as an adhesive and as a sealant [47]. In wood finishing, PU lacquer is a common coating material, extensively used for the protection and decoration of woodware and flooring because of its low cost of manufacture, ease of application and barrier properties against dirt, moisture, oxygen and chemical pollutants [48].

Our understanding of PU coating is lacking, however, since a complete rheological description has not been achieved, and thus incorporating this material into standard models is challenging. There has been a limited amount of research work performed on the mechanical properties of PU coatings but no full description of the essential viscoelastic nature of the material. Some understanding of the relationship between the macroscopic behaviour and the microscopic changes during exposure to fluctuations of relative humidity has been developed. For example, Boubakri [49] established that moisture diffusion in similar materials was Fickian and that absorption results in the movement of macromolecular chain segments, that leads to a reorganisation of the structure and an increase in the free volume. Tensile tests were performed on dried and wet samples to study the influence of moisture, from which the mechanical properties with moisture effect were quantitively summarised, showing a decrease in elastic modulus especially for high deformation values. The evolution of the mechanical properties was related to the microscopic observations from the analysis using scanning electron microscopy (SEM) technique.

2.2.3   UV ageing

2.2.3.1   *Urushi*

It is believed that the main cause of fading and loss of gloss in *urushi* is exposure to UV light [40, 50-51]. The surface of the lacquerware fades and becomes dull as the *urushi* molecular structure changes during sustained exposure to UV light. Some black lacquer pieces, for example, eventually turn a mottled brown and also lose their sheen. Under magnification, one can see that the dull appearance is actually a network of very fine cracks (micro-cracks) that have formed on the surface of the lacquerware. The traditional consolidation technique, *urushi gatame*, is based on the impregnation of micro-cracks with diluted *urushi*. However,

once the micro-cracks have formed they can penetrate through the decorative *urushi* layers and into the foundation layers causing further damage by trapping the solvents being used to clean the lacquer, leaving the lacquer vulnerable to further damage [50]. Lacquer damaged by UV light loses its durability, reduces its normal resistance to water and other solvents, and becomes brittle [3, 52]. It is known that the damage increases with the length of exposure and the intensity of the illumination [53].

Ogawa *et al* [11] investigated the effect of exposure to fluorescent lamps on the mechanical properties of East Asian *urushi* films. The films were exposed to light under three different conditions: uncovered, in an acrylic box, and in a glass box. Hardness was measured and tensile tests carried out. They found that the hardness and the elastic modulus increased with exposure time, while the tensile strength and the elongation at break decreased with exposure time. They concluded that the increased hardness is related to a crosslinking reaction by the enzyme laccase over the whole region of the films. Other studies have shown that following exposure to UV radiation, the surface of *urushi* fades and becomes dull as light breaks down the molecular structure [50].

Hong *et al* [51] investigated the effect of UV-degradation on the chemistry of *urushi*, the effect of photostabilisation on the physical properties of *urushi* coating and the effect of weathering exposure on *urushi*. Hindered amine light stabiliser (HALS) and benzotriazole UV absorber were added to *urushi* to improve the weatherbility (resistance to light degradation) of the *urushi*. Three different mixtures were prepared: 1) unstabilised purified *urushi* (PL); 2) PL plus 2% HALS; and 3) PL plus 2% weight benzotriazole UV absorber. Each mixture was coated on glass substrate slides, 60 μm thick, and dried for one week at room temperature and at $75 \pm 5\%$ RH. The samples were exposed for 300 hours at 50 °C to continuous irradiation with a UVB–313 lamp. Figure 2-8 shows the Fourier Transform Infrared–Attenuated Total Reflectance (FT-IR/ATR) spectra of unexposed and exposed purified lacquer films. The effect of weathering exposure is shown in the difference of the spectra. The presence of negative and positive intensity bands in the difference spectra can be regarded as resulting from the chemical changes due to photo-gradation. The negative absorbance in the difference spectrum reflects structures that were formed during the photo-degradation, and the positive absorbance reflects structures that were lost.

The difference spectrum is dominated by strong bands near 3500, 2900, 1700, 1650, 1480, 990 and 730 cm^{-1}. The broad band near 3500 cm^{-1} was associated with OH stretching in

urushiol. The strong bands related to C-H stretching in the *urushiol* side chain were observed near 2900 cm^{-1}. The strong bands near 1650 cm^{-1} and 990 cm^{-1} may be related to the C-H out-of-plane bending in the quinone group and in conjugated triene, respectively.

Four sets of bands decrease in intensity when the *urushi* films are exposed to UV light. The band near 1480 cm^{-1} is characteristic of CH$_2$ bending; its observed decrease in intensity is partly related to decomposition of *urushiol* side chains. The weak peak at 730 cm^{-1} also decreased due to degradation of the aromatic substitute of *urushiol*. In contrast, the very strong peak near 1700 cm^{-1} increased, and was attributed to C=O stretching in the various carbonyl functional groups formed by photo-oxidation. These results are consistent with the hypothesis that the *urushi* network degrades mostly in the unsaturated side chains. A small number of photosensitive groups had already been formed in *urushi* film during the photo-degradation processing. The photolysis of these groups gives rise to carbonyl products. Carbonyl absorbance starts increasing immediately for the unstabilised *urushi* film during UV exposure. Figure 2-9 shows the IR carbonyl intensity near 1700 cm^{-1} [measure of photo-degradation] as a function of UV exposure time. The rate of increase of carbonyl intensity for photostabilised mixtures is lower than that for an unstabilised mixture [51].
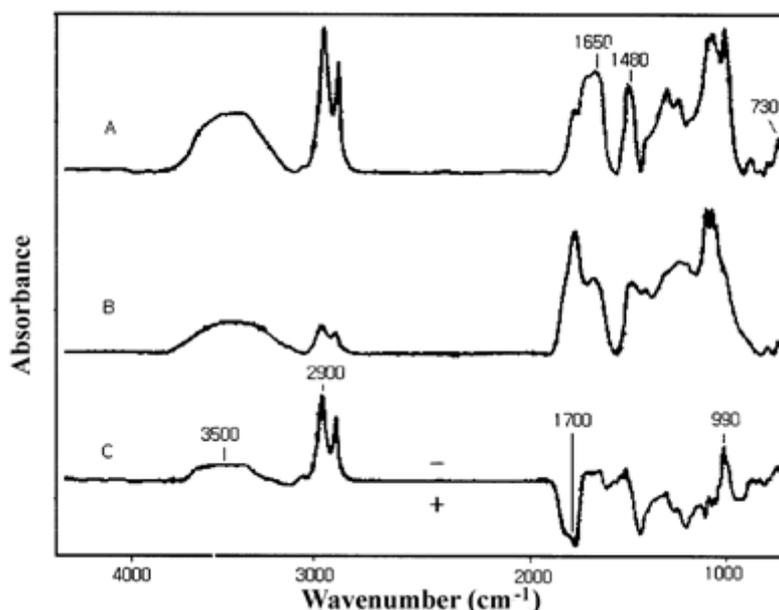
Figure 2-8: FT-IR-ATR spectra of *urushi* film: (a) Original; (b) after 100 hours exposure; (c) difference between spectra in A and B [51].
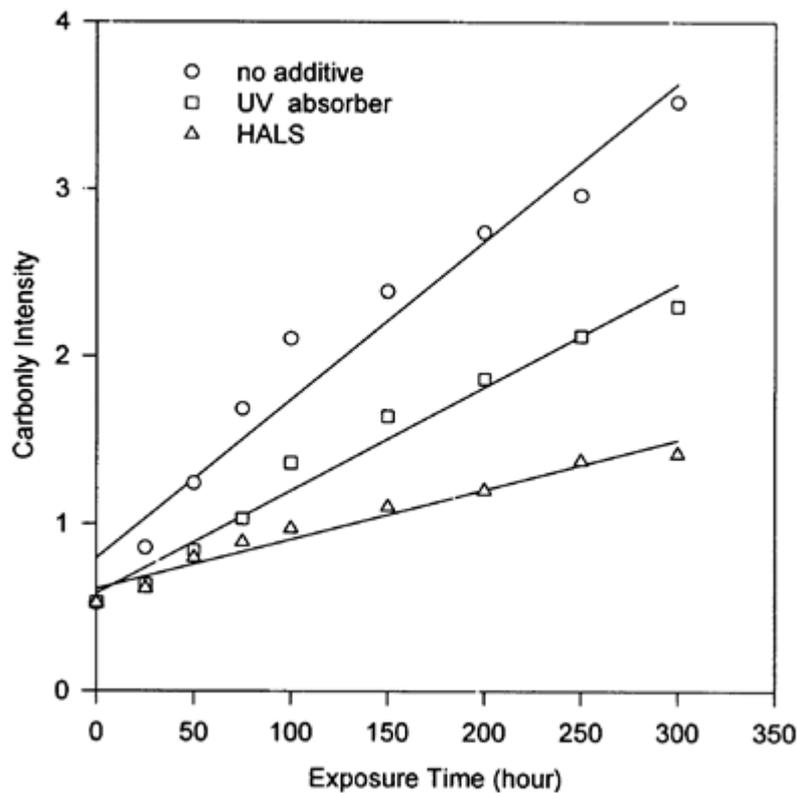
Figure 2-9: Increase in carbonyl intensity with UV exposure time of samples [51].

SEM of the surface of *urushi* are shown in Figure 2-10. The surface of unexposed *urushi* film has small regions 0.1-2 μm diameter, due to polysaccharide particles composed of polymerised *urushiol* and glycoproteins, (Figure 2-2(a)). After exposure to UV light, Figure 2-10(b), large black regions of 10-80 microns in diameter appear together with small regions of 0.1-3 μm diameter. The large black regions may form due to deterioration of the polysaccharide walls and polymerised *urushiol*. After exposure to UV light, the small regions become larger and more numerous [51].
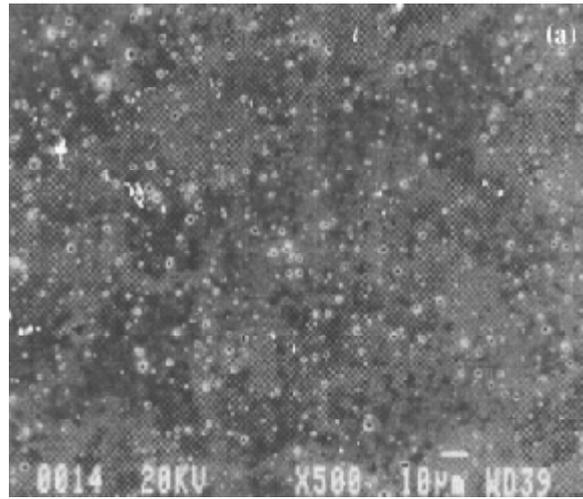
(a)

Polysaccharide
particles
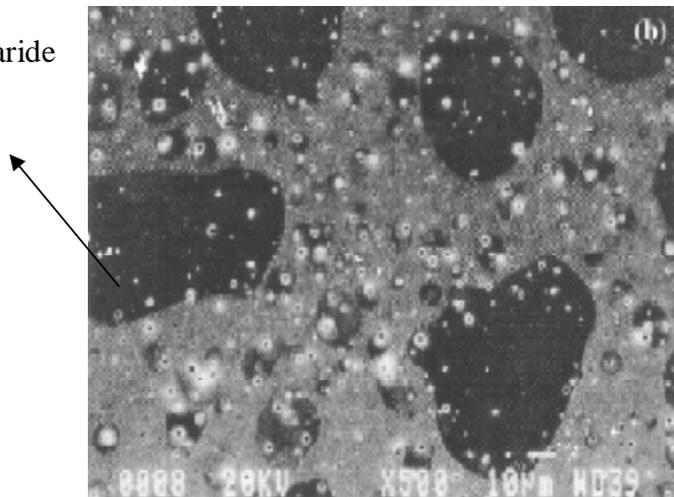
(b)

Figure 2-10: SEM of (a) lacquer film unexposed to UV light and (b) lacquer film exposed to UV light for 100 h [51].

In case of *urushi* containing 2% weight HALS, photo-degradation is significantly inhibited as shown in Figure 2-11.

Polysaccharide particles
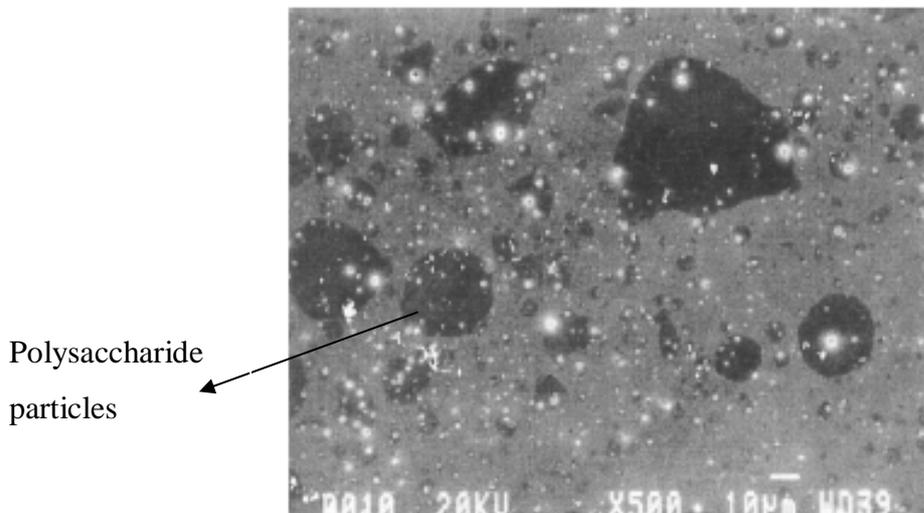
Figure 2-11: SEM of *urushi* film containing 2% wt HALS exposed to UV light for 100 hours [51].

To confirm this result they also measured the weight loss of *urushi* film during photo-degradation as shown in Figure 2-12. All *urushi* films lost weight as a result of photo-degradation. This may be due to evaporation of water in the film. The same result was obtained by Toyoshima [41], where *urushi* film lost weight as a result of photo-degradation with UV explosure.
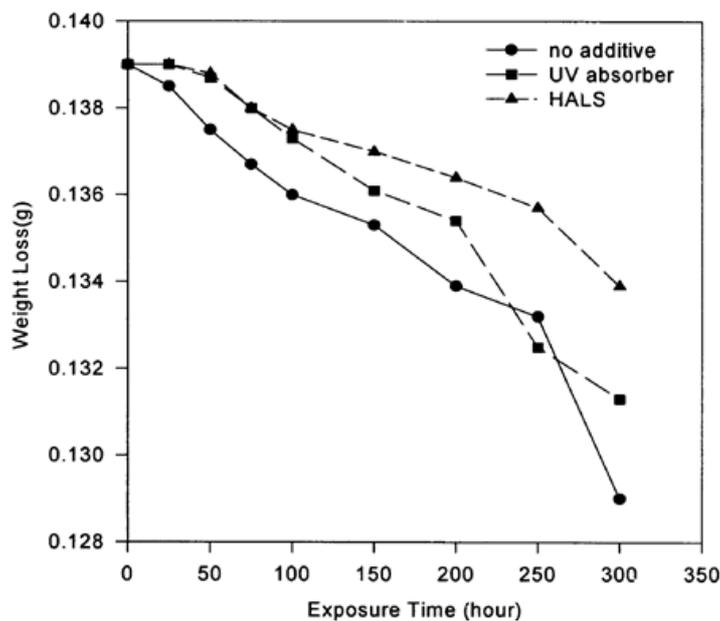
Figure 2-12: Weight loss of lacquer film with exposure time [51].

FT-IR/ATR results from accelerated UV weathering tests showed that the addition of 2 wt% HALS into on *urushi* formulation enhanced photostabilisation up to three times, which was supported by the results of weight loss measurements and SEM analysis [51].

2.2.3.2 Polyurethane

The effect of UV-ageing on the mechanical properties of thermoplastic polyurethane (TPU) was studied by Boubakri *et al* [54]. Mechanical properties, elastic modulus and stress at 200% strain, initially decreased and then increased progressively with UV exposure revealing an increase in crosslink density due to the formation of crosslink structure caused by UV exposure. On the other hand, the wear resistance of the material surface decreased and this degradation became more important with UV exposure time. Finally, a competition between chain scission and crosslinking mechanisms was discerned in this study. The changes in the mechanical properties of coating materials correlate to changes in their microstructure, which has been found from FT-IR spectra [17]. The absorption of UV induces the degradation of PU and photooxidation of the CH_2 groups. Rosu [17] suggested that a photooxidation mechanism was initiated during UV exposure. A related study by Carrasco [55] on high density polyethylene exposed to UV irradiation developed a methodology for establishing the rheology. They measured Young's modulus, tensile strength and rupture strain as functions of irradiation time under room humidity and temperature. They concluded that the majority of the structural and molecular reorganisation occurs during the initial period of irradiation (< 60 days) whereas the chemical changes dominated for irradiation time > 60 days. These structural variations and chemical changes coincide with the evolution of mechanical properties due to UV irradiation, and may suggest different mechanical rheologies at different ageing times. As part of a comparison with *urushi* [45, 56], Obataya *et al* [18] examined the mechanical properties of a PU lacquer at 25°C and 60% RH and found that the mechanical properties of *urushi* lacquer films were very similar to those of the PU lacquer films. An artificial ageing of PU was performed by Skaja *et al* [57], where they exposed samples to cycles of UV irradiation, observing an increasing tensile modulus.

2.3 The Mazarin Chest

2.3.1 The structure of Lacquerware objects

Structurally, lacquerware objects are composed of substrate, foundation, coating and decoration. While wood is the most commonly used substrate material for lacquer objects, there are two kinds of foundation. One type, which can be *kokuso* (mixture of *urushi*, sawdust and hemp fibres), *nonokise* or *kamikise* (adhering of hemp cloth or paper, respectively, to the substrate) is used to reinforce the substrate. The other type, which can be *jinoko* (coarse powdered earth), *tonoko* (fine powdered earth) or *gofun* (calcium carbonate), is used to smooth the surface of the substrate. *Urushi*, wheat flour paste or animal glue is used in making these foundations [3]. Normally several layers of foundation are applied. Over the foundation, several thin layers of *urushi* are applied. After each layer, the substrate is cured in a chamber with a relative humidity of 70-80% at 20-25 °C. The surface of *urushi* is polished with hard and then soft charcoals, with water or oil, then sap is rubbed into the polished surface and cured to obtain a high gloss and durable coating surface. Coating-curing-polishing-rubbing-curing is repeated 10-20 times to obtain a lacquerware finish ready for decoration. This process is called *Roiro Siage*. There are various types of decoration applied to lacquerware objects, the most widely used being [3]:

- *Hiramakie* (flat sprinkled picture).

- *Takamakie* (raised sprinkled picture).

- *Raden* (mother-of-pearl) and *hyomon* (metal foil) inlay.

2.3.2 Nature of damage in Mazarin Chest

In the years since the Mazarin Chest was made, it has suffered significant damage due to fluctuations in RH and exposure to light. The following section summarises the different types of damage [50].

2.3.2.1 Structural damage

Expansion and contraction of the wooden substrate of the lid, in response to fluctuations in RH, has led to:

- Shrinkage across the centre of the lid, preventing the lid from closing. This warps it approximately 4 mm out of its original position.

- Movement of the metal catch of the lock inwards.

- Hairline splits along the corner joints as show in Figure 2-13.

- Cracks are found in parts where the lid and the body join, along parts where the board and frame of the lid join and also on the reverse side of the lid [50, 58].
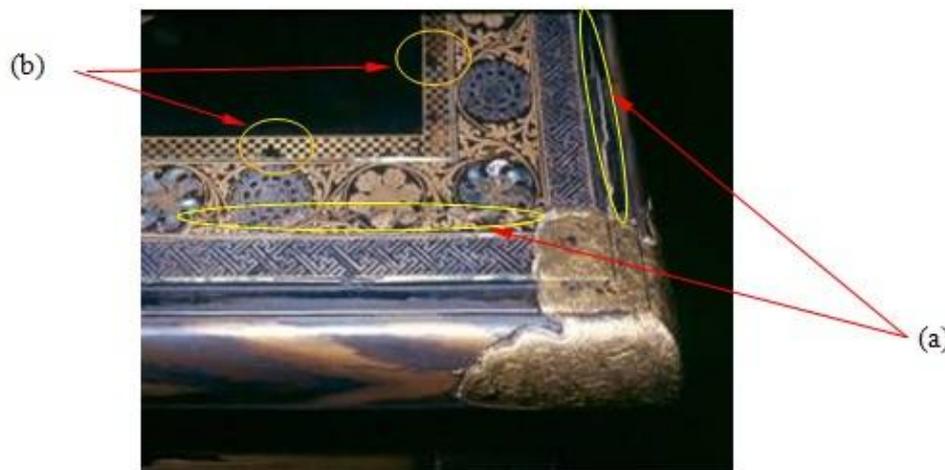
Figure 2-13: Detail of the right corner of the lid showing: (a) Stress fracture of the lacquer along the cleated joint line with associated loss and tenting (up to 3 mm high) of lacquer and decoration; (b) Exposed foundation layers in the inner square gold foil and losses of gold squares, silver and mother of pearl [42].

2.3.2.2 *Urushi* damage

As a result of structural damage mentioned before, *urushi* surface and foundation layers around the cracks are poorly adhered (Figure 2-13) and there are losses of *urushi* in approximately ten places, ranging in size from 1×1 mm to 10×15 mm. Additionally, exposure to light has caused photo-degradation of *urushi* with loss of lustre as micro-cracks have formed on the surface of the *urushi*, as shown in Figure 2-14. Previous applications of black Western natural resin coating to *urushi* surface, in an attempt to restore its shine, resulted in changing the original decorative scheme from the original silver *makie*. Also, the black varnish layer has been lost from some areas, leaving the original partially visible in many areas [59].
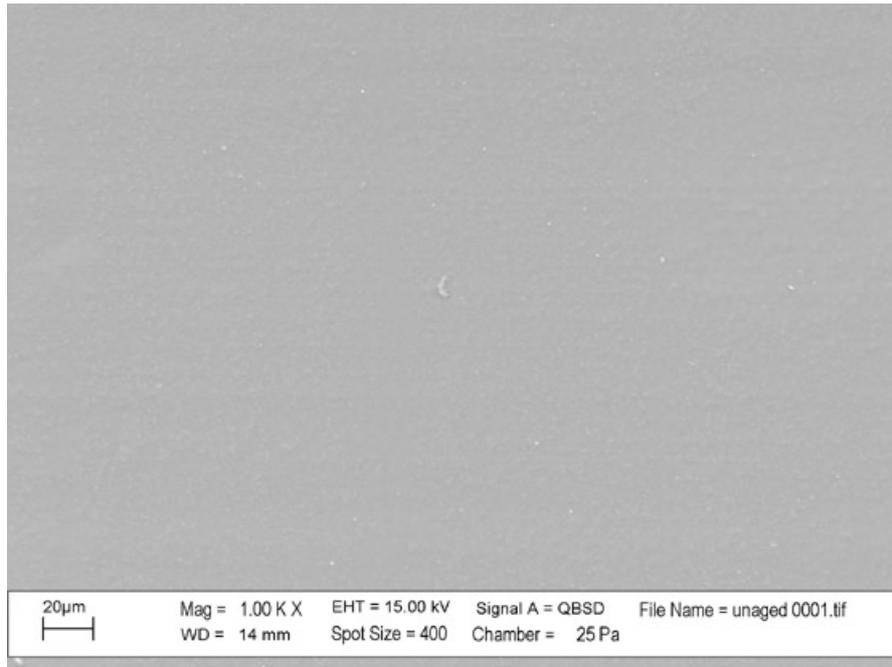
(a)
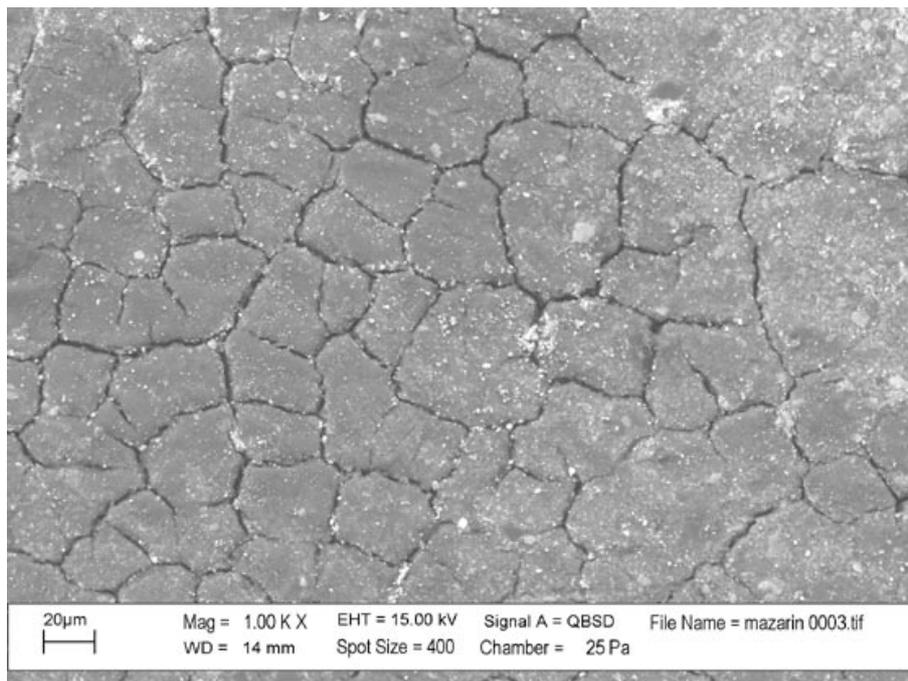
(b)

Figure 2-14: SEM image showing the surface of (a) freshly made *urushi* and (b) Mazarin Chest surface [59].

2.3.2.3 Decoration damage

Passive abrasive cleaning combined with photo-degradation of the *urushi* coating has disfigured some areas of the black background and has exposed parts of the foundation (*shitaji*) layers (Figure 2-15(a)). Polishing of the silver decoration and the applied elements in the past has resulted in loss of detail (e.g. *tsukegaki* decoration on the silver *hyomon*), damage to adjacent lacquer, and loss of poorly adhered decorative silver foil (Figure 2-15(b)). All silver decorative elements are tarnished. There is extensive lifting and wrinkling of gold and silver foil decoration (Figure 2-15(b, c)). There is also extensive lifting of the mother-of-pearl decoration (Figure 2-15(d)) where the shell is broken and has been lost in five places [5].

(a)　　　　　　　　　　　　　　　　(b)

(c)　　　　　　　　　　　　　　　　(d)

Figure 2-15: Examples of decoration damage: (a) Loss of facial detail as a result of corrosion and cleaning; (b) lifting and losses of silver and gold foil decoration; (c) wrinkling of gold foil decoration; (d) poor adhesion and lifting of silver decoration and mother-of-pearl stringing [5].

2.3.3 Record of past storage and display

It is likely that the Mazarin Chest has been on display for long periods since it was acquired by the V&A in 1882. For example, it was on continuous display at the V&A since the early 1960s. From 1986 to 1998 the Mazarin Chest was displayed in the Toshiba Gallery of Art and Design located at the V&A, under light levels of 80 lux and UV levels of less than 5 µW/lumen [5]. The RH in the Toshiba Gallery ranges from 38% to 53% (15% annual variation). In October 1998 the Chest was rotated off display and into an acrylic box as shown in Figure 2-16, located at the V&A main storage repository in Olympia, London. The stores are dark and unlit except when museum staffs visit. The annual RH in storage ranges from 35% to 54% (19% annual variation) as shown in Figure 2-17 [5].
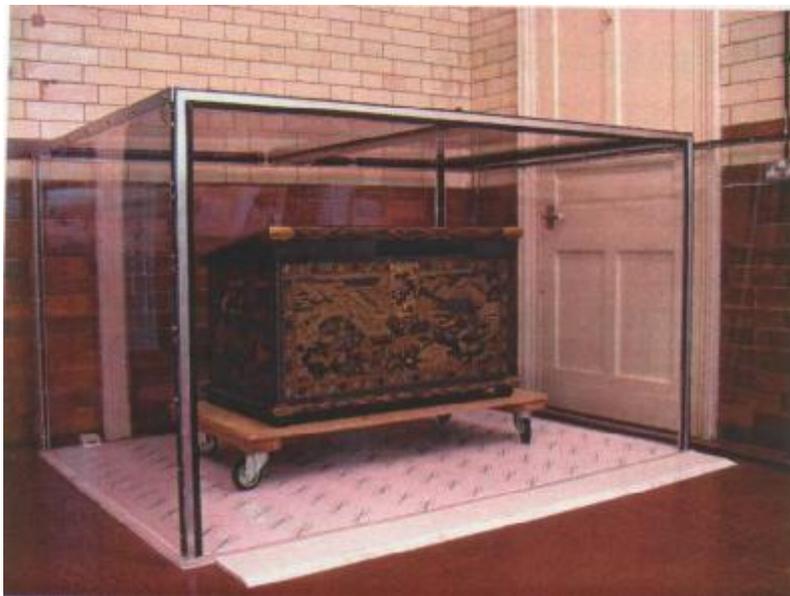
Figure 2-16: Acrylic box for storage and conservation treatment, located at the V&A main storage repository in Olympia, London [5].
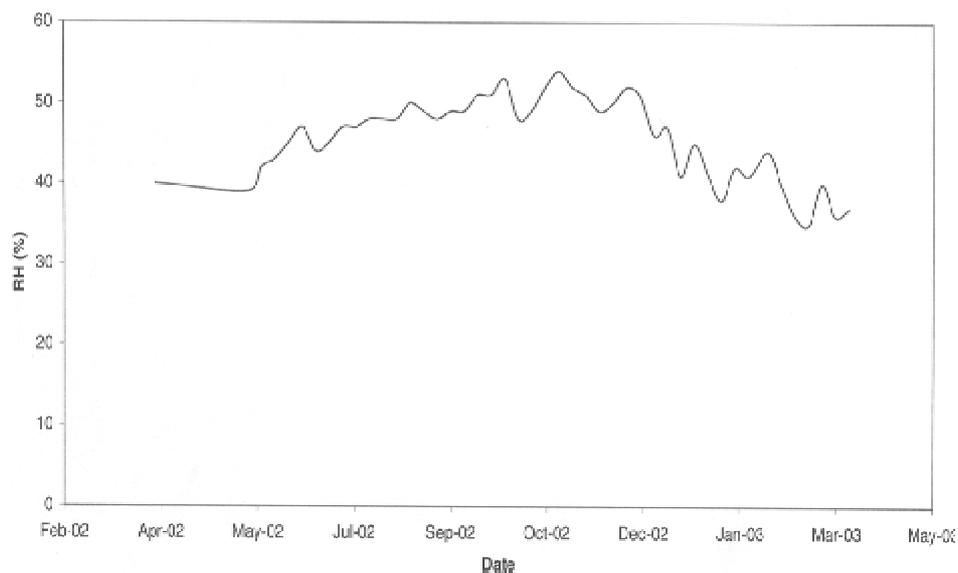
Figure 2-17: The RH variation in the storage April 2002 – March 2003 [5].

2.4   Modelling mechanical-diffusion interaction

2.4.1   Introduction

The process of moisture absorption and subsequent dimensional change lead to hygroscopic stress evolution when the dimensional change is restrained in a coating/substrate structure. This is a cause of concern in conservation of *urushi* lacquerware because it can result in significant damage [60]. Also, environmentally affected material properties during ageing add to the problem. As a general rule, the change of moisture content is considered to greatly affect the adhesiveness of coatings. When water transportation occurs between coating films and the environment, the films will swell or shrink. Porous substrate materials, such as wood, react similarly as water is absorbed, but to a different degree. Consequently, the differential hygroscopic expansion of coating and substrate results in stress at the interface [46]. This has been discussed in a range of literature on different applications of polymeric materials, such as electronic packaging [61], high-temperature adhesives [62] and organic coatings [46, 63-64].

Recently Elmahdy *et al.* [56] were able to measure the stresses in a thin layer of *urushi* as it responded to changes in moisture. They considered the behaviour of a layer of *urushi* deposited on to a small disc which was then placed within a chamber with controlled temperature and humidity. This sample was then subjected to a rapid change in environmental humidity and the curvature induced in the sample measured and related to the

stress developed in the *urushi* layer. The measurements were performed using phase shifting interferometry, a powerful technique for measuring small whole field displacements developed in a range of complex materials, such as composites [65], biological [66], foodstuffs [67-68] and polymers [69]. In this case, Elmahdy *et al* [56] measured the out-of-plane displacements and through an extension of Stoney's equation [70-71], observed the evolution of stresses as moisture was removed and the material responded. This experiment presented an ideal system for validating any proposed model, since the observed behaviour will depend upon the precise details of the constitutive relationships for hygroscopic transport and response, the rheology and their coupling.

Perera and Nguyen [63] examined the role of hygroscopic compressive stress in the failure of coating/metal systems. The stress was measured with an apparatus that monitored the deflection of a coated steel substrate induced by the stress. The determination of this deflection and the knowledge of the elastic properties of the substrate permit this calculation of the stress.

2.4.2 A general model

Mechanical-diffusion interaction of coating material in situ can be studied using a simple coating/substrate bi-material structure [46, 63, 72-73]. Many authors have used this 'curvature method', probably the oldest method for measuring internal stress of coatings and the wide applicability and accuracy of this approach has shown it to be very powerful [70, 74-79]. For a given coating/substrate system, the curvature method provides the internal stress, σ_f, as a function of curvature, δ, (Eq. (2-1)),

$$\boldsymbol{s}_f = f(\boldsymbol{d}),$$

(2-1)

although there are various forms in terms of different hypothesis [70, 80-81].

When used for protective purposes, a thin layer of lacquer is usually cured on the surface of a substrate, usually wood. The resultant stress developed in the coating is then a result of competition between the response to environmental changes (due to, for example, thermal expansion, hygroscopic expansion or volume and material property changes owing to ageing) and the constraints of the substrate (which itself might deform in some manner) as shown in Figure 2-18. In equilibrium, the spatial variation of stresses in a thin layer can be approximated as [82]

$$\frac{\partial s_x}{\partial x} + \frac{\partial s_{xy}}{\partial y} = 0 \qquad (2\text{-}2)$$

$$\frac{\partial s_y}{\partial y} + \frac{\partial s_{xy}}{\partial x} = 0, \qquad (2\text{-}3)$$

where s_x and s_y are normal stress components in the x and y directions respectively and s_{xy} is the shear stress.
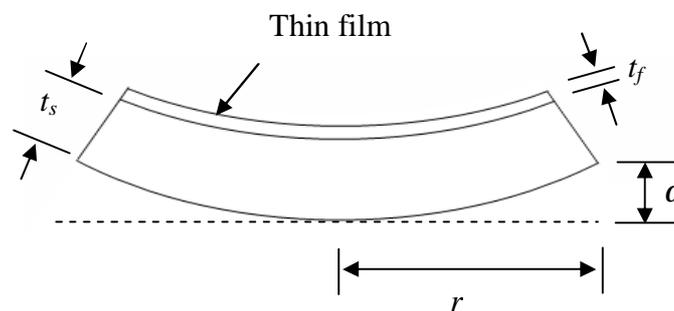
Figure 2-18: Deflection of an initially flat substrate due to film shrinkage.

In order to close the equations, constitutive relations that connect the strain to the stress must be prescribed. These can be quite general, and in the case of polymeric materials, often time dependent, such that the stress is given by

$$s = f(e, \, de/dt), \qquad (2\text{-}4)$$

where the exact functional relationship needs to be determined. Polymeric materials are usually able to absorb moisture, and will change dimensions accordingly. In this case the hygroscopic strain developed as a function of this moisture ingress is given by

$$e_h = bC, \qquad (2\text{-}5)$$

where ε_h, β and C are the hygroscopic strain, coefficient of hygroscopic expansion and moisture concentration, respectively [83], where β needs to be determined experimentally. Finally, the boundary conditions that constrain the system need to be specified and these are problem specific.

Since the moisture can directly affect the strain in the material, a stress analysis will need to be coupled with a model of the moisture absorption and diffusion. In general, diffusion is described by a combination of a continuity equation [84]

$$\frac{\partial j}{\partial t} + \nabla \cdot f = 0 , \tag{2-6}$$

where φ, f, t and   are the density of diffusing material, flux, time and divergence, respectively, and a diffusive constitutive law

$$\frac{\partial j}{\partial t} = \nabla \cdot [D \cdot \nabla j] , \tag{2-7}$$

where D is the diffusion coefficient.

It can be seen, therefore, that in order to develop a model for the development of stresses in *urushi* that are a consequence of environmental changes, a hygro-mechanical definition of material, which is literaturally surveyed in the following sections, is required.

2.4.3   Modelling diffusion behaviour

Water transportation in organic coatings is after considered to occur via diffusion according to Fick's law [85-89]. Fick's first law is based on the hypothesis that the rate of transfer of a diffusing substance through a unit area of a section is proportional to the concentration gradient measured normal to the section. Fick's first law of diffusion in one dimension is given by

$$F = -D \frac{\partial C}{\partial x} , \tag{2-8}$$

where F is the rate of transfer per unit area, C is the concentration of diffusing substance, x is the space coordinate measured normal to the section and D is the diffusion coefficient. This constitutive relation can then be combined with conservation of mass to derive Fick's second law:

$$\frac{\partial C}{\partial t} = D \frac{\partial^2 C}{\partial x^2} . \tag{2-9}$$

Defining $C(t)$ and $C(\infty)$ as the concentration at time t and the concentration at saturation, respectively, the solution to Eq. (2-9) for the case of a plane sheet with a thickness of $2l$ in the region x ($-l < x < l$) is given by [90]

$$\frac{C(t)}{C(\infty)} = 1 - \frac{4}{p} \sum_{n=0}^{\infty} \frac{(-1)^n}{2n+1} e^{\frac{-D(2n+1)^2 p^2 t}{4l^2}} \cos \frac{(2n+1)px}{2l}$$ (2-10)

Eq. (2-10) can be integrated with respect to x to determine the total mass of the diffusing substance at any time using [90]:

$$\frac{M(t)}{M(\infty)} = 1 - \frac{8}{p^2} \sum_{n=0}^{\infty} \frac{1}{(2n+1)^2} e^{\frac{-D(2n+1)^2 p^2 t}{4l^2}}$$ (2-11)

where $M(t)$ indicates the mass of the total amount of penetrant absorbed at time t and $M(\infty)$ is the mass at saturation.

2.4.4   Models of absorption isotherm

A number of absorption isotherm models have been proposed in the literature. Henry's law [91-92] proposes that the weight gain of different materials at equilibrium is linearly related to water activities (relative humidity), i.e.

$$M(\infty) = a\left(\frac{RH}{100}\right),$$ (2-12)

where the $M(\infty)$ is the mass of weight gain at saturation, and a is a constant.

An improvement on Henry's law is the Flory-Huggins model [93-94], which takes into account the large difference in size between the polymer and penetrant molecules and interactions between the two. The Flory-Huggins [95-97] model is described mathematically as

$$\ln a_d = \ln V_d + \left(1 - \frac{u_d}{u_p}\right)V_p + c_d V_p^2,$$ (2-13)

where the subscripts 'd' and 'p' refer to the diluent and polymer respectively, V is volume fraction, u is molar volume, a is diluent activity and c_d is a polymer-penetrant interaction term. As the molar volume of the polymer is generally much greater than that of the penetrant, Eq. (2-13) can be simplified to

$$\ln a_d = \ln V_d + V_p + c_d V_p^2.$$ (2-14)

The moisture content obtained from experiments is mass fraction, therefore Eq. (2-14) needs to be converted using

$$V_p = \frac{1}{M\left(r_p/r_d\right)+1} \qquad (2\text{-}15)$$

$$V_d = 1 - \frac{1}{M\left(r_p/r_d\right)+1}, \qquad (2\text{-}16)$$

where r is density. Eq. (2-14) is then written as

$$\ln a_d = \ln\left(1 - \frac{1}{M\left(r_p/r_d\right)+1}\right) + \frac{1}{M\left(r_p/r_d\right)+1} + c_d\left(\frac{1}{M\left(r_p/r_d\right)+1}\right)^2. \qquad (2\text{-}17)$$

The absorption isotherm for the diffusion of water in organic materials is also commonly modelled using the Guggenheim-Anderson-de-Boer (GAB) equation:

$$M(\infty) = \frac{M_m A C a_w}{(1 - A a_w)(1 - A a_w + A C a_w)}, \qquad (2\text{-}18)$$

where $M(\infty)$ is the weight gain, a_w is water activity, which is equal to RH/100, M_m is the monolayer moisture content, and A and C are constants related to the heat of sorption [98-99].

2.4.5 Hygroscopic expansion

To quantify the swelling behaviour of absorbent material, a material property called the coefficient of hygroscopic expansion (CHE) is introduced to determine the strain distribution for a given change of moisture distribution.

Dimensional change is considered to be the most important consequence of moisture sorption by the wood and lacquer in lacquerware [42]. The swelling behaviour of *urushi* lacquer film as a function of moisture content was determined by Bratasz *et al.* [42]. The *urushi* film samples were categorised into two groups, *urushi* samples exposed to light and those sheltered from light. It was found that both exposed and unexposed samples undergo a considerable dimensional response (up to 1.6% strain for exposed samples and 1% strain for unexposed samples) to the absorption of moisture when the film experiences changes in humidity, especially in high humidity conditions.

2.4.6 Mechanical characterisation of coating materials

It has been observed that many polymers have time dependent elastic and plastic responses to loading [100]. As a natural polymeric material, *urushi* film has been reported to behave viscoelastically [10, 18, 27], but to date no reliable mechanical-diffusion, time dependent material model has been applied and validated for *urushi* [46] despite temporal effects being reported as a major cause of damage to *urushi* films [40, 101]. As a result, obtaining an appropriate material model for characterising the mechanical properties is of great importance prior to modelling the mechanical response of *urushi* film to changes in relative humidity.

2.4.6.1 Phenomenological mechanical models

The classical linear modelling approach is to consider that mechanical behaviour can be represented by a combination of simple mechanical components (springs, dashpots, sliders) connected in parallel and in series. In linear viscoelasticity, materials are represented by combinations of Hookean springs (Figure 2-19(a)), which provide the elastic restorative force component, and Newtonian dashpots (Figure 2-19(b)), which provide the viscous damping components. Various mechanical analogues of these mechanical models are summarised in many polymer texts [43, 102-106].

$$E_0$$

(a)

$$\eta_0$$
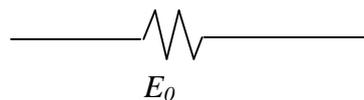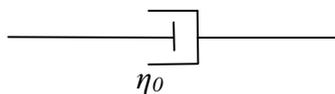
(b)

Figure 2-19: Basic elements: Hookean springs (a) and Newtonian dashpots (b).

For a Hookean spring, strain is proportional to the stress as given by Hooke's law, expressed as

$$s = Ee \, . \qquad (2\text{-}19)$$

For a Newtonian dashpot, stress is proportional to strain rate, which can be expressed as

$$s = h\dot{e} . \qquad (2\text{-}20)$$

There are 3 basic models that are commonly used to represent linear viscoelastic properties of a polymeric material using springs and dashpots. These are the Maxwell model, the Kelvin model and the standard linear solid model (Figure 2-20(a-c)) [107].

(a): Maxwell model

(b): Kelvin model

(c): Standard linear solid model

(d): Burger's model
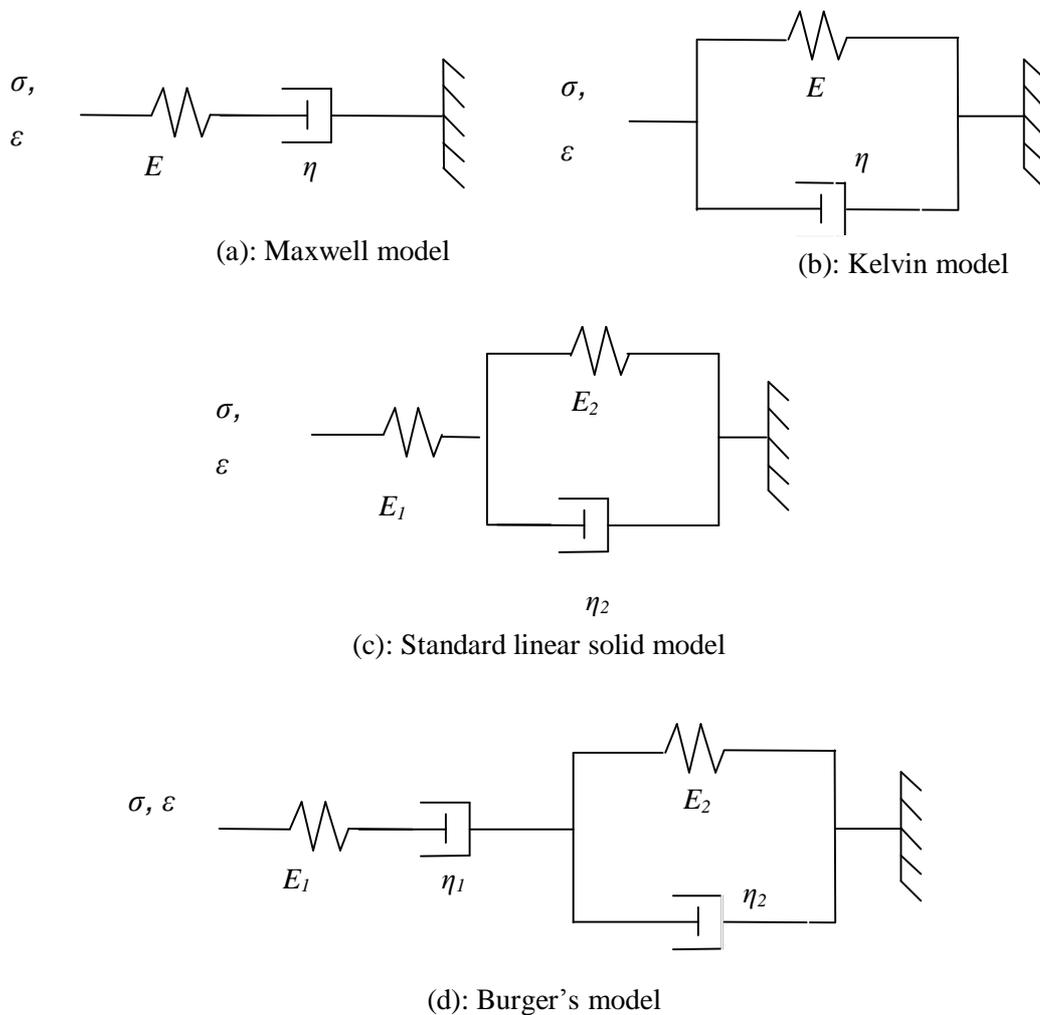
Figure 2-20: Single one-dimensional models of viscoelasticity [107].

2.4.6.1.1 Maxwell model

For a Maxwell model, with a spring and a dashpot in series, the total strain is given by

$$e = e_s + e_d,$$ (2-21)

where s and d refer to spring and dashpot respectively.

Differentiating Eq.(2-21) with respect to time, we can obtain

$$\dot{e} = \dot{e}_s + \dot{e}_d = \frac{\dot{s}}{E} + \frac{s}{h}$$ (2-22)

and

$$s + l\,\dot{s} = h\dot{e},$$ (2-23)

where

$$l = h/E$$ (2-24)

For a creep process where s is a constant, the constitutive equation becomes

$$\frac{de}{dt} = \frac{s}{h}.$$ (2-25)

which indicates that the strain changes linearly over time. This rarely observed in creep experiments except for secondary creep for some materials, suggesting that the Maxwell model is unsuitable for describing creep process [108].

For a stress relaxation process, where strain is a constant, i.e.

$$\frac{de}{dt} = 0,$$ (2-26)

the constitutive equation can be written as

$$\frac{1}{E}\frac{ds}{dt} + \frac{s}{h} = 0.$$ (2-27)

Integrating this equation with respect to time, we can obtain,

$$s(t) = e_o e^{-Et/h} = e_o e^{-t/t},$$ (2-28)

and relaxation modulus

$$E(t) = Ee^{-t/t}, \qquad (2\text{-}29)$$

where

$$t = h/E. \qquad (2\text{-}30)$$

and τ is called retardation time.

The creep and relaxation responses of Maxwell model are presented in Figure 2-21:

(a)   (b)
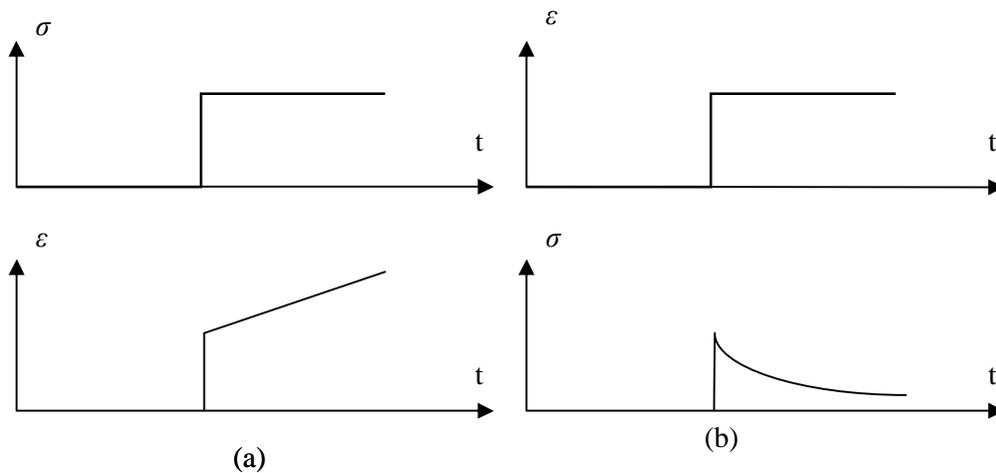
Figure 2-21: (a) Creep and (b) stress relaxation response of the Maxwell model.

2.4.6.1.2 The Kelvin model

Kelvin model is built up of a spring and a dashpot in parallel as shown in Figure 2-20(b). For a creep process, the stress is given by

$$s = Ee + h\frac{de}{dt}. \qquad (2\text{-}31)$$

Integrating with respect of time, the constitutive equation we obtain is,

$$e(t) = \frac{s_o}{E}\left[1 - \exp\left(\frac{-E}{h}t\right)\right], \qquad (2\text{-}32)$$

where σ_0 is creep stress.

The creep compliance $J(t)$ is given by

$$J(t) = \frac{1}{E}\left[1 - \exp\left(\frac{-E}{h}t\right)\right].$$ (2-33)

For stress relaxation, where ε is a constant, the constitutive equation becomes,

$$\pmb{s} = E\pmb{e}.$$ (2-34)

There is no time-dependent stress relaxation for a Kelvin unit according to Eq. (2-34).

The creep and relaxation responses of a Kelvin model, according to constitutive Eq. (2-32) and Eq. (2-34), are illustrated in Figure 2-22.
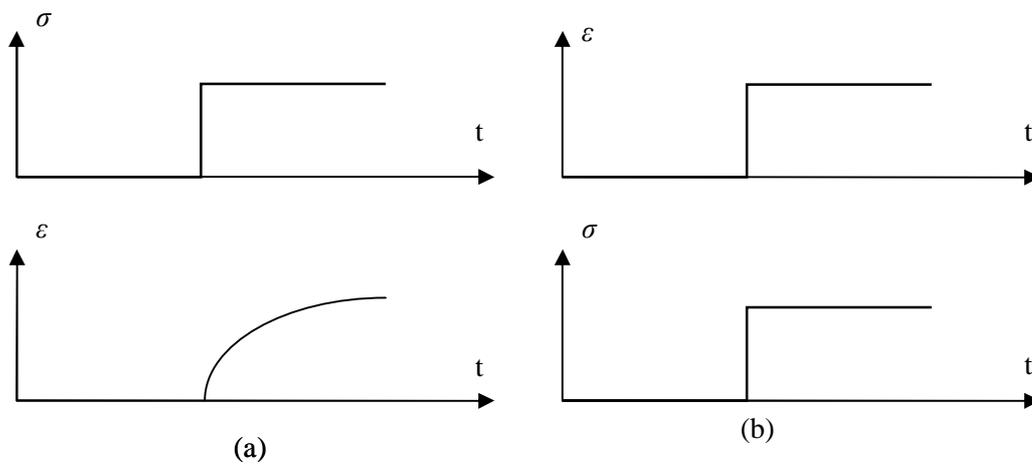
Figure 2-22: Creep according to Kelvin model.

2.4.6.1.3   Standard Linear Solid (SLS) model

One can construct a 3-element model made up of a linear spring in series with a Kelvin model. This is known as the standard linear solid model.

The response of a Kelvin model and linear spring can be expressed as

$$\pmb{s} = E_1\pmb{e}_1,$$ (2-35)

and

$$\pmb{s} = E_2\pmb{e}_K + h_2\dot{\pmb{e}}_K.$$ (2-36)

where ε_1 is the strain of the spring E_1 and ε_K is the strain of the Kelvin model in series with the spring E_1.

Using Laplace transformation, Eq. (2-36) can be transformed to

$$(E_1 + E_2)s + h_2\dot{s} = E_1E_2e + E_1h_2\dot{e}. \tag{2-37}$$

For a creep phase, the constitutive equation is then

$$e(t) = \frac{e_0}{x_1}\left[1\left(1 - e^{-t/l}\right) + x_2 e^{-t/l}\right], \tag{2-38}$$

where,

$$x_1 = \frac{E_1h_2}{E_2 + E_1} \tag{2-39}$$

$$x_2 = \frac{h_2}{E_2 + E_1} \tag{2-40}$$

$$l = \frac{h_2}{E_2} \tag{2-41}$$

and ε_0 is the initial strain when the SLS model is subject to an abrupt stress σ_0.

According to this constitutive equation, the model starts to creep at

$$e_0 = \frac{s_0}{E_1}, \tag{2-42}$$

and the strain asymptotically approaches,

$$e_\infty = e(\infty) = \frac{s_0}{E_\infty}, \tag{2-43}$$

where

$$E_\infty = \frac{E_2E_1}{E_2 + E_1}. \tag{2-44}$$

For a relaxation process, we have

$$s(t) = E_\infty e_0\left(1 - e^{-t/l'}\right) + s_0 e^{-t/l'}, \tag{2-45}$$

where

$$l' = \frac{h_2}{E_2 + E_1} \tag{2-46}$$

This indicates the stress asymptotically approaches

$$s_\infty = s(\infty) = \frac{e_0}{E_\infty}. \tag{2-47}$$

The creep and relaxation response of a SLS model is presented in Figure 2-23.
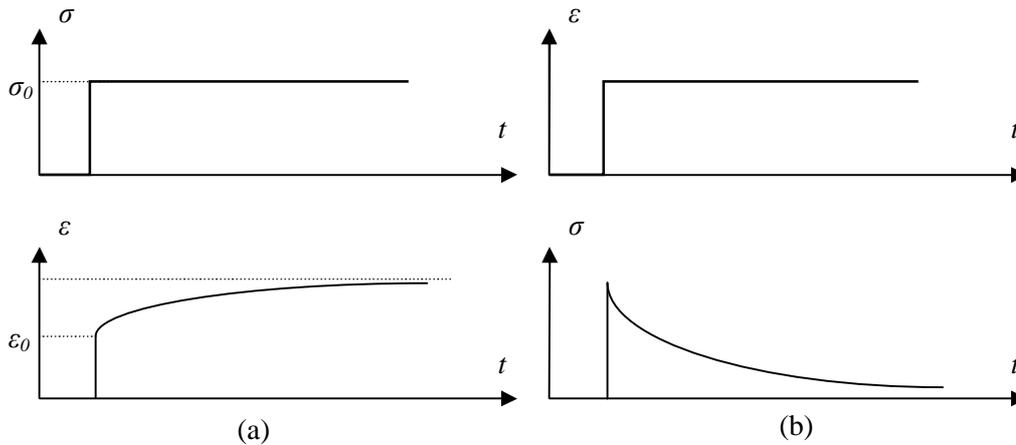
Figure 2-23: Creep (a) and relaxation (b) curves for SLS model.

2.4.6.1.4 Burger's model

One of the most widely used mechanical viscoelastic models is Burger's model due to its simplicity in structure and capability of representing different stages of creep [109-110]. As shown in Figure 2-24, it is composed of a Maxwell and a Kelvin unit connected in series, Burger's model is able to capture all the components of a creep curve with a Maxwell spring defining instantaneous elastic strain ε_1, a Kelvin unit defining transient strain ε_2 and a Maxwell dashpot defining steady strain ε_3. The creep behaviour of Burger's model can be finally obtained following the similar procedures as previously given for Maxwell and Kelvin elements [111-113]. The creep function for Burger's model is:

$$e_c = e_1 + e_2 + e_3 = s\left[\frac{1}{E_1} + \frac{1}{E_2}\left(1 - \exp\left(\frac{-t}{t}\right)\right) + \frac{t}{h_1}\right],$$

(2-48)

where

$$t = h_2/E_2 .$$

(2-49)
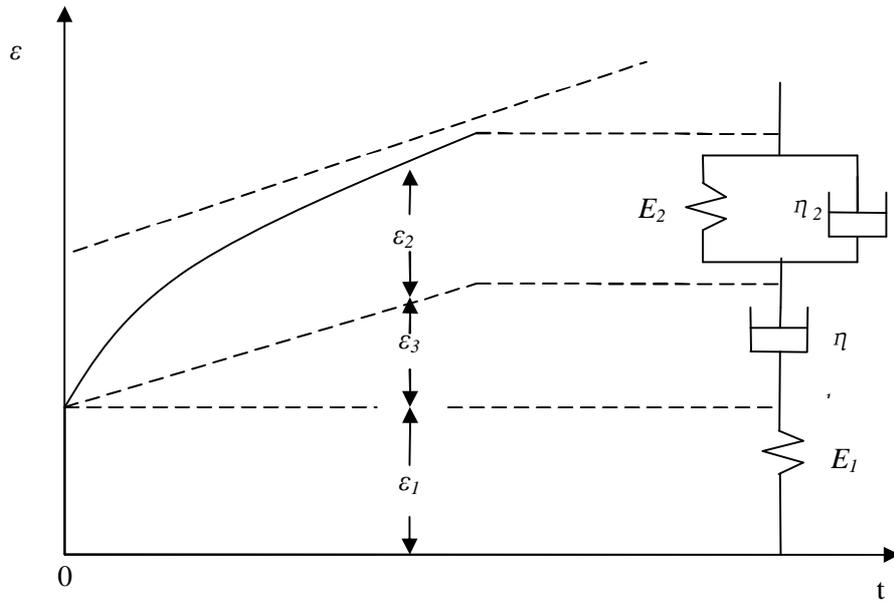
Figure 2-24: Creep response for Burger's model and its mechanical analogue.

2.4.6.1.5 Generalised models

Most polymers have a spectrum of retardation times due to the multiplicity of their structural units and the complexity of molecular movements. Therefore it is often found that having a single Maxwell or Kelvin element in a viscoelastic model is not sufficient to represent the mechanical behaviour of polymeric materials. Generalised models are proposed to deal with this situation [43, 102]. There are two types of generalised mechanical model of particular interest, generalised Maxwell model and generalised Kelvin model.

It is possible to construct several Maxwell models in parallel with a linear spring (Figure 2-25).
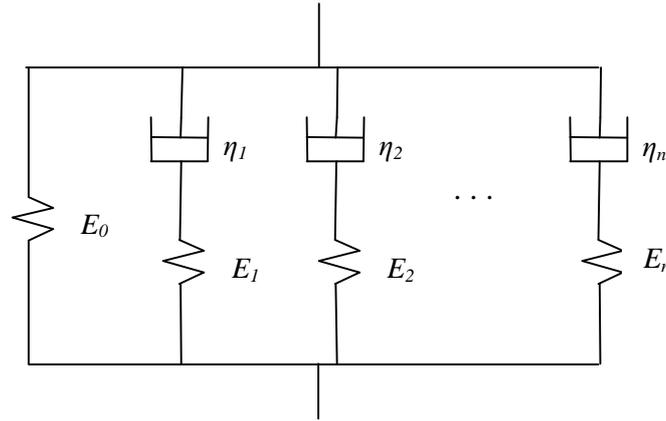
Figure 2-25: A generalised Maxwell model.

The total strain and stress of the generalised Maxwell model are,

$$e = e_i \qquad (2\text{-}50)$$

and

$$s = \sum_{i=1}^{N} s_i . \qquad (2\text{-}51)$$

In a generalised Maxwell model, it is not assumed that the total stress is shared equally by every element. By analogy with Eq. (2-23),

$$\dot{e}(t) = \dot{e}_i(t) = E_i^{-1}(d_t + l_i^{-1})s_i . \qquad (2\text{-}52)$$

The total stress is the sum of the stress in each element,

$$s(t) = \sum_{i=1}^{N} E_i(d_t + l_i^{-1})^{-1}\dot{e}(t) , \qquad (2\text{-}53)$$

where $l_i = h_i/E_i$ and $d_t = d/d_t$ subsequently, the relaxation modulus function can be expressed as [108]

$$E(t) = \sum_{i=1}^{N} E_i \exp(-t/l) . \qquad (2\text{-}54)$$
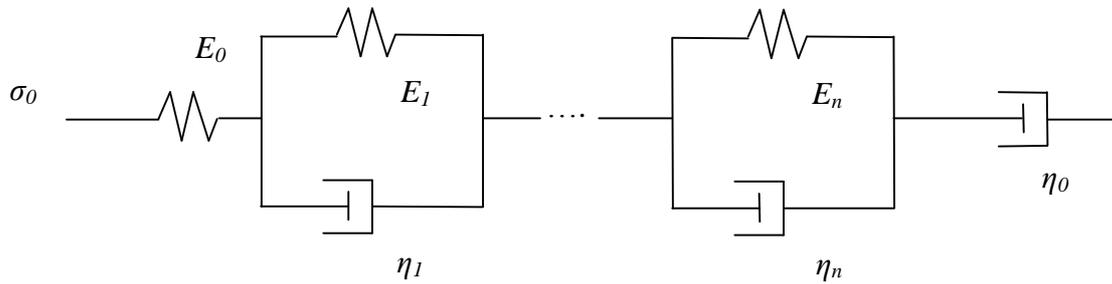
Figure 2-26: A generalised Kelvin model.

Figure 2-26 shows a generalised Kelvin model built up by connecting a number of Kelvin elements in series. In this model, the stress in each element is the same. With reference to Eq. (2-22),

$$\boldsymbol{s}(t) = E_i(1 + d_t\boldsymbol{l}_i)\boldsymbol{e}_i(t)$$

(2-55)

and

$$\boldsymbol{e}(t) = \boldsymbol{s}(t)\sum_{i=1}^{N} E_i^{-1}(1 + d_t\boldsymbol{l}_i)^{-1}$$

(2-56)

where, $\boldsymbol{l}_i = \boldsymbol{h}_i/E_i$ and the creep function of the generalised Kelvin model can be written as [108]

$$J(t) = \sum_{i=1}^{N} \frac{1}{E}\left[1 - \exp\left(\frac{-E_i}{\boldsymbol{h}_i}t\right)\right].$$

(2-57)

Phenomenological models for describing plastic or viscoplastic properties of materials can be described by introducing a slider element which is a rigid body until a yield stress is reached [111, 114-116]. An example of this approach, is with the mechanical analogue shown in Figure 2-27, has been adopted in the stress analysis of adhesive joints [116]. However, the word 'plastic' is best used to denote a type of mechanical behaviour associated with unrecovered deformation or flow and is misleading when used in a generic way to refer to polymers in general [43]. As a result, some researchers consider a viscoelastic solid or fluid model to represent mechanical behaviour of polymers with or without recoverable deformation [117-119]. The difference between a solid model and a fluid model in their

construction is that the former has a dashpot in series (e.g. Burger's model in Figure 2-24) while the latter does not.
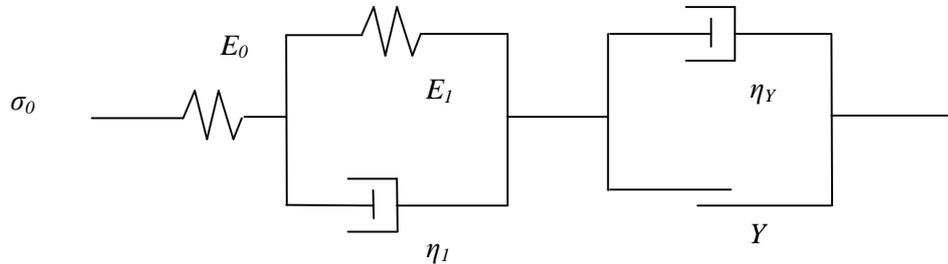
Figure 2-27: A five-parameter viscoelastic-viscoplastic model.

2.4.6.2 Yield criteria and generalised plasticity models

The stress-strain curves of polymers often indicate elastic and plastic regions, although they may be not as distinct as in a typical metal. This behaviour results in the introduction of a yield stress criteria, which is the measured stress level that separates the elastic and plastic behaviour of the material, and is usually obtained from uniaxial tests in laboratory, even though stresses in a structure are multi-axial. To determine a material's yield stress, various theoretical criteria have been suggested for illustrating the yield behaviour of polymers under multi-axial stress conditions. These include the von Mises yield criterion, the Tresca yield criterion, the Mohr-Coulomb criterion and the Ducker-Prager criterion. It is worth noting here that the material this literature review focuses on is assumed to be isotropic (uniform properties in all directions).

In continuum plasticity theory the onset and direction of non-recoverable (inelastic) strains for an isotropic, non-porous material is defined by introducing a yield surface, through a yield function, F_Y, given by

$$F_Y = f(\bar{s}, q, H_a) = 0,$$
(2-58)

where $\bar{s}$ is yield stress, θ is temperature and H_α are a set of hardening parameters to define the hardening behaviour. The subscript α is introduced simply to indicate that there may be several hardening parameters. When the material is flowing inelastically, at $F_Y > 0$, the inelastic part of the deformation is defined by a flow rule which can be written as

$$de^{pl} = dI \frac{\partial g}{\partial s},$$

(2-59)

where g is the flow potential, e^{pl} is the equivalent plastic strain and dI is a scalar defining the equivalent plastic strain increment which is determined in a different way for time dependent and time independent material models [120-121].

The von Mises yield criterion [121], sometimes called the second deviatoric stress invariant (J_2) flow theory or J_2-plasticity, was developed for metals but can also be used for some polymeric materials. The von Mises yield function is given by

$$F_Y = q - s_0(e^{pl}, q)$$

(2-60)

where q is the von Mises equivalent stress, a scalar stress value that can be obtained from the stress tensor and is defined to predict yielding in materials. s_0 is the material uniaxial tensile stress corresponding to the equivalent plastic strain ε^{pl}. The von Mises equivalent stress is defined as

$$s_{eq} = \sqrt{3J_2} = \sqrt{\frac{(s_1 - s_2)^2 + (s_2 - s_3)^2 + (s_1 - s_3)^2}{2}} = \sqrt{\frac{3}{2} s_{ij} s_{ji}},$$

(2-61)

where s_{ij} are the components of the stress deviator tensor σ^{dev}.

According to the definition of the von Mises yield criterion, the von-Mises stress is only a function of the deviatoric stress (seen in Eq. (2-61)). As a result, von Mises plasticity model is not able to capture the commonly observed polymeric hydrostatic stress sensitivity of yielding. A more advanced model, the Drucker-Prager plasticity model, which is hydrostatically dependent and accounts for hydrostatic sensitivity, has been proposed for polymers [120, 122-123]. It is an isotropic elasto-plastic model based on a yield function

$$F_Y = f(s) - t_Y$$

(2-62)

with the pressure-dependent equivalent stress

$$f(s) = aI_1 + \sqrt{J_2}.$$

(2-63)

σ and τ_Y in Eq. (2-62) are the stress tensor and yield stress under pure shear load, respectively. I_1 and J_2 in Eq. (2-63) are the first invariant and second deviatoric invariant of the stress tensor. α is the friction angle, a parameter that controls the influence of the pressure on the yield limit.

Drucker-Prager models have been popular historically in the geotechnical engineering field [81, 124-125]. However, more recently they have also been found to be useful for the

modelling of some polymeric materials [120, 126-127], especially for capturing hydrostatic stress sensitivity [120, 127].

Extensions of the original Drucker-Prager model are commonly used [125] which offering differently shaped yield surfaces in the meridional plane, p-q plane (hydrostatic stress p and von-Mises stress q plane), including a linear form, a hyperbolic form and a general exponent form (shown in Figure 2-28).

The yield function of a linear form of Ducker-Prager model is defined as:

$$F_Y = t - p \tan \boldsymbol{b}' - d \,, \tag{2-64}$$

where β' and d are material parameters. t is a measurement of the degree of the deviation of deviatoric stress and defined as:

$$t = \frac{q}{2}\left[1 + \frac{1}{k} - \left(1 + \frac{1}{k}\right)\left(\frac{r}{q}\right)^3\right], \tag{2-65}$$

where k is a material parameter that may depend on temperature, and other predefined fields. The value of r/q is 1 in uniaxial tension and -1 in uniaxial compression.

The hyperbolic form is defined as

$$F = \sqrt{l_0^2 + q^2} - p \tan \boldsymbol{b} - d^{'}, \tag{2-66}$$

where d' is the d in a hyperbolic form l_0 is defined as:

$$l_0 = d^{'}\big|_0 - p_t\big|_0 \tan \boldsymbol{b} - d^{'}. \tag{2-67}$$

and where $d^{'}\big|_0$ is the initial value of d' and $p_t\big|_0$ is the initial average tensile strength.

The exponent form of Drucker-Prager model is defined as:

$$F_Y = aq^b - p - p_t \tag{2-68}$$

where a and b are material constant parameter, p_t is a hardening parameter.
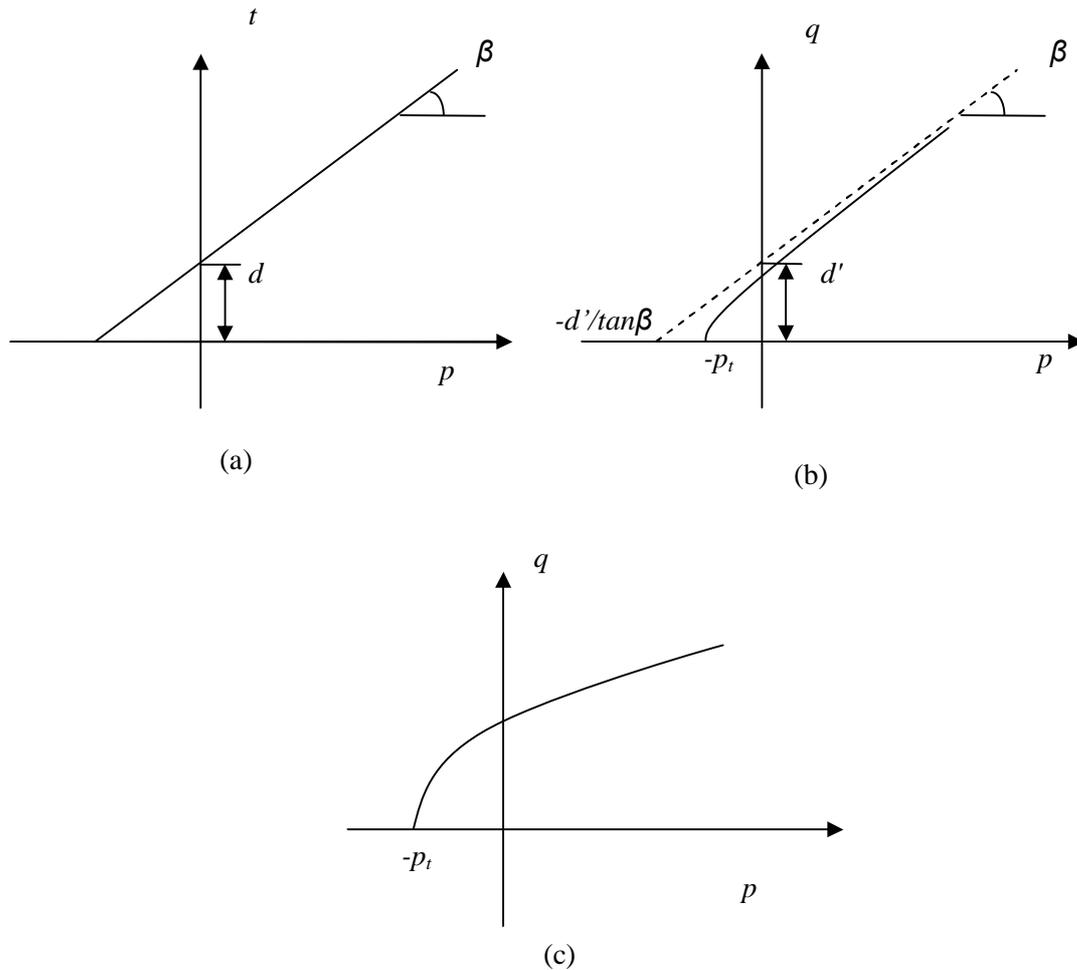
Figure 2-28: Yield criteria in the meridional plane in a linear (a), hyperbolic (b) and a exponent (c) form of Drucker-Prager.

The Drucker-Prager model has a significant advantage over the von-Mises model by introducing hydrostatic sensitivity. However, neither of these two models is able to capture the strain rate dependency of polymeric materials. To overcome this shortage, these two models have been extended to include rate-dependent plasticity by introducing a rate-dependent yield strength (σ_0 and p_t) in the material model in a number of ways, including simple analytical expressions for the yield functions in terms of rate or the specification of a series of hardening curves for various plastic strain rates [120].

In materials science, creep is the tendency of a solid material to slowly move or deform permanently under the influence of stresses. It occurs as a result of long term exposure to high levels of stress that are below the yield strength of the material. Creep is more severe in materials that are subjected to heat for long periods, and near to their melting point. Since

these processes tend to soften the material they counteract the strain hardening produced by plastic deformation. Creep behaviour resembles viscoelasticity since the resulting strain at constant applied stress is a function of time. However, in contrast with solid viscoelastic behaviour, permanent deformation remains following creep. As a result, creep behaviour in some texts, especially for metal creep, is also frequently known as viscoplasticity [128-129].

2.4.6.3   Other advanced models

The classical phenomenological viscoelastic models are linear models and do not represent the behaviour of most polymeric materials very well. Efforts have been put into modifying these linear models to make them able to represent polymeric nonlinear viscoelastic behaviour [44-45, 111, 118, 130]. This modification can be achieved either by specifying stress-dependent model parameters, such as mechanical constants [118] and retardation times [130], or by multiplying constitutive functions by a stress dependent function [44-45, 111]. These modified viscoelastic models manage to represent nonlinear viscoelasticity, but fail to capture elastic-plastic behaviour. One of the best viscoelastoplastic models to date is Schapery's macroscopic model based on thermodynamically consistent theory [131]. It has been successfully applied in modelling non-linear viscoelastic viscoplastic behaviour of synthetic fibres by Chailleux and Davies [132] and FEA of adhesively bonded composite joints by Roy and Reddy [133]. Schapery's model provides good rate-dependency, allows full recovery and non-recoverable deformation.

An advanced form of viscoplastic modelling is the overstress model or unified theory model. The main difference between classical and unified plasticity theory is that classical theory defines plastic behaviour using a yield surface. However unified theories generally generate inelastic strains at all times without using a yield surface, and as a result unified theories resemble power law creep [120, 134]. More general unified theory models that can produce time-dependent recovery have been proposed based on different inelastic flow laws [135-138]. These models have been shown to fit experimental data reasonably well at the expense of the requirement of a large number of model parameters.

2.5   Failure in coatings

In order to achieve an efficient design of a coating system and conservation of coating/substrate structure, e.g. lacquer ware, the stress, deformation mechanisms and failure

modes of the coating needs to be well known. The failure mode of a coating/substrate structure can be categorised mainly into two types: coating-substrate interface failure and in-film failure (entirely within the coating). The prediction of failure in a coating/substrate structure is of great importance in the design and conservation of coating/substrate applications. Several approaches have been developed to model joint failure and have achieved different degrees of success [139-150]. These approaches can be classified as the strength of materials method [139-140, 142, 144, 146-147, 150-151], the fracture mechanics method [141, 145, 149, 151] and the continuum damage modelling method [148].

2.5.1 Strength of materials methods

This method is based on the strength of the materials, in which the stress or strain distribution in a coating/substrate structure is examined, and the structure is assumed to fail when the predicted stress or strain field exceeds a critical value. Some of the most popular strength of material methods is reviewed below.

2.5.1.1 Maximum stress criteria

The maximum stress criterion is commonly used in industry and is one of the most instinctive starting points for strength prediction in coating applications. The method involves determination of the maximum stress in the coating layer and failure is assumed when the stress at any point within the layer exceeds a critical value of stress. This approach allows for the varying stress distributions in the coating layer and the stresses are usually determined by non-linear FEA or closed form analysis. FEA methods are preferred because they are able to account for large displacement rotations that occur in some joints under load. This approach has been applied to thermal barrier coating (TBC) applications with considerable success [142, 144]. Agrawal *et al* [146] proposed a methodology to measure the in-situ ultimate shear strength of coating material on a substrate, and used this to create a tensile-film-cracking model for the interfacial failure prediction of a TiN coating/ AISI 304 stainless steel structure [139].

2.5.1.2 Maximum strain criteria

The maximum strain criterion predicts that failure occurs in the multiaxial state of stress when the maximum principal normal strain becomes equal to or exceeds the maximum normal strain at the time of failure in a simple uniaxial stress test, using a specimen of the

same material [152]. This theory has been adopted to study the structural environment as a factor affecting coating failure of a typical aircraft coating system [150].

2.5.2 Fracture mechanics

The fracture mechanics approach assumes that all materials contain flaws and that failure is by the propagation of flaws of a critical size. Fracture mechanics has been widely used to predict crack growth, fracture and failure in coating/substrate system [141, 145, 149, 151] and bi-material strip structures [153]. The main concepts of fracture mechanics are the energy balance method pioneered by Griffith [154] and the stress intensity factor concept developed by Irwin [155]. One of the fundamental principles of fracture mechanics is that the critical strain energy release rate, G_c (or Jc for non-linear fracture) and the critical stress intensity factor, K_C, are material properties. Although the stress-intensity approach is widely used for the analysis of metals, it is more complicated to apply in adhesion and coating contexts, where constraint effects of the adherend on the adhesive layer make it difficult to define the stress distribution around the crack tip. Therefore, G, is frequently used as the governing fracture parameter in the analysis of bonded joints in preference to K.

2.5.3 Continuum damage modelling

The development of micro-structural damage in engineering materials can be effectively modelled using Continuum Damage Mechanics (CDM) [156]. CDM introduces a field variable to represent the damage in a continuum sense. This concept has been used to model the initiation and growth of cracks. Using the framework of CDM, processes of failure evolution at the microscopic level are introduced into mesoscopic considerations [148, 157]. This approach has also been applied to the failure prediction of a TBC structure, in which it was found that the homogenous CDM model was invalid due to material instability. Thus, a sensitivity analysis was performed to identify a criterion to determine the validity of the homogenous CDM model. It was found that there exists a critical value of damage state variable beyond which the material becomes unstable [142].

2.6 Summary

It is clear that the behaviour of the two coating materials considered in this research is complex and highly influenced by water transportation and UV exposure. *Urushi* and PU are typical viscoelastic materials with significant changes in their mechanical behaviour when

subjected to changes in moisture content and UV illumination. Literature on neither environmentally influenced mechanical properties nor material models for both materials are sufficient at present due to lack of research on these two materials. In order to formulate a predictive mechanical model for *urushi* and PU that includes constitutive relations, a comprehensive analysis of the response of the coatings to changes in environmental conditions is still required in order to determine the precise nature of the relationship between stress, strain, moisture content and thermal and UV conditioning. Moreover, as the ultimate cause for the formation of surface micro-cracks is the surface stress [42, 56], detailed measurements of the dependence of film stress with environmental conditions are required.

Chapter 3 Experimental Methods

3.1 Introduction

Before any predictive model can be applied, material properties must be obtained, usually by means of experiment. In some cases the material model to be used is known beforehand, in which case it is a fairly straightforward procedure to carry out the required experimental tests to determine the material constants. In other cases, such as with *urushi*, it is necessary to carry out initial experiments to characterise the behaviour of the material over the range of conditions to be modelled. An appropriate material law can then be selected (or developed if such a law doesn't exist) and further tests carried out to determine the required material constants. This chapter describes the methods, equipment and procedures used during the experimental programme carried out in this research. A number of investigations were undertaken to generate the following material properties for the PU lacquer and *urushi* film:

- Coefficient of hygroscopic expansion;
- Diffusion coefficient;
- Absorption isotherm.
- Time-dependent mechanical properties.

Other material properties were derived from data available in the literature.

3.2 Control of environment

The material properties of PU lacquer and *urushi* films have a complex dependence on environmental conditions according to the surveyed literature discussed in Chapter 2. Also, sample preparation of PU lacquer and *urushi* requires specified environmental conditions. In this context, a precise control of environmental conditions is a prerequisite to both the design and performance of any experimental work in this project. The three main factors in defining environmental conditions are solar radiation (mainly UV irradiation), temperature, and water (moisture), which are all controlled during the experimental work in this project.

3.2.1 Humidity control

3.2.1.1 Salt solution method

The humidity inside sealed containers can be controlled by saturated salt solution inside [158-160]. Table 3-1 shows saturated salt solutions and the relative humidities they can maintain inside a sealed container under 23±2℃ with error of fluctuation during one day.

Table 3-1: Relative humidities maintained by different salt solutions on saturation inside a container [158].

$MgCl_2$	K_2CO_3	NaBr	NaCl	KCl	K_2S
33.8±0.8% RH	43.2±0.6% RH	58.0±1.2% RH	75.0±0.9% RH	85..0±1.2% RH	95±1.8% RH

3.2.1.2 Dynamic control method

Saturated salt solutions can be used to be able help maintain a specific relative humidity, however, they require a sealed container with solution inside, which is difficult to attach to testing devices (e.g. tensile testers) and cannot generate a dynamic varying relative humidity, if required. To overcome these limitations, a dynamic control method was used, as shown in Figure 3-1. The RH in the chamber can be controlled by changing the moisture content of a stream of air blown through the chamber. The air moisture content can be increased by using a humidifier which consists of a small fan forcing air through a wet pad. The humidifier is connected to a Humidity Controller which switches off the humidifier each time the RH exceeds the desired RH value and switches on the cooler when the RH moves below the desired RH value. With this configuration, the tolerance in the RH was found to be less than ± 1%.
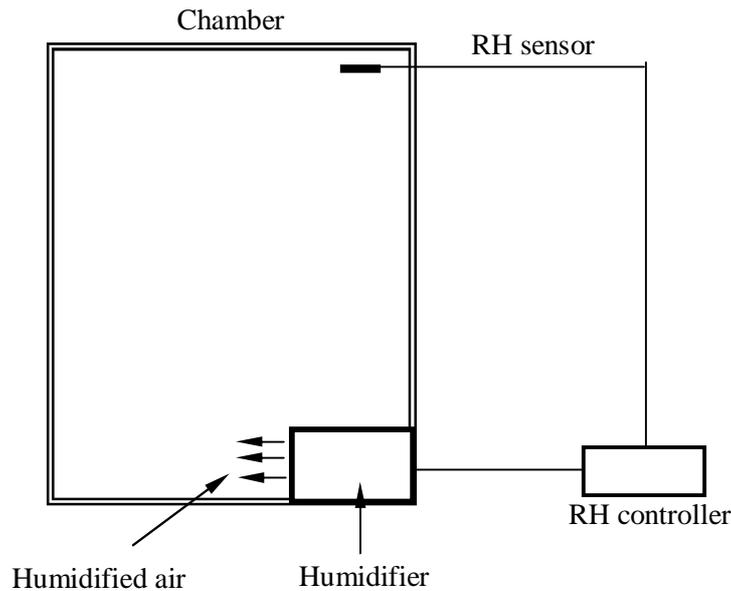
Figure 3-1: Schematic illustration of the chambers (manufactured in Wolfson School, Loughborough University. UK. This is only an illustration to demonstrate the mechanism the control system, with location of components differs in terms of where a chamber is used).

3.2.2 Temperature control

In the V&A Museum, or any other environment where *urushi* lacquerwares are in service or for display, the temperature normally does not vary significantly. As a result, the temperature is considered to be a constant value and is maintained at a constant level that is similar to the in-situ temperature in this project. The temperature controlling system has three main components:

1- Input:

The input is a platinum thermo-couple (PT100) to measure the temperature inside the chamber.

2- Controller:

The controller in Figure 3-2 monitors the input from the PT100 and compares it with the setting point or the desired temperature setting. As required, it increases the temperature by switching on the heating element. It is provided with an on/off and proportional with integral and derivative (PID) control, where PID is used when precise control is required.

3- Output:

The output is the part of the controller that is used for turning the heating element on and off. The output inside the controller is a Solid State Relay.
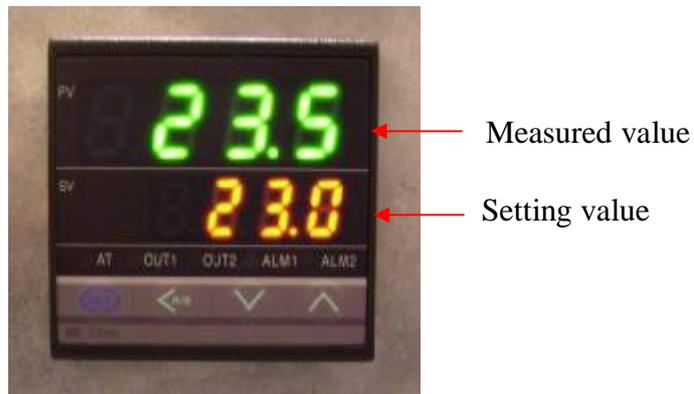
Figure 3-2: Temperature controller.

This approach allowed ones to control RH and temperature to within ±1% RH and ±1℃ respectively.

Using this dynamic temperature controlling technique, the environmental chamber shown in Figure 3-1 can be extended to achieve a dynamic combined environmental control in both temperature and humidity, as shown in Figure 3-3.
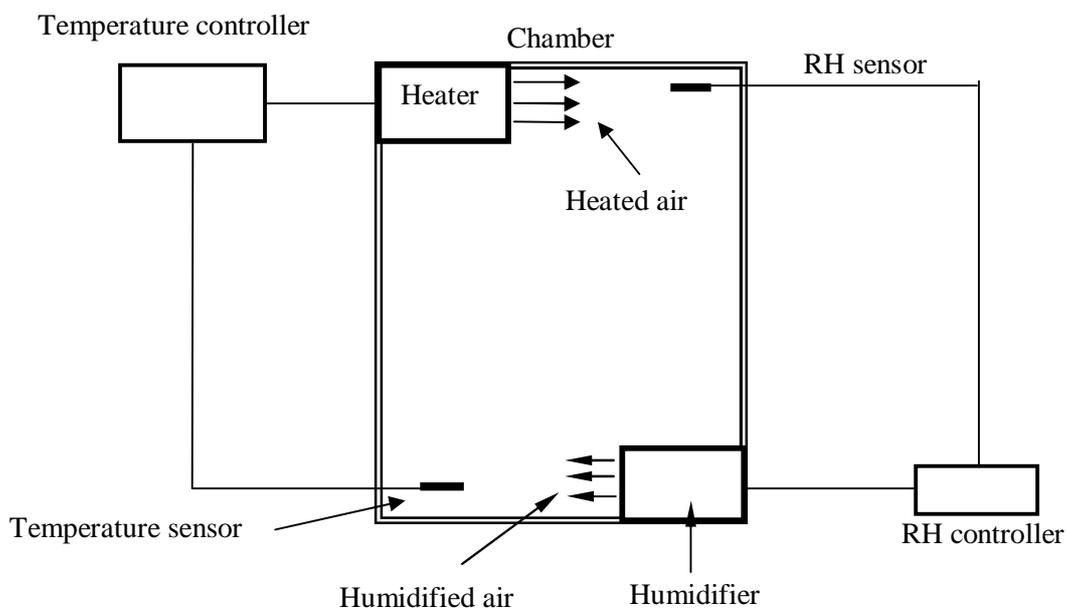
Figure 3-3: Schematic illustration of the controlled environment chamber used to cure *urushi* thin films and to maintain a constant environment during testing.

3.2.3   UV exposure

In order to produce films that were UV aged a subset of the samples were exposed to UV radiation. The UV radiation exposure history of the Mazarin Chest is unknown and therefore any attempt to try to replicate its accumulated ageing will be flawed, Hence rather than replicate the damage to the lacquer exactly, It was attempted to produce damage of a more general kind to understand the broad changes in behaviour that occur during UV ageing. To induce UV damage, a Q-Sun environmental test chamber (Q-SUN Xe-1 manufactured by Q-Lab Corporation, Cleveland, Ohio USA.), equipped with a Xenon arc source, into which the film was exposed to 340 nm, 0.7 $W.m^{-2}$ UV radiation for 400 hours. The only clear data on the exposure of the chest to light is that during the period between 1986 to 1998 it was displayed at the Toshiba Gallery in the V&A, London, where the illuminance was 80 lux, with UV levels less than 5 $\mu W.lumen^{-1}$, resulting in an energy density of 0.0004 $W.m^{-2}$. Considering 52 weeks per year, 5 days per week and 8 hours per day display, this results in a total UV exposure of about 36 $kJ.m^{-2}$ [5]. As a comparison, one can estimate the average (accounting for seasonal and daily variations) exposure to 340 nm UV radiation due to sunlight as 0.08 $W.m^{-2}$. In order to place the tests into context, It can be calculated that the test protocol is equivalent to an average daylight exposure of 0.4 years or an exposure within the Toshiba gallery of 80 years (assuming 80 lux at 340 nm, though the exposure at this wavelength is likely to be much lower in reality) [5]. The same technique and equipment were applied to artificially age the PU lacquer samples to study the effect of UV exposure on material behaviour through mechanical tests for PU film samples.

3.3   Sample preparation

3.3.1   PU lacquer

The material studied was a thermoplastic PU lacquer, No.8 gloss PU lacquer, manufactured by John Myland Ltd, London, UK. It is a one component wood finish lacquer. The samples were made by applying 50-100 grams of lacquer resin onto a glass substrate with a dimension of 260×260 mm^2, which had been surface treated by acetone for better adhesion and placed on a level plane. After curing at room conditions (50±5% RH and 23±2°C) for 48 hours, the dry sample was peeled off and put into a fan oven with a setting temperature of 40°C for 2 weeks of further curing, then stored in a desiccator at room temperature.

3.3.2 *Urushi*

The preparation of *urushi* samples involved several stages, each with the end point in mind of producing consistent thin layers. The stages are as follows:

1. Filtration.

2. Mixing.

3. Glass substrate preparation.

4. Coating.

5. Curing.

In the following sections these processes are described in detail.

3.3.2.1 Filtration

The *urushi* lacquer used in this study was *Kijiro urushi*, product of Wantanabe Syoten Co., Tokyo, Japan. As *urushi* is a natural product, it can often contain unwanted objects and particles. The first stage, therefore, in *urushi* preparation is filtering to eliminate all impurities. *Urushi* was filtered, following the traditional Japanese filtration process of using Rayon sheets, by wrapping and twisting it as shown in Figure 3-4, repeating seven times with three Rayon sheets each time.

Figure 3-4: Traditional Japanese filtration method.

3.3.2.2   Mixing process

Raw *urushi* is a non-stable water-in-oil type emulsion. The water soluble polysaccharides in the raw *urushi* can often aggregate during drying [161] and therefore, the *urushi* was mixed and homogenised for about 3 minutes to avoid aggregate formation. Gentle manual mixing is required to avoid bubble production.

3.3.2.3   Glass substrate

In order to measure depth averaged stresses using the curvature measurement method, it is necessary to deposit layers of known thickness on to a substrate. Dr Adel Elmahdy obtained these *urushi*-substrate samples by casting a small amount of *urushi* on to a BK-7 glass substrate of thickness 190±5 μm and 22 mm in diameter. Prior to applying *urushi*, the glass substrate was tested by Dr Elmahdy to find a substrate with minimum bending. The test was performed using phase shifting interferometry [5].

3.3.2.4   Coating process

Generally, in lacquerware artefacts, plastic or wooden spatulas are used to spread a thin layer of *urushi* over a wooden object. It is found that it was difficult to obtain a homogenously thin layer of *urushi* on a small size glass substrate in a controlled fashion using this technique and opted to use the more reliable spin coating technique instead [162]. The details of incorporating this technique into coating process were presented in Dr Elmahdy's thesis [5].

3.3.2.5   Curing process

As *urushi* cures only in the presence of air and high relative humidity, a controlled humidity chamber was constructed for curing purposes (Figure 3-3). The appropriate RH was maintained at a constant level in the chamber using equipment described in section 3.2.

Urushi films with a thickness of around 20 μm were obtained by spin coating at 3000 rpm for 90 s at room temperature, using a spin coater built by Dr Elmahdy. The back surface of the glass substrate was coated with nickel chromate in a vacuum deposition chamber before coating. Immediately after spin coating, the films were cured at 75±1% RH. For films with a thickness of around 20 μm, it takes at least 3 days for them to fully cure [5]. The film thickness was measured by focusing a microscope (BX-60 Olympus with 50x objective) on

the glass/*air* and the *urushi*/air interfaces and measuring the distance required to refocus. The manufactured films had a thickness of 21 μm±2 μm.

3.4 Measurement of hygroscopic properties

The hygroscopic behaviour of coatings are quantitatively characterised by measuring material constants such as diffusion coefficient, coefficient of hygroscopic expansion and absorption isotherm. The mathematical treatments and experimental techniques used to obtain these constants will be summarised in the following sections.

3.4.1 Measurement of diffusion coefficient

3.4.1.1 PU lacquer

Water absorption and desorption tests were performed under 6 humidities, using the salt solutions listed in Table 3-1, for the measurement of the cyclic water absorption/desorption behaviour of the PU lacquer samples. Eighteen samples, measuring $200 \times 20 \times 0.32$ mm^3 were used in the experiments. Samples with a thickness of 0.44 mm were also manufactured, to investigate the effect of thickness on the diffusion coefficient. Before the first cycle of absorption, the samples were stored in a desiccator with a RH of 5.6% until the weight change was less than 0.1% per week. Six 2-litre flasks with hooks on their stoppers were used to store and moisten PU lacquer film samples which were hooked onto the stoppers to avoid immersion in the salt solutions in the flasks. During the experiment the weight of samples was measured at regular intervals using an electronic balance with a resolution of 0.1 mg, and their percentage increase or decrease rate in weight obtained from

$$M(t) = \frac{m_2 - m_1}{m_1} \times 100$$

(3-1)

where m_1 is the mass of the specimen after drying and m_2 is the mass of the specimen at specified time intervals. In this experiment, 3 repeat samples were used for each test. The average values of the 3 tests were then used to plot the diffusion curve.

3.4.1.2 *Urushi*

The rate of moisture absorption was characterised by gravimetric tests in which the mass of a sample was monitored as a function of time following a change in RH. A digital balance HA180 (A&D Instruments Ltd) with a precision of 0.1 mg was used for all the weight

measurements. Three samples of dimensions 70 mm×50 mm were prepared with a thickness of 0.06-0.08 mm. Samples were allowed to reach a uniform moisture distribution by storing them in a curing chamber at 30% RH until the weight change was less than 0.1% per week. After that the samples' environment was changed to 40%, 50% and then to 60% RH, where each humidity was maintained for 16 hours and the samples' mass was measured every 30 min. Finally, the samples were dried at 100°C for 27 hours to remove the moisture, and the dry weight obtained.

3.4.2 Measurement of hygroscopic expansion

3.4.2.1 PU lacquer

The coefficient of hygroscopic expansion (CHE), β, is defined as Eq. 14:

$$b = \frac{\Delta L}{L \Delta M}$$

(3-2)

where L is the length of a workpiece having a uniform hygroscopic strain, ΔL is linear deformation due to a change in moisture and ΔM is absorbed/released moisture. β determines the swelling behaviour of a material as a function of M. The expansion of the PU lacquer samples due to the uptake of moisture was measured. The samples were marked at regular intervals along their length, photographed and then subjected to a change of environmental humidity. The change in spacing was then determined by the taking of a second photograph and position measurement. The strain can then be determined from a plot of Δx_i (the change in position of the ith mark) against x_i (the position of its mark). An example of determining hygroscopic strain of a PU lacquer film sample from the gradient of this plot is shown in Figure 3-5.
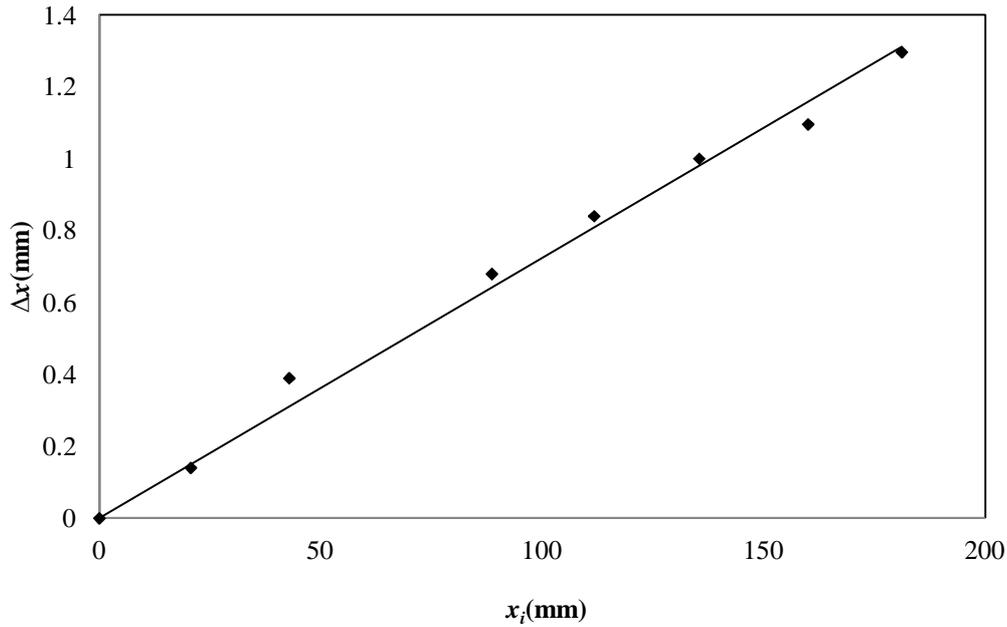
Figure 3-5: Plot of Δx against $x_{i.}$, for measurement of hygroscopic strain of a dry PU lacquer film sample after saturation under 95% RH.

3.4.2.2 *Urushi*

To obtain the coefficient of hygroscopic expansion for *urushi* film, Samples with lateral dimensions of 120×10 mm^2 were manufactured. These were then stored in a desiccator until the weight change was less than 0.1% per week. The dry samples were marked using a 0.5 mm marker pen and photographed, after which they were placed into sealed containers with a range of relative humidities, controlled by the salt solutions presented in Table 3-1. Once saturation had been achieved (2 days after conditioned to make sure complete saturation), the sample was photographed once again and the change in the sample dimensions measured. The measurement repeated three times for each humidify condition, and the average value of extension ratios was used to calculate hygroscopic strain. This was repeated for a number of relative humidities to identify any variance in β with moisture content.

3.4.3 Measurement of absorption isotherm

The absorption isotherm was measured from observing relationships between equilibrium weight gain due to moisture uptake and relative humidity. This was obtained from the hygroscopic tests for measuring the coefficient of hygroscopic expansion. The absorption isotherm was modelled by fitting several absorption isotherm models to the experimental data for the third cycle of absorption data.

3.5 Mechanical properties characterisation

As PU and *urushi* coatings are known to show viscoelastic behaviour (Chapter 2), the experimental test programme needed to include an investigation of time and rate dependent deformation under load. Effective tests for investigating this include isochronous stress-strain tests, creep tests (time dependent deformation under constant load), recovery tests (time dependent recovery of deformation on removal of load) and relaxation tests (time dependent relaxation of stress under constant displacement). To investigate the time dependent mechanical behaviour of PU lacquer and *urushi* coatings, constant displacement rate tensile tests, creep tensile tests and recovery tests were performed for both materials. The temperature was maintained at $23\pm2^{\circ}$C for all the tests.

3.5.1 PU Lacquer

In order to study viscoelastic behaviour and determine a constitutive model for the PU lacquer, uniaxial tensile tests at various displacement rates and constant load (creep) tests were performed. The PU lacquer samples for the mechanical tests were 0.3 mm thick, 10mm wide and 80mm long. These sets of samples were prepared: fresh samples, UV aged samples and moisture conditioned samples. The UV aged samples were aged using a Q-sun Xenon test chamber (Q-SUN Xe-1 manufactured by Q-Lab Corporation, Cleveland, Ohio, USA.), with UV irradiation ($\lambda=340$nm) with an intensity of 0.7 W/m^2 for 2, 4, and 8 days. The samples for moisture conditioning were stored in humidity controlled flasks until saturation. The constant displacement rate tests and creep tests for the UV aged samples were carried out on with an Instron universal testing machine 5569 with a 5kN load cell. The constant loading displacement rate tests under controlled RH were performed on a Hounsfield desktop tensile machine and the creep tests under different RH were performed using a purpose-built creep rig installed in a humidity controlled chamber. In the creep tests, up to 4 stress levels were performed to study the effect of environmental changes on the viscoelastic behaviour of PU lacquer films. Young's modulus was evaluated by taking stress-strain behaviour of the samples linear up to 0.2% strain.

3.5.2 *Urushi*

A series of mechanical tests were performed to identify the characteristic rheological properties of the *urushi*, including constant displacement rate, creep and recovery tests at

different relative humidities. *Urushi* film samples were prepared using the methodology described in Section 3.3 and for these tests, cut into rectangular strips 60×5 mm^2 in size. The thickness of each strip was measured using a Mitutoyo digital micrometer, accurate to 1 μm, and found to take values be between 60 and 100 μm. The mechanical tests were performed using an Instron universal testing machine 5569 with a 100 N load cell at three relative humidities of 30%, 50% and 75% RH. Prior to each test, the films were kept for 1 week under constant RH (30%, 50% and 75%) to ensure that equilibrium had been reached. The gauge length of *urushi* samples between grips of the tester was 5 mm for all the tests. The displacement of the load cell of the tester was measured by a displacement sensor in the tester to measure how much a sample was stretched. Meanwhile, mechanical tests for *urushi* samples with various durations of UV exposure were also performed, with a constant humidity of 50% RH. For a given RH and duration of UV exposure, samples were tested at displacement rates of 0.002 mm/min, 0.02 mm/min and 0.2 mm/min which correspond to initial strain rates of 1.3×10^{-6} s^{-1}, 1.3×10^{-5} s^{-1} and 1.3×10^{-4} s^{-1}. These displacement rates were chosen to be relatively low to reflect the long timescales of straining likely to be experienced by *urushi* films in-service. The force and displacement values are recorded during the test and these data are converted to stress (s) and stain (e). In creep tests, up to 4 stress levels were performed to study the effect of environmentally changes on the viscoelastic behaviour of PU lacquer films. Young's modulus was evaluated by fitting a linear relationship to the stress-strain behaviour of the samples up to 0.2% strain.

3.6   Summary

The hygroscopic and mechanical properties of the materials used in this research, were experimentally determined for use in analytical and numerical models. The bulk PU and *urushi* samples were prepared and dried in a desiccator as the initial condition for experimental work involving different environmental conditions. The moisture diffusion behaviour of the PU lacquer and *urushi* film was studied using a gravimetric method. The absorption isotherm and coefficient of hygroscopic expansion of both materials were determined through swelling tests. Material rheology, with the influence of environmental conditions, was studied by standard mechanical tests. This experimental work provided a comprehensive hygro-UV-mechanical definition of PU and *urushi* lacquers that is essential for the predictive methodology proposed in future chapters.

Chapter 4 Computational Methodology

4.1 Introduction

Experimental observations from the coating material tests provide a phenomenological description of material behaviour. However, in order to obtain a quantitative hygro-UV-mechanical definition of the materials and define material properties in a numerical modelling scheme, mathematical constitutive models need to be fitted to material behaviour. These can then be used in a predictive model of the mechanical response of the coating subjected to variations of environmental conditions and loading using the FEA technique. In this work the FE Analysis was implemented in ABAQUS (v6.9 and 6.10, Dassault Systems, Providence, RI, USA), This chapter gives an overview of the computational methods used in this thesis, including curve fitting techniques, the finite element method (FEM) and its computational scheme in ABAQUS, and a user defined material technique. Specific analysis details, which are only related to a particular model, are further explained in relevant chapters.

4.2 Finite element methods

Very limited work on numerical modelling of the mechanical response of coating materials due to variations in the environmental conditions has been carried out using the FEM. In this work the commercially available FE code ABAQUS was used for the numerical analysis. The geometric model development, problem setup and meshing of two dimensional (2D) and three dimensional (3D) joints was carried out using ABAQUS/CAE, the pre and post-processor for ABAQUS. A consistent system of units based on N, mm and hours was used. This section details the modelling methodology, boundary conditions, meshing methods, element choice and software specific options used during model development and analysis.

4.2.1 Model geometry, boundary conditions and loading

4.2.1.1 Modelling the tensile test

Tensile tests, including constant load and displacement rate tests, can be easily modelled in commercial FEA software package. The geometry and boundary conditions of *urushi* samples for the tensile tests, which were mentioned in Chapter 3, can be represented by a 2D model, as shown in Figure 4-1. To model the *urushi* samples subjected to constant displacement rates, models with the dimensions specified in Chapter 3 were completely

constrained on the left side leaving the sample stretched from the right side with a specified ramped displacement and step time. The modelling of tensile creep tests was achieved by replacing the ramped displacement with a stepped load. To avoid convergence problems, it is worth noting that a small time step followed by long time step is advised to be used initially and this is increased automatically by the FEA code as convergence allows [163].
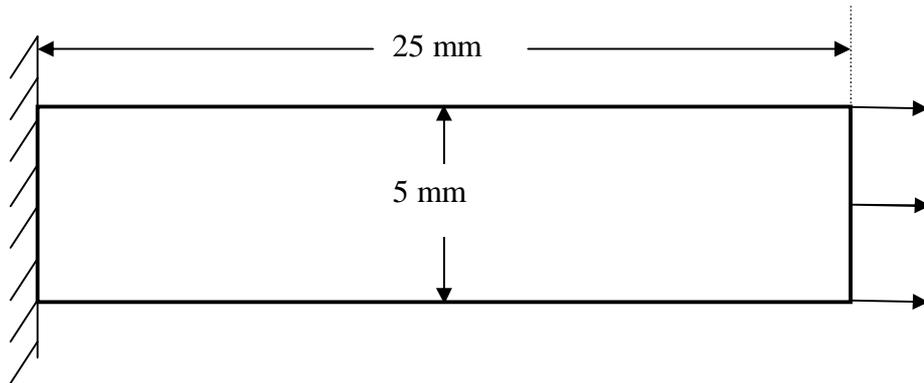
Figure 4-1: Model geometry, boundary condition and loading for FE analysis on tensile tests of *urushi* samples.

4.2.1.2 Modelling the bi-material stress measurement experiment

The response of Japanese lacquer to varying environmental conditions was investigated by examining the deflection of a glass substrate coated with a thin film of *urushi* subjected to changes of humidity. This deflection, measured using phase-shifting interferometry, was then used to determine the two in-plane hygral stress components. Results were compared for two sample conditioning regimes—subjected to intense UV ageing and no ageing—each at a range of relative humidity (RH) steps. The sample structure and dimensions are shown in Figure 4-2, where it can be seen that an *urushi* film of approximately 0.02mm thicknesses is deposited on a glass substrate of approximately 0.2mm thickness and 22mm radius. On exposure to varying humidities, the *urushi* film absorbs or desorbs moisture, resulting in hygroscopic expansion or contraction, respectively. Moisture absorption, and hence hygroscopic expansion, of the glass is assumed to be negligible and, therefore, the glass will provide a constraint against the hygroscopic expansion or contraction of the *urushi* film, creating varying hygroscopic stresses. This mechanism has been modelled using an FE model of the experiments in ABAQUS. The solution domain is shown in Figure 4-2, where the axisymmetry of the problem has enabled simplification of the disc system used in the

experiments. The boundary conditions were such that the lower edge of the disc is only free to displace in the *x* direction, as shown in Figure 4-2. The moisture boundary conditions were constant moisture content at the upper surface to represent the environmental RH and zero flux at the interface between the lacquer and the substrate. Initially the right hand side boundary was allowed to be permeable under the same conditions as the upper surface, but the ratio of depth to breadth was found to be sufficiently small that radial fluxes were insignificant and as a consequence all the numerical experiments discussed in this paper were performed with an impermeable sidewall.
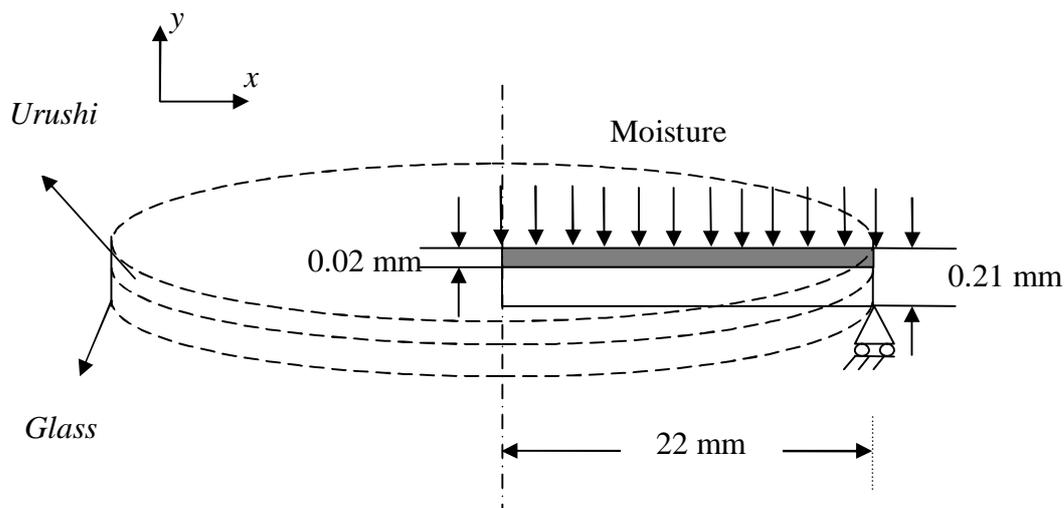
Figure 4-2: Simplified geometry and boundary conditions for the bi-material film samples.

4.2.1.3 Modelling bending behaviour

Over 4 centuries of fluctuating environmental conditions have led to the formation of micro-cracks on the main *urushi*-covered surfaces in the Mazarin Chest. The traditional Japanese consolidation method of lacquerware objects, known as *urushi-gatame,* consists of applying a diluted layer of fresh *urushi* to the damaged (aged) surface in order to fill any micro-cracks and restore its original gloss [164]. It is unknown, however, whether this procedure is effective in arresting crack propagation in the long term or whether it would accelerate damage mechanisms leading to propagation of pre-existing micro-cracks. This poses a dilemma to Western museum conservators, whose approach to conservation is based on minimum impact on the art piece, as opposed to their Japanese counterparts, who apply the traditional methods used in the creation of the art piece to bring it back to its original appearance, even if this means adding or removing substantial parts of it. In order to assess

the effect of the traditional Japanese *urushi gatame* consolidation, a virtual experiment was designed to measure displacement fields around a controlled groove (representing a crack) on an aged *urushi* film before and after the consolidation procedure. The basic idea, illustrated in Figure 4-3, is to predict the displacement field across a crack (or 'v' groove) in the plane of the film surface when the substrate expands and strains the film and to study the effectiveness of this consolidation in the prevention of crack initiation. Making use of the results of material characterisation and a validated modelling methodology, the bending behaviour of *urushi*/aluminium bi-layer strip samples with different shape of notch in the middle, the samples with and without this consolidation and the samples with fresh and aged *urushi* for consolidation were studied through FE analysis. The model geometry, boundary conditions and loading for FE analysis on bending tests for a simple 'v' groove notched *urushi*/aluminium samples are shown in Figure 4-3.
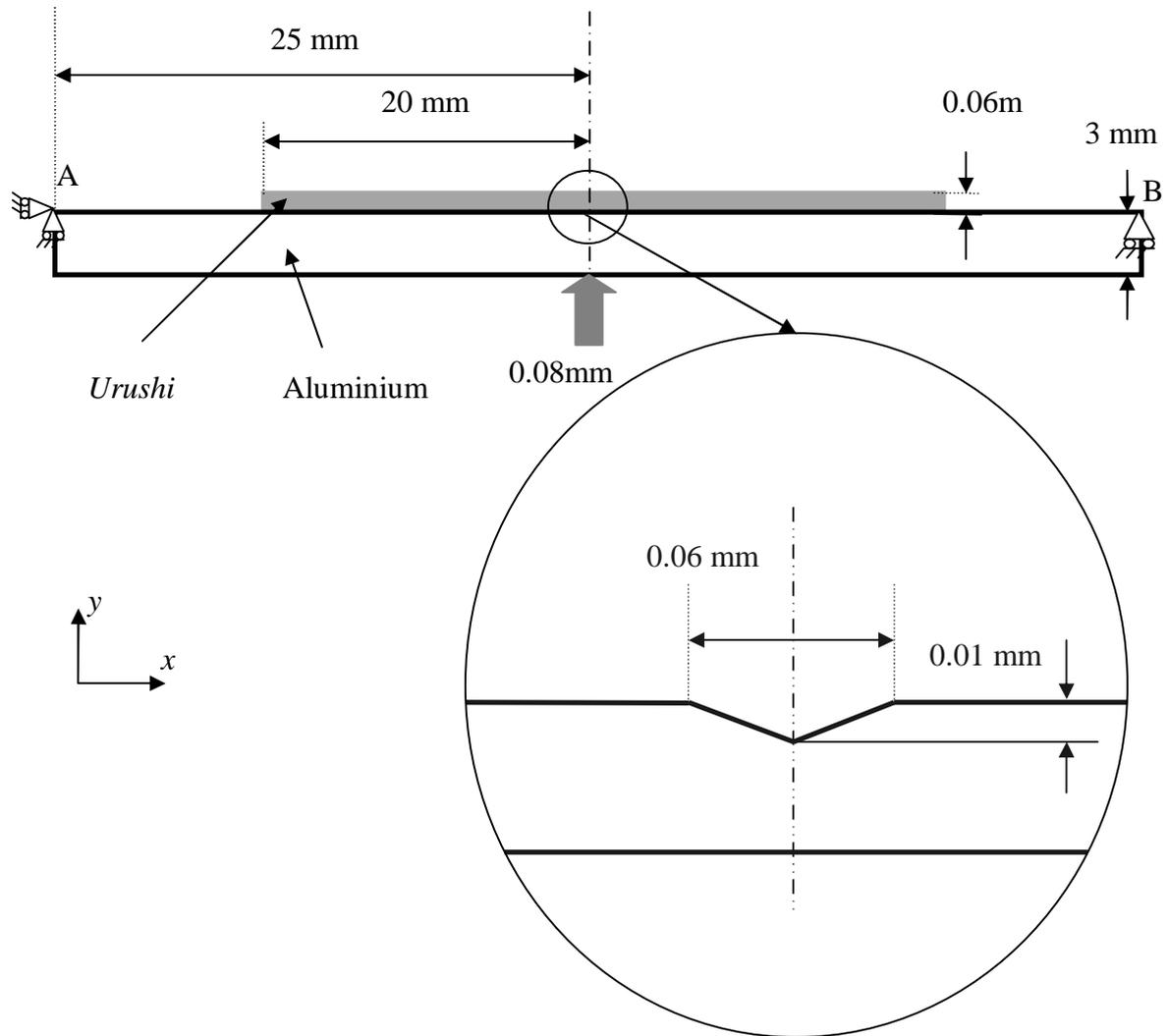
Figure 4-3: Model geometry, boundary condition and loading for FE analysis on bending tests for notched *urushi*/aluminium samples.

This FE model can be simplified significantly by taking advantage of the symmetry of the bi-layer strips. Symmetry can only be considered for use in FEA models if the loading, original and deflected shapes are symmetrical and for the bi-layer strips, planes of symmetry exist on both transverse axes. This is exploited for 2D models as shown in Figure 4-4, resulting in a model half the size of the original geometry and a simplified Model geometry, boundary condition and loading for FE analysis, as shown in Figure 4-5.
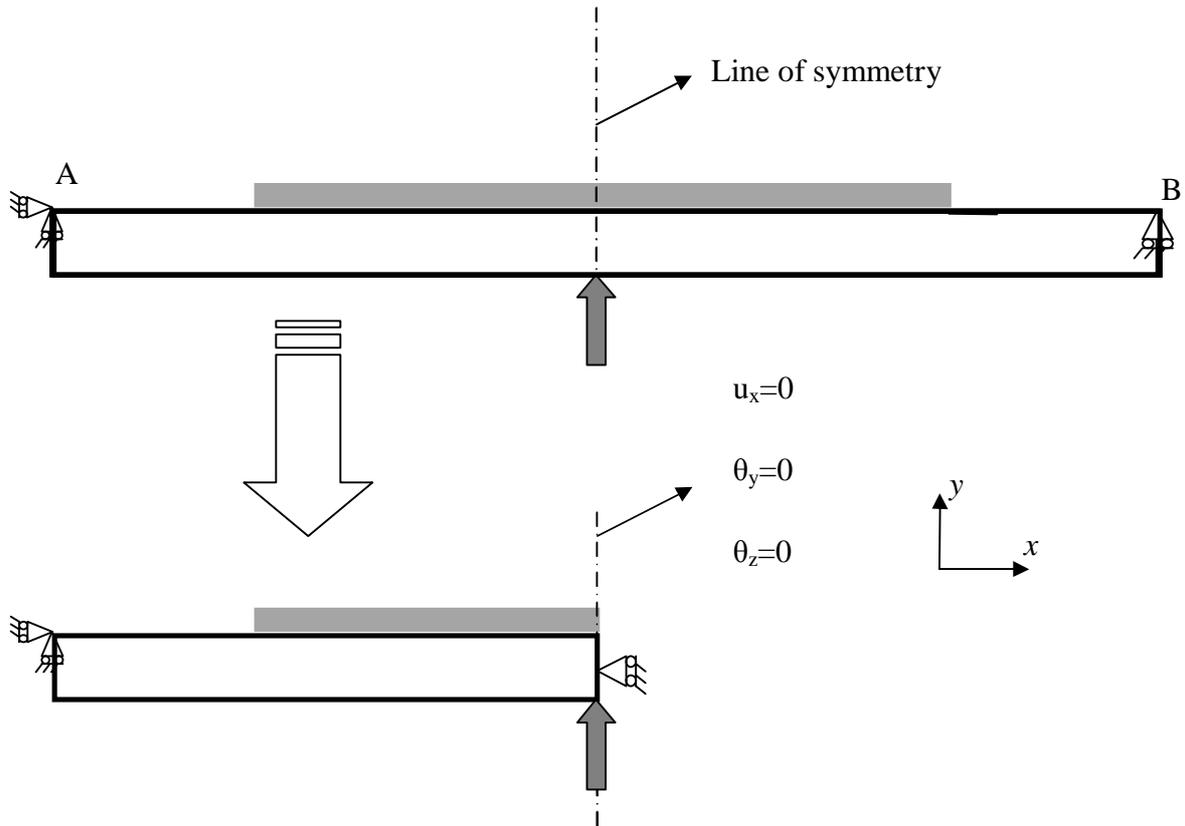
Figure 4-4: Planar symmetry used to simplify the bi-material strip model.
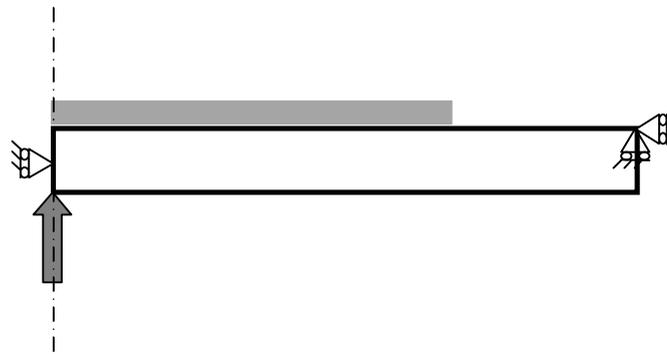
Figure 4-5: Simplified model geometry, boundary conditions and loading for FE analysis on bending tests for notched *urushi*/aluminium samples.

4.2.2 Element choice and meshing

Accurate results from the FEM depend on the choice of element, the number of elements used and where the nodes are located. After creating the geometry within the pre-processor, an FE mesh was applied to it. Several factors were considered when meshing the models created in this work, such as element type, mesh density, geometric and material non-linearity.

The choice of elements is crucial to not only the stress/strain results obtained from an analysis, but the deformed shape as well.

4.2.2.1 Element choice

The ABAQUS element library provides a complete geometric modelling capability. The selection of element types was based on consideration of the samples response under various loads. In this project, the *urushi* bulk samples were stretched by tensile loading, with non-linear deformation observed, bi-layer disc samples were subjected to a hygro-mechanical load resulting in a bending deformation and the bi-layer strip samples experienced 3-point bending, causing a failure if the load was sufficient.

Continuum or solid elements, among the different element families (shell elements, beam elements, rigid elements, membrane elements and so on), can be used to model the widest variety of components. Conceptually, continuum elements simply model small blocks of material in a component. Since they may be connected to other elements on any of their faces, continuum elements, like bricks in a building or tiles in a mosaic, can be used to build models of nearly any shape, subjected to nearly any loading. ABAQUS has a solid element that can be used in coupled temperature-displacement analysis, which can be used for modelling hygro-mechanical interaction in this project.

In this PhD project, 2 dimensional elements were adopted in order to achieve a reduction in computational cost for the bi-layer model. 2D elements can be quadrilateral or triangular. There are three classes that are used most commonly as shown in Figure 4-6. Plane strain elements, normally used to model thick structures, assume that the out-of-plane strain, ε_{33}, is zero. Plane stress elements, suitable for modelling thin structures, assume that the out-of-plane stress, σ_{33} is zero. Axisymmetric elements are suitable for analyzing structures with axisymmetric geometry subjected to axisymmetric loading [165].
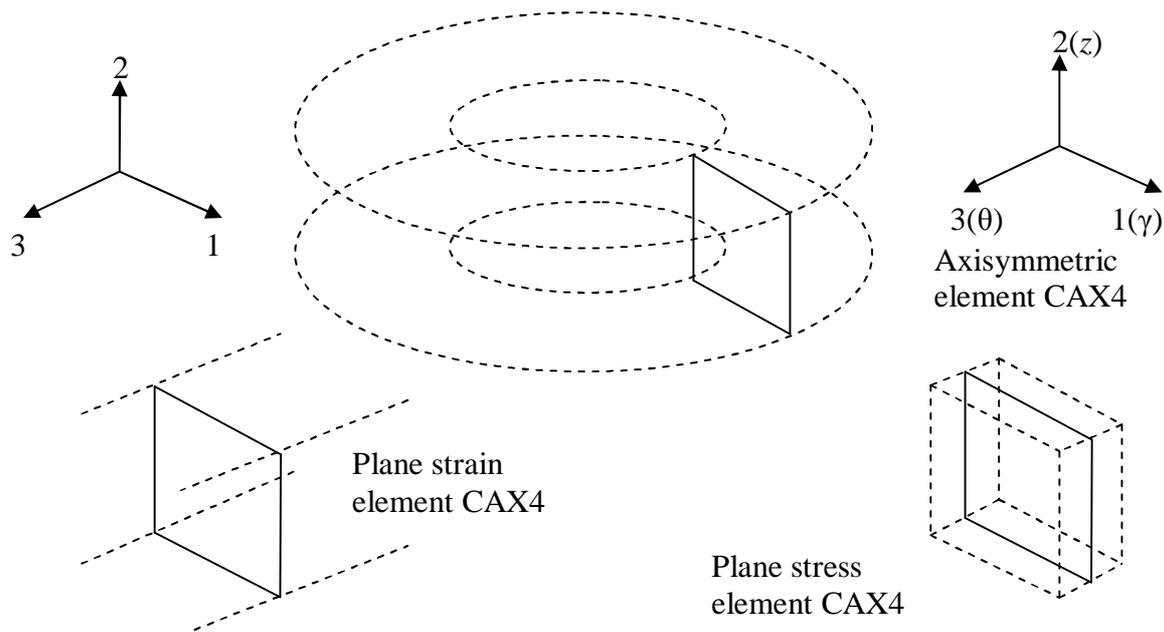
Figure 4-6: Plane strain, plane stress, and axisymmetric elements.

4.2.2.2 Meshing methodology

Meshing the *urushi* bulk sample is simple thanks to its standard rectangular shape and homogenous material properties. Meshing the bi-layer disc sample used for the stress measurement tests and a bi-layer strip sample for the bending tests is more challenging owing to the presence of very thin *urushi* layer compared to the overall dimensions of the substrates. The addition of a groove and *urushi* filling as consolidation in the bending tests further complicates the meshing requirements. The meshing strategy was adopted after considering the geometric factors.

Two methodologies were considered to mesh the bi-layer samples. The first method was to use a continuous mesh, which transitioned from a fine mesh to a course mesh while maintaining mesh continuity by sharing nodes between elements. This method required partitioning of the joint geometry in multiple regions and mesh seeding regions based on the required mesh density. The second method was to use dissimilar meshes in the *urushi* layer and the substrates and to join them using tie constraints. Tie constraints make the translational and rotational motion, as well as all other active degrees of freedom, equal for nodes on the two sides of the tie constraint. The first method required more pre-processing time than the second method. However, the use of tie constraints involves solution of contact

algorithms during the simulation that increases the computational time and resource requirement for an analysis. Thus, the first method was used to develop all the meshes.

A number of meshing methods were available in ABAQUS and each geometric region was meshed based on an appropriate meshing method. In the case of modelling the mechanical test for an *urushi* bulk sample, the rectangular samples were simply meshed with a structured mesh, which provided a mesh of rectangular shaped elements, as shown in Figure 4-7. For modelling the stress measurement experiment using a bi-layer disc *urushi*/glass sample, the rectangular layers of the *urushi* and the substrate layers were both meshed with a structured mesh, which provided a mesh of rectangular shaped elements (seen in Figure 4-8). However, for considerations of the much smaller thickness of the *urushi* layer than that of the substrate layer, the section of the *urushi* layer has a higher density of mesh than that of the substrate layer to avoid excessive computational requirements and achieve adequate accuracy of the analysis in the interesting section, the *urushi* layer. In the case of modelling the bending behaviour of the *urushi*/substrate strip shown in Figure 4-9, the sections of *urushi* and substrate layers were given different mesh density. The area near the notch is meshed using a fine mesh due to a gradient of stresses and strains in this area.
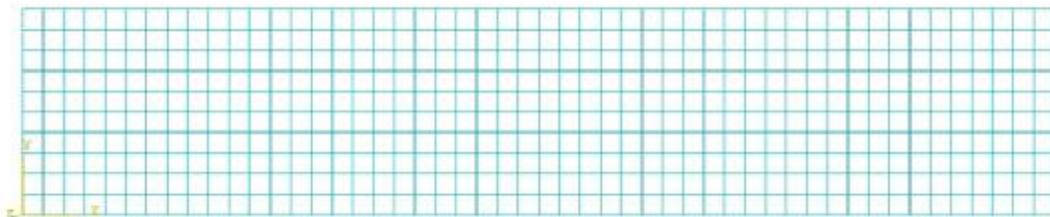
Figure 4-7: Mesh of a bulk sample of rectangular *urushi* film.
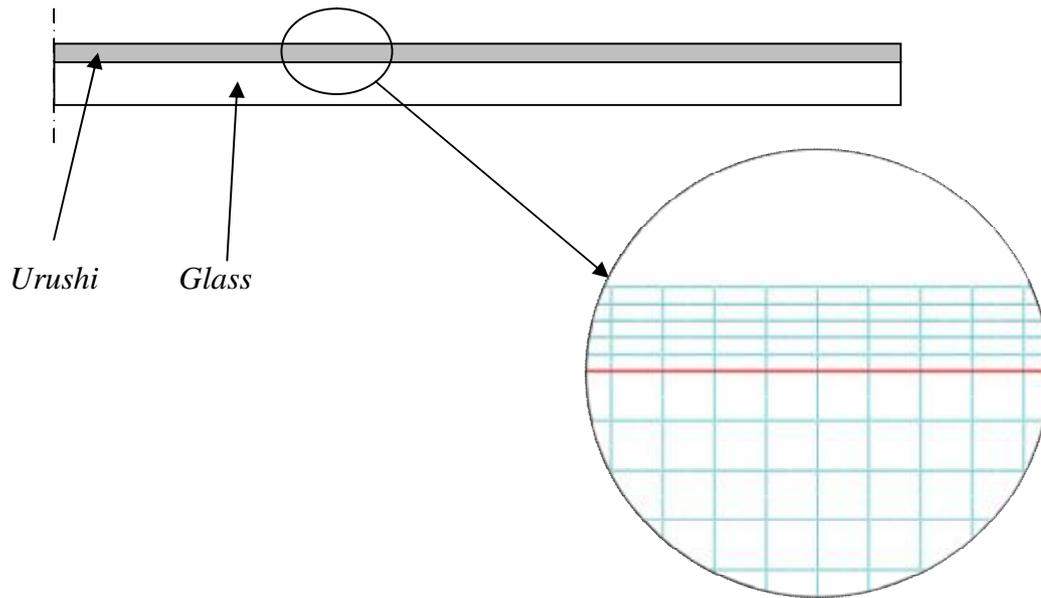
Figure 4-8: Overall and detailed mesh of the bi-layer disc sample used in the stress measurement experiment.
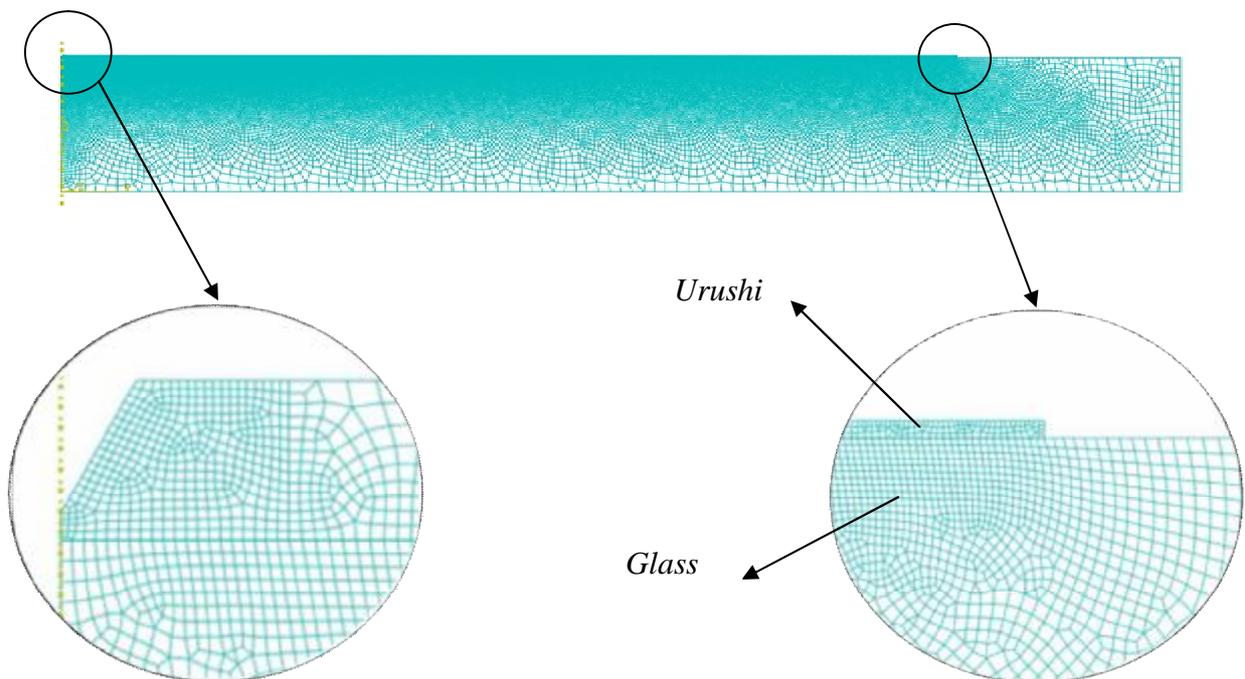
Figure 4-9: Overall and detailed mesh of the bi-layer strip sample used in bending tests.

Urushi/substrate bi-layer structures are difficult to mesh, mainly because of the previously mentioned small thickness of the *urushi* layer compared to the substrate layer and the existence of stress concentrations in the notch area in modelling the bending of the notched

bi-layer strip. To achieve adequate accuracy and computational economy, a convergence study with different mesh densities was performed. A series for models of each modelling case were analysed with various mesh densities, element types and element formulation in order to reduce numerical errors and determine the best compromise between solution times and accuracy.

4.2.3 Thermal and diffusion analysis

ABAQUS provides a capability for both thermal and diffusive analysis. However, only thermal analysis can be coupled with mechanical analysis for the purpose of modelling thermo-mechanical interactions. To model the hygro-mechancial interaction of the bi-layer structure, moisture diffusion analysis was carried out by using the analogy between heat transfer and diffusion equations. The boundary conditions for modelling time dependent diffusion were implemented in the FE models by following this analogy between thermal and moisture diffusion. Temperature dependent moisture diffusion was achieved by including temperature dependent moisture properties. The analogy is illustrated in Table 4-1.

Table 4-1: Analogy between Fickian moisture diffusion and heat transfer.

Properties	Moisture diffusion	Heat Transfer
Field variable	Normalised Moisture concentration C/C_{sat}	Temperature
Density	1	Density
Conductivity	$D \times C_{sat}$	Conductivity
Specific Heat	C_{sat}	Specific Heat

where C_{sat} is the saturated moisture concentration, and D is the diffusion coefficient. In the samples with glass substrates, moisture diffusion through the substrate was assumed to be negligible.

Determination of hygroscopic stresses due to moisture diffusion was carried out using sequentially coupled hygro-mechanical analysis. In the sequentially coupled analysis, an uncoupled transient hygroscopic analysis was carried out to determine the moisture concentration distribution and the results were used as the input to a mechanical analysis to determine the hygroscopic stresses. Identical FE meshes were used for mechanical and diffusion analysis to maintain mesh compatibility for transfer of results between analyses.

4.3 Implementation of user defined material models

ABAQUS provides an extensive library of constitutive models to cope with different materials and analyses. However, if the proposed constitutive model is not available, ABAQUS provides a powerful function which implements user defined material models via a user subroutine, named user material (UMAT).

This function, UMAT, acts as an interface between ABAQUS and user defined material behaviour, and can be used for any procedure involving mechanical behaviour. At the start of a computational increment for an integration point, the ABAQUS main program passes the initial value of variables to the corresponding variables in the UMAT subroutine. The UMAT subroutine updates the stress tensors and state values, which are then passed back to the ABAQUS main program for the next increment. To illustrate this cooperative process of UMAT and ABAQUS, the computational flow of a creep analysis at a given integration point is shown in Figure 4-10.

Step 1

At equilibrium time t_n, ABAQUS Provides:
Total strain $\varepsilon(t_n)$,
Stress $\sigma(t_n)$
Time increment Δt

Step 2

ABAQUS generates strain increment $\triangle\varepsilon(t_n)$,
UMAT is called to calculate:
Creep strain increment $\triangle\varepsilon_c(t_n)$
Stress increment $\triangle\sigma(t_n)$

Update stress tensor:
$\sigma(t_n+\Delta t)=\sigma(t_n)+\triangle\sigma$

UMAT

Step 3

UMAT returns $\sigma(t_n+\Delta t)$ to ABAQUS
and ABAQUS updates total strain
$\varepsilon(t_n+\Delta t)=\varepsilon(t_n)+\triangle\varepsilon(t_n)$

Step 4

ABAQUS judges equilibrium

Yes

No

Iterative times are greater than the default times. ABAQUS reduces time increment and returns to Step 1.

$n=n+1$,ABAQUS returns to Step 1 and starts for next increment.

Return to Step 2 and starts next iteration of this increment

ABAQUS Main Program

Figure 4-10: Flow chart of cooperative computation between UMAT and ABAQUS main program.

FORTRAN is used for coding the UMAT subroutine and ABAQUS 6.9 requires *Intel Visual FORTRAN 9.0* and *Microsoft Visual Studio .NET 2005* for compilation of the code. A detailed description of the compilation of the user subroutine and its implementation is given in Chapter 7.

4.4 Summary

The computational methodology involved in this research was discussed in this chapter. The methods adopted in the development of FE models were discussed. Geometries for 2D models were selected and appropriate simplifications of the model geometries were performed in terms of the models' symmetry. To discretise the geometries, continuous meshes were used, with considerations of element type, mesh density, geometric and material non-linearity. Hygro-mechanical analysis was introduced using a sequentially coupled method. In order to implement non-standard material models, a UMAT subroutine technique was introduced which then cooperates with the ABAQUS main program.

Chapter 5 Characterisation of PU Lacquer Film

5.1 Introduction

Urushi lacquer is expensive and difficult to apply. Hence, it is useful to investigate a synthetic lacquer as a comparison to the *urushi* and as a cost effective substitute for the development of experimental techniques and models [18]. As a result, a PU lacquer was selected as the synthetic lacquer material as it has been found to have similar material properties to *urushi* [18]. PU lacquer is a complex synthetic polymer. The mechanical properties of PU lacquers are influenced by the in-service environment, which may affect their function as protective coatings. To date, limited research work has been published on the mechanical properties of PU lacquer films under environmental ageing conditions. This chapter presents an investigation of the mechanical and hygroscopic behaviour of a commercial PU lacquer film. By means of water absorption and desorption tests, the diffusion coefficient and coefficient of hygroscopic expansion were determined. Tensile tests at constant displacement rates and creep tests under various UV/humidity ageing conditions were used to investigate the dependence of material properties on environmental conditions. A modified Burger's model with environment dependent parameters is introduced to model the mechanical behaviour of the PU lacquer in typical service conditions.

5.2 Material characterisation

5.2.1 Hygroscopic expansion

Figure 5-1 shows the hygroscopic strain from the hygroscopic expansion tests as a function of the moisture content. It can be seen that the data fit a straight line, indicating a moisture independent coefficient of hygroscopic expansion (CHE). The CHE was evaluated from the slope of the best first order fit, giving a value of 0.0025 (wt %)$^{-1}$, which is of the same magnitude with CHE of a similar material [166].
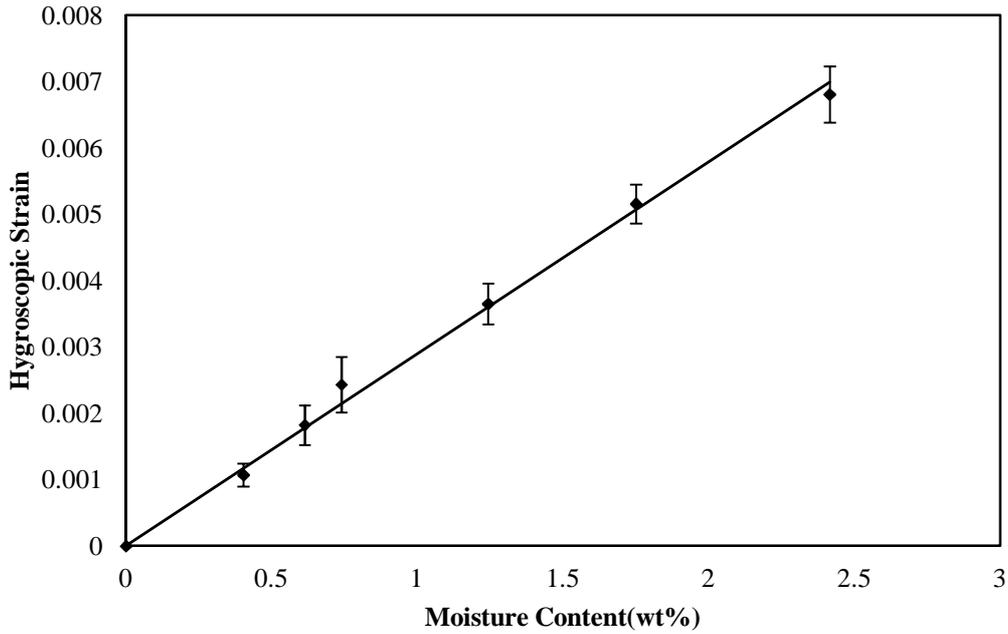
Figure 5-1: Hygroscopic strain for saturated PU samples as a function of moisture content.

5.2.2 Moisture sorption equilibrium and kinetics

Relationships between equilibrium weight gain due to moisture uptake and relative humidity were investigated by fitting several absorption isotherm models to the experimental data of the third cycle of absorption data. The third cycle was chosen because the equilibrium weight gain was found to reach a constant value after 3 cycles of absorption and desorption. Figure 5-2 shows the curve fitting of the two different absorption models, Henry's law and the Flory-Huggins model.

It is evident from Figure 5-2 that Henry's law fails to interpret the relationship between experimental data of equilibrium weight gain and relative humidity. This indicates a concentration dependent interaction of water molecules with the polymer chains, which is not allowed by Henry's law and potentially leads to a concentration dependent diffusion coefficient [98, 167]. The upward curvature of the sorption isotherm curve seen in Figure 5-2 is sometimes attributed to swelling of the polymer which may cause increased exposure of sites for preferential water sorption or the cluster formation of water molecules inside the polymer [168]. This behaviour is found to be satisfactorily modelled by Flory-Huggins model according to the curve fit result shown in Figure 5-2.
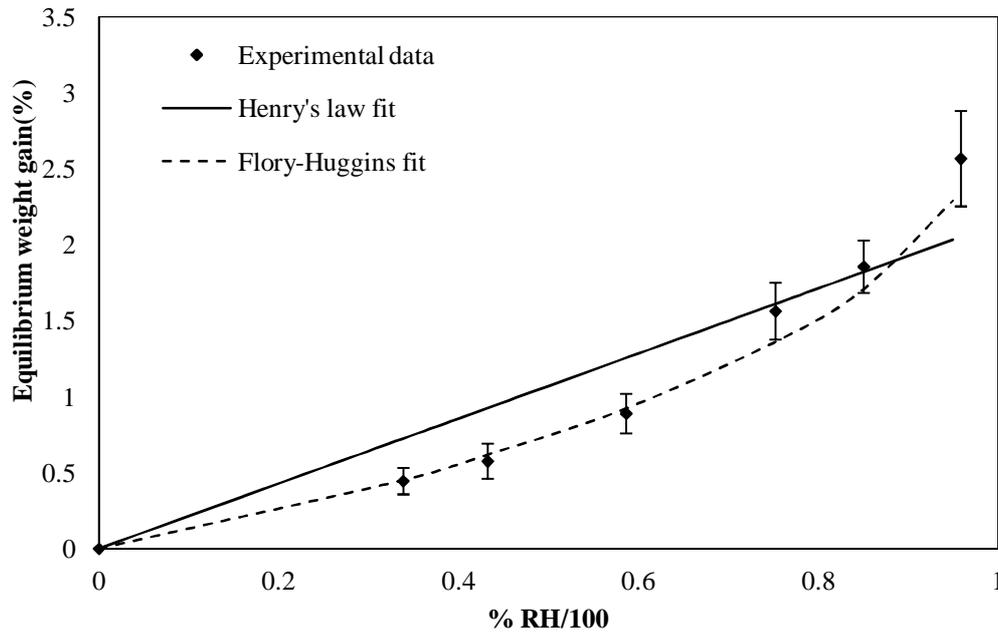
Figure 5-2: Equilibrium weight gain as a function of relative humidity and comparison with the fitted results for two absorption models.

In Figure 5-3 and Figure 5-4 the average percentages of water gain/loss from the first cycle of absorption and desorption (sample thickness, 0.32mm) are plotted as a function of $\sqrt{t}/l$, in which t is the time of absorption/desorption and l is the half thickness of samples in millimetres. As described in Chapter 2, a Fickian diffusion behaviour was assumed and fitted to the experimental data using a nonlinear regression technique [169]. The good fit, quantified by the R^2 value of greater than 0.98 for the fits of Fickian diffusion model to all experimental data, suggests that Fickian behaviour is dominant. The experimental data showed good repeatability with an average standard deviation of 0.13% at each data point of moisture content. The diffusion coefficients obtained for both absorption and desorption at each relative humidity are presented in Table 5-1. Typical diffusion curves are plotted in Figure 5-5 for 3 cycles of absorption and desorption between dry conditions and 85% RH.
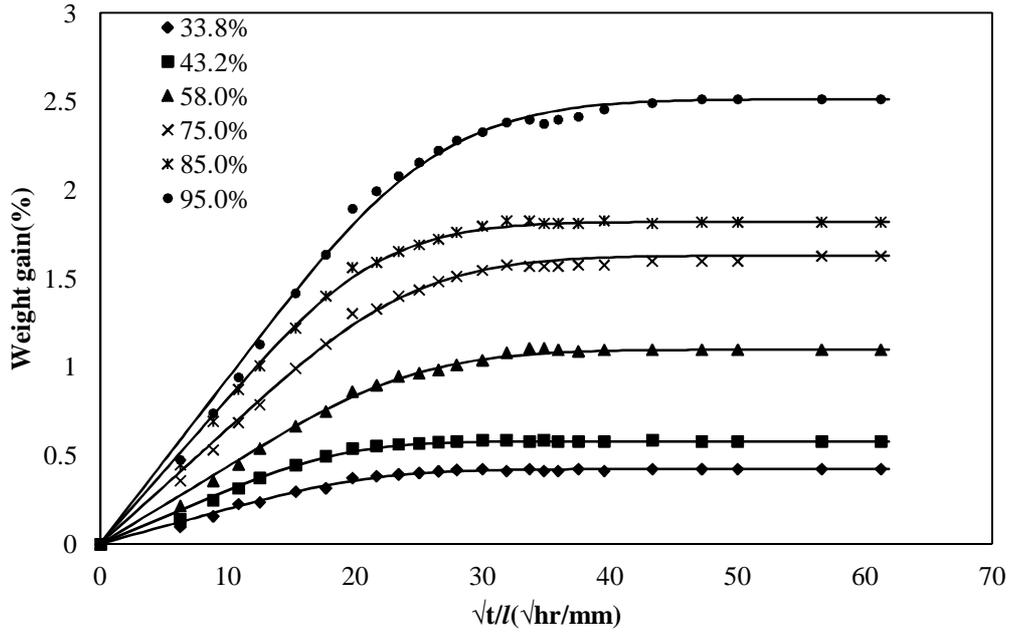
Figure 5-3: Moisture absorption curves for 0.32 mm thick PU lacquer films at different RH during the first cycle. Symbols are used to represent the experiment data points and the solid line the fitted Fickian diffusion model.
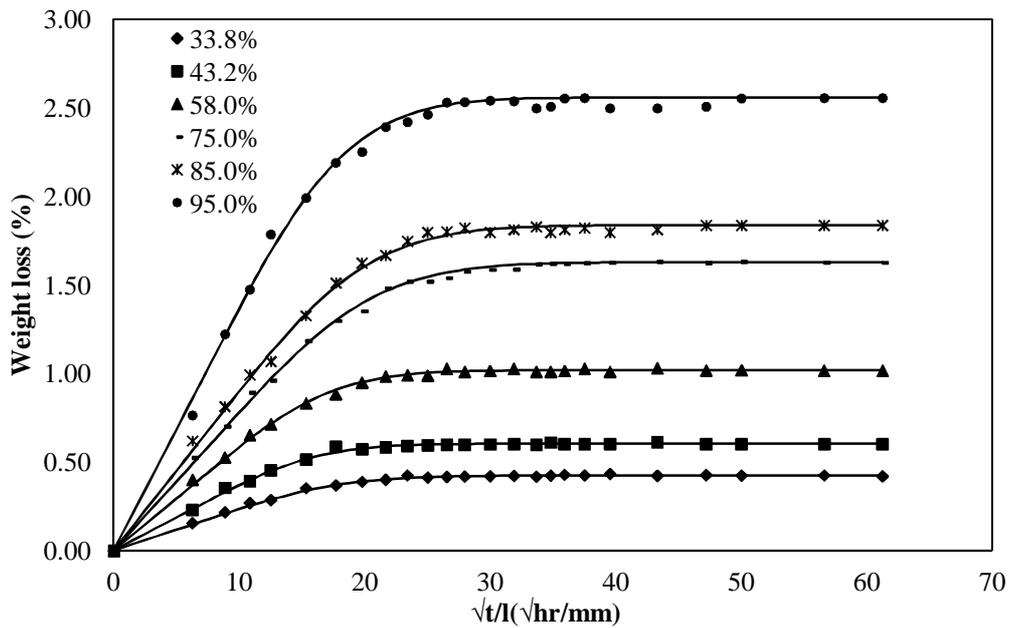
Figure 5-4: Moisture desorption curves for 0.32 mm thick PU lacquer films moistened at different RH during the first cycle. Symbols are used to represent the experiment data points and the solid line the fitted Fickian diffusion model.

Table 5-1: Diffusion coefficients and moisture content of samples during 3 cycles of absorption-desorption test.

	Relative Humidity (%)	Moisture Content (%)	Diffusion coefficient for absorption (10^{-7} mm^2/sec)	Diffusion coefficient for desorption (10^{-7} mm^2/sec)
1st cycle	33.8	0.424±0.037	4.692	6.721
	43.2	0.580±0.049	6.021	8.257
	58.0	0.892±0.021	3.785	4.263
	75.0	1.598±0.069	3.296	5.215
	85.0	1.820±0.043	4.368	5.258
	95.0	2.514±0.078	4.81	6.365
2nd cycle	33.8	0.432±0.023	5.928	6.125
	43.2	0.639±0.054	6.919	6.592
	58.0	0.915±0.058	7.239	7.128
	75.0	1.639±0.047	4.988	6.878
	85.0	1.833±0.098	6.215	5.248
	95.0	2.602±0.103	5.875	5.398
3rd cycle	33.8	0.445±0.035	4.958	5.892
	43.2	0.577±0.082	6.021	6.987
	58.0	0.896±0.051	6.958	7.121
	75.0	1.563±0.073	5.122	5.539
	85.0	1.856±0.119	7.444	7.147
	95.0	2.569±0.090	5.323	6.378
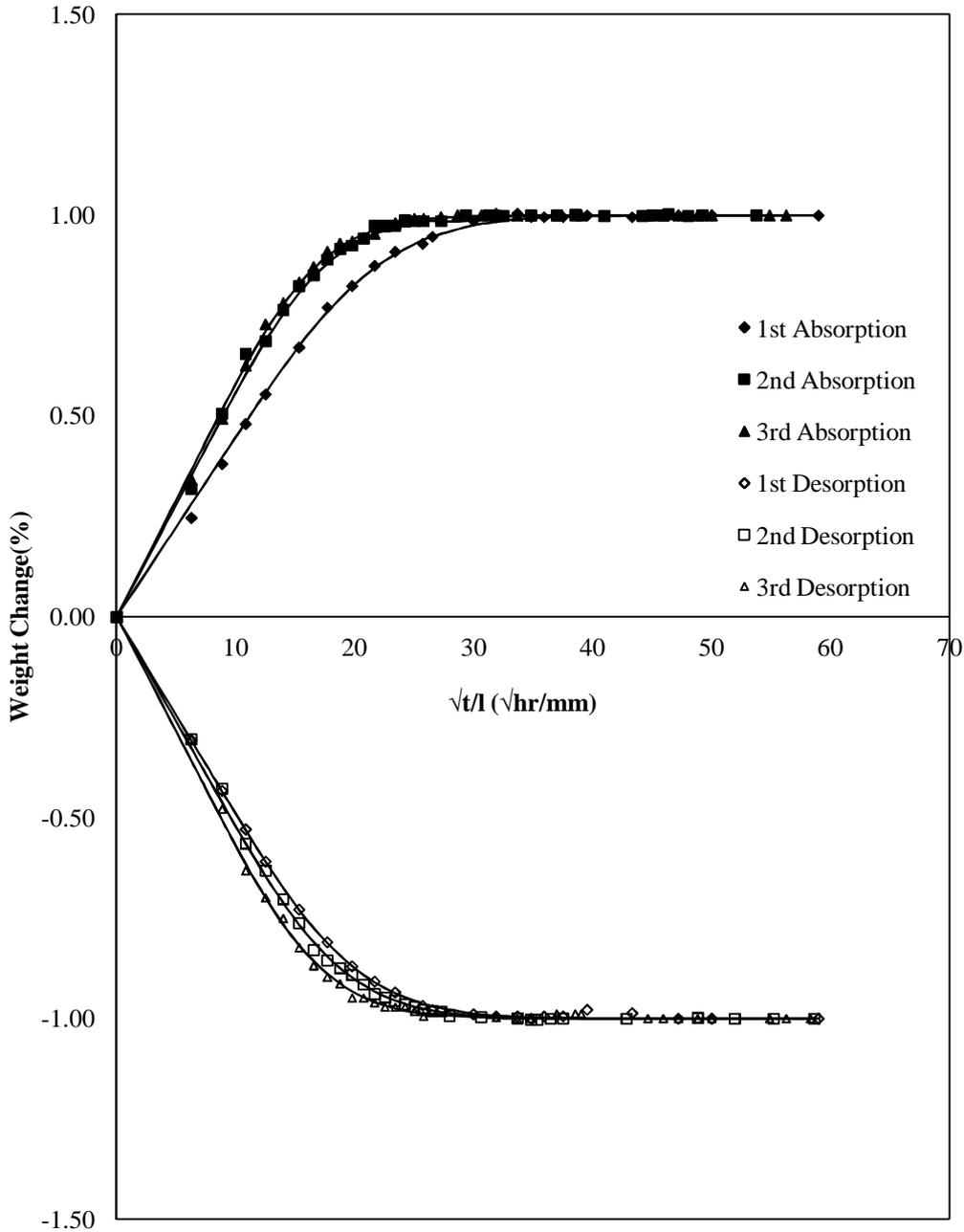
Figure 5-5: Normalised moisture absorption and desorption curves for 0.32 mm thick PU lacquer samples conditioned at 85% RH.

From Figure 5-5, and Table 5-1, which shows the extracted diffusion coefficients, it can be seen that the rate of the first absorption (and desorption) is lower than subsequent cycles, but that the second and third cycles differ little. The similar behaviour has been identified for a single part epoxide adhesive, FM73-M [170]. This may be due to changes in the structure of the polymer occurring during the first cycle, leading to different sorption behaviour of the material diffusion in later cycles. It can also be seen in Table 5-1 that desorption is faster than absorption in the first cycle. A possible explanation for this is that phenomena such as the

chemical binding of water, swelling and micro cracking take place during absorption while desorption is dominated by the release of free water, resulting in a shorter time for desorption to reach equilibrium [171-172].

5.2.3   Stress-strain plots

Tensile stress-strain curves under a constant displacement rate of 1 mm/min were obtained for PU samples previously exposed to UV irradiation. Figure 5-6 shows tensile stress-strain curves from these tests for different periods of irradiation. It can be seen from this figure that as exposure to UV radiation increases the elastic region of the stress-strain curve and Young's modulus and failure stress significantly increase (Table 5-2). This indicates that UV ageing greatly increases the stiffness and strength of PU lacquer films, however, a corresponding decrease in the strain to rupture is also observed. The toughness, which is a measure of the energy material can absorb before rupture, also decreases with time of UV irradiation. The results indicate that PU lacquer films tend to become increasingly strong but brittle on exposure to UV irradiation.
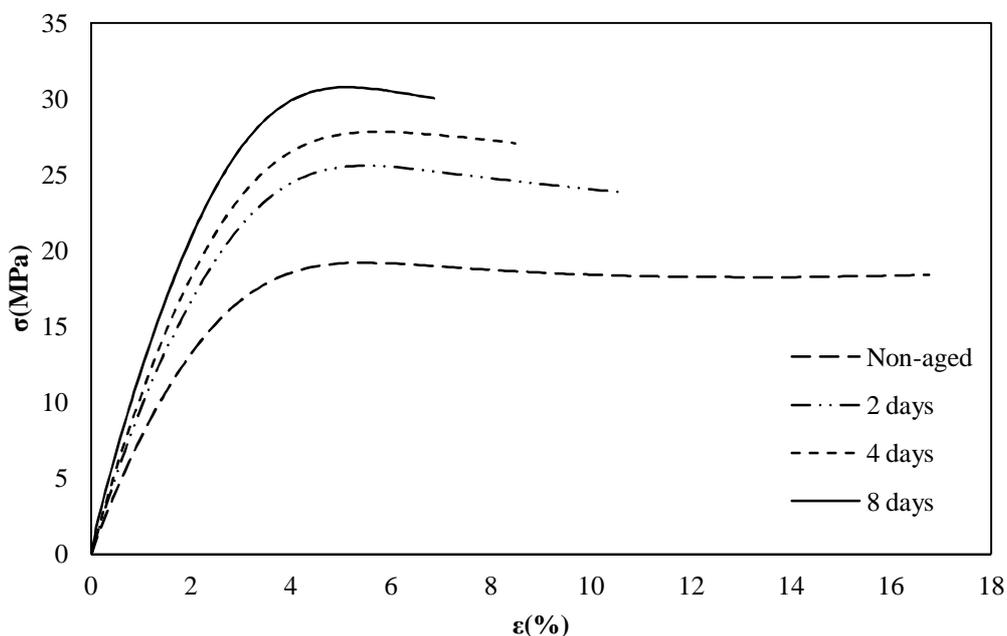
Figure 5-6: Stress-strain curves from tensile tests on PU samples after various periods of UV irradiation.

Table 5-2: Mechanical properties of PU films (obtained from the results of tensile tests with loading displacement speed of 1 mm/min for saturated samples under 45% RH, 25 °C) as a function of UV irradiation time.

Irradiation time (days)	Young's modulus (MPa)	Tensile Strength (MPa)	Rupture strain (%)
0	684.3±66.2	18.8±3.2	16.4±3.6
2	868.1±49.5	25.3±2.7	11.2±4.7
4	1018±54.3	28.2±3.1	9.8±2.2
8	1300±108	31.0±4.5	8.3±1.9

Stress-strain curves from tensile tests on samples conditioned to saturation at different RH are shown in Figure 5-7. Saturated moisture content, tensile strength, and rupture strain are listed in Table 5-3. It is seen that the strain at rupture increases and the Young's modulus decreases with increasing moisture content of samples, which indicates that the PU molecular chains become more flexible with more moisture uptake, with the absorbed moisture serving as a plasticiser [49]. Plasticisers are utilised to reduces the entanglement and bonding between molecules, therefore increases their volume and mobility and improve the workability and flexibility of plastics due to the modification of the free volume of polymer resulting from the water absorption [49, 173-174], often at the sacrifice of strength and stiffness.
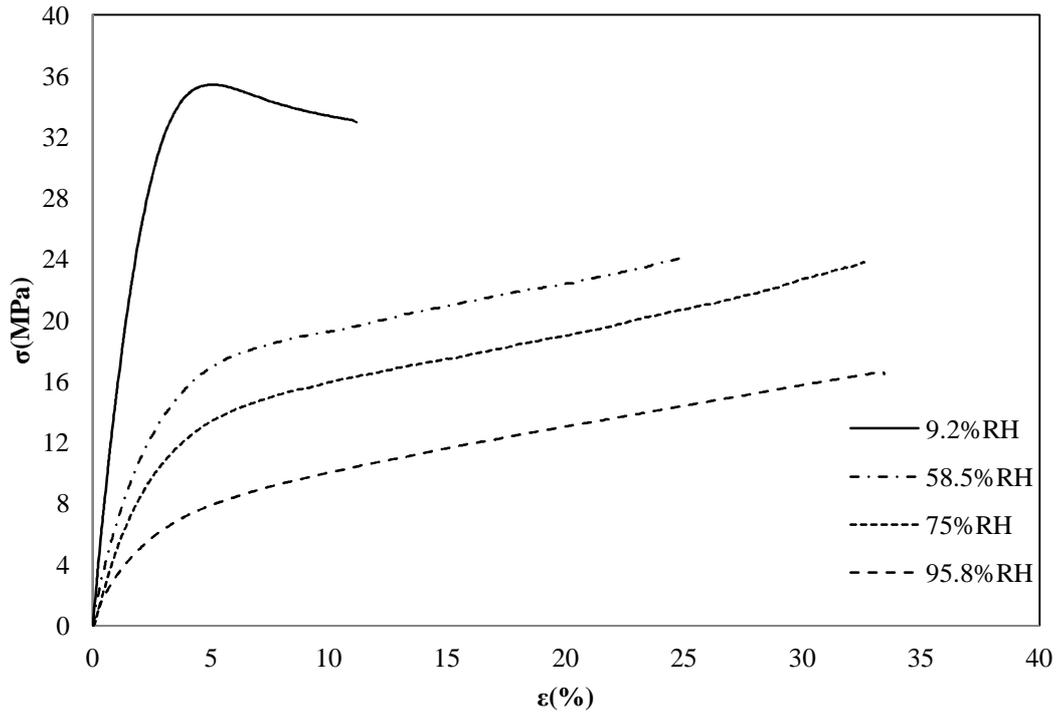
Figure 5-7: Stress-strain curves from tensile tests on non-UV aged samples at different relative humidities at a loading displacement speed of 1 mm/min.

Table 5-3: Mechanical properties of fresh PU lacquer films (obtained from the results of tensile tests with loading displacement speed of 1 mm/min for saturated samples under 25 °C, and different RH) as a function of moisture content.

Relative humidity (%)	Moisture content (%)	Young's modulus (MPa)	Tensile Strength (MPa)	Rupture strain (%)
9.2%	0.05±0.02	1542±152.8	35.4±3.3	11.1±3.8
58%	0.78±0.08	587.3±48.7	24.2±3.5	24.9±7.1
75%	1.29±0.11	341.1±33.6	23.6±5.5	32.5±11.2
95.2%	2.62±0.23	195.3±29.8	16.4±4.7	33.4±9.3

It was also seen that the stress-strain curves showed a strong dependency on the loading rate, which is a typical mechanical property of polymers. Figures 5-8 and 5-9 show that for a specific environmental condition both non-aged and UV-aged PU samples have higher Young's modulus and lower strain to failure at higher loading rates. UV exposure is also found to make PU film stronger through the comparison of the figures 5-8 and 5-9. It seems that UV-ageing involves additional crosslinking to give a more highly ordered structure. This crosslinking is accompanied by an increase of stability which can enhance the material strength [54]. The obtained results are in good agreement with those reported in several papers [175-177]. Subocz et al. [176] have shown that the long-term action of UV mainly

consisted of additional crosslinking to form new supramolecular structures with higher ordering. In the same context, Claude et al. [175] have recently concluded that the formation of a crosslinked structure can be considered to explain the increase of the Young's modulus of the UV-exposed polymer.
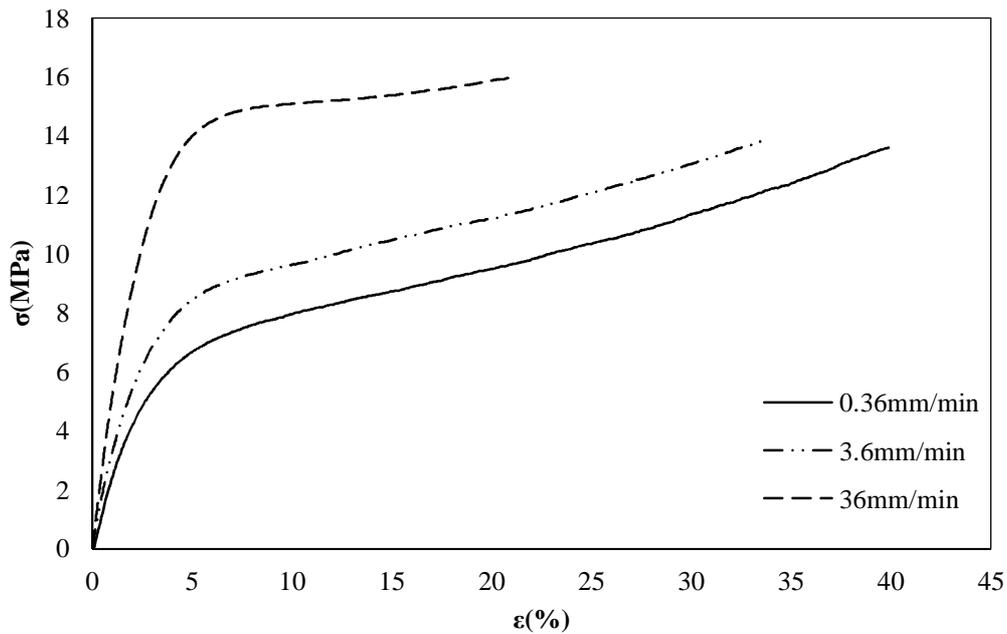
Figure 5-8: Stress-strain curves of tensile tests on non-aged PU lacquer film samples at saturation under 75% RH under different displacement rates.
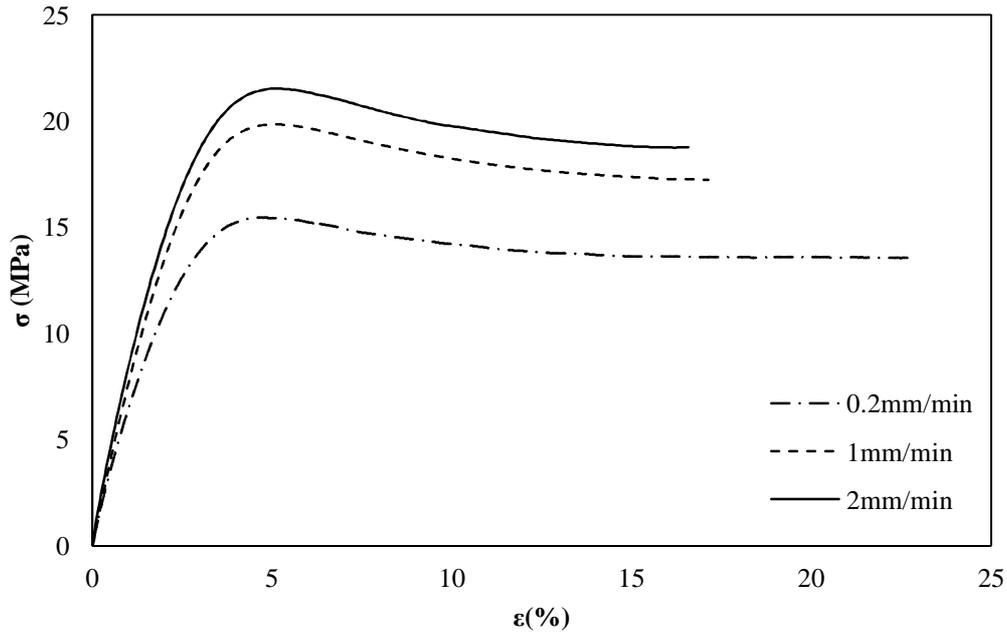
Figure 5-9: Stress-strain curves of tensile tests on 2-day aged PU lacquer film samples under room conditions at different displacement rates.

5.2.4   Creep tests

Creep tests under room humidity and temperature were performed in order to characterise the general viscoelastic behaviour of the PU samples. Figure 5-10 shows tensile creep curves of non-aged PU lacquer at different stresses, indicating the highly time-dependent strain of a typical viscoelastic material. The curves show the initial instantaneous strain, followed by primary and secondary creep.
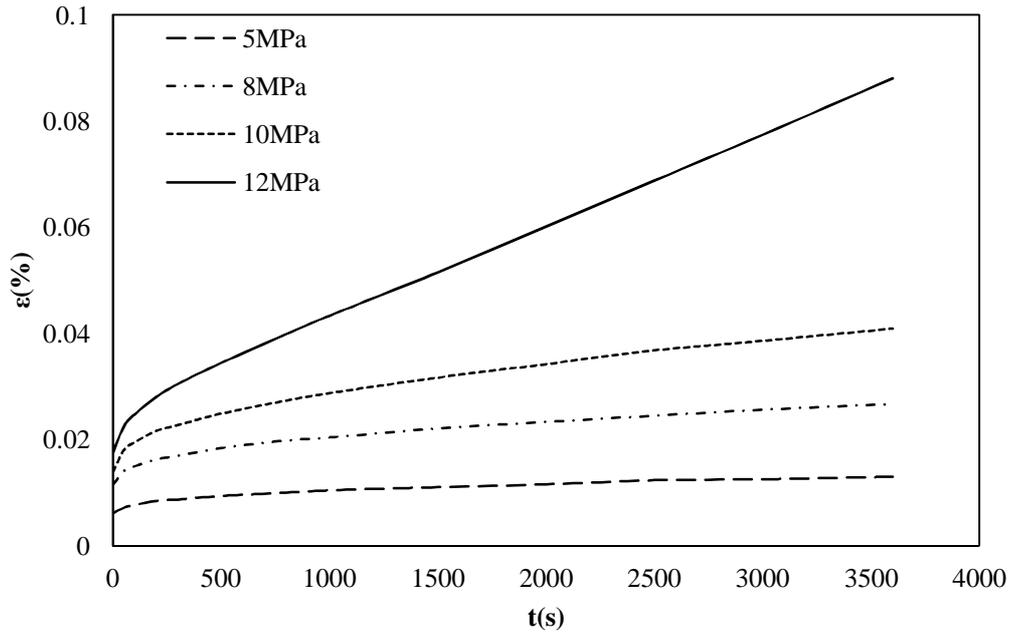
Figure 5-10: Tensile creep curves of non-aged PU lacquer under 5, 8, 10, and 12 MPa.

Secondary creep rates ($\dot{\varepsilon}_3$) were determined from Figure 5-10 by a linear fit to the data in the secondary creep region. $\dot{\varepsilon}_3$ was then plotted against stress for different periods of UV irradiation, as shown in Figure 5-11. It can be seen that $\dot{\varepsilon}_3$ increases with stress and decreases with UV ageing, indicating that UV ageing significantly improves the creep resistance of the PU lacquer. Figure 5-12 shows isochronous stress-strain plots constructed from the creep tests for non-aged samples. It can be seen in this figure that UV ageing makes the PU more brittle, however, it can also be seen that there is a non-linear relationship between the isochronous stress and strain, which means that a non-linear viscoelastic model is needed to accurately model the rheology, as discussed in the Section 5.3.
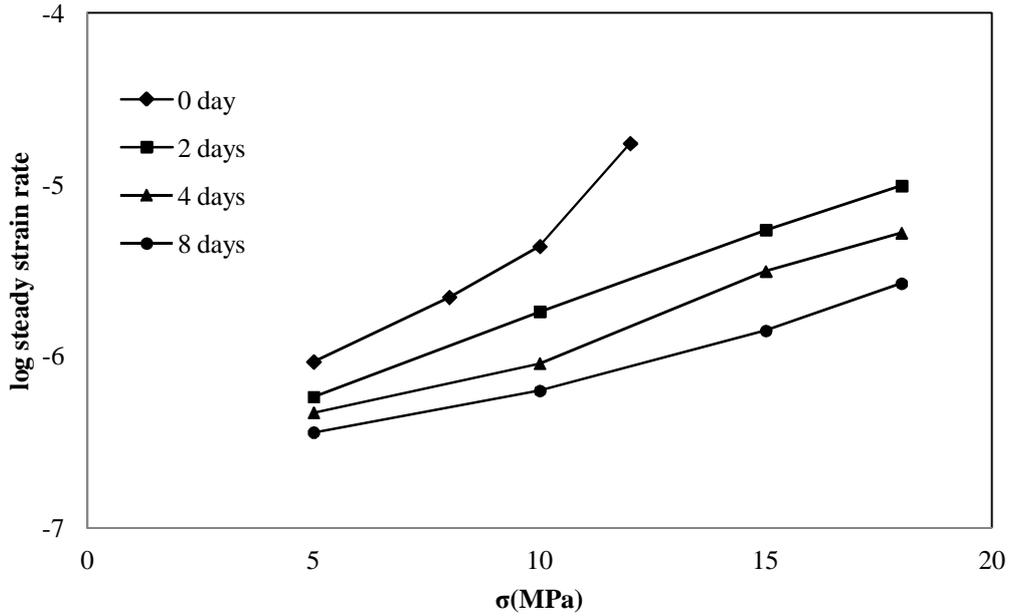
Figure 5-11: Secondary creep rate ($\dot{\varepsilon}_3$) as a function of stress for non-aged and UV-aged PU lacquer films (symbols indicates duration of UV exposure).
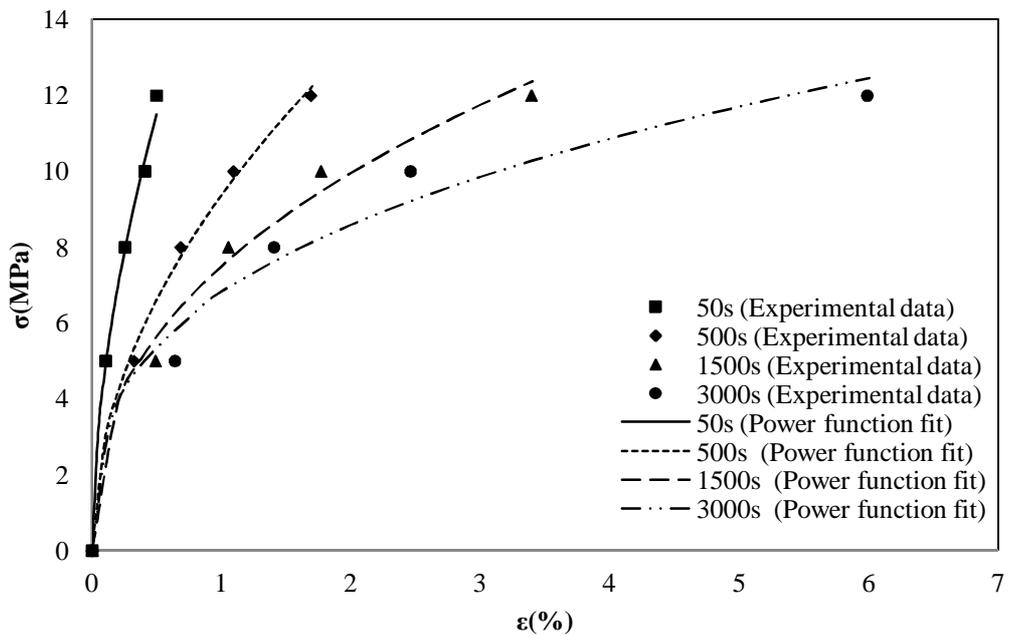
Figure 5-12: Isochronous stress-strain curves for non-aged samples.

5.3 A rheological model for PU lacquers

It can be seen from Figure 5-10 that on application of the load there is an initial elastic strain ε_1. Following this is a phase of decreasing strain rate, the transient creep region ε_2, followed by a period of approximately constant strain rate, the secondary creep region ε_3. Burger's

model is proposed to model this material behaviour as it can capture all these features of the creep process, as described in Chapter 2. As a result, it is used to model the mechanical behaviour of the PU lacquer film on the basis of the viscoelastic behaviour from the experimental results.

As seen, from Figure 5-12, a non-linear viscoelastic model is required for the PU lacquer, hence, the application of a modified Burger's' model is proposed in which the creep strain is given by [111]

$$e_{total}(t) = \frac{s}{E_1} + \left(\frac{s}{m}\right)^m t + \left(\frac{s}{l}\right)^n \left(1 - \exp\left(\frac{-t}{t}\right)\right) \tag{5-1}$$

where m and n are indices representing the non-linearity of the Maxwell dashpot and Kelvin unit, whilst the Maxwell spring remains linear. The procedure for determining the parameters of this model from the experimental data is as follows. First the instantaneous elastic strain was obtained directly from the experimental data, enabling E_1 to be determined, and subtracted from the total strain to obtain the total creep strain. The remaining terms of Eq. (5-1) were then fitted to the experimental creep data to determine the parameters, μ, λ, τ, m and n. The parameters of this model were obtained by fitting the model to experimental data using a non-linear regression analysis using a simplex search algorithm [178] in Matlab (R2007b, The MathWorks, Inc. Massachusetts, U.S.A.). The values of these terms for the various ageing conditions investigated are presented in

Table 5-4 and Table 5-5.

Table 5-4: Parameters of modified Burger's model under different UV ageing conditions under 50% RH.

Days of UV ageing	μ	λ	τ (s)	m	n	R^2
0	82.54	4806	162.3	5.712	0.767	0.999
2	1435	1374	144.8	2.627	1.062	0.997
4	1058	9877	140.1	2.961	0.801	0.993
8	953.1	615.6	130.9	3.203	1.474	0.996

Table 5-5: Parameters of modified Burger's model under different humidity ageing conditions

Moisture content (%)	μ	λ	$\tau(s)$	m	n	R^2
0.88	123.9	59.9	191.1	4.2	1.9	0.987
1.35	867.1	21.0	254.3	2.1	1.9	0.975
2.77	28048	23.8	239.5	1.2	1.7	0.992

Figure 5-13 shows typical fits of this model to the experimental data. It can be observed that the fits are good, and the square of the correlation coefficient (R^2) for all curve fits is greater than 0.97.
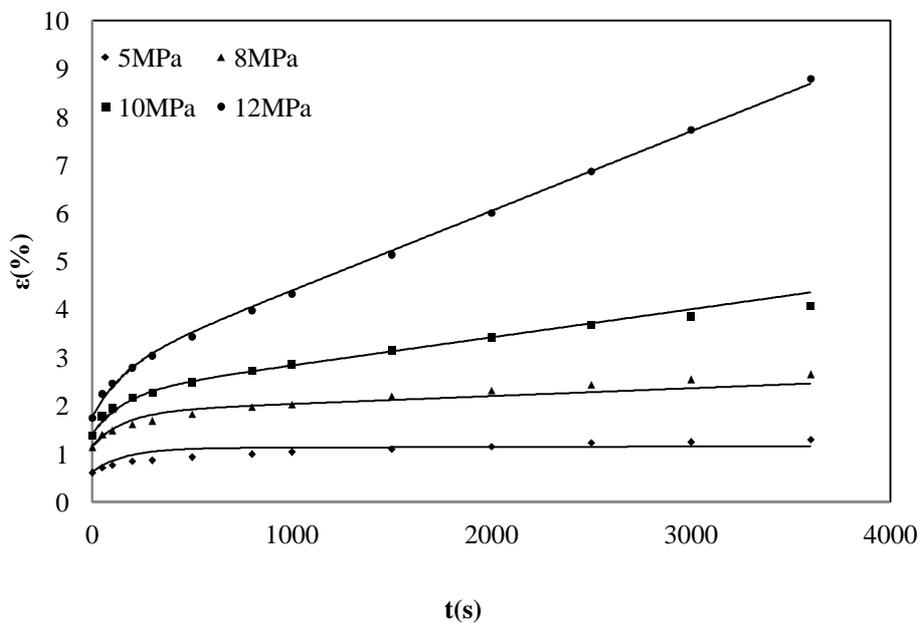
(a) Non-aged/50% RH

Figure 5-13: Experimental data (dots in the figures) and fitted results (solid lines in the figures and using modified Burger's model) of creep tests on PU lacquer films under different environmental conditions: (a) Non-aged/50% RH, (b) 8-day UV aged/50% RH (*To be continued in Page 94*)
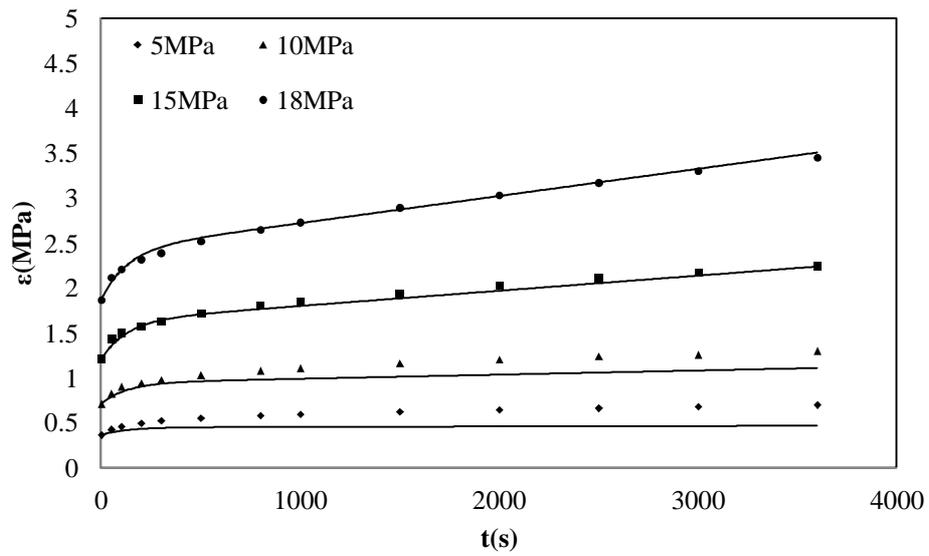
(b) 8-day UV aged/50% RH
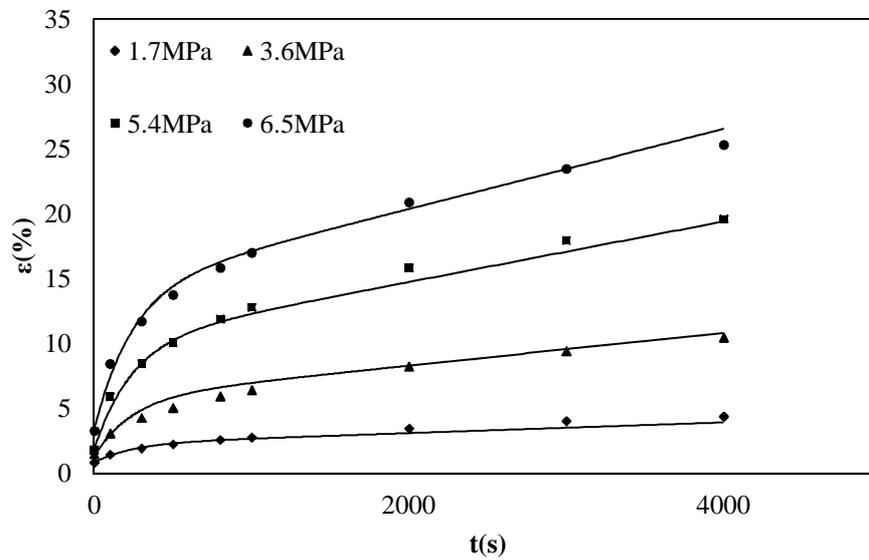
(c) Non-aged/95% RH

Figure 5-13: Experimental data (dots in the figures) and fitted results (solid lines in the figures and using modified Burger's model) of creep tests on PU lacquer films under different environmental conditions: (c) Non-aged/95% RH (*continuing from Page 93*).

The multiplicity of parameters from fitting the modified Burger's model to the creep data makes it difficult to quantify the effect of ageing on the material behaviour. To facilitate our understanding, we calculate three stress-dependent functions from pairs of parameters, given by

$$h_1 \equiv \frac{m^m}{s^{m-1}} \tag{5-2}$$

$$E_2 \equiv \frac{l^n}{s^{n-1}} \tag{5-3}$$

$$h_2 \equiv \frac{tl^n}{s^{n-1}} . \tag{5-4}$$

The dependence of the instantaneous strain response on UV ageing and moisture content is illustrated by Figure 5-14. This shows that the application of UV irradiation increases the instantaneous stiffness of the material, but increasing the relative humidity has the opposite effect. The Kelvin unit parameters E_2 and η_2 and the permanent viscous flow parameter η_1 characterise the transient and secondary creep behaviour. Changes to η_1, E_2 and η_2 with variation in environmental conditions are shown in Figure 5-15. In general, we find that all these parameters respond in a similar way in that they increase with UV ageing and decrease with water absorption.
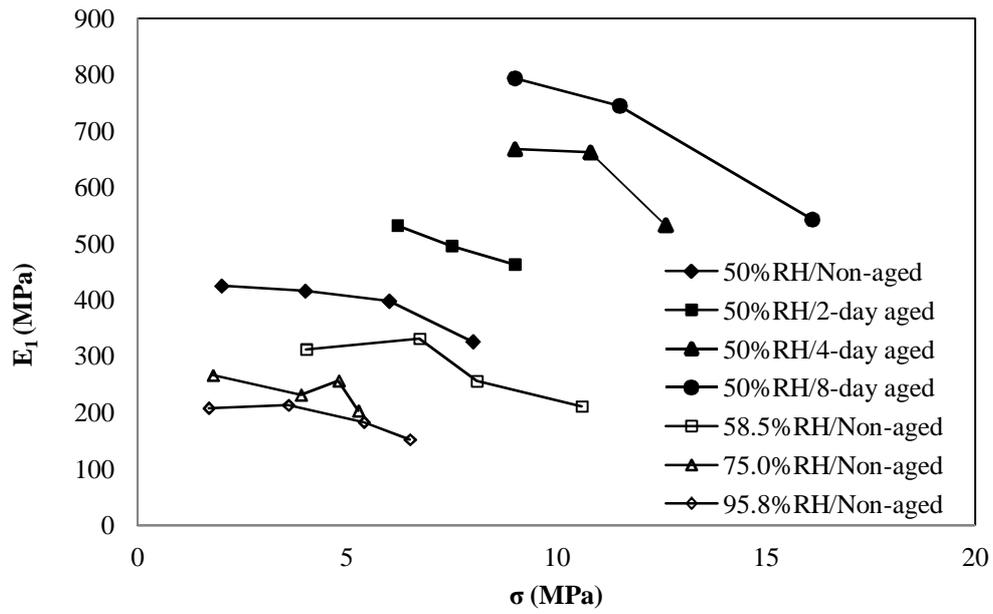
Figure 5-14: Changes of E_1 with different environmental conditions.
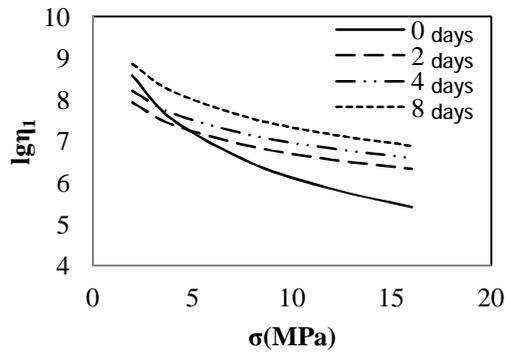
(a)
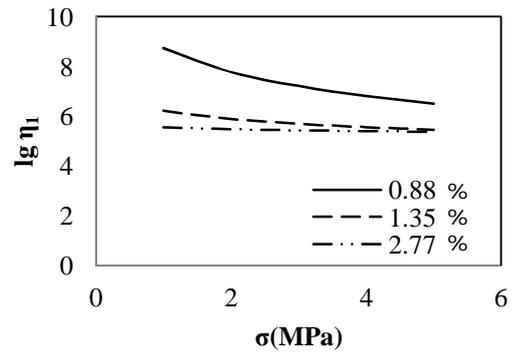
(d)
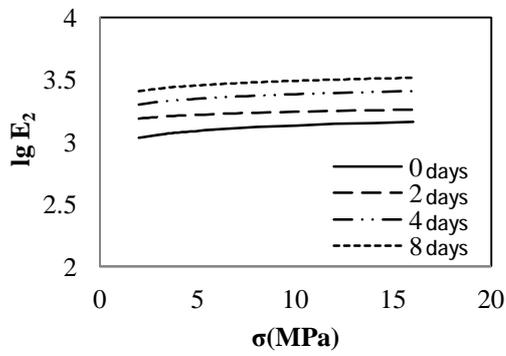
(b)
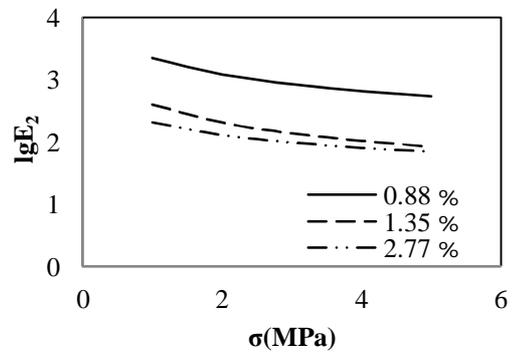
(e)
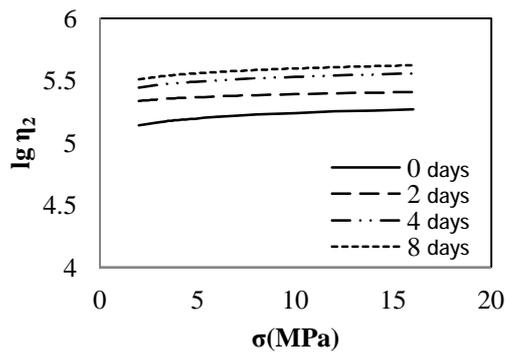
(c)
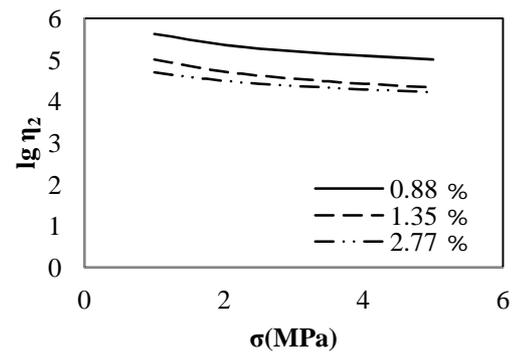
(f)

Figure 5-15: Effect of UV ageing (days of UV exposure in (a-c)) and RH (moisture content in (d-f)) on viscoelastic constants of modified Burger's model for PU lacquer.

5.4   Conclusions

Water transport in between PU lacquer films can be well described by Fick's law, and Flory-Huggins model can be used to represent the sorption isotherm of PU lacquer film. Mechanical properties of PU lacquer films have a complex dependence on environmental conditions. The tensile properties of the PU lacquer were shown to differ significantly after UV ageing. With increasing time of UV irradiation, Young's Modulus and tensile strength increase dramatically, but the maximum strain decreases. With water absorption, both Young's modulus and tensile strength are decreased, but the material tends to sustain more strain. PU lacquer film was also found to behave with a non-linear viscoelasticity, which is highly dependent on environmental conditions. A modified Burger's model was found to fit the experimental data well for different stress levels suggesting this is a satisfactory method for characterising PU rheological behaviour.

Chapter 6 Experimental Investigation and Material Modelling of Fresh and UV aged *Urushi*

6.1 Introduction

As reviewed in Chapter 2, *urushi* is a complex natural polymer that has been used to protect and decorate objects for many hundreds of years. It is an important material as decorated objects can obtain great value and historical worth. These objects are often exposed to environments that are detrimental to both their aesthetic appeal and structural performance and restoration and conservation procedures are needed to preserve these objects over long periods of time. The conservation work requires a detailed understanding of the material properties of the *urushi* lacquer film. However, *urushi* exhibits complex viscoelastic behaviour under load that has not been fully characterised to date. This chapter presents the sample preparation technique and experimental data from a comprehensive mechanical testing programme for *urushi* film. The viscoelastic response was investigated by tests at various displacement rates and creep and recovery tests. In the study on the material behaviour of PU lacquer, it was found that the modified Burger's model could successfully model the viscoelastic behaviour. However, to be confident enough to propose an appropriate model for describing *urushi* material behaviour and modelling its mechanical response to varying environmental conditions, a number of constitutive models were evaluated. The models were implemented in the commercial FEA software ABAQUS, offering the potential to accurately model the *urushi* behaviour in a complex structure.

In this chapter a comprehensive investigation to determine the rheology and mechanical behaviour of *urushi* is presented. The results of a series of rheological experiments designed first to establish the broad rheology of the material and then to characterise it, are described. The results from fresh *urushi* are compared with samples that have been subjected to UV exposure. Various constitutive models are fitted to the data with their advantages and disadvantages assessed.

6.2 Experimental results and analysis of data for fresh urushi

Experimental data from the mechanical tests on fresh *urushi* samples is presented in this section. The usefulness of different models in modelling the behaviour of *urushi* film under

various types of loading, including constant displacement rate tensile tests data, creep and recovery, is assessed using the FE code ABAQUS 6.10. As a general method in this section, proposed constitutive models were fitted to the creep experimental data to determine model parameters using a non-linear regression algorithm. These models were then implemented in ABAQUS to predict the experimental constant tensile displacement rate behaviour in order to assess their applicability.

6.2.1 The time dependent mechanical behaviour of fresh *urushi*

The general behaviour of *urushi* under tensile and creep loading condition was first examined. Figure 6-1 shows tensile stress (σ) - strain (ε) plots for fresh *urushi* samples at different displacement rates. To give an indication of the material properties, elastic properties were estimated from the curves and are listed in Table 6-1. It can be seen that, in general, the material stiffness increases with rate of testing, most likely due to viscous effects, a typical mechanical behaviour of polymeric materials [94]. Also, the ultimate strength increases and ductility decreases with rate of testing. It can be seen that there is little or no strain hardening at any loading rate.
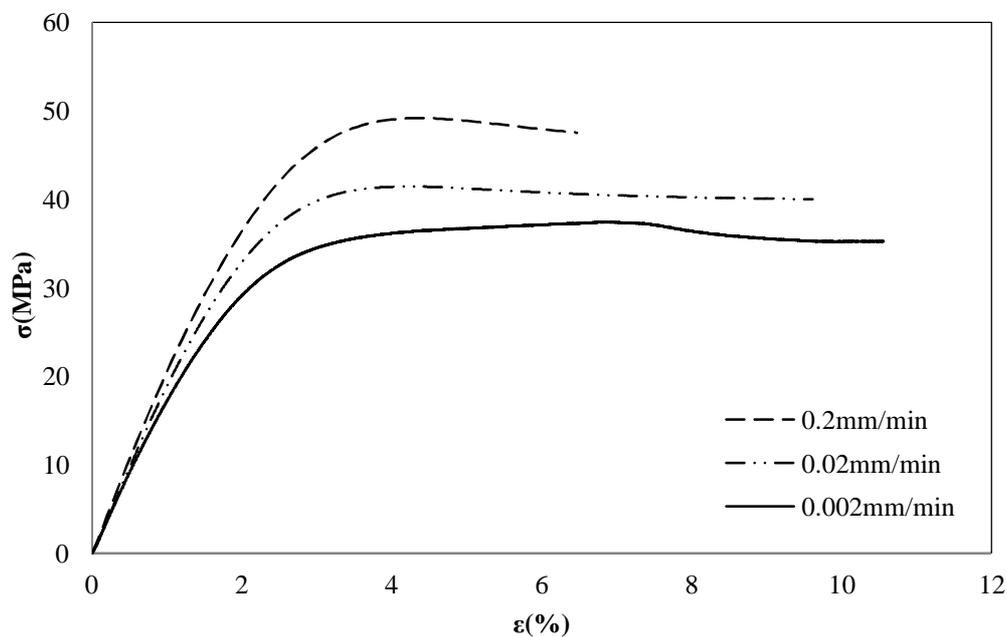
Figure 6-1: Stress-strain curves of tensile tests on fresh *urushi* lacquer film samples at different loading rates at 50% RH and 25°C.

Table 6-1: Tensile elastic modulus (E), tensile strength at break (σ_B), and strain at break (ε_B) for fresh *urushi* samples at different loading rates.

Loading rate (mm/min)	E(MPa)	σ_B (MPa)	ε_B(%)
0.002	1686	35.23	10.56
0.02	1936	40.00	9.61
0.2	2148	47.55	6.48

Typical creep and recovery behaviour for fresh *urushi* can be seen in Figure 6-2. On application of the load there is an instantaneous elastic strain response $\overline{OB}$. This is followed by a phase of decreasing strain rate, known as the primary or transient creep region $\overline{AB}$ and then a period of approximately constant strain rate, the secondary or steady state creep region $\overline{BC}$. On removal of the load there is elastic recovery $\overline{CD}$, followed by a region of decreasing strain rate, $\overline{DE}$. Finally, an unrecoverable strain is left after point E. Similar behaviour is seen at all loads, with greater strains and strain rates seen at the higher loads.

Obviously, a material model is required that can demonstrate all the features observed in the experimental tests. Using the creep behaviour results, it is possible to determine the rheology of the material, and to characterise its response as a function of the degree of ageing. A number of different rheological models were investigated for comparison. These are described in the following sections.
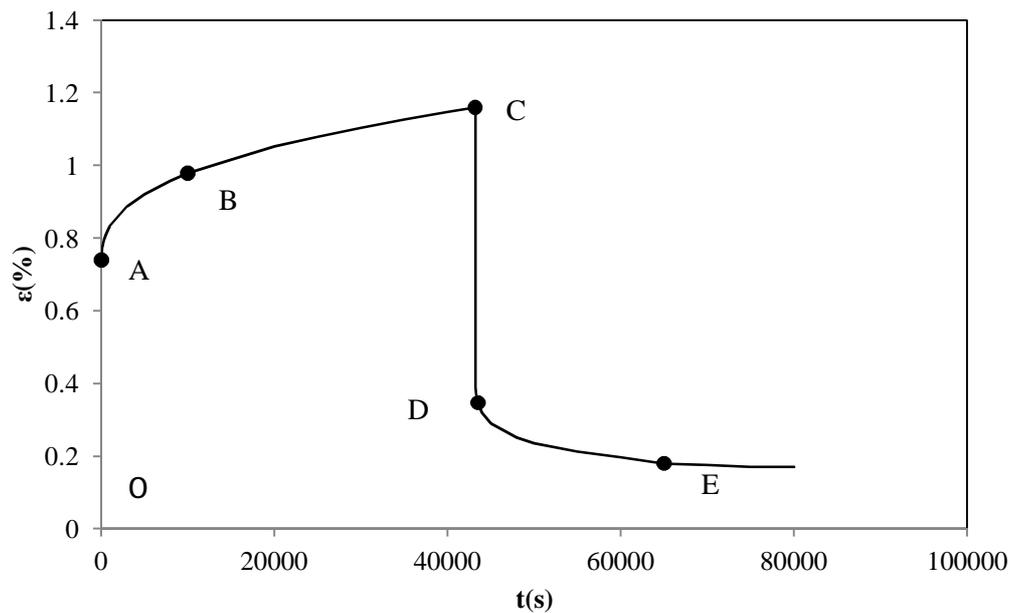
Figure 6-2: A typical tensile creep-recovery curve of fresh *urushi* film (17.5 MPa) at 50% RH and 25 °C.

6.2.2 Plasticity models

A rate dependent plasticity model, von Mises plasticity model, was initially used to describe the rheology. Other yield criteria, such as the Drucker-Prager yield criterion, normally require tests in more stress states, such as compression and shear, in order to define all the model parameters. However, these tests are very difficult to perform with *urushi* film, due to the small thickness of the bulk samples (≤ 0.1 mm) and, hence, only the von Mises yield criterion was investigated in this study. Some commercial FEA codes, such as ABAQUS, provide plasticity models with rate-dependent options by enabling the specification of a series of hardening curves for various plastic strain rates, in order to enhance stress analysis for elastic-plastic rate-dependent materials.

The tensile stress-strain response of fresh *urushi* film at three different loading rates was presented in Figure 6-1. The material model requires stress-plastic strain data under different constant plastic strain rates, which is not directly available from the experimental data. Yu *et al* [120] introduced a manipulation of experimental raw data to extract the stress-plastic strain response under different plastic strain rates. The required constitutive data were obtained and used to define a rate-dependent elasto-plastic FE model by defining hardening curves through

the direct entry of test data. In order to assess the applicability of this model, a FE analysis was performed, with the detailed information on the model presented in Chapter 4 to model the mechanical response of the fresh *urushi* tested at various displacement rates.

Figure 6-3 shows a comparison of the tensile experimental constant displacement rate data with predictions using the FE analysis with rate-dependent von Mises elasto-plastic model. It can be seen that the fitted results agree very well with the experimental data.
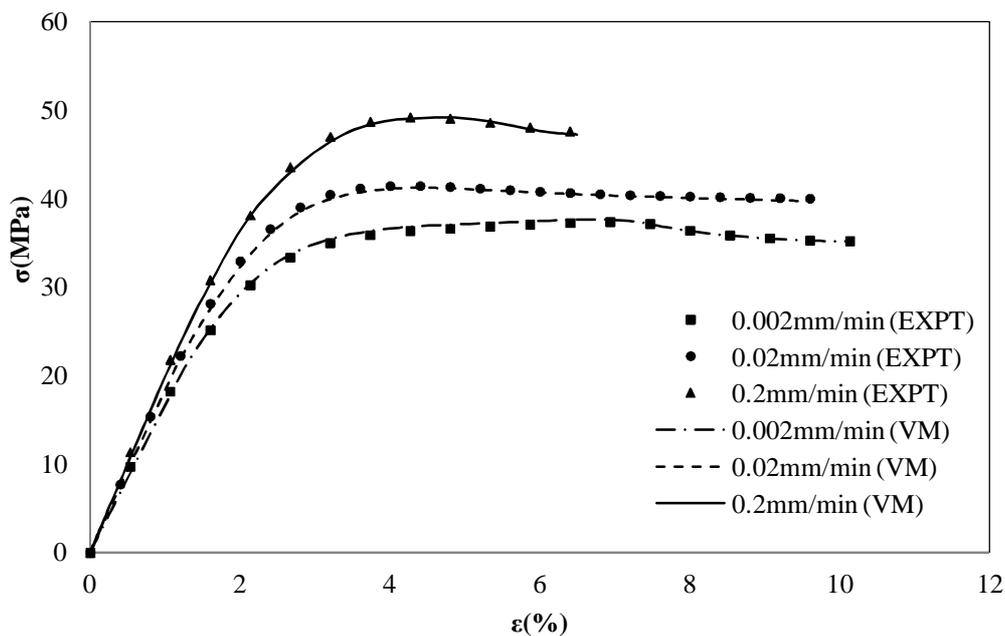
Figure 6-3: A comparison of tensile experimental constant displacement rate data (EXPT) for fresh *urushi* film under with FE predictions (VM) using constant plastic strain rate data in rate-dependent von-Mises elasto-plastic model.

The rate-dependent von Mises model was also used to simulate the creep and recovery tests. The predicted result did not agree satisfactorily with the experimental creep data because stresses in the creep tests were significantly lower than the maximum stress in the constant displacement tests, and in the rate dependent von Mises model time dependent plastic flow does not occur inside the yield surface and is not significant at low stress levels. However, for viscoelastic polymers, time dependent strain occurs under any load. The von Mises plasticity model is unable to model the time dependent recovery response as the strain rate is zero when the load is removed.

6.2.3 Power law creep model

Power law creep models have been found to be useful for empirically characterising the rheological behaviour of many polymers [112, 120, 179]. In this case, the strain rate is considered to be related to the stress through a simple power law relationship, and often this is sufficient to capture the main features of the rheology. The uniaxial equivalent creep strain rate is defined as

$$\dot{\varepsilon}_{eq}^{cr} = A q^n t^m \tag{6-1}$$

where $\dot{\varepsilon}_{eq}^{cr}$ is the uniaxial equivalent creep strain rate, q is the von Mises equivalent stress and t is the total time. A, n and m are material parameters determined from creep test data [8].

The power law creep model was used to model the constant tensile displacement rate data and creep-recovery data in order to investigate its general usefulness. Before implementing the power law creep model in the FE code, the optimised set of model parameters, A, m and n in Eq. (6-1), need to be determined. To achieve this, a least square regression of Eq. (6-1) to the creep experimental data was performed using a non-linear regression analysis based on the Nelder-Mead algorithm, also called simplex search algorithm, in Matlab. The resulting parameters are listed in

Table 6-2.

Table 6-2: Optimised parameters of power law creep model for fresh *urushi* film (stress in MPa and time in seconds)

A	m	n
3.62×10^{-8}	-0.5714	2.2568

The predicted creep and recovery plots using the optimised parameters of the power law creep model for fresh *urushi* film are shown in Figure 6-4, together with the corresponding experimental data. It can be seen that there is satisfactory agreement between the model and the experimental data for the creep phase, however, the power law creep model cannot model the time dependent element of the recovery phase as it can be seen from Eq. (6-1) that the strain rate is zero when the load is removed.
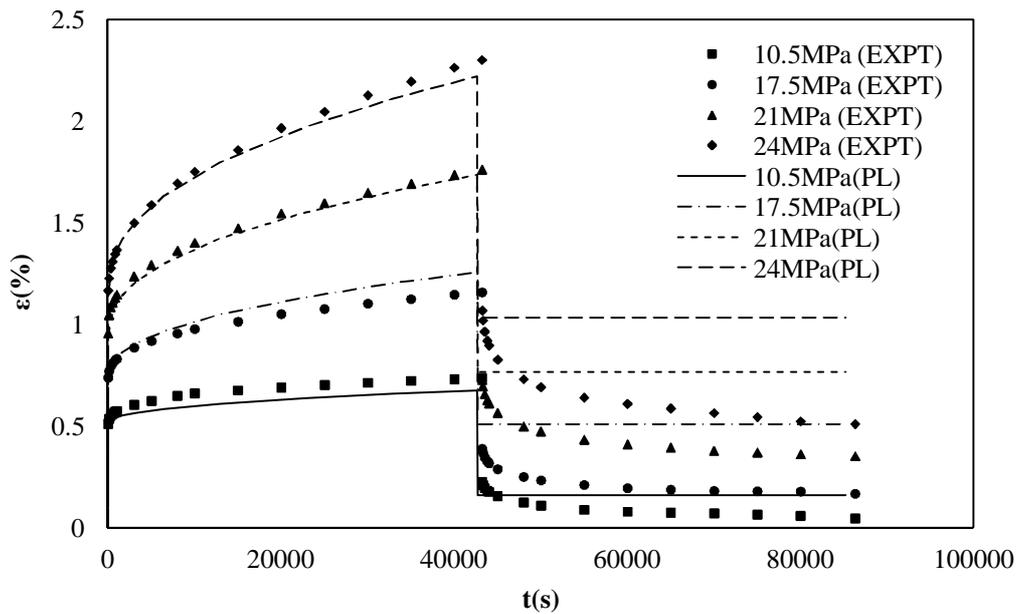
Figure 6-4: A comparison of creep and recovery data (EXPT) for fresh *urushi* film with FE predictions (PL) using the power law creep model.

As a further investigation, the power law creep model was used to predict the constant displacement rate tensile test results. Figure 6-5 shows the comparison between the predicted and experimental results using the parameters given in

Table 6-2. Reasonable agreement was achieved for low strains, but at high strain, the predicted stresses diverge strongly from the experimental observations. This discrepancy is because the creep law parameters were determined from creep tests at relatively low stress (≤24 MPa), as indicated in Figure 6-4, whereas the experimental stress-strain plots show a yield point between 30 and 50 MPa. This behaviour is not captured by the creep-law model and the poor fit of the model at high strains illustrates the dangers of extrapolation beyond the range of data used to determine parameters. In most real applications the strains in *urushi* films are small (< 1%) as they are associated with environmental changes and long term ageing effects [11]. This makes the power law creep model defined here of potential use. However, the inability to predict realistic recovery is a clear drawback if variable loading is experienced.

Figure 6-5: A comparison of tensile experimental constant displacement rate data (EXPT) for fresh *urushi* film with FE predictions (PL) using a power law creep model.

6.2.4 Mechanical models

An alternative to the largely empirical approach of the power law model is to consider that mechanical behaviour can be represented by a combination of simple mechanical components (spring, dashpot, sliders) connected in parallel and in series. In linear viscoelasticity, materials are represented by combinations of Hookean springs, which provide the elastic restorative force component, and Newtonian dashpots, which provide the viscous damping components. Variants of these models include the standard linear solid model, Prony series models, Burger's fluid and the generalised Kelvin fluid. These models will be investigated as a basis for describing the rheological behaviour of *urushi*.

6.2.4.1 Standard linear solid and Maxwell Prony series models

The standard linear model, shown in Figure 2-20 (c), is constructed from a linear spring in parallel with a Maxwell unit (which is a linear dashpot and a linear spring in series). A more realistic extension to this is the Maxwell Prony series model, shown in Figure 2-25, which introduces a series of Maxwell units with different relaxation times in parallel with a spring element. In this model, $G_R(t)$ is the shear stress relaxation modulus and G_∞ and G_0 are defined as:

$$G_\infty = \lim_{t\to\infty} G_R(t) \qquad\qquad \text{(6-2)}$$

and

$$G_0 = G_R(0) \qquad\qquad \text{(6-3)}$$

A dimensionless relaxation modulus can then be defined as:

$$g_R(t) = \frac{G_R(t)}{G_0} \qquad\qquad \text{(6-4)}$$

The normalised shear stress relaxation modulus is represented in the Maxwell Prony series model by a series expansion given by

$$g_R(t) = 1 - \sum_{i=1}^{n} g_i \left[1 - e^{-t/t_i}\right] \qquad\qquad \text{(6-5)}$$

where g is the volumetric modulus, K_i, or deviatoric modulus G_i. The standard linear solid is a special case of the Maxwell Prony series model in which n=1 in Eq. (6-5). In ABAQUS, the creep experimental data was used to determine the material parameters G_i, K_i and t_i used to define the viscoelastic properties of the material with a wide spectrum of retardation time.

In ABAQUS, the Prony series model parameters can be defined in one of four ways: direct specification of the Prony series parameters, inclusion of creep test data, inclusion of relaxation test data, or inclusion of frequency-dependent data obtained from sinusoidal oscillation experiments. To assess the capability of the standard linear solid model to characterise the viscoelastic behaviour of fresh *urushi* films, the normalised experimental creep compliance data was used in the ABAQUS *MATERIAL PROPERTIES* module, with setting the series number *n=1,* to determine the optimum model parameters. The resultant parameters were used in FE models of the creep and recovery tests. A comparison of the predicted and experimental data can be seen in Figure 6-6.
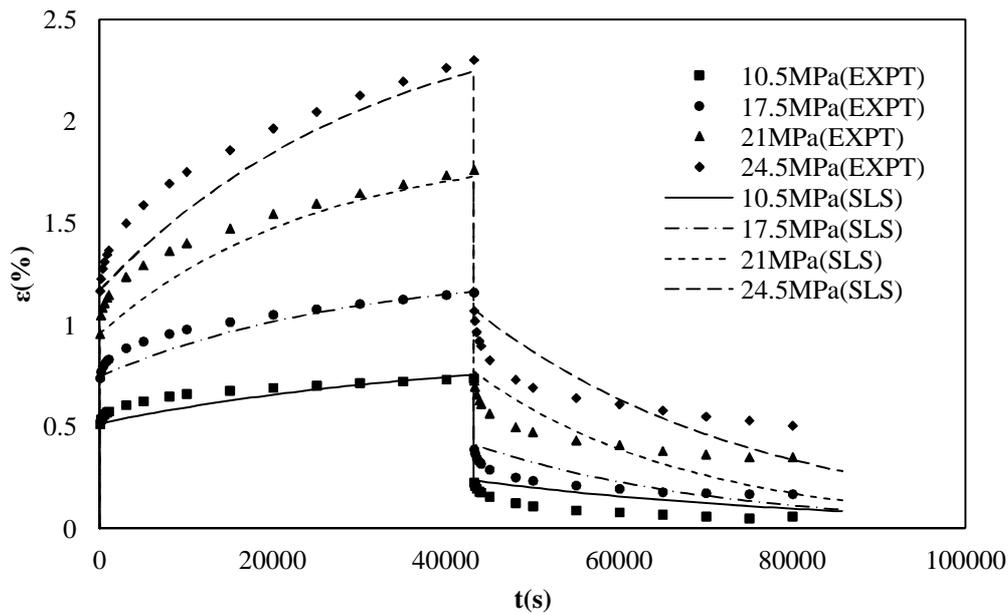
Figure 6-6: Experimental (EXPT) and predicted (SLS) creep and recovery data for fresh *urushi* film samples using standard linear solid model.

Figure 6-6 shows the advantage of the standard linear solid over both the power law creep model and rate-dependent von Mises plastic model in predicting the time-dependent recovery behaviour. However, the prediction of recovery is still unsatisfactory compared with the experimental data. This is because the standard linear solid unit, without a dashpot in series, will recover completely after removal of the creep load, whereas the experimental data appears to indicate a component of unrecovered creep strain. Moreover, the model does not describe the creep behaviour as well as the power law creep model. This is because a single Maxwell unit is not sufficient to describe the time-dependent behaviour, owing to the single dashpot used to represent the relaxation behaviour. In most polymers, including *urushi,* molecular segments will be of various lengths resulting in a distribution of relaxation times [113, 180]. This can be better represented by the Maxwell Prony series model.

Using the same experimental data but setting the maximum number of terms in the Prony series to 13, instead of 1 for the standard linear solid model, the predicted creep and recovery strains were predicted and compared with the experimental data. It can be seen by comparing Figure 6-6 to Figure 6-7 that a much better agreement of predicted results with experimental data has been achieved by increasing the number of Maxwell units in the Prony series model. This model also shows some effectiveness in modelling the time dependent recovery behaviour, although it is still the case that in time all the creep strain will be recovered. In

order to further assess the general usefulness of the Prony series model, it was used to predict the constant displacement rate data, with the results shown in Figure 6-8. It can be seen that the correlation between experimental and predicted data is poor at high strains, for the same reasons discussed for the power law creep model.

Figure 6-7: Experimental (EXPT) and predicted (PS) creep and recovery data for fresh *urushi* film samples using Maxwell Prony series model.
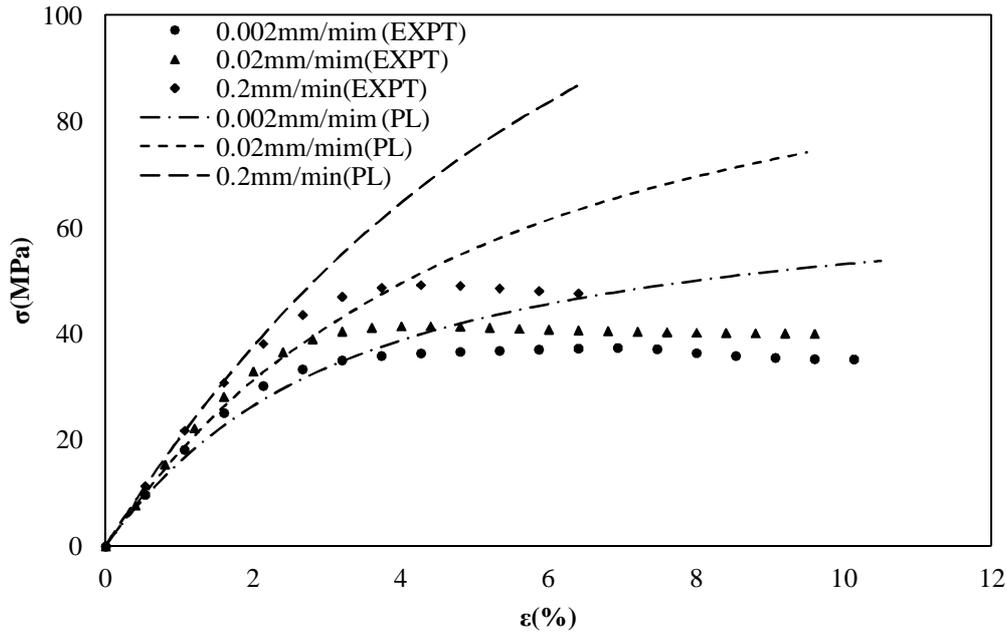
Figure 6-8: A comparison of tensile experimental constant displacement rate data (EXPT) for fresh *urushi* film with FE predictions (PS) using Maxwell Prony series model.

6.2.4.2 Burger's Model

An alternative to the Prony series is to tailor the combinations of mechanical elements to suit the rheological characteristics of the material. A widely used model for viscoelastic materials is the Burger's fluid, which has an advantage over the Maxwell Prony series model in predicting unrecoverable deformation. This model is able to capture all the features of the experimentally observed creep-recovery curve reasonably well. The instantaneous elastic strain is defined as ε_1 (using a Maxwell spring), the transient strain as ε_2 (using a Kelvin unit) and the steady state strain ε_3 (using a Maxwell dashpot). The dashpot in series enables the model to represent irreversible creep strain, unlike the standard linear solid and Maxwell Prony series models. Mathematically, creep and recovery in the Burger's fluid can be represented by:

$$e_c = e_1 + e_2 + e_3 = s \left[\frac{1}{E_0} + \frac{t}{h_0} + \frac{1}{E_1} \left(1 - \exp\left(\frac{-t}{t} \right) \right) \right] , \ (t_0 \leq t < t_1) \qquad (6\text{-}6)$$

$$e_r(t) = e_2^r + e_3^r = s \left[\frac{t_1}{h_0} + \frac{1}{E_1} \left(\exp\left(\frac{t_1}{t} \right) - 1 \right) \exp\left(\frac{-t}{t} \right) \right] , \ (t \geq t_1) \qquad (6\text{-}7)$$

where

$$t = \frac{E_1}{h_1} \qquad (6\text{-}8)$$

and t is time during creep when $t<t_1$ and time during recovery when $t \geq t_1$, and t_1 is the time at which the load is removed.

All the rheological models discussed so far have only contained linear elements and, hence, are only capable of representing linear viscoelasticity. However, isochronous stress-strain plots constructed from the experimental creep data are non-linear, as shown in Figure 6-9, indicating a non-linear viscoelastic model may be needed to accurately characterise the *urushi* material behaviour over a range of loads. The Burger's fluid can be modified to represent non-linear viscoelasticity, such that [111]:

$$e_c(t) = \frac{s}{E_0} + \left(\frac{s}{m}\right)^m t + \left(\frac{s}{l}\right)^n \left(1 - \exp\left(\frac{-t}{t}\right)\right), \ (t_0 \leq t < t_1) \qquad (6\text{-}9)$$

$$e_r(t) = \frac{s}{E_0} + \left(\frac{s_0}{m}\right)^m t_1 + \left(\frac{s_0}{l}\right)^n \left(\exp\left(\frac{t_1}{t}\right) - 1\right)\exp\left(\frac{-t}{t}\right), \ (t \geq t_1) \qquad (6\text{-}10)$$

where σ is the stress during creep or recovery and σ_0 is the stress during recovery. It can be seen from Eqs. (6-9) and (6-10) that a linear elastic component is still assumed but a power law is used to represent non-linearity in the transient and steady state creep components, with m and n being the power law exponents.

To facilitate obtaining the six rheological coefficients in Eqs. (6-9) and (6-10) from the experimental data, the results were analysed in the following way. First, the instantaneous elastic strain was obtained directly from the experimental data in each test, and subsequently subtracted from the total strain to obtain the creep strain. Then a least square regression was performed using Matlab on the experimental data using Eqs. (6-9) and (6-10) to obtain the remaining five parameters: μ, λ, τ, m and n, which are given in
Table 6-3.

The results of fitting the modified Burger's model (MBM) to the creep-recovery data for the fresh *urushi* films are shown in Figure 6-10. One can see that the model is able to capture the creep deformation, although the agreement is less than that seen with the Maxwell Prony series model. However, the recovery is predicted far more accurately with the MBM. This

model is not standard in the FE code, ABAQUS, and hence was incorporated via a user sub-routine. Comparison of the experimental constant displacement rate data with that predicted using the MBM is shown in Figure 6-11. The agreement is better than with the Maxwell Prony series model, although still not satisfactory at high strain because the test data used to define the modified Burger's model is mainly from low strain levels.

Table 6-3: Optimised parameters of modified Burger's creep and recovery model for fresh *urushi* film.

	E_0	μ	λ	$\tau\ (s)$	m	n
Creep	2177±6.5%	2143.35	1742.74	1252.66	3.46	1.32
Recovery		2036.68	10654.23	3430.08	3.55	0.91
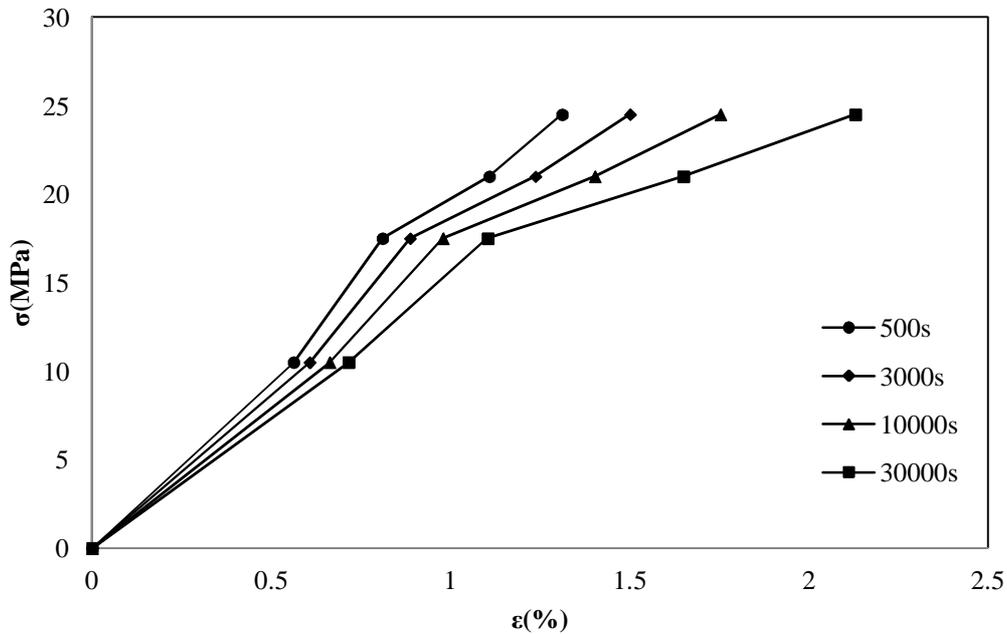
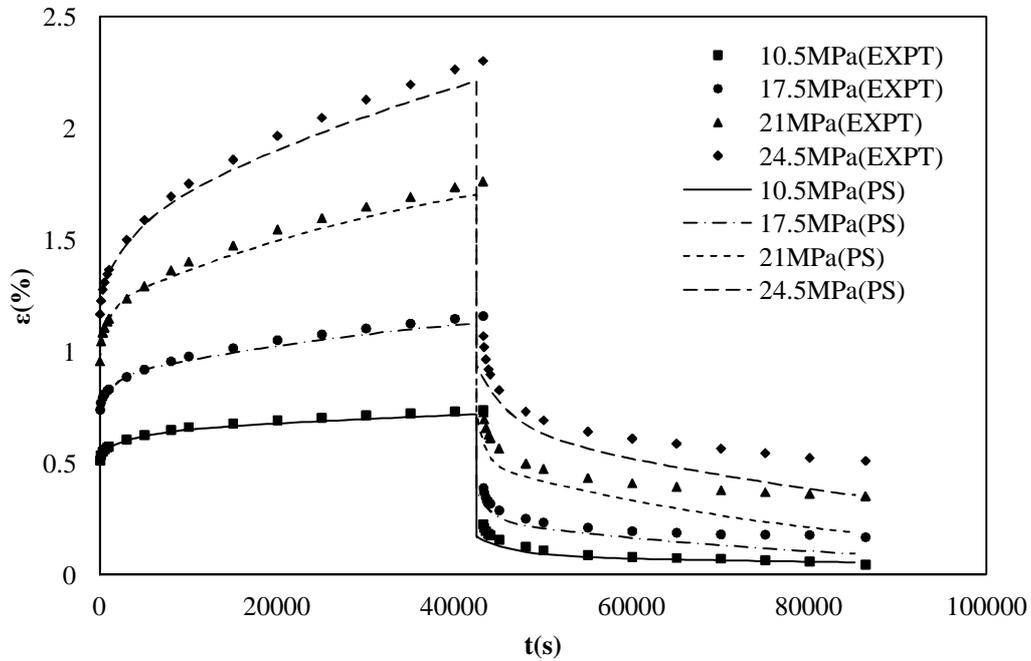Figure 6-9: Isochronous stress-strain curves for fresh *urushi* film.
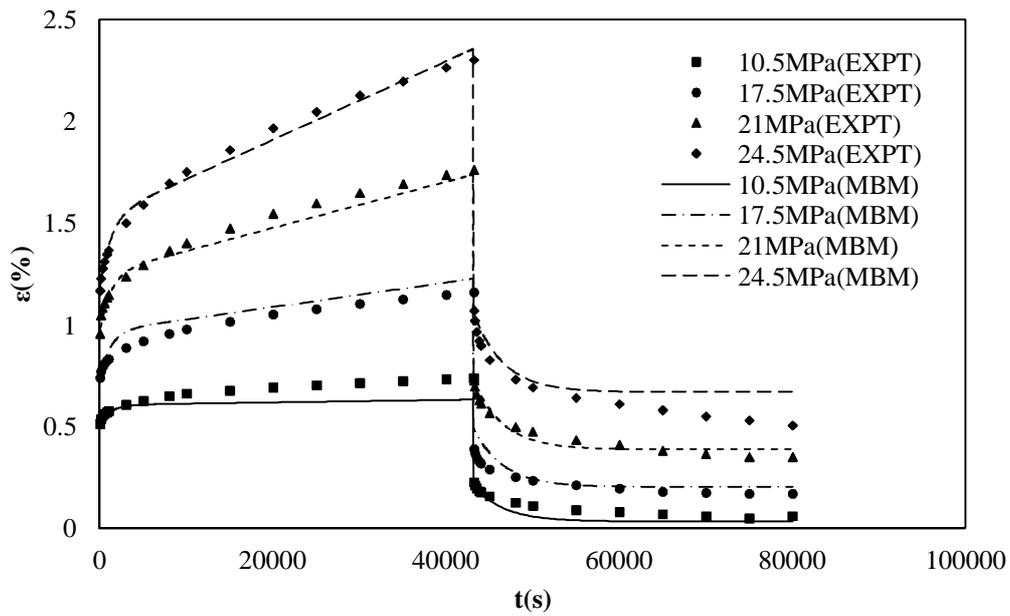
Figure 6-10: Experimental (EXPT)and predicted (MBM) creep and recovery data for fresh *urushi* film samples using modified Burger's model.
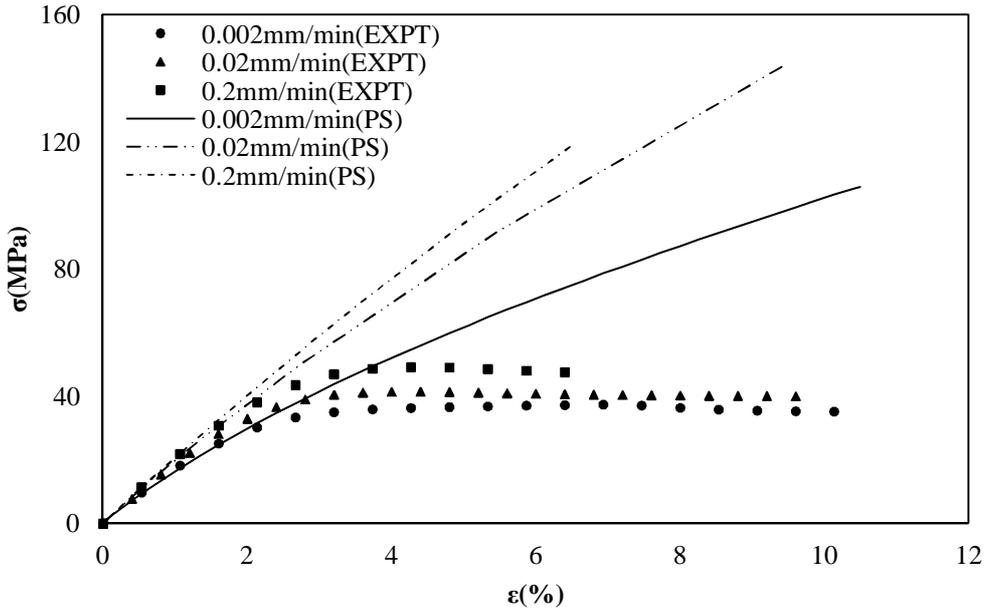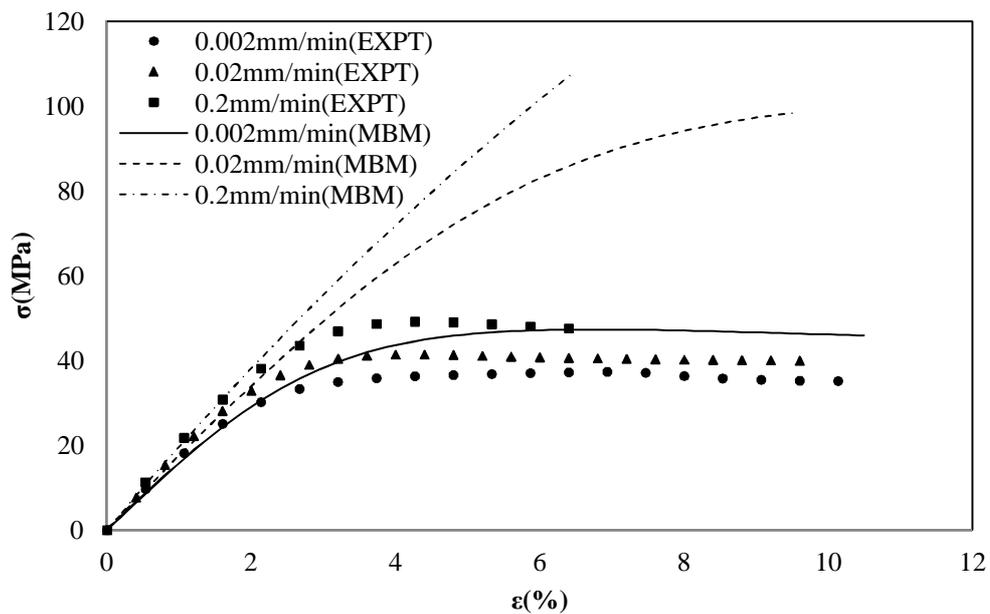

Figure 6-11: A comparison of tensile experimental constant displacement rate data (EXPT) for fresh *urushi* film with FE predictions (MBM) using modified Burger's model.

6.2.4.3 Modified generalised Kelvin fluid model

To overcome the limitations of both the Prony series model and modified Burger's model, a new model, which combines the two models to improve their descriptions of creep and recovery in *urushi* lacquers, is proposed. The Burger's model is first extended by adding further Kelvin units in series to create a generalised Kelvin fluid, as shown in Figure 6-12 [14].
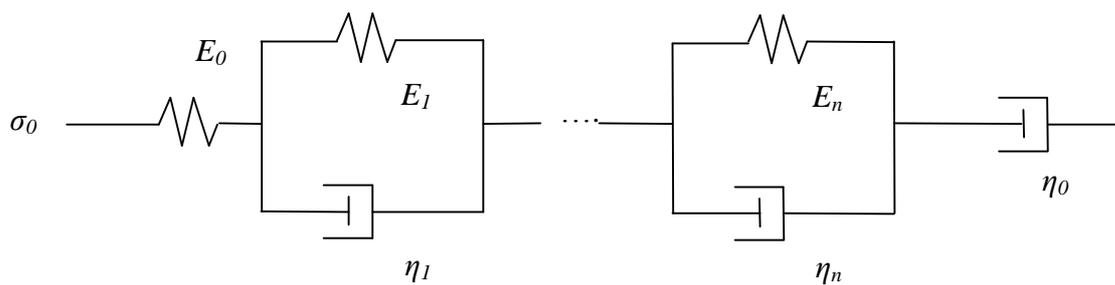
Figure 6-12: Modification of Burger's model to form a generalised Kelvin fluid model.

In order to capture the weak non-linear viscoelasticity of the *urushi* lacquer, the Kelvin units and dashpots are defined as non-linear through the introduction of the stress power law, in a manner similar to that used to create the modified Burger's model. The creep and recovery equations of a modified generalised Kelvin fluid (MGKF) model can then be written as:

$$e_c(t) = \frac{s}{E_0} + \left(\frac{s}{m}\right)^m t + \sum_{i=1}^{N}\left(\frac{s}{l}\right)^n\left(1 - \exp\left(\frac{-t}{t_i}\right)\right), \ (t_0 \leq t < t_1) \qquad (6\text{-}11)$$

and

$$e_r(t) = \frac{s}{E_0} + \left(\frac{s_0}{m}\right)^m t_1 + \sum_{i=1}^{N}\left(\frac{s_0}{l}\right)^n\left(\exp\left(\frac{t_1}{t_i}\right) - 1\right)\exp\left(\frac{-t}{t_i}\right), \ (t \geq t_1). \qquad (6\text{-}12)$$

where μ, λ, $\tau_i(i \geq 1)$, m and n can be determined using a simplex search algorithm as that described in Chapter 4. It was found that good agreement was found with the experimental date for this model with N = 2 and that for N > 3 no significant further improvement was obtained. The parameters for the MGKF model were obtained by fitting the model to the experimental data as discussed previously. The parameters obtained using this procedure are

presented in Table 6-4. From Figure 6-13, it can be seen that this method achieves good agreement with the experimental creep and recovery data.

Table 6-4: Optimised parameters of modified generalised Kelvin fluid creep and recovery model for fresh *urushi* film.

	E_0	μ	λ	$\tau_1(s)$	m	n	$\tau_2(s)$
Creep	2177±6.5%	8009.94	3400.10	531.90	2.70	1.25	10000.31
Recovery		776.56	1746.59	835.26	4.63	1.29	20394.72

Figure 6-13: Experimental (EXPT) and predicted (MGKF) creep and recovery data for fresh *urushi* film samples using modified generalised Kelvin fluid model.

The general effectiveness of the MGKF model was assessed by modelling the constant displacement rate data, and the results are shown in Figure 6-14. It can be seen that the model predicts the experimental data well at low strains.
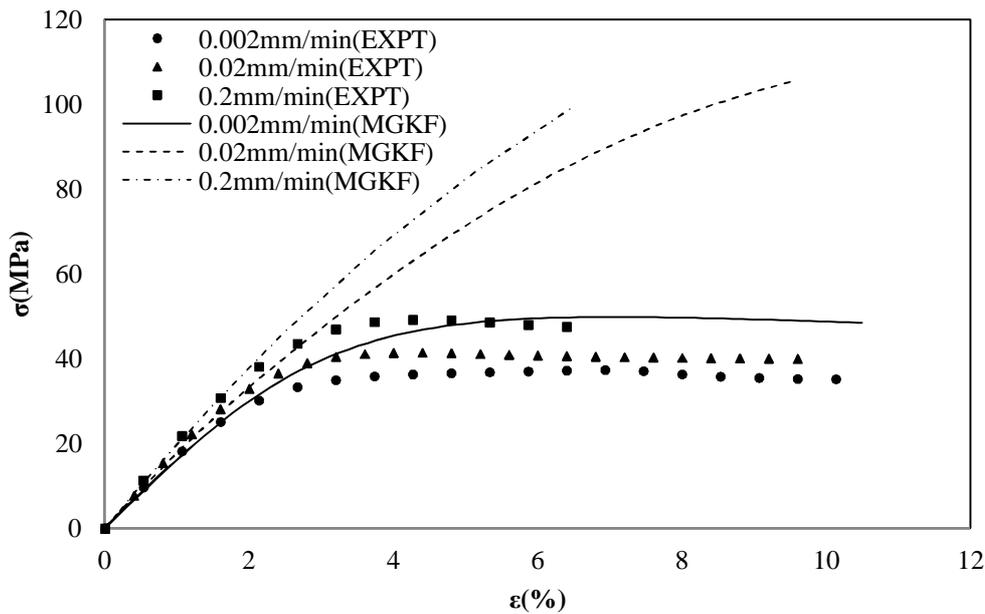
Figure 6-14: A comparison of tensile experimental constant displacement rate data (EXPT) for fresh *urushi* film with FE predictions (MGKF) using modified Kelvin fluid model.

As noted in previous sections, the parameters for the power law creep model, Prony series model, modified Burger's model and modified generalised Kelvin fluid model are determined using creep strain data up to approximately 2.5%, which is below the apparent yield point in the experimental stress-strain plots. As a result, a better comparison of the various models in predicting constant displacement rate behaviour may be gained by only comparing the models with the experimental strain data up to approximately 2.5%, as shown in Figure 6-15. It can be seen in this figure that the Maxwell Prony series model performs the worst while the MBM and MGKF models provide good fits to the data. If a rheological model is required to represent deformation above the yield point then a visco-elastic-plastic model should be used. This can be created by putting a friction plate element in series with a viscoelastic model.

(a)   (b)

(c)   (d)
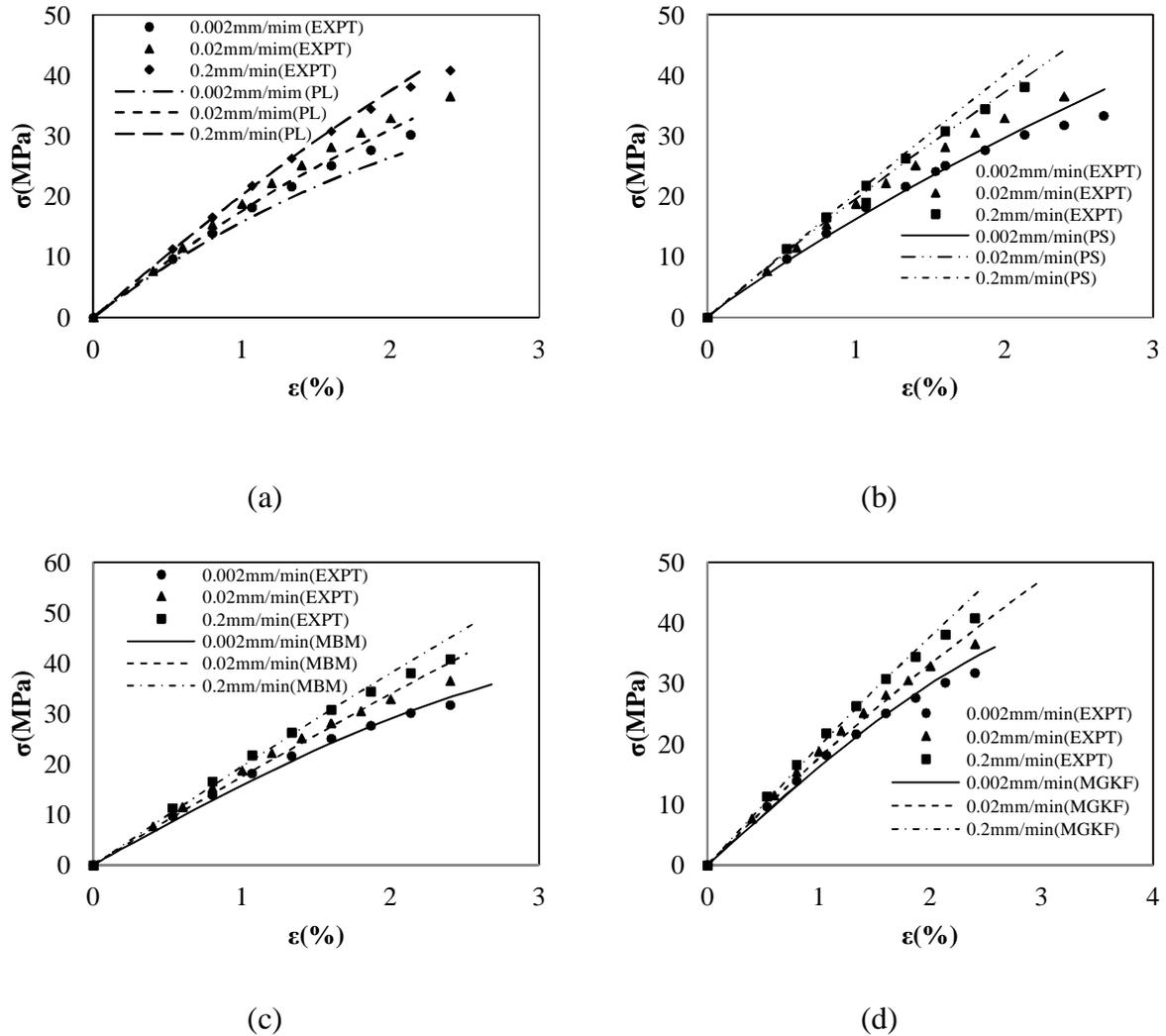
Figure 6-15: Comparison of various models in predicting constant tensile displacement rate behaviour of fresh *urushi* film, (a) The power law creep model, (b) the Maxwell Prony series model, (c) the modified Burger's model, (d) the modified generalised Kelvin fluid model.

6.3   Effect of ageing under ultra-violet illumination

Figure 6-16 shows tensile stress-strain curves for *urushi* samples after different durations of UV exposure, using a displacement rate of 0.002 mm/min. Tensile strength, elastic modulus and fracture strain were determined from the curves and are listed in Table 6-5. It can be seen from Figure 6-16 that as the exposure to UV radiation increases the elastic region of the stress-strain curve is extended but the plastic region is greatly reduced. From Table 6-5 it can be seen that elastic modulus increases from 1686 MPa to 2139 MPa after 400 hours of UV radiation, which indicates that UV ageing increases the stiffness of *urushi* films. However, the deformation at rupture, or the maximum strain that *urushi* films can sustain, strongly decreases from 10.56% to 2.82% after 400 hours ageing. The results indicate that *urushi* films tend to become stiffer and stronger but more brittle with UV ageing which is in good

agreement with testing results of UV-aged PU films and those reported in several papers [175-177]. The possible explanations are formation of a crosslinked structure additional crosslinking to form new supramolecular structures with higher ordering [175-176].
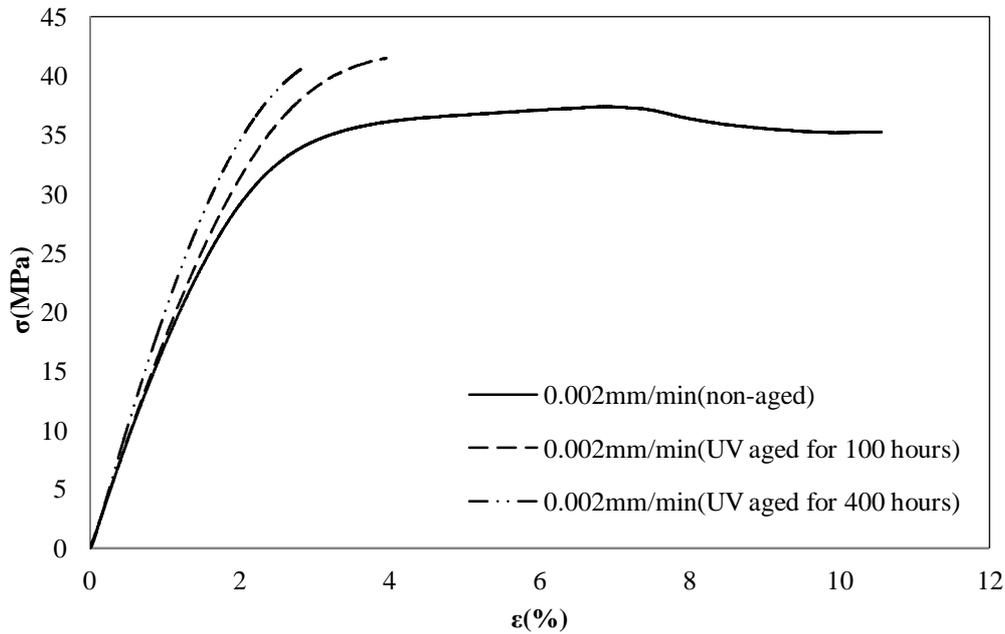
Figure 6-16: Stress-strain curves from tensile tests at 0.002 mm/min on *urushi* film samples after different durations of UV irradiation.

Table 6-5: Tensile elastic modulus (E), tensile strength at break (σ_B) and elongation at break (ε_B) for *urushi* film samples after different durations of UV exposure and fresh from constant displacement rate tests at 0.002 mm/min

UV exposure (hours)	E(MPa)	σ_B (MPa)	ε_B(%)
Fresh/(0.002mm/min)	1686	35.23	10.56
100-hour aged/(0.002mm/min)	1736	40.24	3.95
400-hour aged/(0.002mm/min)	2139	40.55	2.82

To study the UV-ageing effect on the viscoelastic properties of the *urushi* lacquer film, the MGKF model was fitted to the experimental creep and recovery data from samples after various durations of UV radiation, as shown in Figure 6-17 and Figure 6-18, with fitting parameters presented in Table 6-6. It can be seen that the model is capable of representing the UV aged material as well as the fresh *urushi*. The parameters η_0, η_i and E_i ($i\geq1$) can be calculated to analyse the physical meaning of these parameters on the mechanical components in Figure 6-12. The conversion of η_0, η_i and E_i ($i\geq1$) from μ, λ, τ_1, τ_2, m and n are

expressed in the following equations, which can be regarded as a generalised form of Eqs. (5-2), (5-3) and (5-4) in the modified Burger's model for PU, as described in Chapter 5:

$$h_0 = \frac{m^m}{s^{m-1}}$$

(6-13)

$$E_i = \frac{l^n}{s^{n-1}} , (i \geq 1)$$

(6-14)

$$h_i = \frac{t_i l^n}{s^{n-1}} , (i \geq 1).$$

(6-15)

The parameters η_0, η_i and E_i ($i \geq 1$) for different UV ageing conditions are plotted as a function of stress in Figure 6-19. As we can see, there is a strong dependence of the parameters on the UV ageing. It can be seen that both the spring stiffness and dashpot damping coefficient tend to increase with UV ageing, which is consistent with the general observation of increasing stiffness and reduced viscosity following ageing.
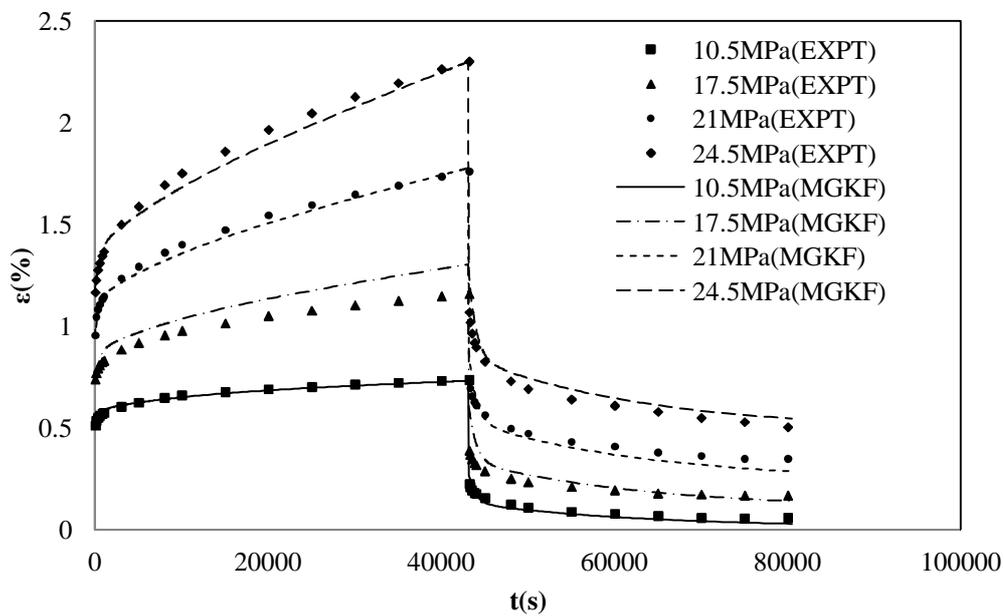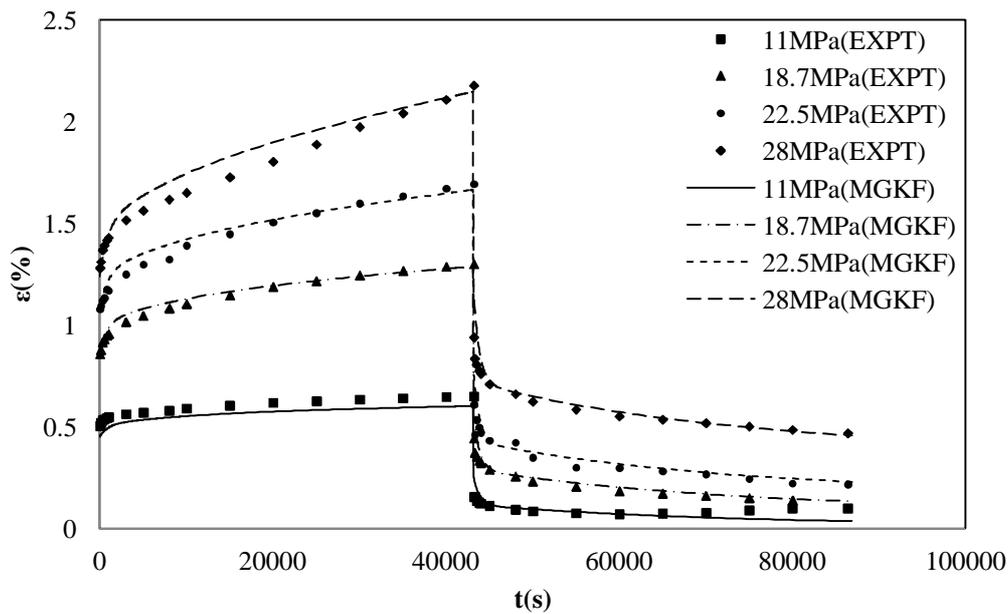

Figure 6-17: Experimental (EXPT) and predicted (MGKF) creep and recovery data for 100-hour aged *urushi* film samples using modified generalised Kelvin fluid model.
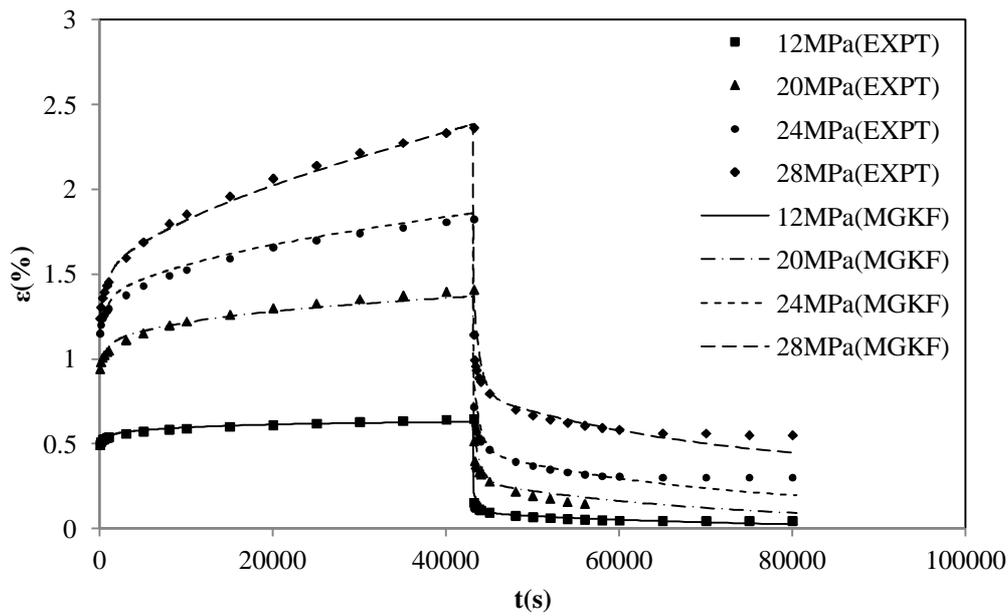
Figure 6-18: Experimental (EXPT) and predicted (MGKF) creep and recovery data for 400-hour UV aged *urushi* film samples using modified generalised Kelvin fluid model.

Table 6-6: Parameters derived from a modified generalised Kelvin fluid creep and recovery model for *urushi* film conditioned at 50% RH after different periods of UV exposure.

UV exposure (hr)		E_0	μ	λ	$\tau_1(s)$	m	n	$\tau_2 (s)$
0	Creep	2177±4.7%	8010	3400	532	2.70	1.25	10000
	Recovery		776	1747	835	4.63	1.29	20395
100	Creep	2193±6.5%	15979	1211	906	2.55	1.59	10320
	Recovery		2362	2013	667	3.66	1.26	30164
400	Creep	2227±4.7%	849	832	847	4.63	1.74	10744
	Recovery		263	408	762	7.33	1.91	27732
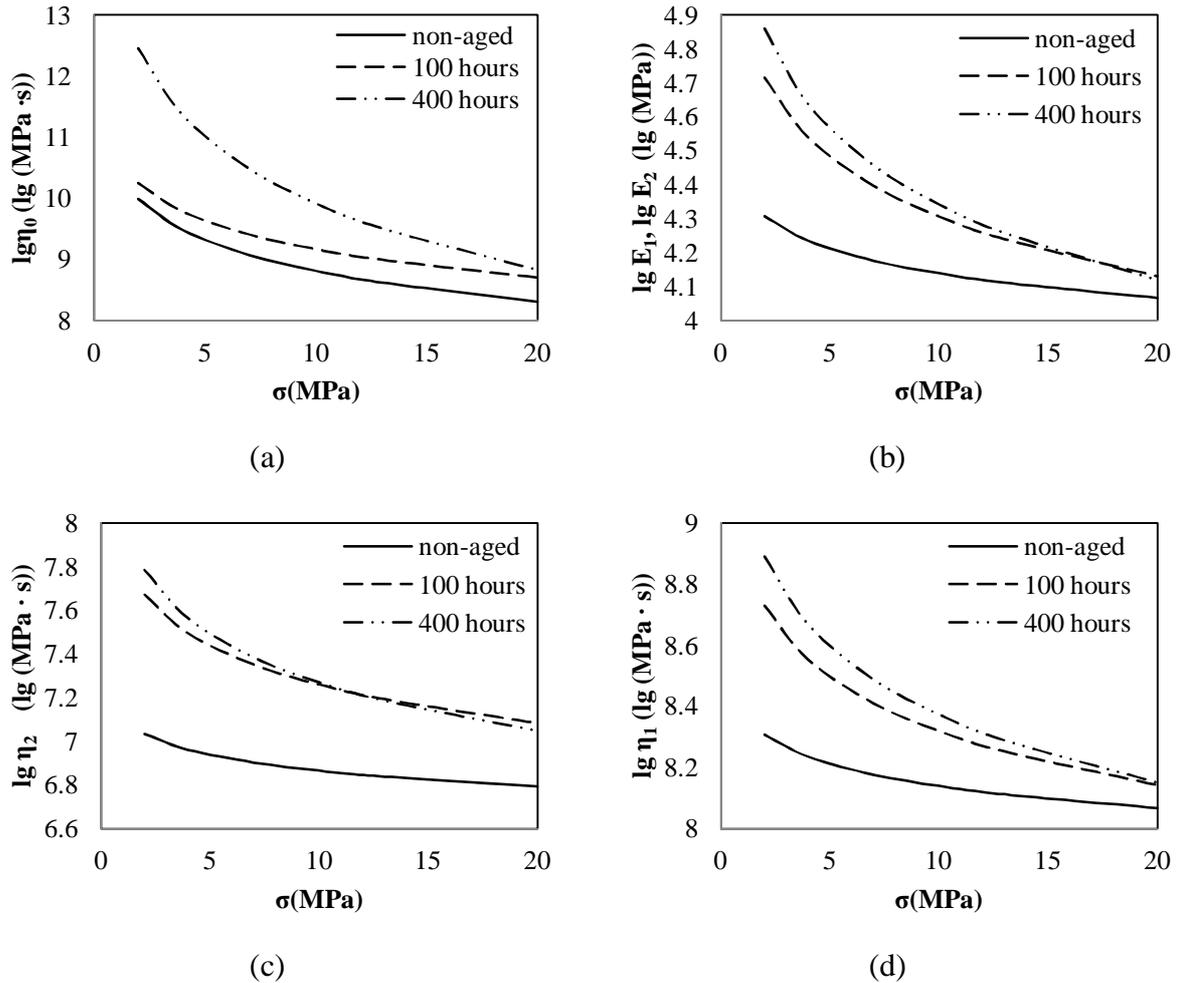
Figure 6-19: Effect of UV ageing on viscoelastic constants of modified generalised Kelvin fluid model for *urushi* film.

6.4 Summary and conclusions

Fresh *urushi* film has been subjected to extensive mechanical testing, comprising constant displacement rate tests at various rates and creep and recovery tests. The *urushi* lacquer film was found to be a nonlinear viscoelastic material at low stress levels with an apparent yield stress. A rate dependent von Mises plasticity model was capable of accurately modelling the full visco-elastic-plastic stress-strain behaviour under constant displacement rate testing but was less successful at modelling the creep behaviour and could not model time dependent recovery. A power law creep model was more successful at predicting creep only, but was also incapable of modelling the time dependent recovery. Mechanical analogue models are capable of describing various types of behaviour and a number of these were assessed. The most successful was the proposed modified generalised Kelvin fluid model, which was also capable of modelling UV aged *urushi* behaviour by using UV ageing time dependent material

constants. The MGKF is a powerful non-linear viscoelastic model capable of representing a wide range of behaviour below the material yield stress. However, in order to include the post yield behaviour a visco-elastic-plastic model is required, or the rate dependent von Mises model can be used. Quantitative analysis based on mechanical tests on samples after different durations of UV ageing show the mechanical properties of *urushi* film to be highly dependent on the duration of UV radiation.

Chapter 7 Modelling the Mechanical Response of *Urushi* Lacquer Subjected to Varying Relative Humidity

7.1 Introduction

Relative humidity is an important factor that contributes to the damage of *urushi* film in service (Chapter 2). When considering the conservation of such an object under varying relative humidity, questions arise regarding the suitability of treatments, and surprisingly there has been little scientific exploration of this to date. A need arises, therefore, to explore the material properties, the environmental conditions, their interaction and the consequences for the conservation of important cultural objects.

The modelling of *urushi* behaviour has been limited. Ogawa and Kamei [46] used FEM to explore the effect of moisture on fracture properties, but limited themselves to an assumption of elastic material properties. Viscoelasticity is not only non-negligible, but the viscoelastic behaviour is strongly affected by both moisture content and UV ageing [42, 44-45, 56]. As a result, it is of great interest to develop a hygro-mechanical model of *urushi* using a phenomenological description of viscoelasticity. The material and mechanical properties need to be measured as a function of the relative humidity (RH) and the relationship between RH and moisture content needs to be determined. These properties serve as inputs to a FE based model which can be tested against experimental measurements of the depth averaged stresses in a thin layer of *urushi* deposited on a substrate and exposed to changes in the environmental conditions [5].

In this chapter, the experimental results used to identify the relevant constitutive relationships will be discussed. Using as a basis the general model for modelling mechanical-diffusion interaction introduced in Chapter 2, a solution for the model will be obtained and the results will be used to validate the predictions against the results of Elmahdy *et al.* [56].

7.2 Material properties

7.2.1 Identification of the material rheology

A series of mechanical tests was performed to identify the characteristic rheological properties including constant displacement rate, and creep and recovery tests at different relative humidities.

Uniaxial loading at constant deformation rate (0.002 mm/min) for *urushi* samples saturated under different relative humidities was performed (Figure 7-1) to obtain estimates of the tensile strength, elastic modulus and fracture strain (Table 7-1). These results show that as the humidity is increased, the elastic region and modulus reduce and the fracture strain increases, consistent with the ingressed moisture acting as a plasticiser [49, 170]. Creep and recovery tests were performed at a range of humidities and constant stresses (30%, 50%, 60% and 70% of their tensile strength at break (Table 7-1)) by applying a constant load and recording the subsequent deformation as a function of time. After 12 hours, the load was removed and a 12 hour recovery observed. The symbols in Figure 7-3 (a-c) show the observed behaviour for different humidities. The behaviour is typical for a viscoelastic response: a rapid increase in strain, followed by a reduction in strain rate to a constant, but non-zero value, and an instantaneous recovery followed by a relaxation to an asymptotic, non-zero strain.
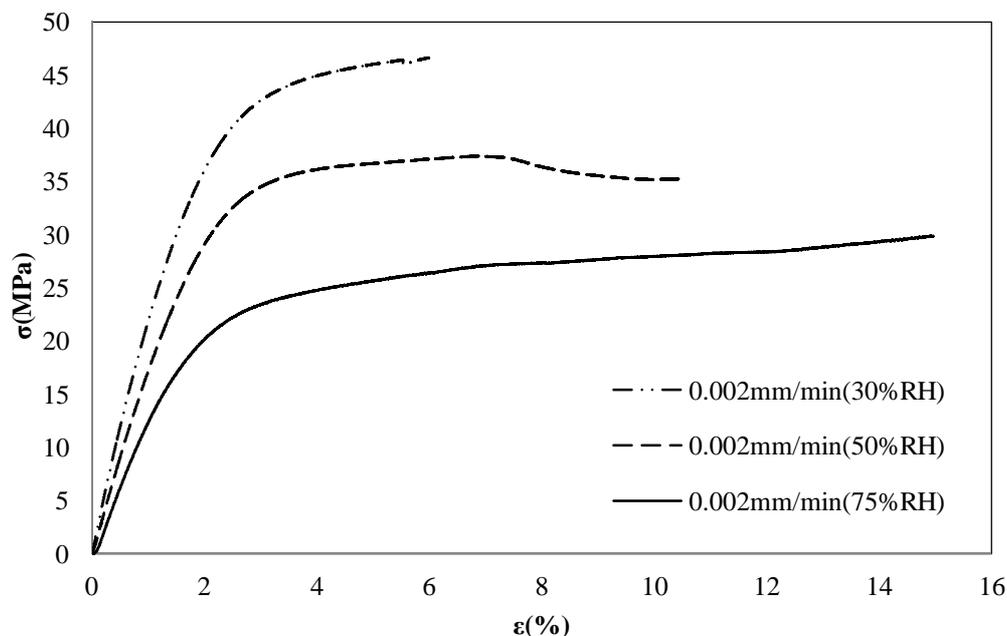
Figure 7-1: Stress-strain curves from tensile tests performed at 0.002 mm/min on *urushi* film samples after saturation at different relative humidities (shown in legend).

Table 7-1: Tensile elastic modulus (E), tensile strength at break (σ_B) and strain at break (ε_B) for *urushi* film samples after saturation at different relative humidities from constant displacement rate tests at 0.002 mm/min.

RH	E (MPa)	σ_B (MPa)	ε_B (%)
30% RH/(0.002mm/min)	2298.2	46.6	5.8
50% RH/(0.002mm/min)	1736.4	35.2	10.4
75% RH/(0.002mm/min)	1356.8	29.7	14.8
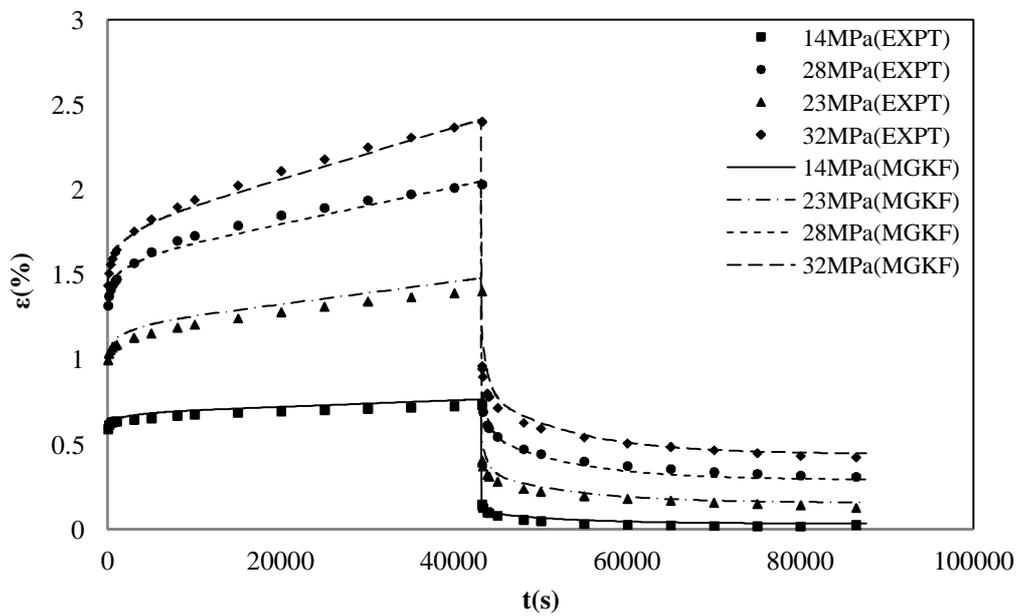
(a)

Figure 7-2: Experimental (EXPT) and predicted (MGKF) creep and recovery data for *urushi* film samples saturated under 30, 50 and 75% RH, (a), (b) and (c) respectively, at a range of constant stresses (shown in legend) (*To be continued in Page 125*).
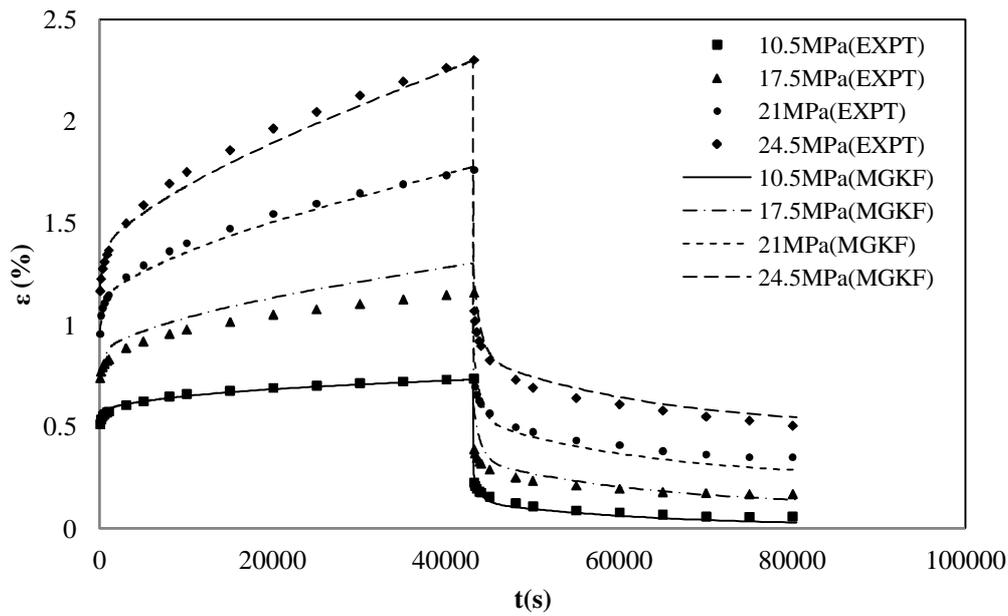
(b)
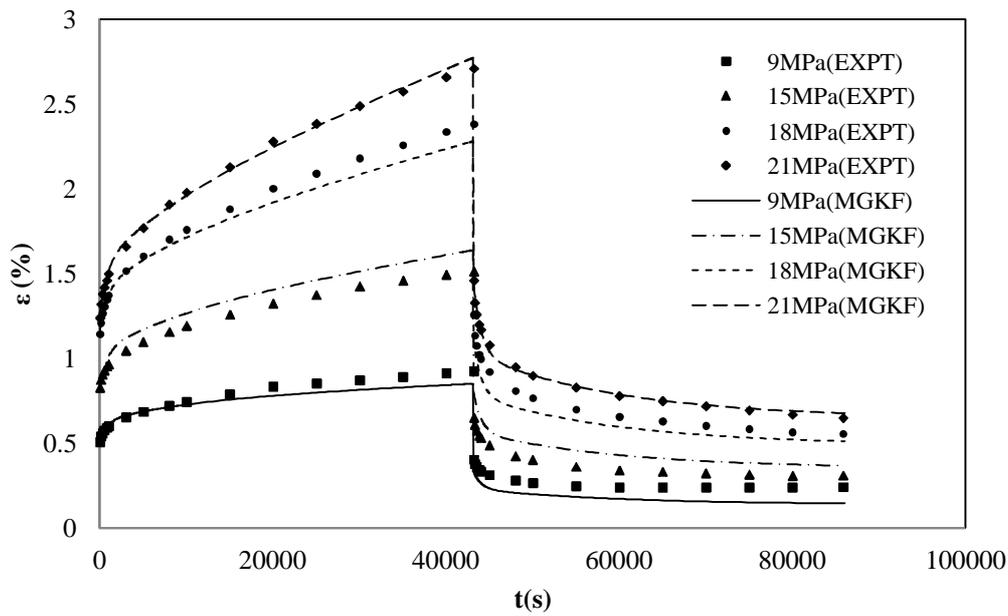
(c)

Figure 7-3: Experimental (EXPT) and predicted (MGKF) creep and recovery data for *urushi* film samples saturated under 30, 50 and 75% RH, (a), (b) and (c) respectively, at a range of constant stresses (shown in legend) (*Continnuing from Page 126*).

The previous analysis of fresh and UV aged *urushi* (Chapter 6) showed that it can be modelled using a modified generalised Kelvin fluid (MGKF) model composed of non-linear Maxwell and multiple Kelvin units connected in series (Figure 6-12). The parameters defined

in Eqs. (6-13)-(6-15) are plotted as functions of stress and RH in Figure 7-4. These were obtained from the parameters which were determined by curve fitting to the MGKF model, as shown in Table 7-2. It can be seen from Figure 7-4 that, firstly, the magnitude of all the parameters decreases as the stress is increased. Secondly in each case, the magnitude of all the parameters decreases as the relative humidity increases, indicating that as moisture is absorbed there is a tendency for the resistance to deformation to reduce.
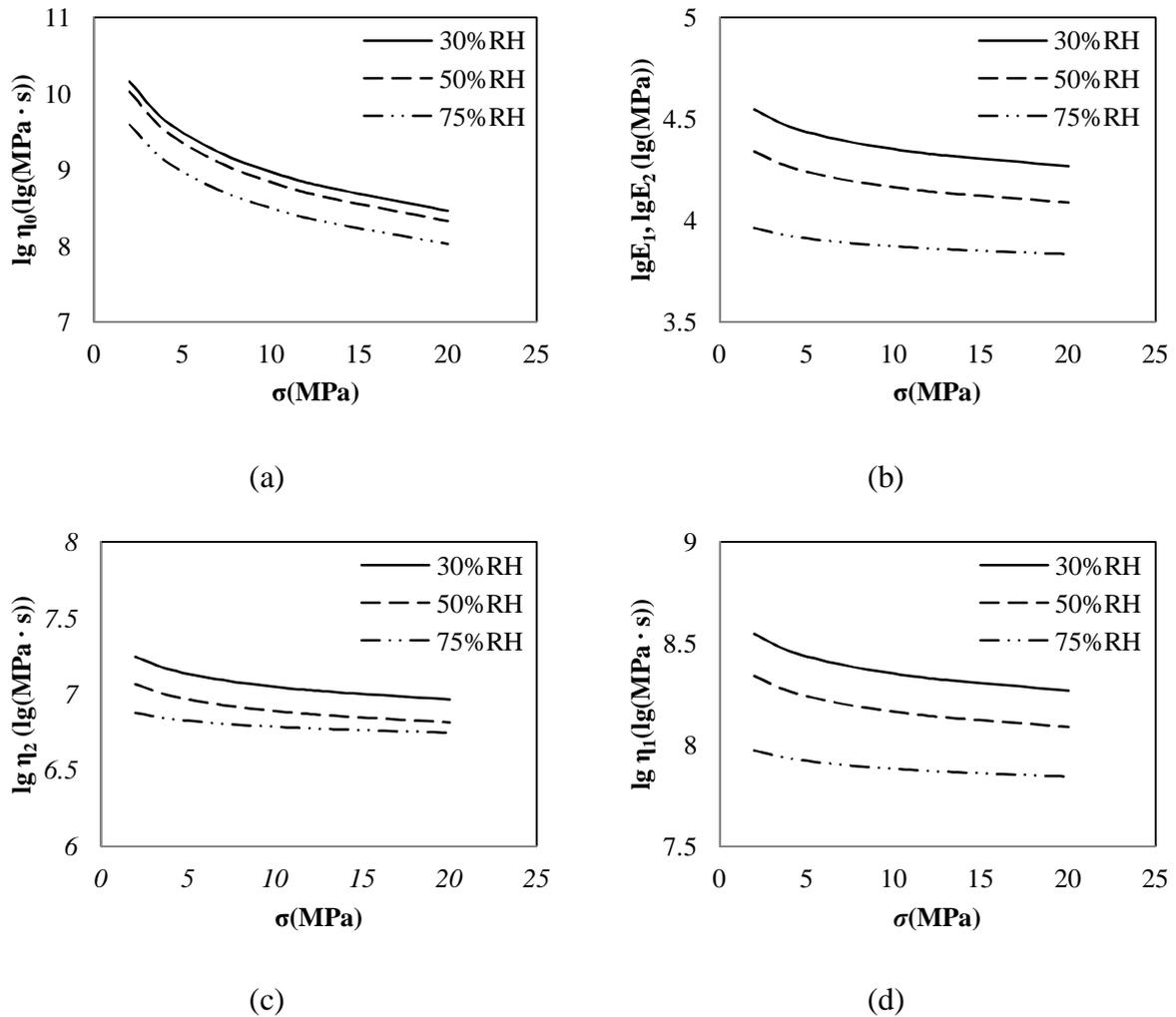
Figure 7-4: Effect of RH on the viscoelastic coefficients of the modified generalised Kelvin fluid model for *urushi* films (Eqs. (6-13)-(6-15)) at different RH (shown in legend).

Table 7-2: Parameters derived from a modified generalised Kelvin fluid creep and recovery model for fresh *urushi* film conditioned at various RH.

RH		E_0	μ	λ	$\tau_1(s)$	m	n	$\tau_2(s)$
30%	Creep	2256±4.7%	8947	4157	500	2.71	1.28	9876
	Recovery		5303	491	724	3.15	2.05	10081
50%	Creep	2177±6.5%	8010	3400	531	2.70	1.25	10000
	Recovery		776	1747	835	4.63	1.29	20394
75%	Creep	1711±6.1%	8488	3487	820	2.56	1.13	10204
	Recovery		117471	567	906	1.82	1.67	16934

7.2.2   Coefficient of hygroscopic expansion

The coefficient of hygroscopic expansion was found to be a constant with a value $b = 0.0027$ (wt %)$^{-1}$. This is in consistency with the value measured by previous work in terms of the magnitude [46].
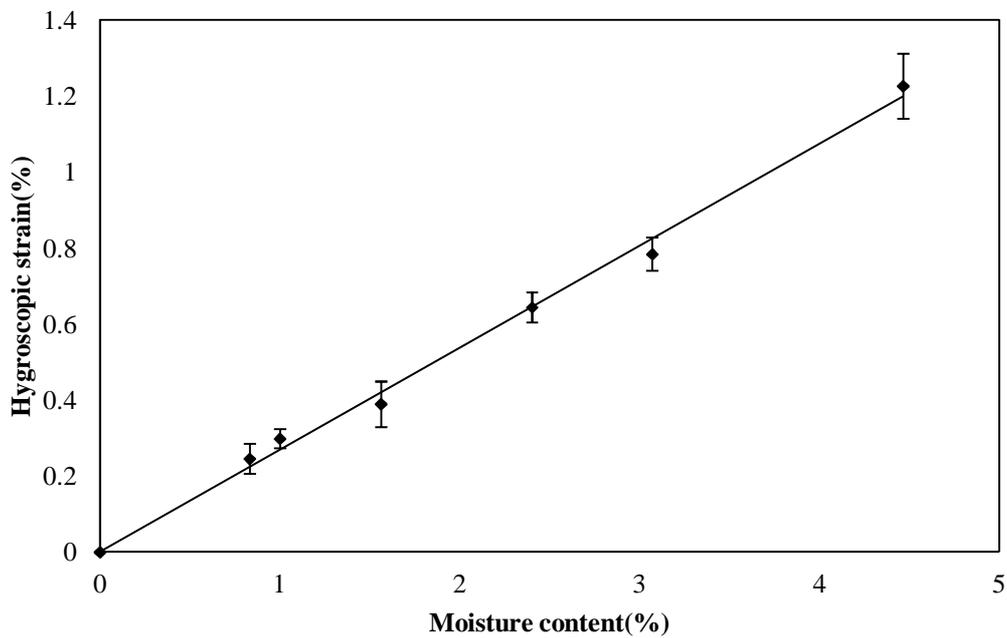
Figure 7-5: The measured hygroscopic strain of saturated samples as a function of moisture content, with error bars showing standard deviation.

7.2.3 Diffusion

The diffusion coefficient was measured using the method described in Chapter 3. The symbols in Figure 7-6 show the moisture content as a function of time for *urushi* film for various changes of RH. The main features that can be seen are that the moisture gain increases with relative humidity and that the experimental data fits well to Fickian diffusion [90]. This suggests that an analysis of the data can be performed to extract the diffusion coefficient, *D*, using the equations of Fickian diffusive transport. The solution of Fick's law, Eq. (2-11) is used to perform a curve fitting to the experimental data, shown by the solid line in Figure 7-6. A satisfactory agreement was found and *D* for different relative humidities is given in Table 7-3. The values of *D* measured at different humidities match the magnitude of the *D* reported in literatures ([46])

The absorption isotherm of water was modelled using the Guggenheim-Anderson-de-Boer (GAB) equation. Figure 7-7 shows a fit of the GAB model (Eq. (2-18)) to the experimental data, demonstrating good agreement (Table 7-4). GAB is commonly used for multi-layer sorption, hence its use here since *urushi* is built up through successive layering. This shape absorption isotherm is also reported in other urushi literatures [27, 46]
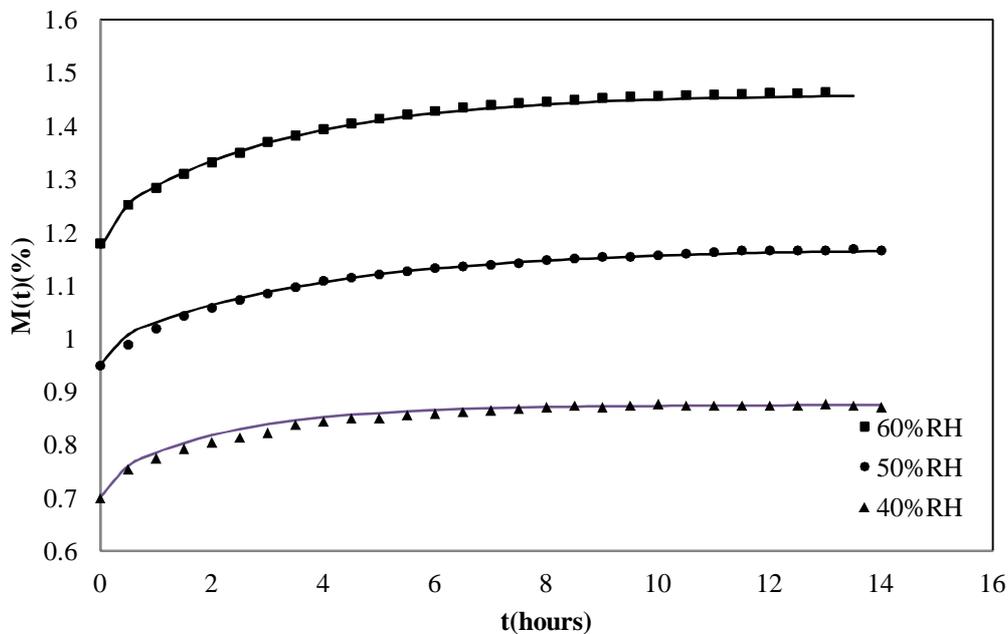
Figure 7-6: Moisture uptake of *urushi* samples as a result of a step change in relative humidity from 30% to 40%, 40% to 50% and 50% to 60%.

Table 7-3: Diffusion coefficient at different relative humidities.

RH	40%	50%	60%
D (m²/s)	2.26×10^{-13}	1.78×10^{-13}	2.02×10^{-13}
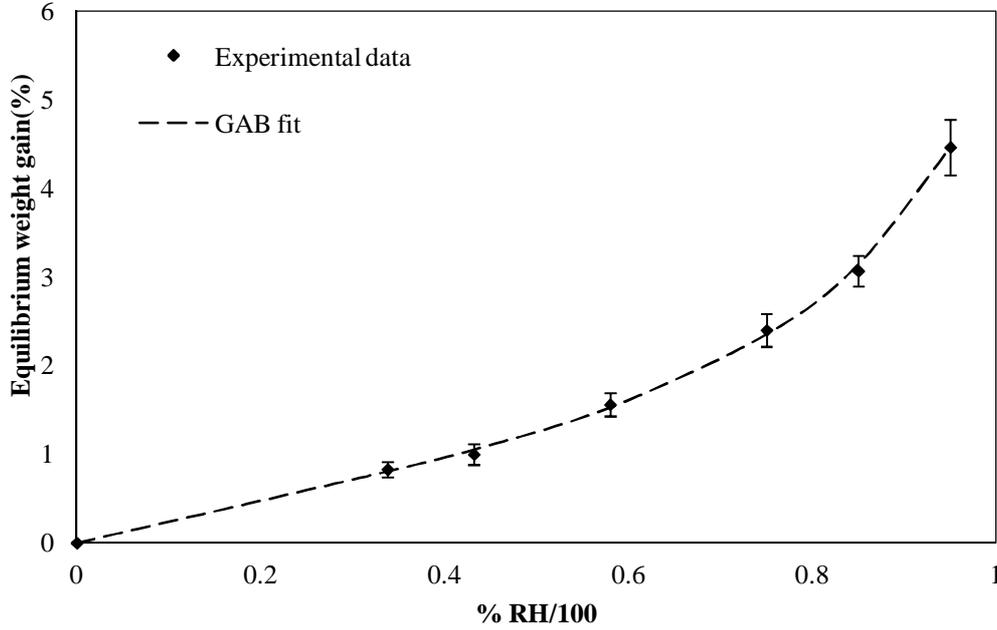
Figure 7-7: Equilibrium weight gain, $M(\infty)$, as a function of relative humidity. The dashed line represents a fit of Eq.(2-18) to the experimental results (symbols), with error bars showing standard deviation.

Table 7-4: Parameters of GAB function for modelling relationship between equilibrium weight gain ($M(\infty)$) and relative humidity for *urushi* films.

M_m	A	C
0.0113	0.811	2.84

7.3 Model solution and results

A FE model of the experiments by Elmahdy *et al.* [56] was created using ABAQUS. Detailed information on the FE pre-processer and solver can be found in Chapter 4. In order to develop a three dimensional model, the rheological model described by Eq. (6-11) was extended to multidimensional stress space. In this case, the multi-direction creep strain rate, $\dot{\varepsilon}_{ij}$, was determined using an associated flow law [181]:

$$\dot{\varepsilon}_{ij} = \dot{\varepsilon}_{eq} \frac{\partial g}{\partial \sigma_{ij}} \tag{7-1}$$

where $\dot{\varepsilon}_{eq}$ is a scalar value representing an equivalent creep strain rate, g is the flow potential which can be related to an equivalent stress function, and i and j represent directions of the stress tensor. The equivalent creep strain rate at any time can then be calculated through a creep constitutive equation, the parameters of which can determined through curve fitting to uniaxial creep tensile test data. In this case a flow law based on the von Mises equivalent stress was used and Eq. (7-1) can then be written as

$$\dot{\varepsilon}_{ij}^c = \frac{3}{2}\dot{\varepsilon}_{eq}^c \frac{s_{ij}}{s_{eq}}. \tag{7-2}$$

This was implemented in ABAQUS using a UMAT.

Apart from UMAT for *urushi*, the rest of material properties for both urushi and glass assigned in FE modelling are listed in Table 7-5.

Table 7-5: Material properties of *urushi* and glass.

	Fresh *urushi*		Glass
Elastic modulus	2256 MPa	30% RH	80000 MPa
	2177 MPa	50% RH	
	1711 MPa	75% RH	
Poisson's ratio	0.29		0.3
Diffusion coefficient (m^2/s)	2.02		0
Expansion coefficient	0.0027 (wt %)$^{-1}$		0

The boundary conditions in the bi-material disc model were such that the lower edge of the disc is only free to displace in a direction that is perpendicular to the disc's axis of symmetry. The moisture boundary conditions were constant moisture content at the upper surface determined using Eq. (2-18) for the set environmental RH and zero flux at the interface between the lacquer and the substrate. Initially the right hand boundary was allowed to be permeable under the same conditions as the upper surface, but the ratio of depth to breadth was found to be sufficiently small that radial fluxes were insignificant and as a consequence all the numerical experiments discussed in this paper were performed with an impermeable sidewall. The values of the material properties were all specified from the experimentally determined parameters discussed in Section 2 of this Chapter, and the boundary conditions were specified to replicate the experimental conditions for the bi-layer disc.

Figure 7-8(a-c) shows the variation in the longitudinal stress, σ_{xx}, with time for the middle point of the coating layer through thickness of bi-material samples exposed to three different conditions: changing the relative humidity from 75% RH to 30% RH, 36% RH and 42% RH respectively. The plotted points indicate the experimental results and the error bars indicate the standard error in the measurement. The initial behaviour of the *urushi* film following a reduction in humidity is a hygroscopic shrinkage, which is constrained by the substrate, resulting in a tensile in-plane stress developing in the film. It can be seen from Figure 7-8(a) that the stress increases rapidly in the first few minutes, reaching a maximum value of approximately 11 MPa after approximately 8000s. After this time, there is a gradual reduction in the stress. A second effect of the desorption of the moisture is that the viscoelastic properties of the *urushi* film change, as discussed in last section, and this effect was also included in the model by having moisture dependent properties in the mechanical analysis. Following the initial increase in film stress, there is a gradual reduction of the stress, which can be attributed to the relaxation of the material that arises as a result of its viscoelastic nature. The solid lines in Figure 7-8 indicate the results from the semi-coupled hygro-stress model with the measured constitutive parameters discussed in last section. It can be seen that there is a close correspondence between the model predictions and the experimental results, with the model results lying within the bounds of the experimental error at all times. In particular, it can be seen that the model captures the rapid increase in depth-averaged stress during the early ingress phase, and accurately predicts the relaxation of the material at longer times. The good agreement between model and experiment suggests that the proposed hygro-mechanical model and the viscoelastic constitutive model provide a good phenomenological description of the observed behaviour, presenting a platform on which descriptions of models for the conservation of *urushi* can be built.
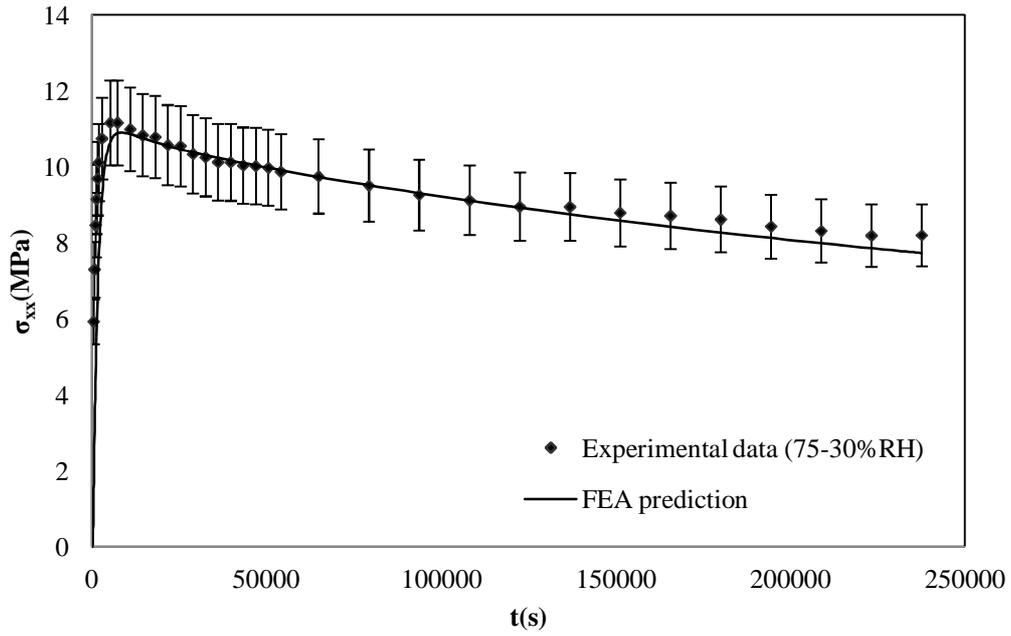
(a)
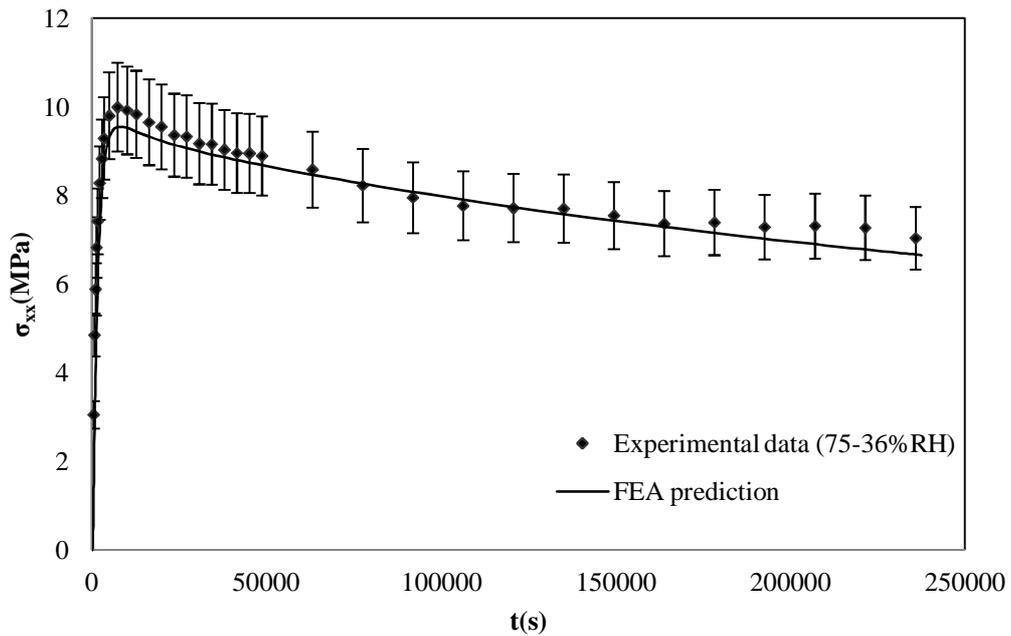
(b)

Figure 7-7: Comparison of experimental (symbols) and predicted (solid line) depth averaged stress as a function of conditioning time ((Experimental data in figures are provided by Dr Elmahdy, and the error was calculated based on a uncertainty analysis [5]).) when a bi-material sample saturated under 75% RH was placed into a chamber with humidity of (a) 30% RH, (b) 36% RH and (c) 42% RH (*to be continued in Page 134*)
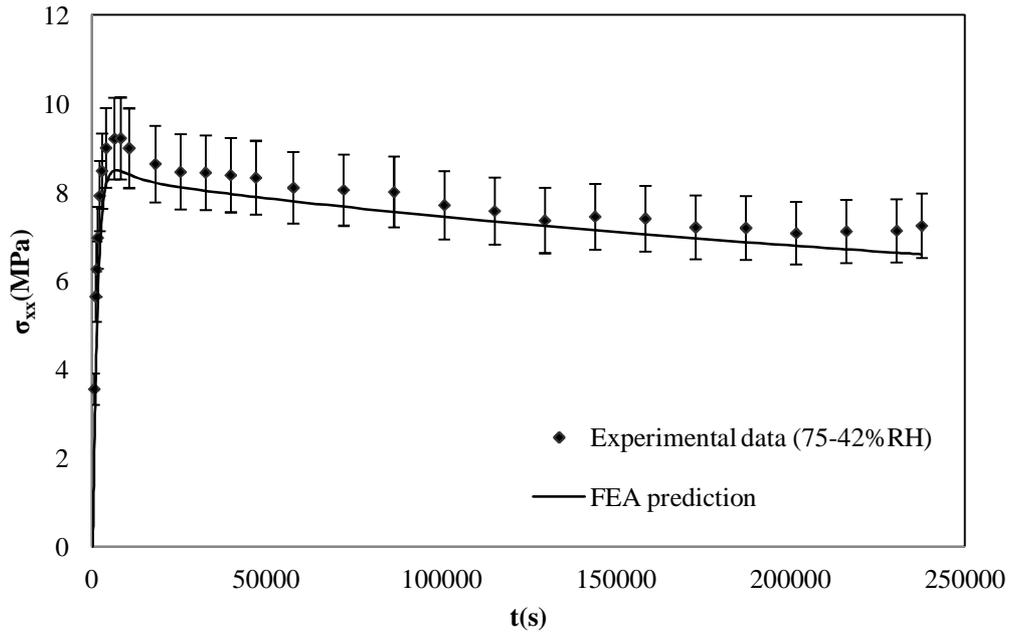
(c)

Figure 7-8: Comparison of experimental (symbols) and predicted (solid line) depth averaged stress as a function of conditioning time (Experimental data in figures are provided by Dr Elmahdy, and the error was calculated based on a uncertainty analysis [5]) when a bi-material sample saturated under 75% RH was placed into a chamber with humidity of (a) 30% RH, (b) 36% RH and (c) 42% RH (*continuing from Page 133*).

Having validated the method, it is interesting to examine the development of stresses as a function of depth. In Figure 7-9 (a) the evolution of the moisture concentration (normalised values on a basis of saturated concentration under 100% RH calculated using solved GAB model parameters in Table 7-4), through the *urushi* film thickness over time after the RH is reduced from 75% to 30% is shown. It can be seen that shortly after the change in RH, e.g. at 67 s, the change in moisture concentration is localised to the region near to the upper surface and the moisture concentration gradient near to the substrate is zero, suggesting that a gradient in stress should be expected. Indeed, from the calculated stresses at the corresponding times, as shown in Figure 7-9b, it can be seen that at short times the hygroscopic stresses are limited to the area to the surface. As the experiment proceeds, the moisture concentration gradient reduces and as the moisture approaches a constant as a function of depth, an almost uniform longitudinal stress is reached, although it is noted that the peak stress is largest at short times. This is clarified in Figure 7-10 which shows that although at short times the peak stress, occurring near to the upper surface, is significantly larger than the mean stress, that after a period of less than 30 minutes the range of stresses becomes small. It is also shown in Figure 7-10 that the maximum stress, occurring near to the upper surface during the first 60 minutes, is less than the depth averaged stress. This is because of the stress relaxation effect due to the viscoelasticity of the *urushi,* causing a decreased stress near to the surface.
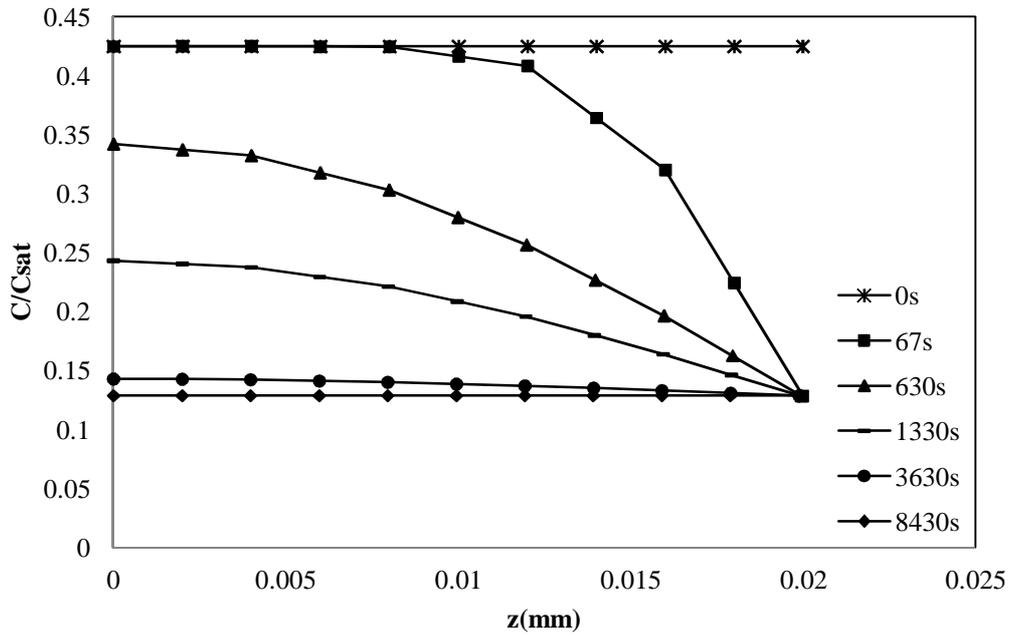
(a)
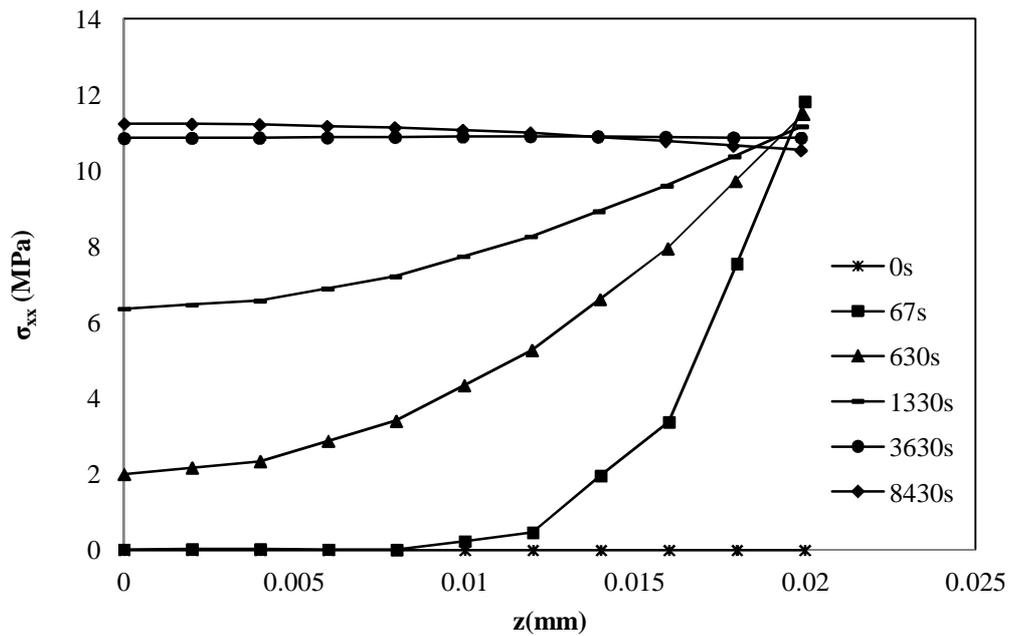
(b)

Figure 7-9: Distributions of (a) normalised moisture concentration, *C*, and (b) longitudinal stress (s_{xx}) as a function of depth, y, where y = 0 is the *urushi*-substrate interface and the *urushi* upper surface is at *y* = 0.02, under the boundary conditions shown in Figure 4-2 with the moisture variation from 75% to 30% RH.
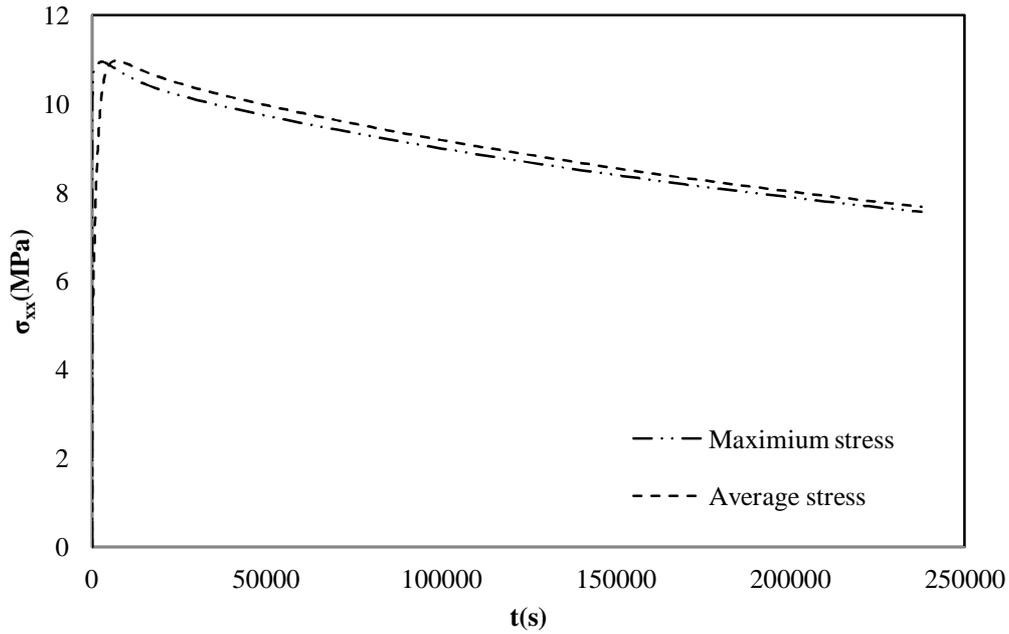
Figure 7-10: Comparison of depth averaged stress, $\sigma_{xx(avg)}$, and maximum stresses, $\sigma_{xx(max)}$, in longitudinal direction.

The model also allows the effects of a slowly cycling moisture content to be predicted, which is likely to be of interest since museum stored artifacts are not always stored in constant environmental conditions [42]. Figure 7-11 shows a time dependent relative humidity profile that varies between 70 and 30% RH with a period of 24h. The model predicts a time dependent depth averaged stress profile that oscillates in phase with the moisture variation, but with a decaying envelope attributable to the viscoelasticity, as shown in Figure 7-11 interestingly. Periods of compression can be seen after the first cycle as shown in Figure 7-12, which may cause in-film buckling after delamination. This indicates that further work should be done on the response of the material to dynamic loads and on the modes of failure in the material to study the damage initiation and propagation due to the dynamic loads caused by varying environmental conditions.
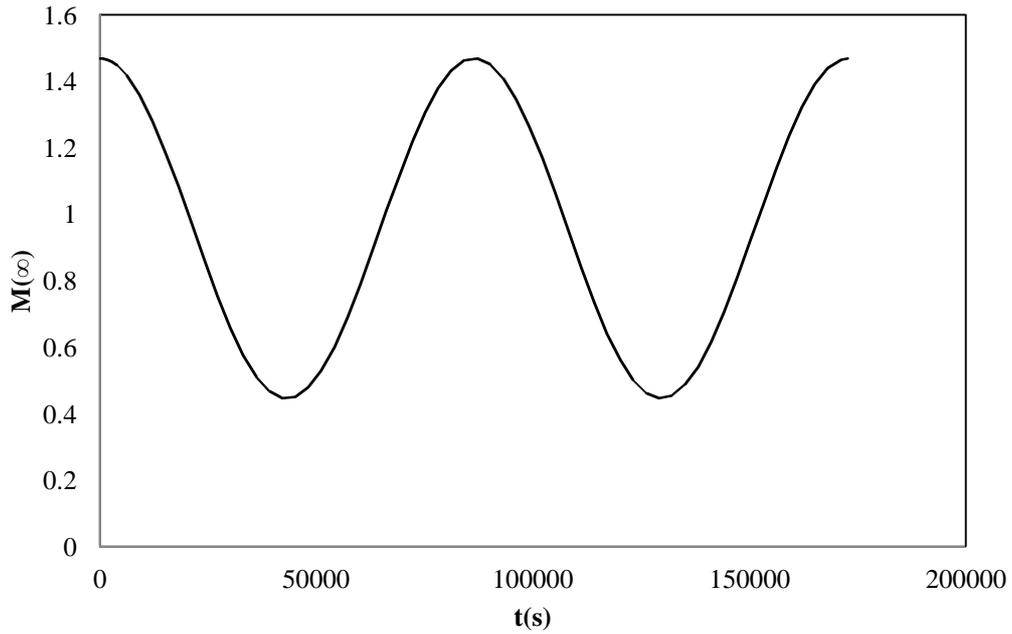
Figure 7-11: Changes of normalised moisture content of *urushi* film at surface when a sample experiences a sinusoidally varying humidity during 48 hours, with a peak to peak RH of 75 to 30%.
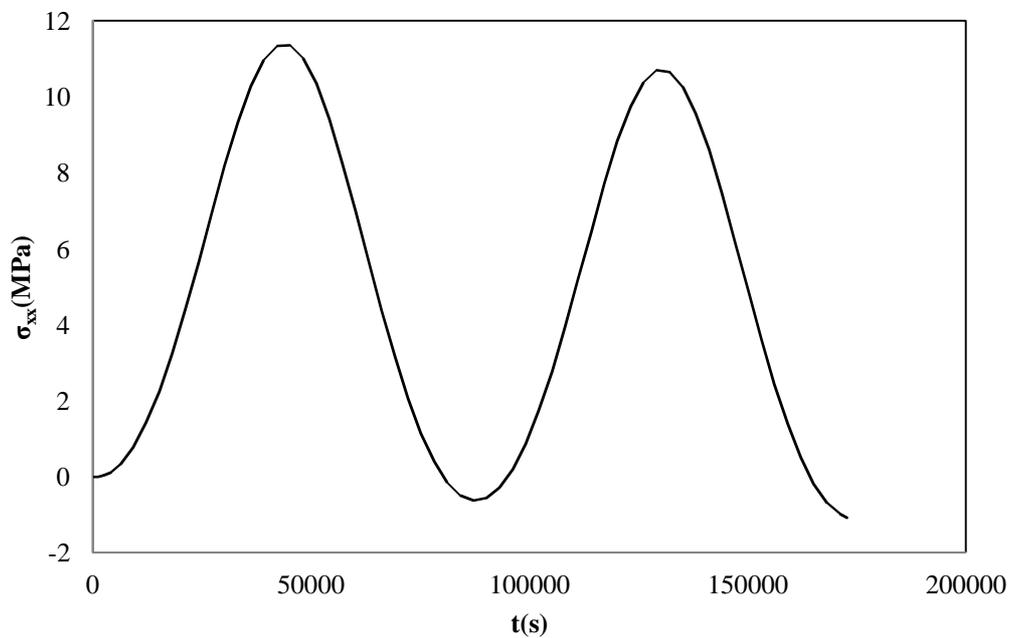
Figure 7-12: Stress evolution of *urushi* film when a bi-material sample saturated under 75% RH experiences a sinusoidally varying humidity during 48 hours, with a peak to peak RH of 75 to 30%.

7.4 Summary

A hygro-mechanical FE model of *urushi* behaviour based on a moisture dependent viscoelastic phenomenology has been developed and tested. Through careful determination of the mechanical behaviour the constitutive properties of a thin layer of lacquer were determined and used as an input to a FE based model of the deformation and stresses that develop in response to changes in the environmental conditions. The model was validated using experimental results that show the depth averaged stress in a thin layer of *urushi* deposited on a glass substrate. The model was used to gain insight into the time dependent and spatially varying stresses within the layer. These showed that the regions of highest stress were to found in areas of highest moisture transport, emphasising the need to control the environment in which *urushi* coated artefacts are stored.

Chapter 8 Modelling Mechanical Effects of Traditional Japanese Consolidation on Aged *Urushi* Films

8.1 Introduction

Over 4 centuries of fluctuating environmental conditions have led to the formation of micro-cracks in the main *urushi*-covered surfaces of the Mazarin Chest. The traditional Japanese consolidation method of lacquerware objects, known as *urushi-gatame,* consists of applying a diluted layer of fresh *urushi* to the damaged (aged) surface in order to fill any micro-cracks and restore its original gloss [182]. It is unknown, however, whether this procedure is effective in arresting crack propagation in the long term or whether it would accelerate damage mechanisms leading to the propagation of pre-existing micro-cracks. This poses a dilemma to Western museum curators and restorers, whose approach to conservation is based on minimum impact on the art piece, as opposed to their Japanese counterparts, who would apply the traditional methods used in the creation of the art piece to bring it back to its original appearance, even if this means adding or removing substantial parts of it [42]. In fracture mechanics, engineers are interested in the stress field near the crack tip and whether a failure criterion, such as the fracture toughness is exceeded. By determining the stress or strain fields around a crack on a plane along which the crack propagates they can evaluate the stress intensity factors, from which the maximum stress can be estimated. Some experimental work has been carried out to study mechanical effects of traditional Japanese consolidation on aged *urushi* films [183]. It managed to measure the displacement field across a crack (or 'v' groove) in the plane of the film surface. However, it has been found to be difficult to measure the displacement field at the crack tip with current techniques due to the extremely small localised dimension. In order to assess the effect of the traditional Japanese *urushi gatame* consolidation, an FEA model of the consolidation procedure was developed to evaluate the response of the consolidated film to changes in relative humidity. This model introduces an *urushi*/aluminium strip to mimic the previous experimental study [5]. This chapter initially studies the mechanical response of this bi-material structure to a bending load with consideration of the shape of the notch. The failure behaviour of the bi-material structure is modelled with the introduction of a maximum strain failure criterion to study the effectiveness of the traditional Japanese *urushi gatame* consolidation which is being used by conservators at the V&A Museum, London.

8.2 Mechanical response of grooved bi-material sample to bending load

8.2.1 Modelling bending behaviour

In Elmahdy *et al.*'s experiment [183], the aluminium substrates were mounted on a three-point-bending loading rig to strain the *urushi* film in a controlled and repeatable way. This was replicated in the FEA model. Detailed information on model geometry, mesh and boundary conditions is given in Chapter 4. The bi-layer model was initially subjected to a 0.08 mm displacement in the middle of the aluminium surface in a direction towards the *urushi* layer, in order to introduce bending of the structure. The displacement and stress fields around a crack (or 'v' groove), initially 0.05 mm in depth and 0.06 mm in width, in the plane of the film surface was studied after application of the deflection. The geometry of the crack is shown in Figure 8-1. As an initial study on mechanical response of this bi-material structure to a bending load, the material behaviour in this analysis was assumed to be time independent. The time-dependent behaviour will be studied in the next section.
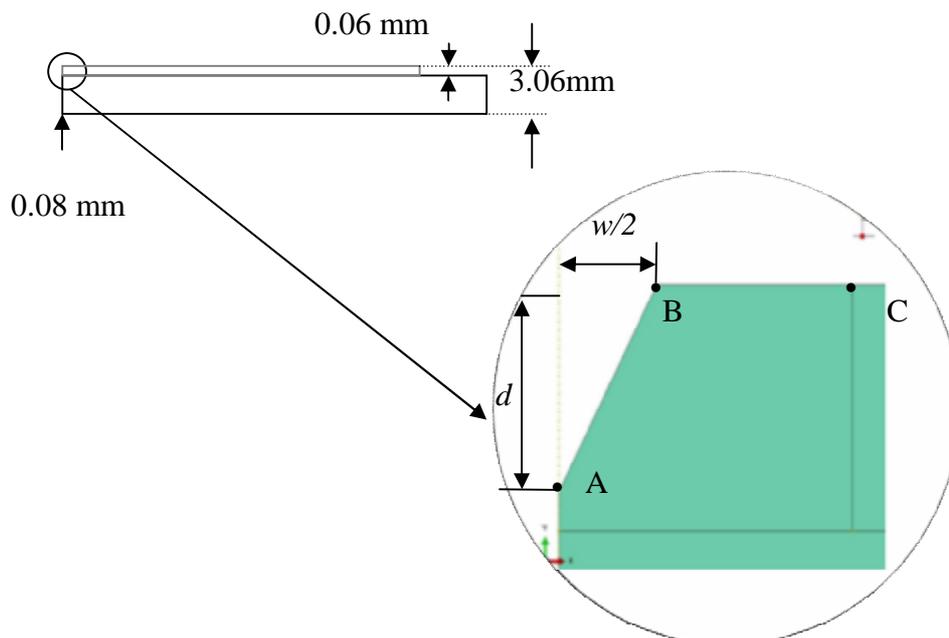
Figure 8-1: Simplified geometry of a grooved *urushi*/aluminium bi-material sample for FE analysis.

The time independent material properties assigned for *urushi* and aluminium are listed in the

Table 8-1: Material properties of *urushi* and aluminium

	Urushi		Aluminium
Elastic Modulus, *E* (MPa)	2148	Fresh	65000
	2214	100-hour-UV aged/50% RH	
	2289	400-hour-UV aged/50% RH	
Poisson's ratio, υ	0.29		0.33

Longitudinal displacement profiles around the groove were obtained from FEA and presented in Figure 8-2 for the nodes in path $\overline{ABC}$ in Figure 8-1. As shown in Figure 8-2, an anomaly in the displacement profile is visible in the vicinity of the groove, showing there is a discontinuity at the edge of the groove.
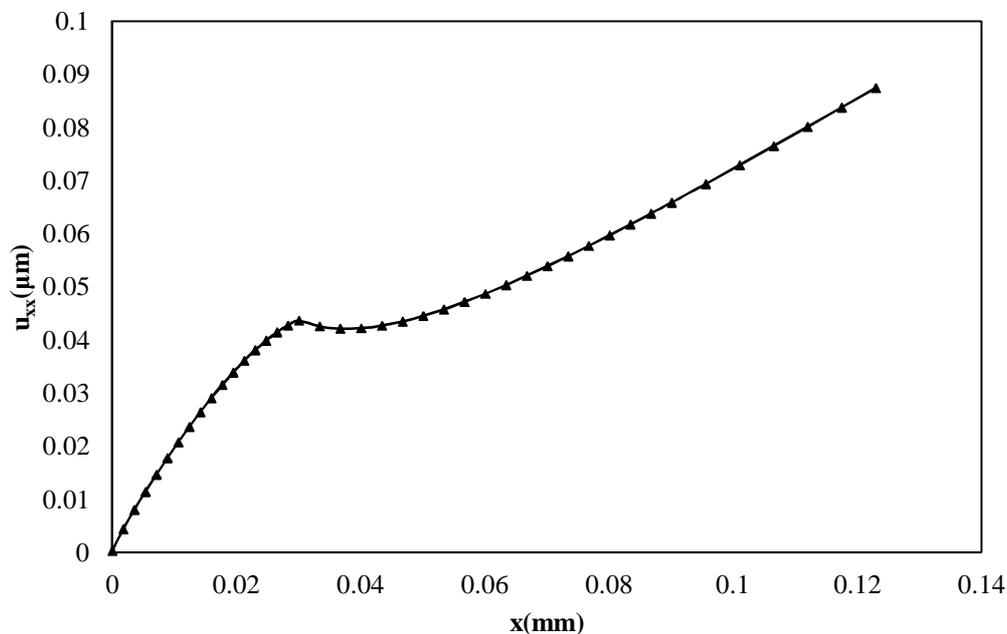
Figure 8-2: Displacement field profile around a groove (w=0.06, d=0.05, B and D indicate the points between which there is a negative slope).

8.2.2 Time dependent behaviour

The Time dependent bending behaviour of the grooved *urushi*/aluminium bi-material structure, which occurs as a result of the viscoelasticity of *urushi* film (Chapters 6 and 7), was studied by performing a similar FEA to that discussed in the previous section but holding the bending load for various periods and substituting to elastic material model used for the *urushi* in the previous model with the MGKF viscoelastic model. The longitudinal displacement along path $\overline{ABC}$ for the time dependent model is shown in Figure 8-3 for different periods of

time. It can be seen that the effect of holding time is small but some creep can be observed at the edge of the groove. It can be seen from this study that the mechanical response of this bi-material structure to a bending load is little affected by time, hence, the material properties of the *urushi* in this chapter are assumed to be time independent, if not specified otherwise.
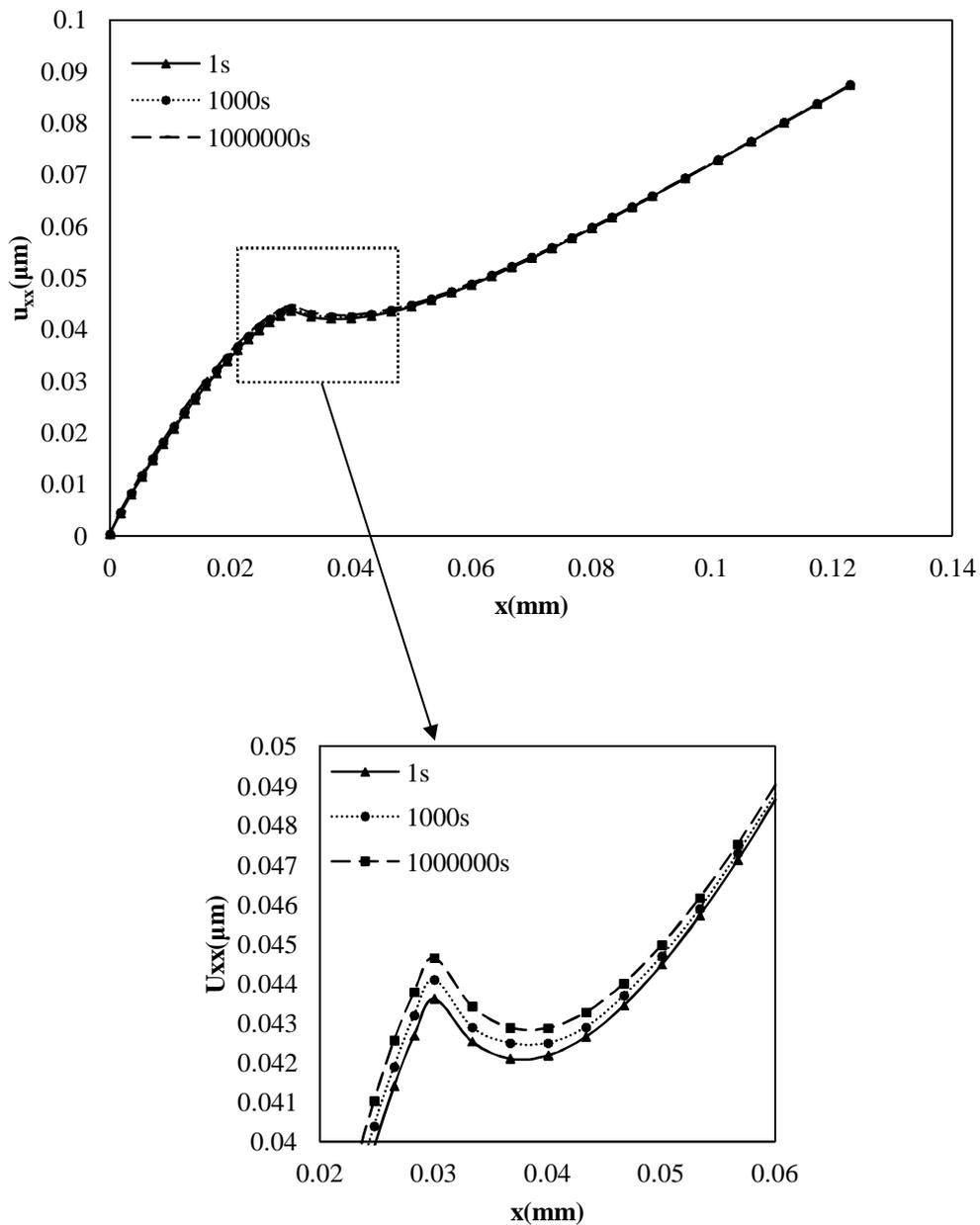
Figure 8-3: Displacement profile around groove in *urushi*/aluminium bi-material sample subjected to different periods of bending load.

8.2.3 Pile-up and sink-in effect

In the work of Elmahdy [5], the 'v' groove was created in the middle of the *urushi* film using a sharp blade [183]. It was difficult, due to the lack of understanding in response of *urushi* to cutting process, to determine the exact shape of the groove caused by this cutting process presenting difficulties when building the geometric model in FEA. In this analysis, therefore, two possible extremes of the surface profiles caused by the cutting process were considered. Pile-ups and sink-ins have been frequently reported in the literature for thin films [184-185], and present a possibility for exploring the range of possible behaviour. As a result, it was proposed to examine the limits of these conditions and compare displacements fields for these extremes of behaviour. Figure 8-4 illustrates pile-up and sink-in, showing the difference between a process which conserves material and one that removes all the material.

Pile-up

Sink-in

(a)   (b)
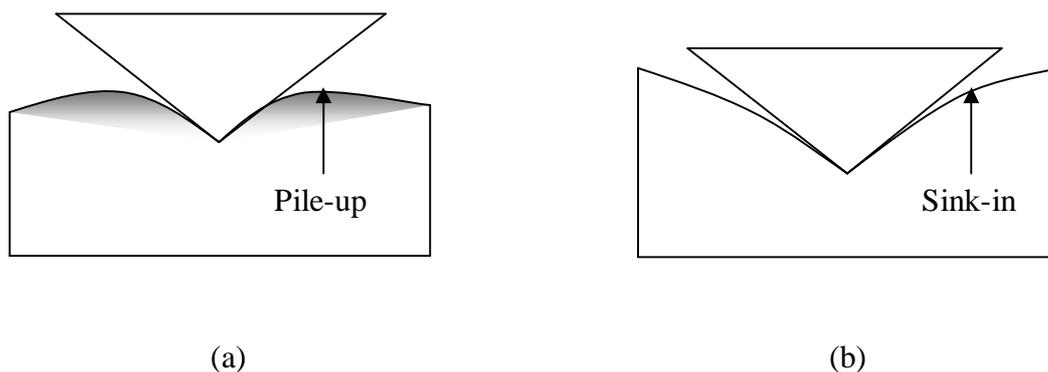
Figure 8-4: Pile-up (a) and sink-in (b).

An FE analysis was performed to study the displacement field around a 0.02 mm deep groove, with pile-up or sink-in caused by cutting the groove, for the same *urushi*/aluminium bi-material structure model explored in Section 8.2.1. The geometries of the pile-up and the sink-in were estimated using spline curves on a basis of the given geometry (width, height and depth of the groove). A comparison of the displacement fields around the two grooves can be seen in Figure 8-5. Here a significant difference in behaviour can be seen with the displacement field for pile-up and sink-in. This suggests that the discontinuity at the edge of the groove is enhanced by the presence of piled up regions surrounding the cut, whereas sink-in reduces this discontinuity.
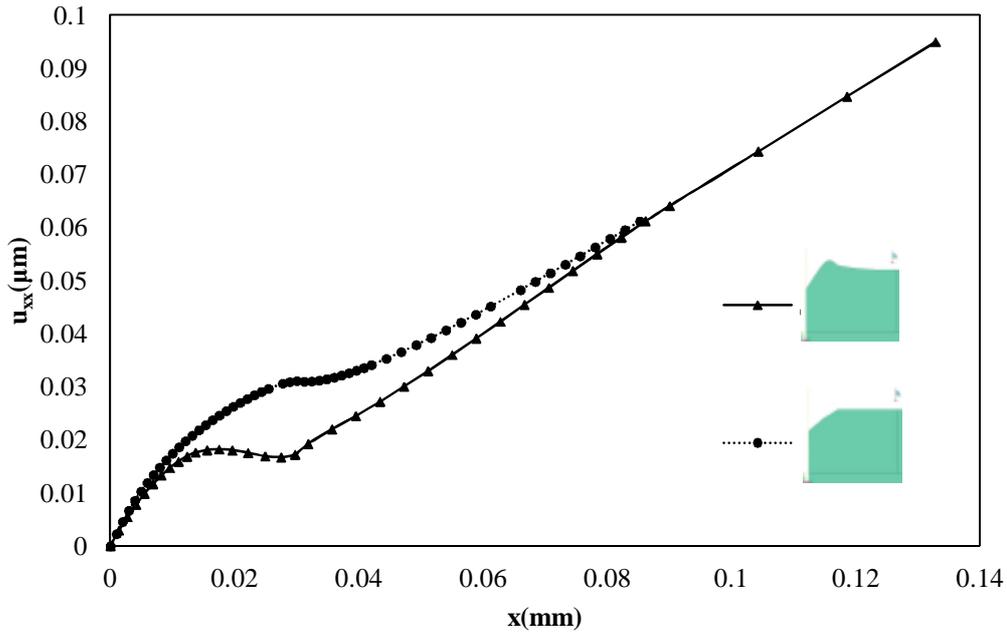
Figure 8-5: Profiles of longitudinal displacement for grooved *urushi*/aluminium bi-material strips with pile-up and sink-in.

8.2.4 Depth effect

The effect of groove depth on the displacement field around a groove was studied by analysing models of the grooved bi-material *urushi*/aluminium strip, with a constant groove width (0.03mm) and various depths, without pile-up and sink-in. The profiles of longitudinal displacement around the grooves are shown in Figure 8-6. It can be seen that the groove caused an increase in the longitudinal strain around the groove region with increasing groove depth. As a distance from the groove, the longitudinal strain is insensitive to groove depth, however, the deeper the groove, the greater distance over which the groove has an effect.
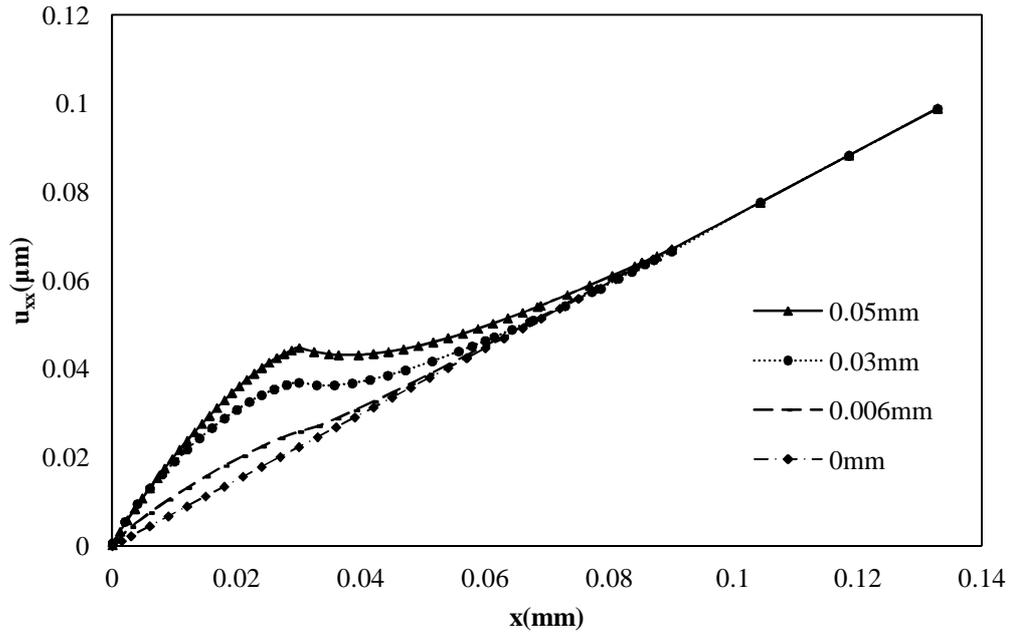
Figure 8-6: Profiles of longitudinal displacement around grooves with a width of 0.03 mm and different depths.

8.2.5 Width effect

The effect of groove width on the displacement field around a groove was studied by performing an analysis using a grooved bi-material *urushi*/aluminium strip model with a groove of a depth of 0.03mm but with varying width and no pile-up or sink-in. The profiles of the longitudinal displacement around the grooves of the grooved bi-material strips are shown in Figure 8-7. It can be seen that the longitudinal displacement in the region of the groove increases with groove width, as does the area over which the groove has an effect. However, the longitudinal displacement fields tend to have the same slope at distance from the groove [186].
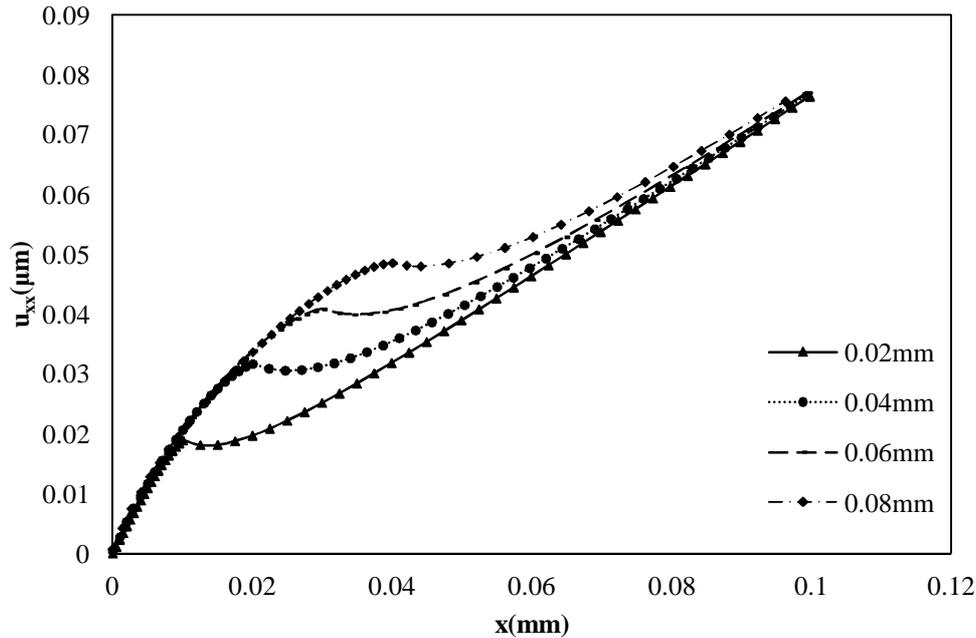
Figure 8-7: Profiles of longitudinal displacement around grooves with a depth of 0.03 mm and different widths.

8.2.6 Height effect

The effect of height of pile-up on the profiles of longitudinal displacement was studied by performing an analysis of the grooved bi-material *urushi*/aluminium strip model with different heights of pile-up, *H* (Figure 8-8). The pile-ups were made to have the same groove cross-sectional area to replicate a situation with no material loss. All the grooves had the same width and depth (0.08 mm wide and 0.03 mm deep), with an example shown in Figure 8-8. The profiles of displacement around the groove with different *H* are shown in Figure 8-9. It can be seen that the discontinuity at the edge of the groove increases with pile-up height. This suggests that a combination of pile-up and groove depth control the magnitude of the discontinuity in the displacement field at the edge of the groove.

These studies have shown that the displacement and, hence, strain and stress fields around a scratch or crack in an *urushi* coating are highly dependent on the geometry of the "groove". A detailed knowledge of groove geometry is therefore required to accurately model the effect of the groove on coating performance.
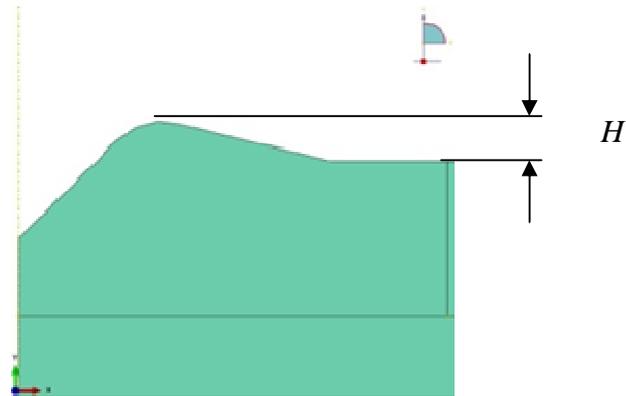
Figure 8-8: Pile-up of a groove with a height of *H*.
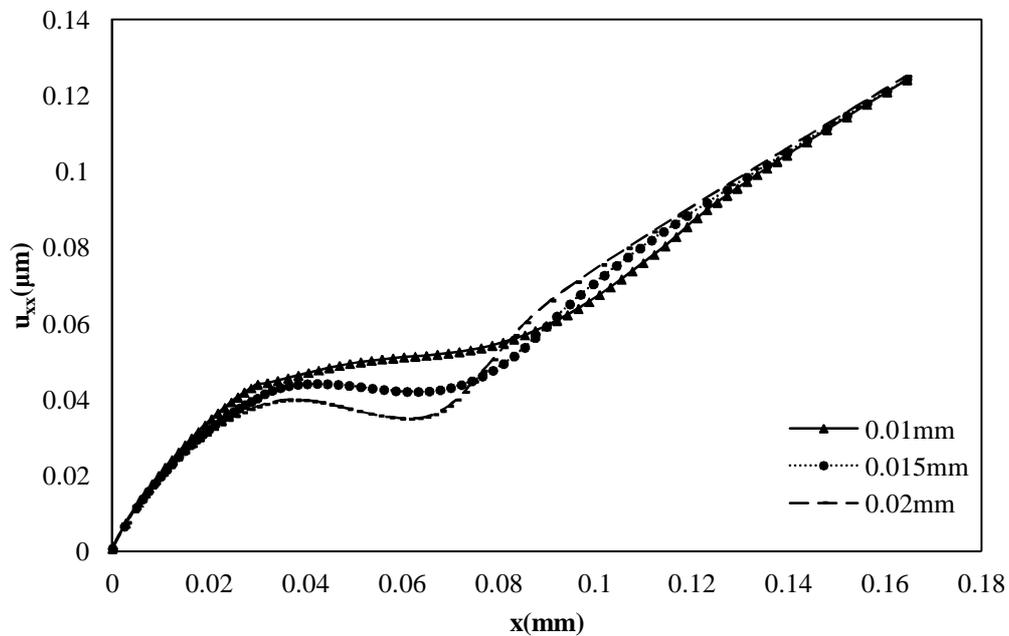
Figure 8-9: Profiles of longitudinal displacement field around a groove with different height of pile-up (*H*).

8.3 Failure behaviour and consolidation

The failure behaviour of a grooved *urushi*/aluminium bi-material strip subjected to bending load and the effectiveness of the traditional Japanese *urushi gatame* consolidation was also studied. A strain-based failure model was adopted using the FEA package ABAQUS, which can not only predict the strength, but also the damage initiation and propagation for both in-film and interfacial damage. This strain-based cohesive failure model is a simple and effective method of modelling progressive continuum damage and failure in adhesively

bonded joints [187]. The only parameter required in this method is the moisture dependent critical failure strain.

8.3.1 Predictive modelling using the strain-based failure model

The grooved *urushi*/aluminium bi-material strip shown in Figure 8-1 was considered first to study the bending failure behaviour using a strain-based failure model. To avoid a stress concentration due to a singular geometry, a small fillet was created at the bottom of the groove as shown in Figure 8-10. A 2-D FE model of an *urushi*/aluminium bi-material strip was created with the same geometry as that shown in Figure 4-5. A rate-independent elastic-plastic model with material properties determined from experimental results (constant displacement rate tensile tests of fresh *urushi* film at 0.2 mm/min), was adopted to define the material behaviour of the *urushi* film. The raw stress-strain data was treated by an Abaqus plug-in software, *EP Calibrate*, to obtain plastic strain-stress data which is used to input into Abaqus MATERIAL PROPERTIES module. A material damage model was defined with the failure plastic strain as a damage initiation parameter and zero fracture energy as a damage evolution parameter. This means the material response followed the non-linear constitutive response until the equivalent plastic strain (corresponding to Mises equivalent stress) reached a critical value to fail at any element integration point. It is worth noting that this failure model can only be used in conjunction with von Mises yielding and ABAQUS Explicit [165]. The explicit analysis was applied with a mass scaling factor of 1000 to reduce computational time and prevent dynamic instability. Non-linear geometric behaviour was also introduced into the modelling as large deformations were observed in this analysis.
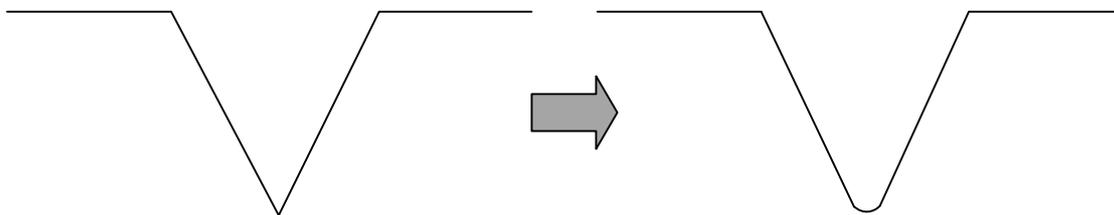
Figure 8-10: Fillet used to avoid singularity at the bottom of the groove.

ABAQUS supports real time elimination of failed elements and assign a STATUS value to the element (0 for failure and 1 for no failure). It also outputs and records the results after each load increment, which makes it possible to study the evolution of damage in the model

with increasing load. Figure 8-11 shows the predicted damage initiation and evolution around the groove of an *urushi*/aluminium bi-material strip during application of the bending load at deflections of 1.2 mm, 1.35 mm and 1.5 mm. The failed elements are shown in white indicating zero stress. It can be seen that damage initiates around the bottom of the groove, propagates first along the thickness direction, down to the interface of the bi-material strip, and interfacial failure initiates when the deflection reaches 1.5 mm, extending mainly along the interface to both ends, as shown in Figure 8-12.

(a)

(b)

(c)
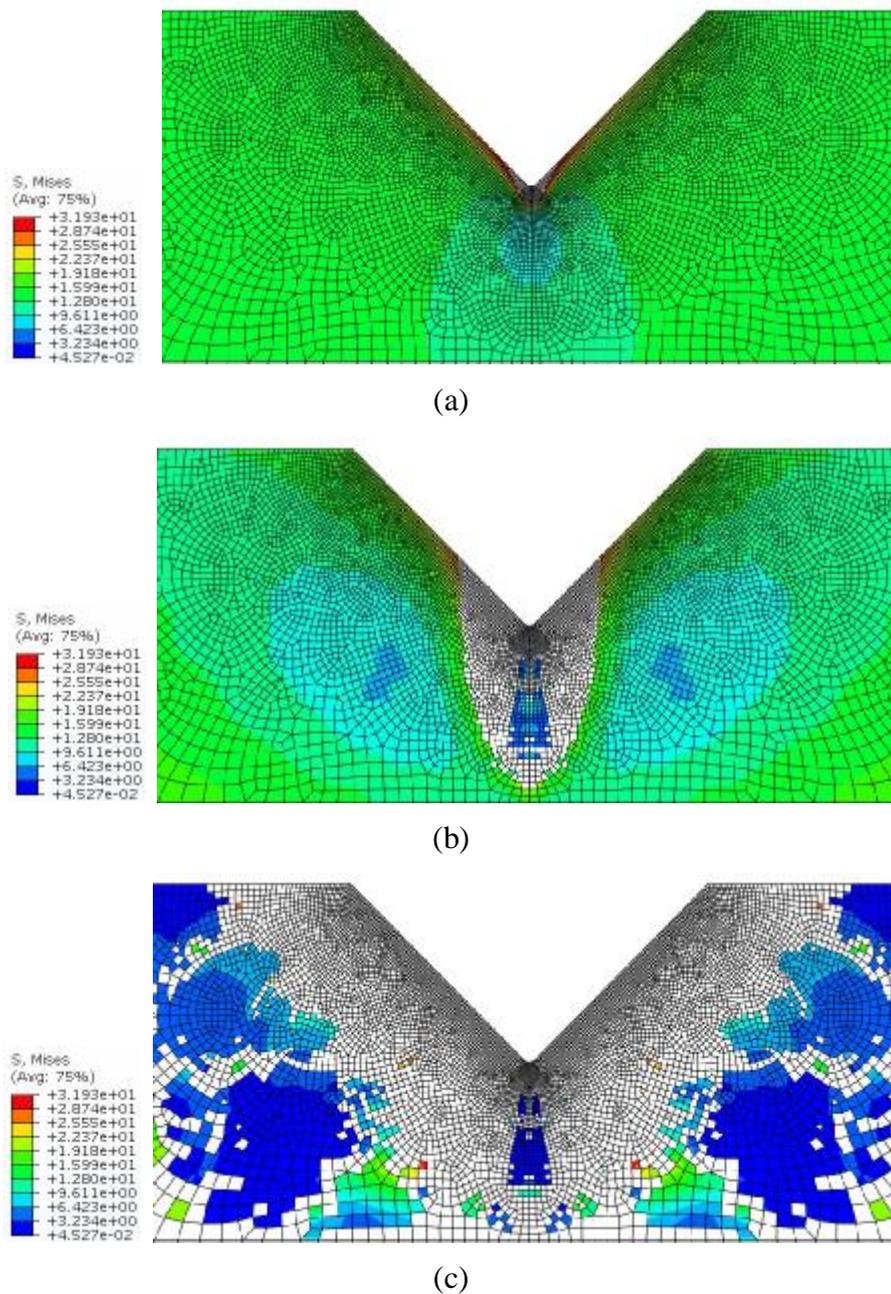
Figure 8-11: Predictive damage around the groove of a *urushi*/aluminium bi-material strip under a bending load with a deflection of (a) 1.2 mm, (b) 1.35 mm, and (c) 1.5 mm (von Mises stress contour with blank elements indicating failure).
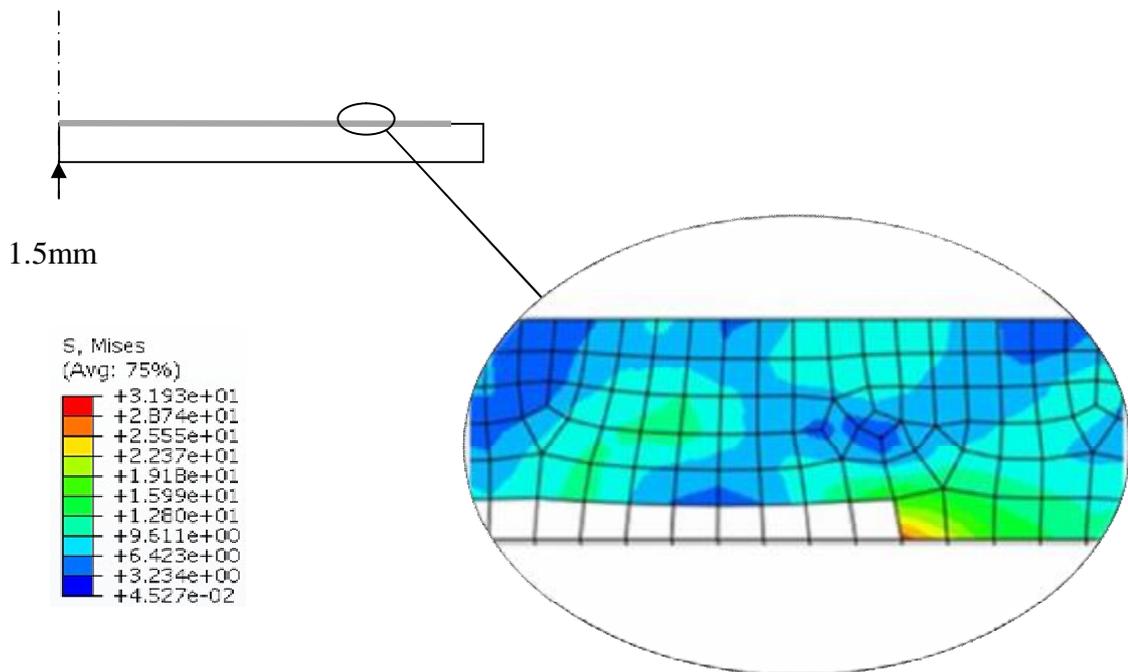
Figure 8-12: Predictive interfacial failure of an *urushi*/aluminium bi-material strip subjected to a bending load with a deflection of 1.5 mm (von Mises stress contour).

8.3.2 Predictive evaluation of consolidation

To evaluate the effectiveness of the traditional Japanese *urushi-gatame* consolidation method of lacquerware objects, the consolidated film was modelled by filling a grooved *urushi*/aluminium bi-material strip with *urushi* filler, marked in red as shown in Figure 8-13. Ageing was simulated by filling the groove with *urushi* with different UV-aged properties. Material properties of fresh, 100 hour-aged and 400 hours aged *urushi* films were assigned to the filler, The *urushi* film that is to be consolidated, i.e. all the *urushi* coating except the filler, is 400 hours aged as it is usually aged *urushi* lacquerwares that require consolidation.
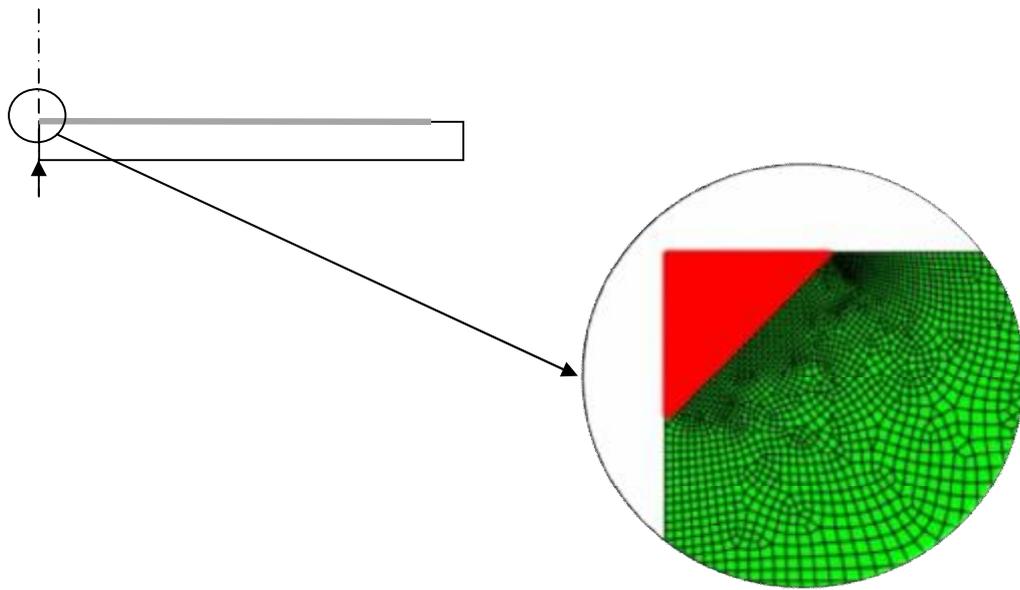
Figure 8-13: Modelling consolidated bi-material sample with *urushi* filler.

In order to study the damage initiation and propagation of the bi-layer filled with fresh *urushi* filler, the model shown in Figure 8-13 was subjected to a series of increasing bending deflections. The results from these analysis show that the damage in the filled bi-material model with fresh *urushi* filler, as shown in Figure 8-14, initiates when the deflection reaches 4 mm. It can be seen that the damage mainly occurs in the aged *urushi* film, which is easy to be understood as fresh *urushi* is able to sustain more strain than aged *urushi* (Section 6.2). It can also be seen that on the first appearance of damage, the damage is actually very comprehensive including both in-film and interfacial damage. However, the load which is required to achieve this damage is much higher than for the unfilled strips, in other words, the structure is consolidated by filling the groove using *urushi*.

(a) Around the filled groove

S, Mises
(Avg: 75%)
+3.193e+01
+2.874e+01
+2.555e+01
+2.237e+01
+1.918e+01
+1.599e+01
+1.280e+01
+9.611e+00
+6.423e+00
+3.234e+00
+4.527e-02

4 mm
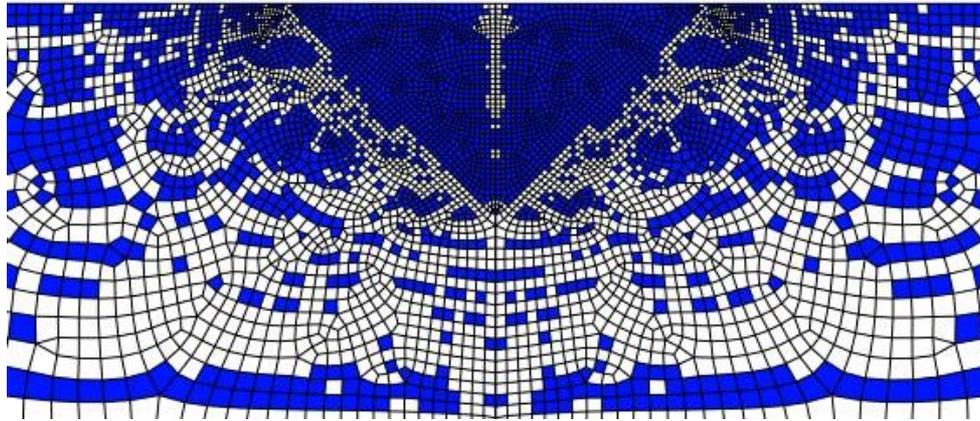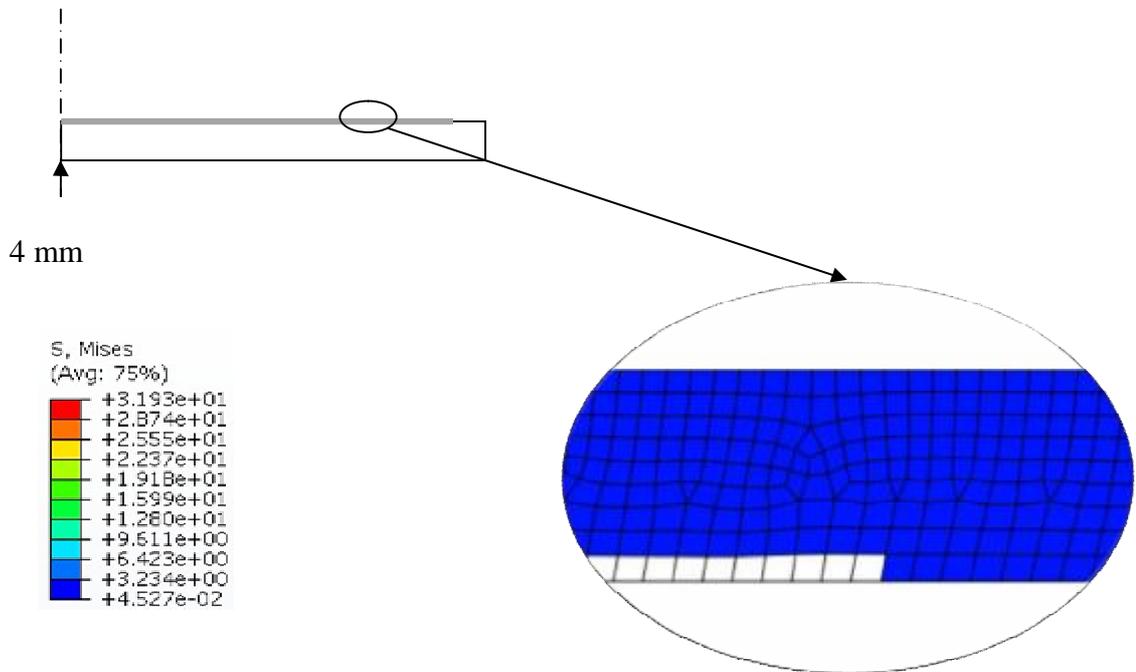
(b) At the end of the delamination

Figure 8-14: Damage in the grooved bi-material model filled with fresh *urushi* (von Mises stress contour) occurs when the deflection reaches 4 mm.

The effect of UV ageing of *urushi* fillers on the damage of the bi-material strip was studied by performing the same analysis but changing the material properties of the red section in Figure 8-13 from fresh to 400-hour aged *urushi*. The damage was found to initiate when the deflection reached 1.65 mm. With similarity to the bi-material strip with fresh filler, the structure damages comprehensively including in-film and interfacial failure. However, in this case there is much greater damage in the filler material.
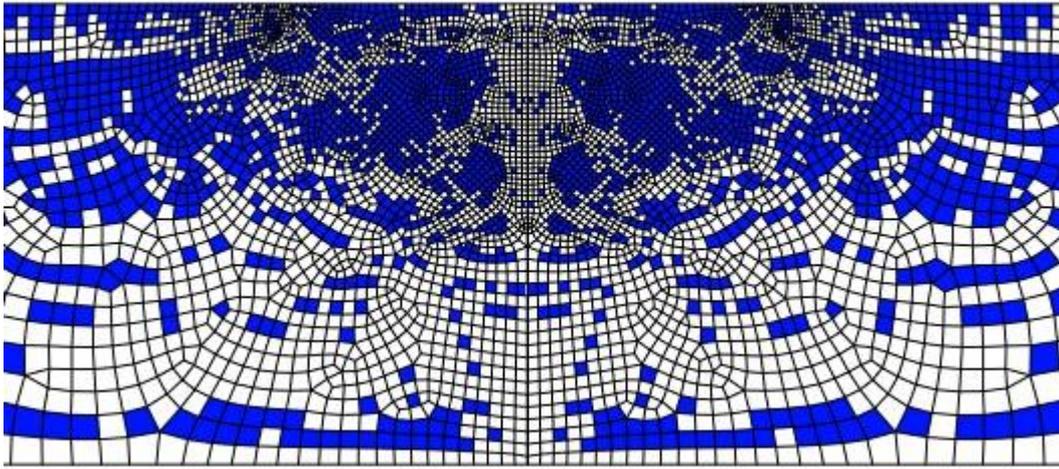
(a) Around the filled groove
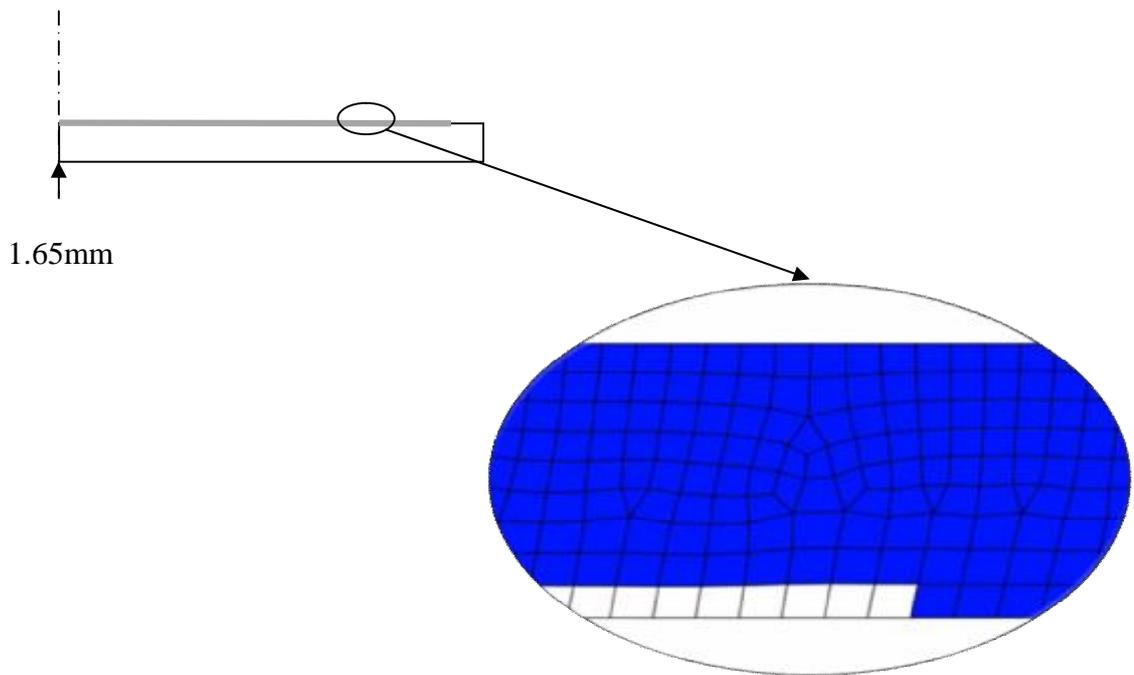
1.65mm

(b) At the end of the delamination

Figure 8-15: Damage in the grooved bi-material model filled with 400 hour UV aged *urushi* (Mises stress contour) occurs when the deflection is 1.65 mm.

A quantitative analysis of the damage behaviour of both in-film and interfacial damage was performed. To compare the effectiveness of the consolidation methods, crack depth, d_c is introduced and defined as the vertical distance from the bottom of the groove towards the

interface, with a maximum value of 0.03 meaning a through-depth crack. Figure 8-16 shows d_c as a function of the deflection. It can be seen that the unfilled strips are predicted to start cracking at a relatively low bending load, followed by a rapid evolution with increasing load. The introduction of the filler enabled the strip to sustain more bending load, with the fresh filler being more effective than the aged filler. Interfacial damage occurs once the bending load reaches a critical deflection, which is greater for filled strips than unfilled. Interfacial damage is studied by introducing a quantity l_d, delamination length, defined as the length of delamination from the central line to the end of the delamination. It can be seen from Figure 8-17 that initiation of interfacial damage is dependent on the filler material, but that after initiation, the delamination length is dependent on the deflection but not the filler material.
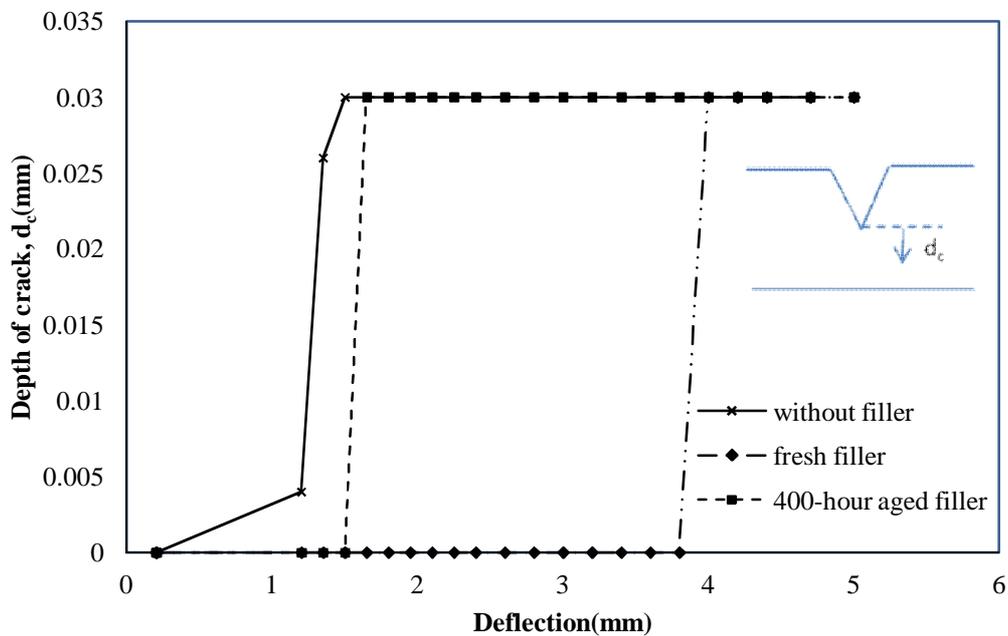
Figure 8-16: Predicted crack depth for grooved *urushi* coatings with fresh and UV aged fillers.
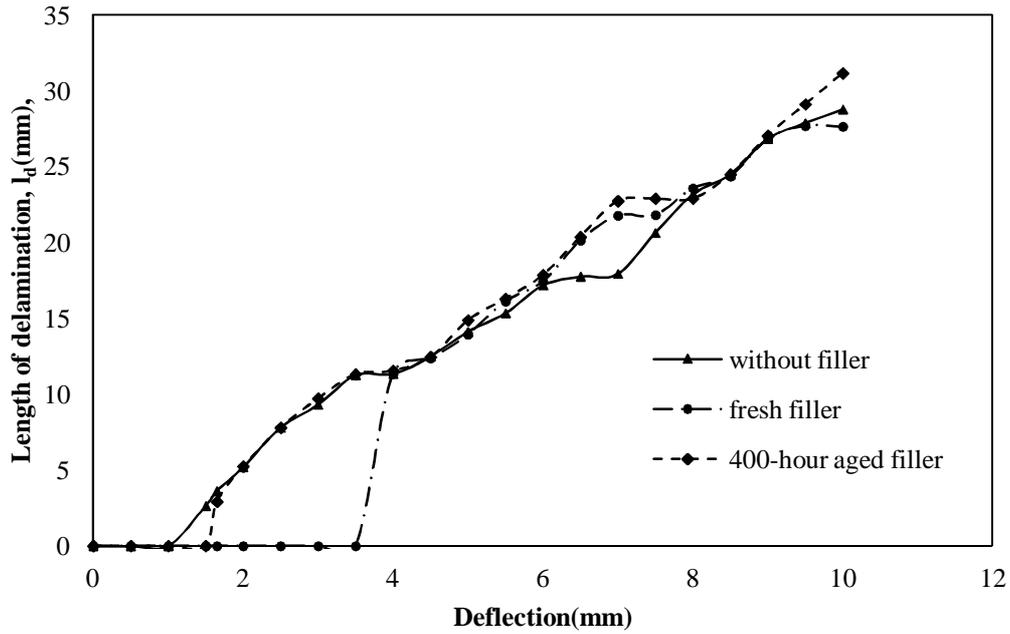
Figure 8-17: Predicted length of delamination of for bi-material strips with fresh and UV aged fillers.

The FE modelling above was also performed on an assignment of 100-hour-UV aged material properties to the filler to study the UV ageing effect to the effectiveness of the consolidation. The critical deflections of the bi-material samples subjected to a bending load are plotted as a function of duration of UV ageing of the filler *urushi* as shown in Figure 8-18. As expected, with the UV ageing of filler *urushi*, the filled bi-material strip appears to sustain less and less bending load due to the filler becoming more and more brittle (Chapter 6).
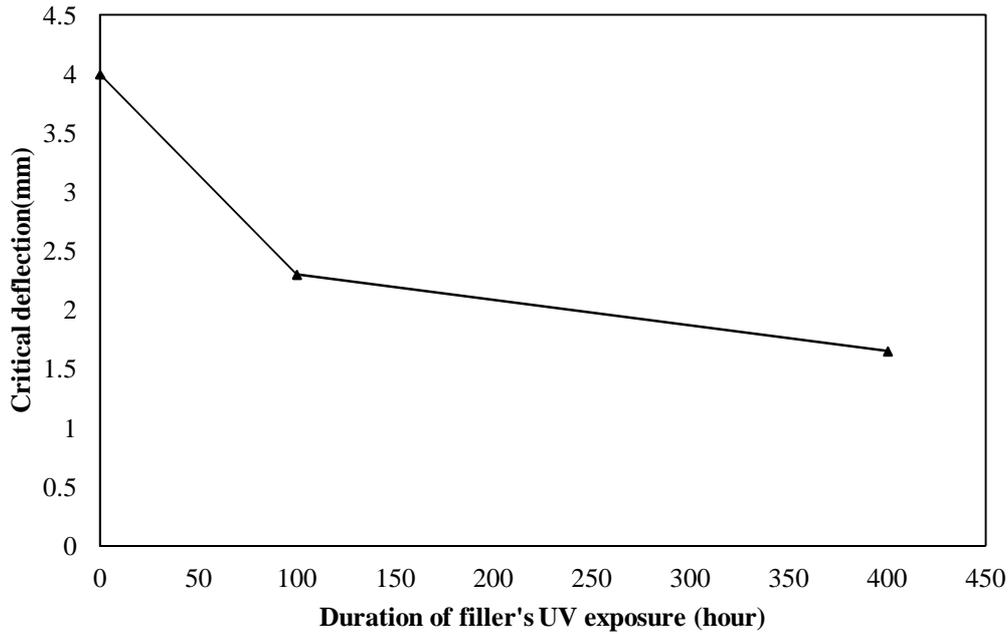
Figure 8-18: The critical deflections of bi-material strips subjected to a bending load as a function of duration of UV ageing of the filler *urushi*.

8.4 Summary

In order to perform a predictive study on the bending behaviour of *urushi* films with a crack (or scratch), a model with a grooved *urushi* film on an aluminium substrate was created and subjected to bending loads. The time-dependency of the *urushi* material properties seems to have little effect on the bending behaviour of the model when using a midpoint deflection of 0.08mm. The profile of the displacement field around the groove was found to be considerably affected by the geometry of the groove.

To evaluate the effectiveness of a traditional Japanese consolidation method of lacquerware objects, known as *urushi-gatame,* a strain-based progressive damage failure model was used to model continuum failure in the bi-material strip under an increasing bending load. The behaviour of damage initiation and evolution was modelled for an unfilled strip, and a filled strip with fresh filler and UV aged filler. From the FEA results, the introduction of the fillers, as a simple mimic of the consolidation method, does enable the strip to sustain a higher bending load. However, this effectiveness is weakened as the material is aged, with it then behaving quite similarly to a groove without any filler.

Chapter 9 Conclusions and future work

The research work presented in this thesis has made a useful and original contribution to the characterisation and modelling of the mechanical response of *urushi* coatings to varying environmental conditions, UV ageing and mechanical damage. The conclusions from the research and suggestions for future work are summarised in the following two sections.

9.1 Conclusions

The main conclusions of this research are as follows:

1. Moisture transport in both PU lacquer and *urushi* is found to follow Fick's law. However, the absorption isotherms of PU and *urushi* are best described by Flory-Huggins and GAB models, respectively.

2. Both PU and *urushi* lacquer films undergo a considerable dimensional change on the water absorption, which causes hygroscopic stresses to develop when considering a coating/substrate bi-material structure.

3. The mechanical properties of both *urushi* and PU lacquer films have a complex dependence on environmental conditions, including UV irradiation and relative humidity.

4. PU lacquer films behave with a non-linear viscoelasticity, which is highly dependent on environmental conditions. A modified Burger's model was found to fit the experimental data with satisfactory agreement at different stress levels, suggesting this is a suitable model for characterising PU rheological behaviour.

5. In the case of *urushi* films, the most successful material model is the proposed modified generalised Kelvin fluid model, which is capable of modelling *urushi* behaviour under various environmental ageing conditions by using specific material constants that represent the environmental ageing effects.

6. A method of modelling the environmental ageing behaviour of *urushi* film using FEA, introduced in this thesis, provides a powerful and generally applicable method of predicting the ageing behaviour of *urushi* film under variable environmental conditions. It is envisaged that the method could also be extended to the evaluation of the effects of various conservation and repair procedures.

7. The proposed FEA method, together with the MGKF model implemented through a user defined subroutine, is able to satisfactorily model the hygro-UV-mechanical response of *urushi* coated structures to varying environmental conditions.

8. The traditional Japanese consolidation method of lacquerware objects is considered, through the proposed and validated FE model, to be an effective way of consolidating the Mazarin Chest, or at least reducing the risk of further damage, however, the effect decreases as the filler material ages.

9.2   Future Work

Future experimental work is required to validate of the predicted results from modelling the bending behaviour of grooved *urushi*/substrate bi-material strips. A controlled and repeatable technique is required to cut the *urushi* film for a specified crack (or groove), and a reliable measurement setup needs to be designed and calibrate to accurately obtain the displacement field around a groove in an *urushi*/substrate bi-material sample.

It would be interesting to study further, by means of the proposed FEA technique, the conditions, dynamic loading caused by varying environmental conditions under which the Mazarin Chest was stored, that initiate and propagate micro-cracking in East Asian lacquer surfaces. A more complex model than the current bi-material strip would be needed that would represent the layered structure of real lacquerware and indicate the effect of moisture absorption in the wooden substrate.

More detailed experimental work would be useful to further study the failure behaviour of *urushi* film in service, both in-film and interfacial, by adopting more advanced failure models. For example, it would be of great interest to study whether the interfacial and in-film failure behaves with different characteristics and can be distinguished in the failure modelling, in order to perform a more convincing predictive investigation on the effectiveness of traditional Japanese consolidation method of lacquer ware objects.

It would also be of great interest to apply the developed model to a full scale and 3-D application for the sake of validity. This would however require a lot of computer power.

Reference

[1]   V&A. *Japanese Lacquer: Integrated Research and collaborative Conservation Project.* Available: http://www.vam.ac.uk/

[2]   V&A. *The Mazarin Chest conservation project.* Available: http://www.vam.ac.uk/content/articles/t/mazarin-chest-conservation-project/

[3]   V&A. *History of the Mazarin Chest: Design Elements on the Mazarin Chest.* Available: http://www.vam.ac.uk/content/articles/d/design-elements-on-the-mazarin-chest/

[4]   "The Mazarin Chest Major Anglo-Japanese Conservation project to start in 2004," in *The Japan Foundation London Newsletter*, ed, 2003.

[5]   A. Elmahdy, "Optical and Numerical Examination of the Effect of Western and Japanese Consolidation Treatments of Micro-cracks in the Surface of Aged Japanese Lacquer (Urushi)," PhD, Loughborough University 2011.

[6]   V&A. *Conservation of the Mazarin Chest, Further Investigation & Academic Partners.* Available: http://www.vam.ac.uk/res_cons/conservation/mazarin_chest/Conservation/iInvestigation/index.html

[7]   Z. W. Wicks*, et al.*, *Organic coatings : science and technology*, 2nd ed. New York: Wiley-Interscience, 1999.

[8]   S. K. Ghosh, *Functional coatings : by polymer microencapsulation*. Weinheim Chichester: Wiley-VCH ; John Wiley distributor, 2006.

[9]   D. G. Weldon, *Failure analysis of paints and coatings*, Rev. ed. Chichester, U.K.: Wiley, 2009.

[10]   T. Ogawa*, et al.*, "Effect of Water on Viscoelastic Properties of Oriental Lacquer Film," *Journal of Applied Polymer Science,* vol. 69, pp. 315-321, 1998.

[11]   T. Ogawa*, et al.*, "Light Stability of Oriental Lacquer Films Irradiated by a Fluorescent Lamp," *Journal of Polymers and the Environment,* vol. 6, pp. 59-65, 1998.

[12]   K. Awazu*, et al.*, "Effects of H-implantation energy on the optical stability of implanted urushi films under photo-irradiation," *Nuclear Instruments and Methods in Physics Research Section B: Beam Interactions with Materials and Atoms,* vol. 148, pp. 1121-1125, 1999.

[13]   L. B. Freund and S. Suresh, *Thin film materials: stress, defect formation, and surface evolution* vol. 1st. Cambridge: Cambridge University Press, 2003.

[14]   R. Lu and T. Yoshida, "Structure and molecular weight of Asian lacquer polysaccharides," *Carbohydrate Polymers,* vol. 54, pp. 419-424, 2003.

[15]   H. F. Brinson and L. C. Brinson, *Polymer engineering science and viscoelasticity : an introduction / Hal F. Brinson* vol. 1st. New York: Springer, 2007.

[16]   T. Brock*, et al.*, *European coatings handbook* Hannover, Germany: Vincentz Network GmbH & Co KG, 2000.

[17]   D. Rosu*, et al.*, "IR-change and yellowing of polyurethane as a result of UV irradiation," *Polymer Degradation and Stability,* vol. 94, pp. 591-596, 2009.

[18]   E. Obataya*, et al.*, "Effects of oriental lacquer(urushi) coating on the vibrational properties of wood used for the soundboards of musical instruments," *Acoust Sci Technol,* vol. 22, pp. 27-34, 2001.

[19]   E. Agostinelli*, et al.*, "Stability of Japanese-lacquer-tree (Rhus vernicifera) laccase to thermal and chemical denaturation: comparison with ascorbate oxidase.," *Biochemical Journal* vol. 306, pp. 697-702, 1995.

[20] R. Lu, *et al.*, "Development of a fast drying hybrid lacquer in a low-relative-humidity environment based on kurome lacquer sap," *Journal of Applied Polymer Science,* vol. 98, pp. 1055-1061, 2005.

[21] J. Kumanotani, "Urushi (oriental lacquer) -- a natural aesthetic durable and future-promising coating," *Progress in Organic Coatings,* vol. 26, pp. 163-195, 1995.

[22] N. Niimura and T. Miyakoshi, "Structural study of oriental lacquer films during the hardening process," *Talanta,* vol. 70, pp. 146-152, 2006.

[23] N. Niimura, *et al.*, "Characterization of Synthesized Lacquer Analogue Films by Two Stage Pyrolysis-Gas Chromatography/Mass Spectrometry and X-Ray Photoelectron Spectroscopy," *Analytical Sciences* vol. 17, pp. 155-158, 2001.

[24] H. K. Kim, *et al.*, "Surface and Curing Properties of Oriental Lacqur Modified by Acryl Monomer," *J. Korean Ind. Eng. Chem.,* vol. 12, pp. 444-448, 2001.

[25] N. Niimura and T. Miyakoshi, *Characterization of natural resin films and identification of ancient coating* vol. 51. Tokyo, JAPON: Mass Spectrometry Society of Japan, 2003.

[26] R. Lu, *et al.*, "Design and characterization of modified urethane lacquer coating," *Progress in Organic Coatings,* vol. 57, pp. 215-222, 2006.

[27] E. Obataya, *et al.*, "Effects of aging and moisture on the dynamic viscoelastic properties of oriental lacquer (urushi) film," *Journal of Applied Polymer Science,* vol. 83, pp. 2288-2294, 2002.

[28] O. Vogl, "Oriental lacquer, poison ivy, and drying oils," *Journal of Polymer Science Part A: Polymer Chemistry,* vol. 38, pp. 4327-4335, 2000.

[29] K. Taguchi, *et al.*, "Photo-curing composite paint containing urushi (Oriental lacquer), and wrinkled coating caused by phase separation," *Progress in Organic Coatings,* vol. 58, pp. 290-295, 2007.

[30] J. Kumanotani, "Enzyme catalyzed durable and authentic oriental lacquer: a natural microgel-printable coating by polysaccharide-glycoprotein-phenolic lipid complexes," *Progress in Organic Coatings,* vol. 34, pp. 135-146, 1997.

[31] Shiihara, *et al.*, *Studies on confirming the type of dried urushi film and its formation mechanism (urushi hardening study report II)* vol. 75. Tokyo, JAPON: Chemical Society of Japan, 2002.

[32] O. Bayer, "The diisocyanate polyaddition process (polyurethanes). Description of a new principle for building up high-molecular compounds," *Angewandte Chemie* vol. A, 1947.

[33] W. F. Gum, *et al.*, *Reaction polymers : polyurethanes, epoxies, unsaturated polyesters, phenolics, special monomers, and additives : chemistry, technology, applications, markets.* Munich ; New York. New York: Hanser Publishers; Distributed in the U.S.A. and Canada by Oxford University Press, 1992.

[34] G. Oertel and L. Abele, *Polyurethane handbook : chemistry, raw materials, processing, application, properties*, 2nd ed. Munich; New York. Cincinnati: Hanser ; Hanser/Gardner distributor, 1994.

[35] H. Ulrich, *Chemistry and technology of isocyanates.* Chichester ; New York: J. Wiley & Sons, 1996.

[36] G. Woods and ICI Polyurethanes (Firm), *The ICI Polyurethanes book*, 2nd ed. Chichester ; New York: Published jointly by ICI Polyurethanes and Wiley, 1990.

[37] J. H. Saunders and K. C. Frisch, *Polyurethanes--chemistry and technology.* Huntington, N.Y.: R.E. Krieger Pub. Co., 1978.

[38] R. V. Herren, *Agricultural mechanics : fundamentals and applications*, 6th ed. Clifton Park, NY: Delmar, Cengage Learning, 2009.

[39]   M. Webb, "Methods and materials for filling losses on lacquer objects," *Journal of American Institute for Conservation,* vol. 37, pp. 117-133, 1998.

[40]   Bishop. Museum. *Art Conservation Handout: Lacquer.* Available: http://www.bishopmuseum.org/research/pdf/cnsv-lacquer.pdf

[41]   K. Toyoshima, "Study of Deterioration of Urushi Film with Ultraviolet Radiation, Material Life Society," *Material Life Society,* vol. 8, pp. 28-35, 1996.

[42]   L. Bratasz, *et al.*, "Conservation of the Mazarin Chest: structural response of Japanese lacquer to variations in relative humidity," presented at the ICOM-CC triennial meeting, New Delhi, India, 2008.

[43]   H. F. Brinson, *Polymer engineering science and viscoelasticity : an introduction.* New York: Springer, 2007.

[44]   X. Liu, *et al.*, *A Methodology for Modelling the Mechanical Response of Urushi Lacquer under Varying Environmental Conditions.* London: Archetype Publications 2010.

[45]   X. Liu, *et al.*, "Experimental investigation and material modelling of fresh and UV aged Japanese lacquer (Urushi) . In-press," *Progress in Organic Coatings,* 2010.

[46]   T. Ogawa and T. Kamei, "The Fracture of Lacquer Films on Oriental Lacquerware Resulting from Absorption and Desorption of Water," presented at the in Japanese and European Lacquerware, Munich, Arbeitshefte des Bayerischen Landesamtes fur Denkmalpflege, 2000.

[47]   D. K. Chattopadhyay and D. C. Webster, "Thermal stability and flame retardancy of polyurethanes," *Progress in Polymer Science,* vol. In Press, Corrected Proof, 2009.

[48]   J. Hu, *et al.*, "Ageing behavior of acrylic polyurethane varnish coating in artificial weathering environments," *Progress in Organic Coatings,* vol. 65, pp. 504-509, 2009.

[49]   A. Boubakri, *et al.*, "Investigations on hygrothermal aging of thermoplastic polyurethane material," *Materials & Design,* vol. 30, pp. 3958-3965, 2009.

[50]   S. Rivers, "On the conservation of the Mazarin Chest.," presented at the 27th International Symposium on the Conservation and Restoration of Cultural Property, Tokyo National Research Institute for Cultural Property/Tokyo National Museum, Japan., 2003.

[51]   J.-W. Hong, *et al.*, "UV-Degradation Chemistry of Oriental Lacquer Coating Containing Hindered Amine Light Stabilizer," *Bulletin of Korean Chem. Society,* vol. 21, pp. 61-64, 2000.

[52]   R. Lu, *et al.*, "Development of a fast drying lacquer based on raw lacquer sap," *Progress in Organic Coatings,* vol. 51, pp. 238-243, 2004.

[53]   H. Römich, *et al.* (2004 *V&A: Lightcheck®: A New Tool in Preventive Conservation.* Available: http://www.vam.ac.uk/res_cons/conservation/journal/number_47/lightcheck/index.html

[54]   A. Boubakri, *et al.*, "Study of UV-aging of thermoplastic polyurethane material," *Materials Science and Engineering: A,* vol. 527, pp. 1649-1654, 2010.

[55]   F. Carrasco, *et al.*, "Artificial aging of high-density polyethylene by ultraviolet irradiation," *European Polymer Journal,* vol. 37, pp. 1457-1464, 2001.

[56]   A. E. Elmahdy, *et al.*, "Stress measurement in East Asian lacquer thin films owing to changes in relative humidity using phase-shifting interferometry. In press," *Proceedings of The Royal Society, A* 2010.

[57]   A. Skaja, *et al.*, "Mechanical property changes and degradation during accelerated weathering of polyester-urethane coatings," *Journal of Coatings Technology and Research,* vol. 3, pp. 41-51, 2006.

[58]   Y. Yamashita, "On the Plan for the Conservation of the Mazarin Chest: The Role of Urushi in International Exchange," presented at the 27th International Symposium on the Conservation and Restoration of Cultural Property December 2003, Tokyo National Museum, Tokyo, 2005.

[59]   V&A. *Mazarin Chest - further investigation & academic partners.* Available: http://www.vam.ac.uk/content/articles/m/album-with-nested-carousel13/

[60]   M. F. Mecklenburg, *et al.*, "Structural response of painted wood surfaces to changes in ambient relative humidity," in *Painted wood: history and conservation* V. Dorge and F. C. Howlett, Eds., ed Los Angeles: The Getty Conservation Institute 1998, pp. 464-483.

[61]   E. H. Wong, *et al.*, "The Mechanics and Impact of Hygroscopic Swelling of Polymeric Materials in Electronic Packaging," *Journal of Electronic Packaging,* vol. 124, pp. 122-126, 2002.

[62]   J.-H. Jou, *et al.*, "Structure effect on water diffusion and hygroscopic stress in polyimide films," *Journal of Applied Polymer Science,* vol. 43, pp. 857-875, 1991.

[63]   D. Y. Perera, *et al.*, "Stress Development and Weathering of Organic Coatings," in *Service Life Prediction of Organic Coatings.* vol. 722, ed: American Chemical Society, 1999, pp. 323-331.

[64]   D. Y. Perera, "On adhesion and stress in organic coatings," *Progress in Organic Coatings,* vol. 28, pp. 21-23, 1996.

[65]   P. D. Ruiz, *et al.*, "Numerical and experimental investigation of three-dimensional strains in adhesively bonded joints," *The Journal of Strain Analysis for Engineering Design,* vol. 41, pp. 583-596, 2006.

[66]   L. Yang, *et al.*, "Measurement of strain distributions in mouse femora with 3D-digital speckle pattern interferometry," *Optics and Lasers in Engineering,* vol. 45, pp. 843-851, 2007.

[67]   Q. Saleem, *et al.*, "A novel application of speckle interferometry for the measurement of strain distributions in semi-sweet biscuits " *Meas. Sci. Tech.,* vol. 14, pp. 2027–2033, 2003.

[68]   Q. Saleem, *et al.*, "Improved understanding of biscuit checking using speckle interferometry and finite-element modelling techniques," *Proceedings of the Royal Society A: Mathematical, Physical and Engineering Science,* vol. 461, pp. 2135-2154, July 8, 2005 2005.

[69]   Y. Morita, *et al.*, "Experimental analysis of thermal displacement and strain distributions in a small outline J-leaded electronic package by using wedged-glass phase-shifting moiré interferometry," *Optics and Lasers in Engineering,* vol. 46, pp. 18-26, 2008.

[70]   G. Stoney, "The Tension of Metallic Films Deposited by Electrolysis," *Proceedings of the Royal Society. A* vol. 82, pp. 172-175 1909.

[71]   A. Atkinson, "Generation and relief of stress in ceramic films," *British Ceramic Proceedings (UK). ,* vol. 54, pp. 1-14, 1997.

[72]   Y. Perera Dan, *et al.*, "Stress Development and Weathering of Organic Coatings," in *Service Life Prediction of Organic Coatings.* vol. 722, ed: American Chemical Society, 1999, pp. 323-331.

[73]   G. Mills and J. Eliasson, "Factors Influencing Early Crack Development in Marine Cargo and Ballast Tank Coating " *Journal of Protective Coatings and Linings,* 2006.

[74]   T. Clyne and S. Gill, "Residual Stresses in Thermal Spray Coatings and Their Effect on Interfacial Adhesion: A Review of Recent Work," *Journal of Thermal Spray Technology,* vol. 5, pp. 401-418, 1996.

[75]   Y. C. Tsui and T. W. Clyne, "An analytical model for predicting residual stresses in progressively deposited coatings Part 1: Planar geometry," *Thin Solid Films,* vol. 306, pp. 23-33, 1997.

[76]   J. Chen and I. D. Wolf, "Study of damage and stress induced by backgrinding in Si wafers," *Semiconductor Science and Technology,* vol. 18, pp. 261-268, 2003.

[77]   J. D. Schafer*, et al.*, "Macro- and microstress analysis in sol-gel derived Pb(Zr[sub x]Ti[sub 1 - x])O[sub 3] thin films," *Journal of Applied Physics,* vol. 85, pp. 8023-8031, 1999.

[78]   J. Matejicek and S. Sampath, "In situ measurement of residual stresses and elastic moduli in thermal sprayed coatings: Part 1: apparatus and analysis," *Acta Materialia,* vol. 51, pp. 863-872, 2003.

[79]   C. A. Klein, "How accurate are Stoney's equation and recent modifications," *Journal of Applied Physics,* vol. 88, pp. 5487-5489, 2000.

[80]   P. E. Gill*, et al.*, *Practical optimization.* London ; New York: Academic Press, 1981.

[81]   L. B. Freund*, et al.*, "Extensions of the Stoney formula for substrate curvature to configurations with thin substrates or large deformations," *Applied Physics Letters,* vol. 74, pp. 1987-1989, 1999.

[82]   H.-C. Wu, *Continuum mechanics and plasticity.* Boca Raton: Chapman & Hall/CRC, 2005.

[83]   J. Zhou, "Transient analysis on hygroscopic swelling characterization using sequentially coupled moisture diffusion and hygroscopic stress modeling method," *Microelectronics Reliability,* vol. 48, pp. 805-810, 2008.

[84]   C. T. Crowe*, et al.*, *Engineering fluid mechanics*, 8th ed ; Just ask! ed. Hoboken, NJ: Wiley, 2006.

[85]   Z. Kolek, "Water absorption by lacquer coatings," *Packaging Technology and Science,* vol. 9, pp. 99-110, 1996.

[86]   Y. Sato, "Mechanism and evaluation of protective properties of paints," *Progress in Organic Coatings,* vol. 9, pp. 85-104, 1981.

[87]   V. B. Miskovic-stankovic*, et al.*, "Electrolyte penetration through epoxy coatings electrodeposited on steel," *Corrosion Science,* vol. 37, pp. 241-252, 1995.

[88]   S. J. Shaw*, et al.*, "The mechanical and water absorption behavior of fluoroepoxy resins," ed New York Plenum 1988, pp. 45-66.

[89]   M. I. Karyakina and A. E. Kuzmak, "Protection by organic coatings: criteria, testing methods and modelling," *Progress in Organic Coatings,* vol. 18, pp. 325-388, 1990.

[90]   J. Crank, *The Mathematics of Diffusion* vol. 2nd. Oxford: Clarendon Press, 1975.

[91]   G. J. Van Amerongen, "Diffusion in Elastomers," in *Rubber Chemistry and Technology*. vol. 37, ed, 1964, pp. 1065-1152.

[92]   D. M. Ruthven, *Principles of adsorption and adsorption processes.* New York: Wiley, 1984.

[93]   R. J. Young and P. A. Lovell, *Introduction to Polymers* vol. 1st. London: Chapman and Hall, 1991.

[94]   J. Fried, *Polymer science and technology*: Prentice Hall Professional Technical Reference, 2003.

[95]   P. Bhargava*, et al.*, "Moisture diffusion properties of HFPE-II-52 polyimide," *Journal of Applied Polymer Science,* vol. 102, pp. 3471-3479, 2006.

[96]   P. J. Flory, *Principles of polymer chemistry.* Ithaca,: Cornell University Press, 1953.

[97]   L.-T. Lim*, et al.*, "Sorption and transport of water vapor in nylon 6,6 film," *Journal of Applied Polymer Science,* vol. 71, pp. 197-206, 1999.

[98]   H. Weisser*, et al.*, *Properties of Water in Foods NATO ASI Series E: Applied Sciences-No. 90* vol. 1st. PA: West Conshohocken, 1978.

[99]   E. O. Timmermann*, et al.*, "Water sorption isotherms of foods and foodstuffs: BET or GAB parameters?," *Journal of Food Engineering,* vol. 48, pp. 19-31, 2001.

[100] A. G. Fredrickson, *Principles and applications of rheology*. Englewood Cliffs, N.J.,: Prentice-Hall, 1964.

[101] M. Webb, "Methods and Materials for Filling Losses on Lacquer Objects," *Journal of the American Institute for Conservation* vol. 37, pp. 117-133, 1998.

[102] W. Findley and J. Lai, *Creep and relaxation of nonlinear viscoelastic materials : with an introduction to linear viscoelasticity* vol. 1st. Amsterdam: North-Holland, 1976.

[103] I. M. Ward and J. Sweeney, *An introduction to the mechanical properties of solid polymers*, 2nd ed. Chichester, West Sussex, England: Wiley, 2004.

[104] J. Gittus, *Creep, viscoelasticity and creep fracture in solids*. London: Applied Science Publishers, 1975.

[105] L. E. Nielsen, *Mechanical properties of polymers*. New York,: Van Nostrand Reinhold, 1962.

[106] N. M. Bikales, *Mechanical properties of polymers*. New York,: Wiley-Interscience, 1971.

[107] Y. M. Haddad, *Viscoelasticity of Engineering Materials*. Cornwall: Chapman & Hall, 1995.

[108] J. Gittus, *Creep, viscoelasticity, and creep fracture in solids*. New York: Wiley, 1975.

[109] F. Li*, et al.*, "Fish oil thermosetting polymers: creep and recovery behavior," *Polymer,* vol. 41, pp. 4849-4862, 2000.

[110] Y. Xu*, et al.*, "Study on creep properties of indica rice gel," *Journal of Food Engineering,* vol. 86, pp. 10-16, 2008.

[111] I. H. Shames and F. A. Cozzarelli, *Elastic And Inelastic Stress Analysis* vol. 1st. Englewood Cliffs: Prentice-Hall, 1992.

[112] Z. D. Wang and X. X. Zhao, "Modeling and characterization of viscoelasticity of PI/SiO2 nanocomposite films under constant and fatigue loading," *Materials Science and Engineering: A,* vol. 486, pp. 517-527, 2008.

[113] I. M. Ward, *Mechanical properties of solid polymers*. Weinheim: John Wiley and Sons Ltd, 1983.

[114] E. C. Bingham, "An Investigation of the Laws of Plastic Flow," *U.S. Bureau of Standards Bulletin,* vol. 13, pp. 309-353, 1916.

[115] E. C. Bingham, *Fluidity and Plasticity*. New York: McGraw-Hill 1922.

[116] H. L. Groth, "Viscoelastic and viscoplastic stress analysis of adhesive joints," *International Journal of Adhesion and Adhesives,* vol. 10, pp. 207-213, 1990.

[117] S. Yang*, et al.*, "Analysis of nanoindentation creep for polymeric materials," *Journal of Applied Physics,* vol. 95, pp. 3655-3666, 2004.

[118] P. Majda and J. Skrodzewicz, "A modified creep model of epoxy adhesive at ambient temperature," *International Journal of Adhesion and Adhesives,* vol. 29, pp. 396-404, 2009.

[119] M. P. Kruijer*, et al.*, "Modelling of the viscoelastic behaviour of steel reinforced thermoplastic pipes," *Composites Part A: Applied Science and Manufacturing,* vol. 37, pp. 356-367, 2006.

[120] X. X. Yu*, et al.*, "Material modelling for rate-dependent adhesives," *International Journal of Adhesion and Adhesives,* vol. 21, pp. 197-210, 2001.

[121] D. Systèmes, "Plasticity Models: General Discussion," in *Section 4.2.1 of the 10Abaqus Analysis User's Manual*, ed, 2009.

[122] G. D. Dean and L. Crocker, "Comparison of the Measured and Predicted Deformation of an Adhesively Bonded Lap-Joint Specimen," 2000.

[123] C. H. Wang and P. Chalkley, "Plastic yielding of a film adhesive under multiaxial stresses," *International Journal of Adhesion and Adhesives,* vol. 20, pp. 155-164, 2000.

[124] B. Loret and J. H. Prevost, "Accurate numerical solutions for drucker-prager elastic-plastic models," *Computer Methods in Applied Mechanics and Engineering,* vol. 54, pp. 259-277, 1986.

[125] D. C. Drucker and W. Prager, "Soil Mechanics and Plastic Analysis or Limit Design," *Quarterly of Applied Mathematics,* vol. 10, pp. 157-165, 1952.

[126] P. A. D. Bois*, et al.*, "Material behaviour of polymers under impact loading," *International Journal of Impact Engineering,* vol. 32, pp. 725-740, 2006.

[127] P. Bardia and R. Narasimhan, "Characterisation of Pressure-sensitive Yielding in Polymers," *Strain,* vol. 42, pp. 187-196, 2006.

[128] E. G. Miravete. (2005, 8th Jan). *Classical and Computational Solid Mechanics for Materials Engineers.* Available: http://www.ewp.rpi.edu/hartford/~ernesto/F2005/CINVESTAV/

[129] M. A. Meyers and K. K. Chawla, *Mechanical behavior of materials*, 2nd ed. Cambridge ; New York: Cambridge University Press, 2009.

[130] G. Dean, "Modelling non-linear creep behaviour of an epoxy adhesive," *International Journal of Adhesion and Adhesives,* vol. 27, pp. 636-646, 2007.

[131] R. A. Schapery, "Further development of a thermodynamic constitutive theory: stress formulation " Purdue University1969.

[132] E. Chailleux and P. Davies, "A Non-Linear Viscoelastic Viscoplastic Model for the Behaviour of Polyester Fibres," *Mechanics of Time-Dependent Materials,* vol. 9, pp. 147-160, 2005.

[133] S. Roy and J. N. Reddy, "A finite element analysis of adhesively bonded composite joints with moisture diffusion and delayed failure," *Computers & Structures,* vol. 29, pp. 1011-1031, 1988.

[134] A. D. Crocombe*, et al.*, "A unified visco-plastic model for the stress analysis of adhesively bonded structures," *Journal of Adhesion Science and Technology,* vol. 15, pp. 279-302, 2001.

[135] E. P. Cernocky, "Comparison of the unloading and reversed loading behavior of three viscoplastic constitutive theories," *International Journal of Non-Linear Mechanics,* vol. 17, pp. 255-266, 1982.

[136] S. R. Bodner and Y. Partom, "Constitutive Equations for Elastic-Viscoplastic Strain-Hardening Materials," *Journal of Applied Mechanics,* vol. 42, pp. 385-389, 1975.

[137] W. K. Chiu and R. Jones, "Unified constitutive model for thermoset adhesive, FM73," *International Journal of Adhesion and Adhesives,* vol. 15, pp. 131-136, 1995.

[138] V. G. Ramaswamy*, et al.*, "A Unified Constitutive Model for the Inelastic Uniaxial Response of Rene' 80 at Temperatures Between 538C and 982C," *Journal of Engineering Materials and Technology,* vol. 112, pp. 280-286, 1990.

[139] B. F. Chen*, et al.*, "A tensile-film-cracking model for evaluating interfacial shear strength of elastic film on ductile substrate," *Surface and Coatings Technology,* vol. 126, pp. 91-95, 2000.

[140] H. Yuan and J. Chen, "Computational analysis of thin coating layer failure using a cohesive model and gradient plasticity," *Engineering Fracture Mechanics,* vol. 70, pp. 1929-1942, 2003.

[141] H. Lei*, et al.*, "Modeling Stress and Failure in Shrinking Coatings," *Materials Research Society,* vol. 653, pp. Z10.5.1-Z10.5.7, 2001.

[142] H. Bhatnagar, "Computational modeling of failure in thermal barrier coatings under cyclic thermal loads ", Mechanical engineering, The Ohio State University, Columbus, 2008.

[143] L. Nicodemo, *et al.*, "Failure Mode Prediction of Organic Coating-Metallic Substrate Systems," in *Organic Coatings for Corrosion Control*. vol. 689, ed: American Chemical Society, 1998, pp. 199-210.

[144] P. Seiler, *et al.*, "FEM simulation of TBC failure in a model system," presented at the 15th International Conference on the Strength of Materials, Dresden, 2010.

[145] A. Strawbridge and H. E. Evans, "Mechanical failure of thin brittle coatings," *Engineering Failure Analysis,* vol. 2, pp. 85-103, 1995.

[146] D. C. Agrawal and R. Raj, "Measurement of the ultimate shear strength of a metal-ceramic interface," *Acta Metallurgica,* vol. 37, pp. 1265-1270, 1989.

[147] J. Rösler, *et al.*, "Stress state and failure mechanisms of thermal barrier coatings: role of creep in thermally grown oxide," *Acta Materialia,* vol. 49, pp. 3659-3670, 2001.

[148] V. V. Silberschmidt and J. Zhao, "A computational model for damage evolution in ceramic coatings: effect of random microstructure," presented at the 11th International Conference on Fracture, Turin, Italy, 2005.

[149] H. Bhatnagar, *et al.*, "Parametric studies of failure mechanisms in elastic EB-PVD thermal barrier coatings using FEM," *International Journal of Solids and Structures,* vol. 43, pp. 4384-4406, 2006.

[150] U. H. Tiong and G. Clark, "The structural environment as a factor affecting coating failure in aircraft joints," *Procedia Engineering,* vol. 2, pp. 1393-1401, 2010.

[151] P. S. Lam, "Failure Analysis of Coating Defects," Westinghouse Savannah River Company, Aiken 2002.

[152] J. A. Collins, *Failure of materials in mechanical design : analysis, prediction, prevention*, 2nd ed. New York: Wiley, 1993.

[153] A. R. Akisanya and N. A. Fleck, "Interfacial cracking from the freeedge of a long bi-material strip," *International Journal of Solids and Structures,* vol. 34, pp. 1645-1665, 1997.

[154] A. A. Griffith, "The Phenomena of Rupture and Flow in Solids," *Philosophical Transactions of the Royal Society of London. Series A,,* vol. 221, pp. 163-198, 1921.

[155] G. Irwin, "Analysis of stresses and strains near the end of a crack traversing a plate," *Journal of Applied Mechanics* vol. 24, pp. 361-364, 1957.

[156] J. Lemaitre, *A Course on Damage Mechanics*. Berlin: Springer, 1996.

[157] J. Zhao and V. V. Silberschmidt, "Microstructure-based damage and fracture modelling of alumina coatings," *Computational Materials Science,* vol. 32, pp. 620-628, 2005.

[158] T. D. Hong, *et al.*, "Saturated salt solutions for humidity control and the survival of dry powder and oil formulations of Beauveria bassiana conidia," *Journal of Invertebrate Pathology,* vol. 89, pp. 136-143, 2005.

[159] L. Greenspan, "Humidity Fixed Points of Binary Saturated Aqueous Solutions," *Journal of Research of the National Bureau of Standards,* vol. 81A, pp. 89-96, 1977.

[160] F. E. M. O'Brien, "The Control of Humidity by Saturated Salt Solutions," *Journal of Scientific Instruments,* vol. 25, p. 73, 1948.

[161] E. Obataya, *et al.*, "Effect of aging and moisture on the dynamic viscoelastic properties of oriental (urushi) film," *Journal of Applied Polymer Science,* vol. 83, pp. 2288-2294, 2002.

[162] D. A. H. Hanaor, *et al.*, "Morphology and photocatalytic activity of highly oriented mixed phase titanium dioxide thin films," *Surface and Coatings Technology,* vol. 205, pp. 3658-3664, 2011.

[163] Dassault, "Heat Transfer and Thermal-Stress Analysis." vol. 6.9, ed United States of America: ABAQUS 6.9 Documentation Collection, 2009.

[164] R. D. Adams and J. A. Harris, "The influence of local geometry on the strength of adhesive joints," *International Journal of Adhesion and Adhesives,* vol. 7, pp. 69-80, 1987.

[165] D. Systemes. (2010) Dassault Systemes, ABAQUS analysis' user manual.

[166] J. N. Tey*, et al.*, "Ink and moisture sorption study in UV-curable polyurethane acrylate," *Journal of Applied Polymer Science,* vol. 103, pp. 1985-1991, 2007.

[167] P. Bhargava*, et al.*, "Moisture Diffusion Properties of HFPE-II-52 Polyimide," *Journal of Applied Polymer Science,* vol. 102, pp. 3471-3479, 2006.

[168] H. W. Starkweather and S. P. Rowland, *Water in Polymers, ACS Symposium Series* vol. 1st. Washington, DC: American Chemical Society, 1980.

[169] G. A. F. Seber and C. J. Wild, *Nonlinear regression*. New York: Wiley, 1989.

[170] A. Mubashar, "Modelling Degradation in Adhesive Joints Subjected to Fluctuating Service Conditions," PhD, Wolfson School of Mechanical and Manufacturing Engineering, Loughborough, Leicestershire, 2010.

[171] A. Mubashar*, et al.*, "Moisture absorption–desorption effects in adhesive joints," *International Journal of Adhesion and Adhesives,* vol. 29, pp. 751-760, 2009.

[172] A. Mubashar*, et al.*, "Modelling Cyclic Moisture Uptake in an Epoxy Adhesive," *The Journal of Adhesion,* vol. 85, pp. 711-735, 2009/09/18 2009.

[173] J. Zhang*, et al.*, "Aqueous processing of SiC green sheets II: Binder and plasticizer," *Jounal of Material Reseach,* vol. 17, pp. 2019-2025, 2002.

[174] M. I. Kohan, *Nylon plastics handbook*. Munich; New York Cincinnati: Hanser Publishers; Distributed in the USA and in Canada by Hanser/Gardner Publications, 1995.

[175] B. Claude*, et al.*, "Surface cross-linking of polycarbonate under irradiation at long wavelengths," *Polymer Degradation and Stability,* vol. 83, pp. 237-240, 2004.

[176] J. Subocz*, et al.*, "Changes in the thermoluminescence of epoxy resin aged by UV radiation," *Polymer Degradation and Stability,* vol. 24, pp. 335-339, 1989.

[177] P. V. Zamotaev and Z. O. Streltsova, "Thermo-oxidative stabilization of photochemically crosslinked polyethylene," *Polymer Degradation and Stability,* vol. 36, pp. 267-274, 1992.

[178] J. C. Lagarias*, et al.*, "Convergence Properties of the Nelder--Mead Simplex Method in Low Dimensions," *SIAM J. on Optimization,* vol. 9, pp. 112-147, 1998.

[179] N. Phienwej*, et al.*, "Time-Dependent Response of Tunnels Considering Creep Effect," *International Journal of Geomechanics,* vol. 7, pp. 296-306, 2007.

[180] W. Stark, "The Phenomenological theory of linear viscoelastic behavior. An introduction. Von NICHOLAS W. TSCHOEGL. ISBN 3-540-19173-9. Berlin/Heidelbere/New York/London/Paris/Tokyo/Hong Kong: Springer-Verlag 1989. XXV, 769 S., geb., DM 148,00," *Acta Polymerica,* vol. 41, pp. 425-425, 1990.

[181] F. Dunne and N. Petrinic, *Introduction to computational plasticity*. Oxford ; New York: Oxford University Press, 2005.

[182] R. D. Adams and J. A. Harris, "The influence of local geometry on the strength of adhesive joints," *International Journal of Adhesion and Adhesives,* vol. 7, pp. 69-80, 1987.

[183] E. Adel, "Examination of the Response of East Asian Lacquer Films to Changes in Environmental Conditions," PhD, Wolfson School of Mechanical and Manufacturing Engineering Loughborough University Leicestershire, 2011.

[184] D. Bantz, "Springer Handbook of Nanotechnology (Book)," *Choice: Current Reviews for Academic Libraries,* vol. 42, pp. 324-324, 2004.

[185] A. A. Elmustafa, "Pile-up/sink-in of rate-sensitive nanoindentation creeping solids," *Modelling and Simulation in Materials Science and Engineering,* vol. 15, p. 823, 2007.

[186] A. E. H. Love, *A treatise on the mathematical theory of elasticity*, 4th ed. New York: Dover Publications, 1944.

[187] Y. Hua, "Modelling Environmental Degradation in Adhesively Bonded Joints," PhD, School of Engineering, Surrey University Surrey, 2006.